IDENTIFICATION OF FUNCTIONAL TARGETS IN EPITHELIAL OVARIAN CANCER

MIOW QING HAO

(B. Sci. (Hons.), NUS)

A THESIS SUBMITTED

FOR THE DEGREE OF DOCTOR OF PHILOSOPHY

NUS GRADUATE SCHOOL FOR INTEGRATIVE SCIENCES AND ENGINEERING

NATIONAL UNIVERSITY OF SINGAPORE

2014

DECLARATION

I hereby declare that the thesis is my original work and it has been written by me in its entirety. I have duly acknowledged all the sources of information which has been used in the thesis.

This thesis has also not been submitted for any degree in any university previously.

Miow Qing Hao

27 March 2014

ACKNOWLEDGEMENTS

This dissertation would not be possible without the guidance and the input of several people. First and foremost, I would like to express my sincerest thanks to my supervisor, Prof. Jean Paul Thiery for his unrelenting guidance, support and patience. It is my honour to meet such a nice professor. I would also like to thank my former supervisor, Dr Seiichi Mori for his selfless dedication to my training. His stimulating suggestions and immense knowledge helped me greatly throughout the project.

I am also grateful to my co-supervisor, Prof. Yoshiaki Ito for his insightful advice and guidance. I also extend my thanks to my thesis advisory committee members: Assoc Prof. Thilo Hagen and Dr. Chan Shing Leng for sharing their knowledge and counsel.

My heartfelt thanks also go to Dr. Tan Tuan Zea who is ever so approachable and patient in giving me advice. The project would not have progressed smoothly without his help. I would also want to extend my gratitude to Ye Jieru and Amelia Lau for helping me in some of the experiments. I would also like to thank all JPTians: Dr. Ruby Huang, Katty Kuang, Chung Vin Yee, Wong Meng Kang, Tan Ming, Mohammed Asad and Jane Anthony for their informative discussions and timely help.

This work is a product of a collaborative effort. I would like to thank Prof. Goh Boon Cher, Dr. Wang Ling-Zhi, Dr. Noriomi Matsumura, Assoc Prof. Richie Soong, Dr. Wu Meng Chu, Prof. Michael Sheetz and Dr. Pascale Monzo for their contributions to the project.

I am grateful to the NUS Graduate School for Integrative Sciences and Engineering for providing me with a valuable research scholarship and the Cancer Science Institute of Singapore for supporting my research work.

Special thanks go to my friends, Dr. Chua Kian Ngiap, Dr. Azhar Ali and Kong Liren for all their help and precious friendships. I also wish to express my deepest appreciations to my parents, who have always been supportive and encouraging. Last but not least, I would like to thank my wife, Hong Jia Mei for her accompaniment and giving me the support when it was most required.

TABLE OF CONTENTS

SUMMARY

Epithelial ovarian carcinoma (EOC) is the most lethal gynaecologic malignancy, with a low 5-year relative survival of only 44%. The possible reasons for these low survival rates are the high incidence of chemoresistance found with EOC and a lack of consideration of the high degree of heterogeneity of EOC in the current standard of care. Thus, the thesis is divided into two parts in an attempt to address these two concerns.

A classification scheme was previously developed to assess this high degree of heterogeneity in EOC, based on gene expression patterns of 1,538 tumours. Five, biologically distinct subgroups (Epi-A, Epi-B, Mes, Stem-A and Stem-B) were identified, each with significantly distinct clinicopathological characteristics, deregulated pathways, and patient prognoses. Rather than the current scheme of grouping patients together, the proposed classification scheme could be used to stratify patients and align them to subtype-specific therapies with the highest likelihood of benefit. Thus, in the first part of the thesis, the objective was to identify potential molecular targets that can be utilised for subtype-specific therapies. For this purpose, a pooled lentivirus library of short-hairpin RNAs (shRNAs) targeting 16,000 genes was screened for shRNAs that modulate cell growth (proliferation and/or viability) in a subtype-specific manner. The screen indeed revealed growth determinants that can be distinguished amongst the proposed subtypes. Focusing on the poor-prognosis Stem-A subtype, two genes involved in tubulin processing— *TUBGCP4* and *NAT10*—were found to be functionally relevant for cell growth. In support of these findings, the pathway analyses of

ovarian clinical tumours and ovarian cancer cell lines predicted the Stem-A subtype to have a significantly higher activity of microtubule/tubulin-related pathways than the non-Stem-A subtype. Furthermore, Stem-A representative cell lines were found to be specifically more susceptible to the tubulin polymerisation inhibitor drugs, vincristine and vinorelbine, but not to the microtubule stabilising drug, paclitaxel. These findings highlight the significance of TUBGCP4, NAT10 and tubulin polymerisation to Stem-A cells, and may serve as a potential platform to develop subtype-specific therapies.

The second focus of this thesis was to address the high incidence of chemoresistance. Since their introduction in the late 1970s, platinum-based drugs, such as cisplatin, have been the standard of care for EOC patients. Unfortunately, despite initial results, a large fraction of EOC acquires platinum resistance, leading to relapse and treatment failure. Thus, the objective for the second part of the thesis was to identify potential molecular targets that might be exploited for reverting platinum resistance in EOC.

Here, the pooled shRNA lentivirus library was screened for shRNAs that would decrease the cell viability of a cisplatin-resistant cell line in the presence of cisplatin. shRNAs targeting *ABCC3*, *KCNH3*, *KCNN1*, *MLH1*, *MRPL3* and *RPS6KA1* were found to enhance cisplatin sensitivity of the resistant cell line. In particular, the combinatorial treatment of cisplatin with a RPS6KA1-specific inhibitor, SL0101, specifically rendered Epi-A representative cell lines, but not Stem-A representative cell lines, more sensitive to cisplatin. Further investigation of these findings may lead to an

increased understanding of cisplatin resistance mechanisms and facilitate the development of chemosensitisation strategies.

LIST OF TABLES

LIST OF FIGURES

LIST OF SYMBOLS AND ABBREVIATIONS

ABC	ATP-binding cassette
ABCB1	ATP-binding cassette, sub-family B (MDR/TAP), member 1
ABCC1	ATP-binding cassette, sub-family C (CFTR/MRP), member 1
ABCC3	ATP-binding cassette, sub-family C (CFTR/MRP), member 3
ABCG2	ATP-binding cassette, sub-family G (WHITE), member 2
ACTB	Actin, beta
ADP	Adenosine diphosphate
ALK	Anaplastic lymphoma kinase
AMP	Adenosine monophosphate
AOCS	Australian Ovarian Cancer Study
ATCC	American Type Culture Collection
ATP	Adenosine triphosphate
ATP6V0D2	ATPase, H+ transporting, lysosomal 38kDa, V0 subunit D2
AURKB	Aurora Kinase B
B2M	Beta-2-microglobulin
BCL-2	B-cell CLL/lymphoma 2
BinReg	Binary regression
BLOC1S1	Biogenesis of lysosomal organelle complex-1, subunit 1
bp	Base pair
BR	Binary regression
BRAF	v-raf murine sarcoma viral oncogene homolog B1
BRCA1	Breast cancer 1, early onset
BRCA2	Breast cancer 2, early onset
BSA	Bovine serum albumin
BUB1	Budding uninhibited by benzimidazole 1
CA125	Cancer associated antigen 125
CCLE	Cancer Cell Line Encyclopedia
CCNE1	Cyclin E1
CD24	CD24 molecule
CDC2	Cyclin-dependent kinase 1
CDDP	*cis*-diamminedichloroplatinum(II) or Cisplatin
CDH1	Cadherin 1, type 1, E-cadherin (Epithelial)
CDH2	Cadherin 2, type 1, N-cadherin (Neuronal)

CDK12	Cyclin-dependent kinase 12
CI	Confidence interval
cm	Centimetres
CML	chronic myeloid leukemia
CO_2	Carbon dioxide
CR	Complete response
CREB	Cyclic AMP response element-binding protein
CRT	Cancer Research Technology
CTR1	Copper transporter 1
CXCL10	Chemokine (C-X-C motif) ligand 10
CXCL11	Chemokine (C-X-C motif) ligand 11
CXCR3	Chemokine (C-X-C motif) receptor 3
Cy	Cyanine
DAPI	4',6-diamidino-2-phenylindole
DAPK	Death-associated protein kinase
DMEM	Dulbecco's Modified Eagle Medium
DMSO	Dimethyl sulfoxide
DNA	Deoxyribonucleic acid
EB3	End-binding protein 3
ECACC	European Collection of Cell Cultures
EDTA	Ethylenediaminetetraacetic acid
EGFR	Epidermal growth factor receptor
ELISA	Enzyme-linked immunosorbent assay
EML4	Echinoderm microtubule associated protein like 4
EMT	Epithelial to mesenchymal transition
EOC	Epithelial ovarian carcinoma
EPCAM	Epithelial cell adhesion molecule
Epi-A	Epithelial-A
Epi-B	Epithelial-B
ER	Oestrogen receptor
ERK	Extracellular signal-regulated kinase
ESR1	Oestrogen receptor 1
ExpO	Expression Project for Oncology
FDA	Food and Drug Administration
FDR	False discovery rate

FIGO	International Federation of Gynaecology and Obstetrics
FN1	Fibronectin 1
GAPDH	Glyceraldehyde-3-phosphate dehydrogenase
GEO	Gene Expression Omnibus
GI50	Growth inhibition of 50%
GSEA	Gene set enrichment analysis
GTF3C1	General transcription factor IIIC, polypeptide 1, alpha 220kDa
h	Hour
HBOC	Hereditary breast and ovarian cancer
Her2	Human epidermal growth factor receptor 2
HGSOC	High-grade serous ovarian cancer
HNPCC	Hereditary nonpolyposis colorectal cancer
HPRT1	Hypoxanthine phosphoribosyltransferase 1
HR	Hazard ratio
i.e.	*id est*
ICON	International Collaboration on Ovarian Neoplasms
KCNH3	Potassium voltage-gated channel, subfamily H (Eag-related), member 3
KCNN1	Potassium intermediate/small conductance calcium-activated channel, subfamily N, member 1
KRAS	v-Ki-ras2 Kirsten rat sarcoma viral oncogene homolog
Kyoto U.	Kyoto University
LGR5	Leucine-rich repeat containing G protein-coupled receptor 5
LRRC59	Leucine rich repeat containing 59
M	Molar
MAPK	Mitogen-activated protein kinase
MCM2	Minichromosome maintenance complex component 2
MEK	MAPK/ERK kinase
Mes	Mesenchymal
MET	Mesenchymal to epithelial transition
MHC	Major histocompatibility complex
min	Minute
ml	Milliliter
MLH1	mutL homolog 1
MLH1	mutL homolog 1
MMR	Mismatch repair

MMR	mismatch repair
MOI	Muliplicity of infection
mRNA	messenger RNA
MRPL3	Mitochondrial ribosomal protein L3
ms	Millisecond
MSH2	mutS homolog 2
MSigDB	Molecular Signature Database
MTS	3-(4,5-dimethylthiazol-2-yl)-5-(3-carboxymethoxyphenyl)-2-(4-sulfophenyl)-2H-tetrazolium, inner salt
MYCN	v-myc myelocytomatosis viral related oncogene, neuroblastoma derived (avian)
NAT10	N-acetyltransferase 10 (GCN5-related)
NCAM	Neural cell adhesion molecule 1
NCI-Frederick	National Cancer Institute-Frederick National Laboratory for Cancer Research
NER	Nucleotide excision repair
NES	Normalised enrichment score
NF-κB	Nuclear factor-κB
NGS	Next-generation sequencing
nM	Nanomolar
No.	Number
NR	Non-responder
NSCLC	Non-small cell lung cancer
nt	Nucleotide
OSE	Ovarian surface epithelium
PARP1/2	Poly (ADP-ribose) polymerase 1/2
PBS	Phosphate buffered saline
PCA	Principle component analysis
PCNA	Proliferating cell nuclear antigen
PCR	Polymerase chain reaction
PDGFRA	Platelet-derived growth factor receptor, alpha polypeptide
PGK1	Phosphoglycerate kinase 1
PGK2	Phosphoglycerate kinase 2
PI3K	Phosphoinositide-3-kinase, regulatory subunit 5
PIM3	Pim-3 oncogene
PKMYT1	Membrane-associated tyrosine- and threonine-specific CDC2-

	inhibitory kinase 1
PLCO	Prostate, Lung, Colorectal and Ovarian
PPP1CA	Protein phosphatase 1, catalytic subunit, alpha isozyme
PPV	Positive predictive value
PR	Partial response
PROM1	Prominin 1
qPCR	Quantitative polymerase chain reaction
RAS	Rat sarcoma
RB1	Retinoblastoma 1
RECIST	Response Evaluation Criteria In Solid Tumour
RFP	Red fluorescence protein
RIGER	RNAi gene enrichment ranking
RIPA	Radioimmunoprecipitation assay
RMA	Robust Multichip Average
RNA	Ribonuclei acid
RNAi	RNA interference
ROC	Receiver Operation Curve
RPL13A	Ribosomal protein L13A
RPMI	Roswell Park Memorial Institute
RPS6KA1	Ribosomal protein S6 kinase, 90kDa, polypeptide 1
RPS6KA3	Ribosomal protein S6 kinase, 90kDa, polypeptide 3
RSK	p90 ribosomal S6 kinase
RT-PCR	Reverse transcriptase-polymerase chain reaction
s	Second
SAM	Significance Analysis of Microarrays
SE	Standard error
SEM	Standard error of measurement
shRNA	Short-hairpin RNA
SigClust	Statistical significance of clustering
siRNA	Small interfering RNA
SRF	Serum response factor
ss-GSEA	Single sample gene set enrichment analysis
StemA	Stem-like-A
StemB	Stem-like-B
SW	Silhouette width

TBE	Tris-borate-EDTA
TBP	TATA box binding protein
TCGA	The Cancer Genome Atlas
TFRC	Transferrin receptor
TIRF	Total internal reflection fluorescence
TP53	Tumour protein P53
TRC	The RNAi Consortium
TUBGCP4	Tubulin, gamma complex associated protein 4
TVU	Transvaginal ultrasonography
TWIST1	Twist basic helix-loop-helix transcription factor 1
VCAM1	Vascular cell adhesion molecule 1
ZEB1	Zinc finger E-box binding homeobox 1
β-catenin	Catenin (cadherin-associated protein), beta 1, 88kDa
γTuRC	gamma-tubulin ring complex
γTuSC	gamma-tubulin sub-complex
μg	Microgram
μl	Microliter
μM	Micromolar

LIST OF PUBLICATION

1. Tan TZ*, **Miow QH***, Huang RY*, Wong MK, Ye J, Lau JA, Wu MC, Bin Abdul Hadi LH, Soong R, Choolani M, Davidson B, Nesland JM, Wang LZ, Matsumura N, Mandai M, Konishi I, Goh BC, Chang JT, Thiery JP**, Mori S**. (2013). Functional genomics identifies five distinct molecular subtypes with clinical relevance and pathways for growth control in epithelial ovarian cancer. *EMBO Mol. Med.* Jul;5(7):983-98. *These authors contributed equally to this work. **Corresponding authors.

2. **Miow QH**, Tan TZ, Ye J, Lau JA, Thiery JP, Mori S. Epithelial-mesenchymal status renders differential responses to cisplatin in ovarian cancer. *Oncogene*. Under revision.

DECLARATION OF CONTRIBUTIONS

Title of article: Functional Genomics Identifies Five Distinct Molecular Subtypes with Clinical Relevance and Pathways for Growth Control in Epithelial Ovarian Cancer

Authors: Tuan Zea Tan*, **Qing Hao Miow***, Ruby Yun-Ju Huang*, Meng Kang Wong, Jieru Ye, Jieying Amelia Lau, Meng Chu Wu, Luqman Hakim Bin Abdul Hadi, Richie Soong, Mahesh Choolani, Ben Davidson, Jahn M Nesland, Ling-Zhi Wang, Noriomi Matsumura, Masaki Mandai, Ikuo Konishi, Boon-Cher Goh, Jeffrey T. Chang, Jean-Paul Thiery**, Seiichi Mori**

* Equally contributing authors
** Equally contributing corresponding authors

Journal: EMBO Mol. Med. 2013 Jul;5(7):983-98.

SM conceived the idea. SM, JPT, BCG and RYH devised the project and obtained funding. SM and JPT supervised the project. SM, TZT, QHM and JPT designed all experiments. SM, TZT and JTC performed all bioinformatics analyses, including the identification of epithelial ovarian cancer molecular subtypes, correlation of subtype with clinicopathological parameters, construction of predictive framework for subtype classification and identification of subtype representative cell lines. MC performed clinical parameter analyses. MKW, NM, MM and IK performed microarray analysis on ovarian cancer cell lines. SM, QHM, JY and JAL performed genome-wide shRNA screens. MCW, LHBAH and RS performed next-generation sequencing analysis. SM and QHM performed validation of subtype-specific growth-promoting genes. SM, QHM, JY, JAL and LZW performed drug sensitivity assays. SM, TZT, QHM, JTC and JPT wrote the paper. BD and JMN provided OSLO ovarian cancer samples. NM, MM, and IK provided ovarian cancer cell lines.

CHAPTER 1

INTRODUCTION

1.1 Overview of ovarian cancer

1.1.1 Definition of ovarian cancer

According to the description by the National Cancer Institute, United States of America, ovarian cancer is defined as any malignant tumours that develop in the ovarian tissues. Based on the presumed cells of origin, ovarian cancer is commonly classified as epithelial ovarian carcinoma (EOC), ovarian germ cell tumour or sex cord-stromal tumour. EOC is believed to derive from epithelial cells that cover the outer surface of the ovary (Auersperg et al, 1998), and alone accounts for 95% of all cancers in the ovaries (Quirk & Natarajan, 2005). In addition, EOC is the most lethal group among ovarian cancers and the prime cause of death for patients with gynaecological malignancies (Auersperg et al, 2001). Hence, being the most common and most dangerous type of ovarian cancer, EOC has been the focus of most ovarian cancer research and is also the focal point in this thesis.

On the other hand, ovarian germ cell tumours and sex cord-stromal tumours are rare events, accounting for only 2% to 3% and 1.2% of all ovarian cancers, respectively (Matei et al, 2013; Quirk & Natarajan, 2005). Ovarian germ cell tumours arise from primitive germ cells in the embryonic gonad (Downs & Boente, 2003), which tend to occur in teenagers and women in their twenties. The age of diagnosis ranges from 6 to 40 years (Gershenson et al, 1984; Matei et al, 2013). Sex cord-stromal tumours are a morphologically

diverse group of neoplasms composed of cells derived from gonadal sex cords, specialised gonadal stroma and fibroblasts (Deavers et al, 2003), and account for most hormone producing tumours (Judson & Boente, 2003). Unlike germ cell tumours, sex cord-stromal tumours are more common in adult women and can be found in peri- and post-menopausal women (Judson & Boente, 2003). The majority of germ cell tumours as well as sex cord-stromal tumours are presented as early-stage disease and usually considered as low-grade malignancies (Colombo et al, 2012; Koulouris & Penson, 2009). Owing to the advancements in surgical management and chemotherapy regimens, the overall prognosis of these rare tumours are very favourable today, and most patients survive the disease devoid of treatment-related toxicities, such as the loss of fertility (Matei et al, 2013). Even in the setting of advanced disease, the patients can be cured (Downs & Boente, 2003; Judson & Boente, 2003).

1.1.2 Epidemiology of ovarian cancer

Globally, ovarian cancer represents the eighth most common type of cancer among females, with 225,500 women estimated to be diagnosed with ovarian cancer in 2008 (Jemal et al, 2011). Despite its relatively low incidence, ovarian cancer is the seventh most frequent cause of cancer-related deaths in females, causing more than 140,000 deaths worldwide every year (Jemal et al, 2011). It accounts for 4.2% of all cancer deaths in women and has the highest mortality rates of any gynaecologic malignancy (Jemal et al, 2011). In the United States, it was reported that more women died from

ovarian cancer than from all other gynaecologic cancers combined (Howlader et al, 2013).

Like most types of cancer, notable geographic variation in ovarian cancer incidence and mortality patterns have been observed. For example, the lifetime risk of developing ovarian cancer for the average woman in economically developed regions is 1.0%, compared to only 0.5% in less economically developed regions (Jemal et al, 2011). Similarly, the mortality rate in developed regions (5.1 per 100,000 women) is almost twice as high as developing regions (3.1 per 100,000 women) (Jemal et al, 2011). Even within the same region, ethnic factors can also influence the incidence rates of ovarian cancer. In the United States, incidence rates are the highest among white women, but the lowest among Native American women (Runnebaum & Stickeler, 2001). Such demographic disparities may be attributed to the availability of advanced detection services, and/or the regional differences in prevalence and distribution of major risk factors.

Ovarian cancer most commonly occurs in peri- or post-menopausal women. The median age of diagnosis is at 58 years, with about 90% of patients older than 40 years (Runnebaum & Stickeler, 2001). Overall incidence of ovarian cancer rose with increasing age up to mid-70s, before declining slightly among women beyond 80 years (Goodman et al, 2003). It is thought that with each passing decade of aging, more time is afforded to accumulate random genetic alterations favourable for ovarian carcinogenesis. Furthermore, ovarian cancer patients beyond 65 years have higher case-fatality

ratios than patients less than 65 years (Lowe et al, 2013). These make age as one of the greatest risk factor of ovarian cancer.

Today the overall 5-year relative survival for women diagnosed with ovarian cancer is 44% (Howlader et al, 2013; Roland et al, 2013), having only minimal, but statistically significant improvements in the last several decades (Lowe et al, 2013). Compared to the substantial decreases in mortality rates observed in cancers of the breast and cervix, the modest improvements for ovarian cancer may or may not have meaningful clinical significance (Lowe et al, 2013; Siegel et al, 2013).

The poor prognosis of ovarian cancer is largely due to the lack of reliable screening strategies, late stage of disease presentation, high recurrence rate of the disease, and poor response of recurrent disease to current chemotherapeutic regimens. Because of its insidious onset, the majority of ovarian cancers are detected at an advanced stage with metastases present beyond the ovaries, at which point the disease is rarely curable using existing treatment schemes. Accordingly, more than half of the patients (61%) in the United States are diagnosed with disseminated disease, for whom the 5-year relative survival is only 27.3% (Howlader et al, 2013). In contrast, only 15% of the patients present with localised disease and have a high 5-year relative survival of 91.9% (Howlader et al, 2013). Additionally, patients with advanced ovarian cancer have increased risk of recurrence, with almost 90% of patients diagnosed with distant disease experiencing recurrence of the disease compared to less than 10% among patients diagnosed with localised disease (Lowe et al, 2013). Given the low 5-year survival rate of advanced

ovarian cancer, there is still significant unmet need to develop reliable screening strategies and more effective therapeutic regimens.

1.1.3 Risk factors of ovarian cancer

Women with a family history of ovarian or breast cancer are of particular risk for having an inherited predisposition. The increased risk for the disease is largely due to the inheritance of a germline mutation in high-penetrance cancer susceptibility genes, such as *BRCA1, BRCA2, MLH1, MSH2* (Schorge et al, 2010). Hereditary ovarian cancer occurs in two different forms. The more common is the hereditary breast and ovarian cancer (HBOC) syndrome, accounting for more than 90% of all inherited ovarian cancers (Schorge et al, 2010). HBOC syndrome is due to the germline mutations in *BRCA1* or *BRCA2* genes, with at least two-thirds of the cases associated with *BRCA1* mutations, and up to one-third linked to *BRCA2* mutations (Holschneider & Berek, 2000). Both *BRCA1* and *BRCA2* are tumour suppressor genes that are involved in the maintenance of genome integrity. Thus, inheritance of a mutation in these genes dramatically elevates lifetime risk of ovarian cancer from a baseline of 1.0% to 39% for *BRCA1* carriers and 22% for *BRCA2* carriers (Chen et al, 2006). Of particular note, women who are of Ashkenazi ancestry are especially susceptible to hereditary ovarian cancer, owing to the high prevalence of *BRCA1* or *BRCA2* mutation (1 in 40 carrier rate). However, in the general population, such germline mutations are rare, and are carried by less than 1 in 500 individuals (Szabo & King, 1997).

The other form of hereditary ovarian cancer is the association with hereditary nonpolyposis colon cancer (HNPCC) syndrome, also called Lynch

II syndrome. HNPCC syndrome is caused by the germline mutations of genes involved in the DNA mismatch-repair pathway, and almost 10% of women with this syndrome develop ovarian cancer (Aarnio et al, 1999).

As it would be expected for familial diseases, the average age of diagnosis for hereditary ovarian cancer is 48 years, significantly lower than that of sporadic ovarian cancers in the general population (Boyd & Rubin, 1997). However, only an estimated 10% of ovarian cancers are based on inherited predisposition (Runnebaum & Stickeler, 2001), and thus, its overall impact on mortality is relatively small.

The other ovarian cancers are believed to develop sporadically without an obvious autosomal-dominant inheritance (Runnebaum & Stickeler, 2001), and numerous risk factors, besides age, have been identified. Among them, reproductive factors received the widest attention. As first proposed by Fathalla in 1971, it was surmised that incessant ovulation results in the repeated rupture of the ovarian epithelium and subsequent repair by clonal expansion may increase the rate of mutations, which may confer increased malignancy (Fathalla, 1971). In addition, the increase in sex steroid hormones production during ovulation may enhance cell proliferation and transformation in the ovarian epithelium (Berchuck et al, 2008). These has been supported by a case-control study showing that increase in 1 year worth of ovulation was associated with a 6% increase in ovarian cancer risk (Purdie et al, 2003).

On the other hand, reduction in ovulatory events by pregnancy or oral contraceptive use was found to dramatically reduce ovarian cancer risk (Riman et al, 2002; Risch et al, 1994), as reflected in observations that

regardless of the age at first pregnancy, each child delivery confers a 16% risk reduction (Hankinson et al, 1995), while prolonged consumption of oral contraceptives reduce risk by up to 53% (Schlesselman, 1995). Additionally, the progestogenic hormonal milieu associated with pregnancy and oral contraceptive use may also exert a protective effect against ovarian cancer by stimulating apoptosis of genetically damaged epithelial cells that otherwise might evolve to a malignant phenotype (Rodriguez et al, 2002).

Interestingly, surgical interventions, such as tubal ligation and hysterectomy can also reduce ovarian cancer risk by 18-35% (Miracle-McMahill et al, 1997; Rice et al, 2013). The inverse associations observed may be explained by the possible impediment of retrograde transport of inflammatory agents or other potential carcinogens through the fallopian tubes to the ovaries after tubal ligation or hysterectomy, and thereby prevent tumour formation (Green et al, 1997; Hankinson et al, 1993). Alternatively, surgical interventions may possibly lower ovarian cancer risk through the disruption of blood supply towards the ovaries, resulting in the loss of ovarian function (Hankinson et al, 1993).

A variety of dietary and environmental factors have also been found by numerous studies to be associated with ovarian carcinogenesis, but with weak or inconsistent correlation. Examples of such factors include alcohol consumption (Runnebaum & Stickeler, 2001), amount and composition of dietary fats (La Vecchia et al, 1987), use of talc in genital hygiene (Cramer et al, 1999), radiation exposure (Pettersson et al, 1985), and high-level physical activity (Mink et al, 1996). Several of these risk factors are highly related to

the diverse cultural habits and lifestyle practices of the world (Runnebaum & Stickeler, 2001), and as mentioned earlier, may possibly explain for the notable geographic disparities in ovarian cancer incidence and mortality patterns.

It is important to note that very few or none of the numerous epidemiological risk factors identified to date, are presently used in the clinic to guide clinical surveillance or interventions, with the exception of those rare cases with family history of ovarian or breast cancer. Thus, a deeper understanding of the molecular genetic features of ovarian cancer would be an essential and complementary approach to epidemiologic and clinical studies.

1.1.4 Cell of origin of epithelial ovarian carcinoma

Epithelial ovarian carcinoma which makes up more than 85% of human ovarian cancers, is the focus of most ovarian cancer research. Even so, early events in ovarian carcinogenesis remain remarkably unknown, and are complicated by the recent controversy with regards to the cell of origin of this disease. The long-held view was that EOC arises by malignant transformation of epithelium lining the ovarian surface (Auersperg et al, 1998), also referred as ovarian surface epithelium (OSE). Normal OSE is a phenotypically uncommitted mesothelium, composing of a monolayer of flat to cuboidal epithelial cells, having both epithelial and mesenchymal characteristics. The invaginations of OSE into the ovarian stroma (Feeley & Wells, 2001) and/or aggregation of OSE within the stroma during postovulatory repair (Ahmed et al, 2007) may result in the formation of inclusion cysts, which are believed to

be the most likely site of early neoplastic transformation. Sequentially, accumulation of stromal-derived growth factors, OSE-derived cytokines and/or other bioactive molecules within the confined sites of inclusion cysts may promote the neoplastic progression of OSE-lined cysts (Auersperg et al, 2001).

However, recent publications suggested that EOC develops from cells of extra-ovarian origins, such as the fallopian tube epithelium (O'Shannessy et al, 2013), other derivatives of the secondary Mullerian system (Dubeau, 2008) or the transitional area between the OSE, mesothelium and tubal epithelium (hilum region) (Cheng et al, 2005). The dilemma as to where EOC actually originates, rises from the fact that ovarian epithelial neoplasms are morphologically, as well as genetically similar to normal non-ovarian epithelial cells of the female reproductive tract, even though they are not developmentally related to the ovary (Cheng et al, 2005; Dubeau, 2008; O'Shannessy et al, 2013). In comparison, none of the normal cellular constituents of the ovary show morphologic features that resemble EOCs (Dubeau, 2008). Proponents of OSE as the cell of origin account for these observations by stipulating that OSE-lined cells become more differentiated as it transform and acquire complex epithelial characteristics of the Mullerian duct-derived epithelia, *i.e.*, the oviduct, endometrium, and uterine cervix (Auersperg et al, 2001). On the other hand, others argue that this notion is at odds with our current understanding of cancer development, whereby malignant cells become less differentiated than the epithelium from which they arise. Instead, it would seem much more likely that EOCs originate from

cells in which epithelial features of Mullerian epithelium are already present (Dubeau, 2008).

Presently, the contribution of ovary and various segments of the Mullerian system to the genesis of EOC is unclear, complicated by the fact that majority of the patients are presented with advanced disease, where wide-spread growth of tumour tissue extend throughout the peritoneal cavity and obscures the primary site (Bowtell, 2010).

1.1.5 Heterogeneity in epithelial ovarian carcinoma

Epithelial ovarian carcinoma is a series of molecularly and etiologically distinct diseases. Even when all patients with EOC are given the same treatment regimen, they display a broad range of clinical outcomes (Sabatier et al, 2009). To date, multiple genetic and epigenetic abnormalities have been detected in different patients with EOC (Bast et al, 2009). Such abnormalities are linked to signalling pathways that are involved in proliferation, apoptosis, motility, adhesion and invasion, but how these changes are selected during carcinogenesis and drive the heterogeneous clinical behaviour of EOC is not yet clear. Consequently, EOC is highly heterogeneous and also, among the least understood of all major human malignancies.

It is currently accepted that the tumour progression of EOC can be broadly divided into two categories termed Type I and Type II, which correspond to two distinct pathways of tumorigenesis (Shih Ie & Kurman, 2004; Singer et al, 2003). Type I includes low-grade tumours and borderline

tumours of low malignant potential whereas Type II, accounting for three fourths of all EOCs, is composed of high-grade tumours with very aggressive clinical behaviour (Gadducci et al, 2012). In general, Type I tumours have an indolent clinical behaviour, are poorly responsive to conventional chemotherapy, lack TP53 gene mutations, and are genetically stable (Bowtell, 2010). These neoplasms arise by progressive transformation from clearly recognised precursor lesions, such as cystadenoma, atypical proliferative tumour and noninvasive carcinoma, reminiscent of the adenoma-carcinoma sequence in colorectal cancer (Shih Ie & Kurman, 2004). Nevertheless, Type I ovarian carcinomas form a heterogeneous group of tumours, with each of the various histological types categorised as Type I having distinct mutations of genes involved in different signalling pathways (Singer et al, 2003). For example, high frequency of *BRAF* or *KRAS* mutations were found in low-grade serous tumours (Singer et al, 2003), while mucinous and endometrioid tumours are associated with *KRAS* and *β–catenin* mutations respectively (Auner et al, 2009; Catasus et al, 2004; Lengyel, 2010).

Conversely, Type II tumours have a more direct and aggressive development from either OSE-lined cysts or other epithelial source, and also disseminate early to the peritoneal cavity (Lengyel, 2010). These neoplasms have a high incidence of TP53 mutations, rarely harbour mutations of *BRAF*, *KRAS* and *β–catenin*, and are often found with widespread DNA copy number aberrations (Kuo et al, 2009; Singer et al, 2005). Such high levels of DNA amplifications and deletions are believed to be the determinant of further Type II tumours evolution, through the enhancement of the expression of genes in favour of tumour growth, as well as the suppression of tumour suppressor

genes (Bowtell, 2010). However, little is known about the potential contributions of thousands of genes whose expressions could be altered by the highly aberrant genome.

Heterogeneity in EOC is also apparent in tumour histopathology, where based on morphological criteria, EOC can be classified into four distinct main histotypes; serous, mucinous, endometrioid and clear cell. Among them, high-grade serous carcinoma is the most common, accounting for approximately 70% of all ovarian carcinoma and almost two-thirds of ovarian cancer deaths (Bowtell, 2010).

Recent genomic findings indicate that these distinct histotypes resemble well-differentiated normal cells that line the fallopian tube (serous), endometrium (endometrioid), endocervix (mucinous), or cells that form nests within the vagina (clear cell) (Bast et al, 2009; Kurman & Shih, 2010). Moreover, some of these histotypes bear more resemblance with certain types of breast cancer or renal cancer than with other histotypes similarly classified as ovarian cancer. For example, high-grade serous ovarian carcinoma and clear cell ovarian carcinoma share similar transcriptional features with basal-like breast carcinoma and renal clear cell carcinoma respectively (Bowtell, 2010; The Cancer Genome Atlas Research Network, 2012; Zorn et al, 2005).

These discrete histological types also differ with respect to variable clinical features, including epidemiological risk, spread patterns, somatic mutations, chemotherapeutic response and patient prognosis (Gilks & Prat, 2009). For instance, only 15% of patients with clear cell carcinoma respond to conventional chemotherapy, in sharp contrast with the high response rate

(80%) observed for high-grade serous carcinoma (du Bois et al, 2003; Takano et al, 2006).

Even with similar histological features, heterogeneity can still be observed in each of the histotypes. This is illustrated by the diverse clinical outcomes displayed in patients with high-grade serous carcinoma, in spite of the same or very similar treatment regimens (Gilks & Prat, 2009). In addition, heterogeneous pattern of genomic aberrations, which are of clinical significance, has also been observed in clear cell carcinoma (Tan et al, 2011). Essentially, EOC should not be viewed and treated as a single disease entity.

1.1.6 Metastasis in epithelial ovarian carcinoma

The spread of ovarian carcinoma differs markedly from the classic pattern of hematogenous metastasis found in most other cancers. For instance, metastasis in breast cancer involves the following steps: partial loss or complete loss of the epithelial phenotype, increased motility and invasiveness, intravasation into the blood circulation, survival in the circulation, extravasation to secondary sites, and finally the establishment of metastases in distant organs (Chambers et al, 2002; Gupta & Massague, 2006). In the case of ovarian carcinoma, primary tumour cells do also experience profound phenotypic changes, including the disruption of E-cadherin-mediated intercellular adhesion and the acquisition of migratory and invasive properties, through the epithelial to mesenchymal transition (EMT) process (Ahmed et al, 2007; Thiery et al, 2009). These changes allow the detachment of malignant cells from the primary tumour into the peritoneal cavity. Once in the

peritoneum, the cells often aggregate and form spheroid-like structures, which can be transported throughout the cavity by the physiological movement of peritoneal fluid, resulting in the extensive seeding of malignant cells onto the mesothelial lining of the peritoneum (Lengyel, 2010). Upon adhesion to the mesothelial cells, the metastatic colonies undergo mesenchymal to epithelial transition (MET) to an epithelial phenotype for enhanced proliferation and forms the bulk of the secondary tumour mass (Ahmed et al, 2007; Thiery et al, 2009). Hence, it is thought that ovarian carcinomas metastasize through a passive and relatively easy mechanism, without any anatomical barrier to prevent widespread metastasis throughout the peritoneal cavity. This was supported by clinical observations and retrospective clinical studies which suggest that EOCs grow efficiently within the peritoneal cavity, but rarely metastasize through the hematogenous circulation to distant organs (Lengyel, 2010).

The unique metastatic behaviour of ovarian carcinoma may account for the high percentage of ovarian cancer patients diagnosed with disseminated disease. In fact, making use of ovarian carcinomas from women with *BRCA1* mutations as a model for sporadic ovarian carcinomas, it was estimated that more than half of ovarian carcinomas had already spread into the space around the gut, stomach and liver (Stage III), or to the distant organs (Stage IV) when they are only 3cm in size (Brown & Palmer, 2009). Hence, together with heterogeneity, the metastatic behaviour of EOC augments the challenge of improving the mortality rate of this so-often fatal disease.

1.1.7 Screening strategies for epithelial ovarian carcinoma

The high mortality rate of EOC is believed to be attributed to the late stage of disease presentation, while survival is longer when cancer remains localised at the time of diagnosis. However, non-specific symptoms and the lack of reliable early screening strategy hinder the diagnosis of EOC at the more curable early stage. Consequently, only 15% of the patients present with localised disease (Howlader et al, 2013). Moreover, it was suggested that on average, EOCs have already progressed to a late stage for approximately 1 year prior to their discovery (Brown & Palmer, 2009). Thus, given the inverse relationship between survival and disease stage at diagnosis, the ability to detect early disease and prevent their progression to invasive disease will offer the most effective way to save lives.

In order for early detection tests to be clinically useful, they should be able to identify the precursors of advanced stage disease with both high sensitivity and specificity (Clarke-Pearson, 2009). Unfortunately, we currently know little of the early natural history of EOCs. The low percentages of EOCs that present clinically at early stages are typically not precursors to those that present at late stages (Vaughan et al, 2011), and thus, cannot be used as models for rational design of effective screening strategy. The challenge is further complicated by recent evidences suggesting that to achieve even 50% sensitivity in detecting early stage EOC in normal-risk women, any screening test has to be able to detect tumours less than 1.3cm in diameter (Brown & Palmer, 2009). Accordingly, it is a great challenge to identify specific molecular markers and develop assays that can provide the necessary sensitivity and specificity to detect this low prevalence disease.

Presently, CA125 tumour antigen measurement, transvaginal ultrasonography (TVU) and pelvic examination are used as diagnostic tests to detect presence of EOC. Among these tests, only CA125 is recommended for monitoring ovarian cancer patients' response to therapy, as well as post-treatment monitoring for recurrent disease (Sturgeon et al, 2008). However, for the purpose of early detection, these tests have limited clinical utility, as they are often associated with false-positive and false negative results (Johnson et al, 2008; Schorge et al, 2010). Since further diagnostic evaluation usually involves invasive surgical procedure, such false-positive results will lead to unnecessary surgical intervention and could even cause serious complications. Indeed, the recently completed Prostate, Lung, Colorectal and Ovarian (PLCO) trial concluded that annual screening performed with CA125 and TVU does not reduce ovarian cancer mortality in normal-risk women, but instead increases unnecessary surgical interventions (Buys et al, 2011; Partridge et al, 2009). Even when ovarian cancers were detected, 72% of the cases were late stage (Partridge et al, 2009). On the basis of current data, widespread screening for ovarian cancer is not recommended (Sawyers et al, 2013).

1.1.8 Therapeutic regimens for epithelial ovarian carcinoma

Surgery followed by chemotherapy has been the mainstays of first-line treatment regimen for ovarian cancer patients. Patients are first subjected to surgical cytoreduction to remove all grossly visible tumours, and at the same time provide opportunities for clinicians to accurately establish the diagnosis

and extent of the disease (Coleman et al, 2013; du Bois et al, 2009). Although such surgical procedure is rarely practiced in other malignancies, the removal of tumours in ovarian cancer patients to less than 1 cm residual disease has consistently been associated with better overall survival (Eisenkop et al, 1998; Hoskins et al, 1994).

Given the high chemosensitivity of EOC, chemotherapy was often administered to patients following surgery, so as to eradicate residual disease. In the past, commonly used drugs included cyclophosphamide, melphalan and chlorambucil (Vella et al, 2011). When cisplatin was introduced to clinical practice in 1978, platinum-based therapy was shown to generate a higher number of responsive patients, increase response duration and progression-free interval (Vella et al, 2011). Since then, platinum derivatives, such as cisplatin and carboplatin, become the standard of care for ovarian cancer patients.

In the late 1990s, two randomised phase III trials led to the combination of cisplatin with paclitaxel as adjuvant treatment of advanced stage ovarian cancer (McGuire et al, 1996; Piccart et al, 2000). Compared with cisplatin and cyclophosphamide combination, patients treated with cisplatin and paclitaxel were shown in both studies to have significantly higher overall clinical response rate and complete clinical remission rate, and also experienced significantly longer progression-free survival and overall survival (McGuire et al, 1996; Piccart et al, 2000). Therefore, the combination of platinum and paclitaxel is presently the treatment of choice as first-line therapy for all ovarian cancer patients.

Briefly, paclitaxel is a taxane that binds to the taxoid-binding site of β-tubulin, resulting in the enhancement of microtubule polymerization (Schiff et al, 1979). Such microtubule stabilising activity suppresses microtubule dynamics, and thus, arrest cell proliferation. Apart from taxanes, other microtubule-targeted agents, such as vinca alkaloids are also currently administered in a broad range of solid tumours and haematological malignancies, while extensive research are dedicated to examine the clinical relevance of other agents (Dimitroulis & Stathopoulos, 2005; Dumontet & Jordan, 2010).

Although the administration of platinum-taxane based therapy has been standardised (intravenously once every 3 weeks for 6 to 9 cycles), there are still doubts over its optimal dose and schedule. A recent study in Japan suggested that dose-intensification schedule of weekly paclitaxel administration at lower doses together with standard doses and schedules of carboplatin prolonged progression-free survival and overall survival compared to the conventional regimen (Katsumata et al, 2009). In addition, peritoneal delivery of chemotherapy has been shown to increase overall survival compared to intravenous therapy (Armstrong et al, 2006). Since most of the tumours are confined within the peritoneal cavity, this route of administration will be able to achieve high local concentration of the drugs, but is also highly toxic to the patients (Gore et al, 2006). Both of these approaches are still under evaluation and may well have a role in future management of ovarian cancer patients (Coleman et al, 2013).

At the present time, 60 to 80% of patients with advanced EOC will respond to the combination of platinum- and taxane-based chemotherapy and achieve complete clinical remission (Kigawa, 2013), while approximately 20% to 30% of the advanced-stage patients present with platinum-refractory disease (intrinsic platinum resistance) and continue to have progressive disease even during treatment (Cannistra, 2004). Despite the high chemosensitivity of the disease to first-line therapy, maintenance of disease-free status has proven to be elusive, with over two-thirds of the patients experiencing recurrent disease (Herzog & Pothuri, 2006). Depending on the time interval from completion of first-line platinum-based chemotherapy until recurrence, patients usually receive non-platinum single agent regimen (relapsed disease within 6 months after treatment) or platinum-based chemotherapy (relapsed disease more than 6 months after treatment) (Coleman et al, 2013). However, due to the development of drug resistance, the response rates and time to progression typically fall with each relapse (Vaughan et al, 2011).

Collectively, intrinsic and acquired platinum resistance are among the major reasons of treatment failures, resulting in the low 5-year relative survival of 27.3% for advanced stage disease (Howlader et al, 2013). Additionally, current therapeutic regimens fail to take into account the high degree of heterogeneity in EOC (Vaughan et al, 2011). Hence, identification of new therapeutic approaches is necessary to improve the survival outcome of patients with advanced EOC.

1.1.9 Strategies to improve therapeutic for epithelial ovarian carcinoma

Ovarian cancer research lags behind more advanced stages of investigations in other cancer types, leading to delayed introduction of new targeted therapeutics into clinical practice. In fact, the drugs used in the clinic today for EOC are similar to those used in the late-70s, albeit with reduced side effects (Vaughan et al, 2011). With the possible exception of angiogenesis inhibitors, such as bevacizumab, attempts to improve patient survival by including other drugs have not been encouraging (Bookman et al, 2009). The recently concluded phase 3 randomised trial conducted by International Collaboration on Ovarian Neoplasms (ICON7) indeed showed that bevacizumab treatment improved progression-free survival, particularly in patients at high risk of disease progression (Perren et al, 2011), but at the same time, it is also associated with a small but clinically significant decrement in quality-of-life (Canevari et al, 2013; Stark et al, 2013). Hence, much effort is still needed to develop therapeutic regimens with better therapeutic index and smaller negative impact on patients' quality-of-life.

Rather than the current scheme of grouping patients together, one potential approach could be the stratification of patients to molecularly targeted therapies with the highest likelihood of benefit. Such therapies have been successfully incorporated into standard treatment for other malignancies, such as chronic myelogenous leukaemia, ER- or Her2-positive breast cancer, and EGFR-mutated lung cancer (Quintas-Cardama et al, 2009; Rosell et al, 2010; Yaziji et al, 2004). A key point of these successes is the development of

precision medicine – the use of the right treatment for the right patient at the right time. Despite the high degree of heterogeneity in EOC, all women diagnosed with EOC are given the same regimen, with no prognostic classifications currently powerful enough to identify patients who are most likely to benefit from any particular regimen (Vaughan et al, 2011). As a result, therapeutic regimens are less than perfectly adapted to each patient (Sabatier et al, 2009). Therefore, there is an urgent need to define molecularly homogeneous subsets that respond similarly to treatment, followed by the development / identification of compounds that can inhibit the biological drivers of each individual subset.

Another approach to improve patient survival would be to circumvent resistance of recurrent EOC disease to standard chemotherapy. Many women respond well to the initial platinum-based treatment, but often relapse with platinum-resistant disease (Vaughan et al, 2011). Despite extensive research dedicated to this area, the precise mechanisms of platinum resistance remain elusive and are likely to be multi-factorial (Coleman et al, 2013). Thus, in order to achieve more durable response to therapy, genome-wide knockdown and expression approaches could be used as a strategy to identify promising candidates for which inhibition would revert the resistance to platinum-based therapy. In fact, application of such approaches has led to the successful identification of CDK12 as a synthetic lethal partner of the PARP1/2 inhibitor, olaparib (Bajrami et al, 2013).

Therefore, this thesis is divided into two parts; addressing the two aforementioned approaches that will hopefully lead to better therapeutic regimens for EOC.

1.2 Dissecting heterogeneity in epithelial ovarian carcinoma

1.2.1 Basis for dissecting cancer heterogeneity

In the multistep process of tumorigenesis, normal cells acquire a series of random abnormalities that ultimately lead to the development of most of the hallmarks of cancer – enhanced proliferation, reduced apoptosis, resistance to anoikis, angiogenesis, increased invasion and metastasis, etc (Hanahan & Weinberg, 2011). As a result, the spectrum of somatic genomic and epigenomic aberrations can vary substantially among individual tumours that appear clinically similar (Garay & Gray, 2012). However, certain driver aberrations can occur frequently enough, such that they can define molecularly homogeneous subsets that respond similarly to treatment (Alizadeh et al, 2000; Collisson et al, 2011; Sorlie et al, 2001). Hence, the utility of such classification scheme to identify patients' subgroups and direct them to appropriate targeted therapies can have substantial therapeutic benefit (Druker et al, 2001; Slamon et al, 2001).

With the help of high throughput technologies, homogeneous subgroups can be defined based on transcriptional profiles, genomic aberrations, promoter methylation patterns and protein expression. mRNA expression profiling is particularly well established and has been instrumental in characterising the complex biological diversity of human cancers (Alizadeh

et al, 2000; Perou et al, 2000; Verhaak et al, 2010). Subtypes identified through expression microarray analyses are coupled with multiple clinical parameters, such as patient prognosis, age of onset and molecular marker expression (Perou et al, 2000; Verhaak et al, 2010). Already, predictors of prognosis, as well as the ability to identify patient subgroups that are most likely to benefit from particular therapies have been developed for other cancers and are being tested in prospective randomised clinical trials. For example, the basal expression subtype of breast cancer, which has an unfavourable prognosis, and does not benefit from anti-oestrogenics or Herceptin is currently being investigated in relation to response to simvastatin (http://www.clinicaltrials.gov/ct/ show/NCT00807950). Here, I describe some major studies that have attempted to define molecularly homogenous subgroups in EOC.

1.2.2 Published studies on molecular classification of epithelial ovarian carcinoma

Efforts to dissect EOC heterogeneity have correlated expression patterns with clinical features, such as histological types, aggressiveness and patient outcomes (Denkert et al, 2009; Helland et al, 2011; Mok et al, 2009; The Cancer Genome Atlas Research Network, 2011; Tothill et al, 2008). Of particular note, The Cancer Genome Atlas (TCGA) and the Australian Ovarian Cancer Study (AOCS) have in recent years demonstrated the existence of molecular subtypes in EOC defined by transcriptional patterns (The Cancer Genome Atlas Research Network, 2011; Tothill et al, 2008).

Making use of expression microarray data from 285 serous and endometrioid invasive tumours of the ovary, peritoneum, and fallopian tube, AOCS identified six molecular subtypes - C1, C2, C3, C4, C5 and C6, which are associated with molecular and histopathological characteristics, and patient survival (Tothill et al, 2008). Both C1 and C5 subtypes were found to confer poorer clinical outcomes as compared with other subtypes (Tothill et al, 2008). On further investigation, they found *Let-7* pathway to be specifically altered in the poor prognosis C5 subtype, and suggested it as one of the drivers responsible for the biological and clinical behaviour of C5 subtype (Helland et al, 2011).

On the other hand, TCGA analysed promoter methylation, DNA copy number aberration, as well as expression patterns of messenger RNA and microRNA in 489 high-grade serous ovarian adenocarcinomas (The Cancer Genome Atlas Research Network, 2011). Focusing on their mRNA expression analysis, the existence of at least four expression subtypes - differentiated, immunoreactive, mesenchymal, proliferative, was reported (The Cancer Genome Atlas Research Network, 2011). The subtypes were named based on their distinct gene clusters. For instance, the immunoreactive subtype is characterised by T-cell chemokine ligands *CXCL11*, *CXCL10*, and the receptor *CXCR3*, while high expression of proliferative markers such as *MCM2* and *PCNA* defined the proliferative subtype. These subtypes were originally found to be not significantly correlated with survival duration (The Cancer Genome Atlas Research Network, 2011), but subsequent study observed association with survival duration when the TCGA classification scheme was applied onto expression profiles obtained from other published

studies (Verhaak et al, 2013).

Due to varied histotype presentation, samples sizes and analytical criteria, the reported molecular subtypes of EOC by TCGA and AOCS are similar but not completely the same (The Cancer Genome Atlas Research Network, 2011; Tothill et al, 2008). Thus, a refined classification scheme with intense phenotypic characterisation remains to be established. Also, the molecular targets relevant to cancer cell growth in these transcriptional subtypes have not been identified.

1.2.3 Proposed molecular classification of epithelial ovarian carcinoma

Previously, our group also proposed a classification scheme to address the high degree of heterogeneity in EOC. This scheme was published together with the results in Chapter 3 and 4 in EMBO Molecular Medicine (Tan et al, 2013).

For our proposed molecular classification, we used a large collection of ovarian tumour gene expression data (n = 1,538; serous: 1,335, mucinous: 27, clear cell: 25, endometrioid: 96, and others: 55 samples) derived from 16 independent studies (Anglesio et al, 2008; Bild et al, 2006; Bowen et al, 2009; Denkert et al, 2009; Hendrix et al, 2006; Hogdall et al, 2003; Hsu et al, 2007; Iorio et al, 2010; Jochumsen et al, 2009; Jochumsen et al, 2007; Mok et al, 2009; Pejovic et al, 2009; The Cancer Genome Atlas Research Network, 2011; Tone et al, 2008; Tothill et al, 2008; Tung et al, 2009). The strong batch-effect among the independent datasets was removed by ComBat, through the elimination of technical differences across data collection sites, while

conserving meaningful variations (Fig. 1.1) (Chen et al, 2011; Johnson et al, 2007). A preliminary statistical power analysis showed that 1,500 or more samples were required to achieve sufficient statistical power (≥ 0.8) in capturing the complexity and dynamicity of EOC (Fig. 1.2) (Fox & Mathers, 1997). Importantly, known prognostic factors were correlated with patient overall survival by univariate and multivariate Cox proportional hazards analyses (Table 1.1).

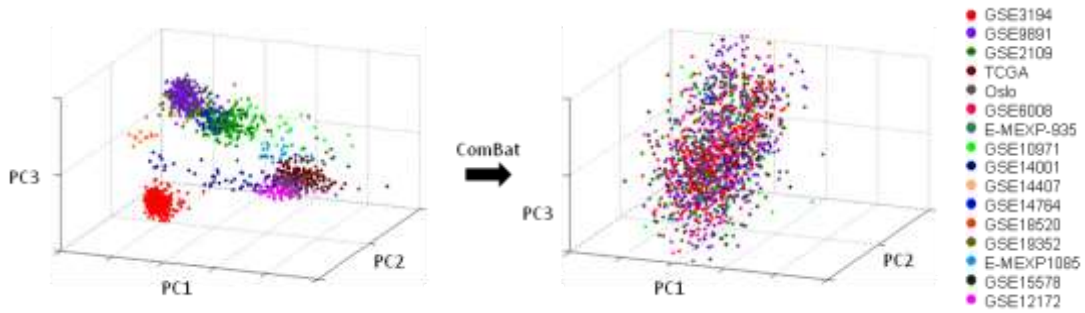

Figure 1.1 Removal of batch effect from combined expression microarray data for epithelial ovarian carcinoma.
Effect of ComBat standardisation in the principle component analysis (PCA) of 16 independent cohorts. Left panel. Prior to ComBat standardisation, the combined ovarian cancer gene expression data showed technical variations. Right panel. After ComBat standardisation of the same data, the technical variations were eliminated. Tan et al (2013).

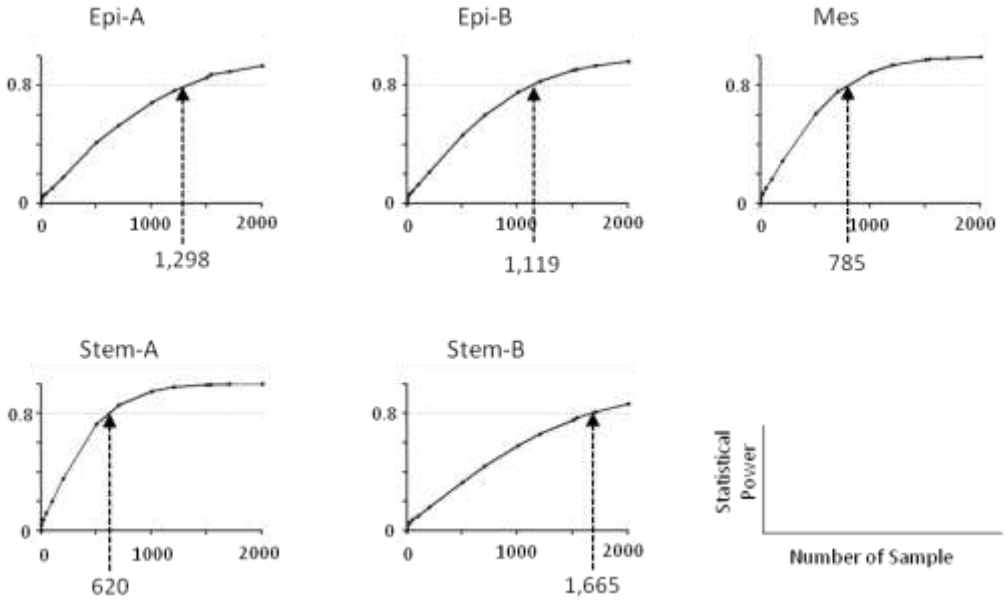

Figure 1.2 Statistical power plots for each molecular subtype.
Statistical power plots to distinguish one subtype from the others. Arrows indicate the number of samples required to attain a statistical power of 0.8 for distinguishing amongst molecular subtypes. *x*-axis is the number of samples; *y*-axis is statistical power. Tan et al (2013).

Table 1.1. Univariate and multivariate Cox proportional hazards regression analysis for multiple known clinical variables and proposed tumour subtypes.

Clinical Variables	Sample size (Total *n* = 539)	Univariate (HR, 95% CI)	*p*-value	Multivariate (HR, 95% CI)	*p*-value
Age (yr)					
< 55	175 (32.47%)	1		1	
≥ 55	364 (67.53%)	1.403 (1.071 - 1.839)	0.0141	1.285 (0.9781-1.687) *	0. 07173 *
Stage					
I or II	47 (8.72%)	1		1	
III or IV	492 (91.28%)	3.907 (1.843-8.285)	0.00038	3.429 (1.591-7.389) *	0.00165 *
Grade					
1	17 (3.15%)	1		1	
≥ 2	522 (96.85%)	2.58 (0.9578-6.949)	0.0608	1.365 (0.494-3.763) *	0.54799 *
Metastasis					
Primary	500 (92.76%)	1		1	
Metastasis	39 (7.24%)	1.349 (0.8323-2.185)	0.224	1.391 (0.854-2.27) *	0.1853 *
Subtype					
Non-Epi-A	483 (89.61%)	1		1	
Epi-A	56 (10.39%)	0.7103 (0.4498-1.122)	0.142	0.9449 (0.583-1.53) **	0.8176 **
Non-Epi-B	384 (71.24%)	1		1	
Epi-B	155 (28.76%)	0.69 (0.5206-0.9144)	0.0098	0.7347 (0.553-0.976) **	0.033 **
Non-Mes	361 (66.98%)	1		1	
Mes	178 (33.02%)	1.171 (0.907-1.513)	0.225	1.01 (0.777-1.324) **	0.9164 **
Non-Stem-A	411 (76.25%)	1		1	
Stem-A	128 (23.75%)	1.417 (1.075-1.868)	0.0135	1.382 (1.045-1.83) *	0.0234 *
Non-Stem-B	517 (95.92%)	1		1	
Stem-B	22 (4.08%)	1.204 (0.6383-2.271)	0.567	1.14 (0.603-2.149) **	0.6886 **

* Multivariate Cox regression analysis of clinical variables with Stem-A subtype.
** For multivariate Cox regression, each subtype was independently analysed with the other clinical variables (age, stage, grade, and metastasis) from the remaining subtypes.
p-values below 0.05 are shown in red.
Tan et al (2013).

To identify EOC molecular subtypes, consensus clustering was applied to the collection and five clusters – Epithelial-A (Epi-A), Epithelial-B (Epi-B), Mesenchymal (Mes), Stem-like-A (Stem-A) and Stem-like-B (Stem-B), that were characterised by markers of differentiation or cell-type status and stromal components were detected (Fig. 1.3A) (Tan et al, 2013). For instance, Epi-A and Epi-B tumour clusters are characterised by epithelial cell markers, such as *CDH1*, *EPCAM*, *CD24* and various keratin genes. The Mes tumour subtype predominantly expressed fibroblastic/mesenchymal genes, such as *PDGFRA*, *VCAM1*, *ZEB1*, *TWIST1*, and extracellular matrix genes, including collagen and *FN1*. The Stem-A and Stem-B tumour clusters did not share many gene markers, but expressed typical markers for epithelial stem cells: *LGR5* and *PROM1* respectively (Fodde, 2009). Stem-A tumours also expressed more *MYCN*, *NCAM*, *CDH2* and proliferation-related genes, suggesting neural characteristics. Epi-B and Mes tumours expressed inflammatory genes, such as multiple interferon down-stream genes, MHC class II genes and immunoglobulin genes. The silhouette plot (Rousseeuw, 1987) and SigClust (Liu et al, 2008) analysis confirmed tumour similarity within each subtype, indicating the robustness of the proposed classification (Fig. 1.3B).

On comparison of our proposed subgrouping scheme with that of AOCS (Tothill et al, 2008), an overall concordance of 82.9% for all of the subtypes was found (Fig. 1.4A), implying that the proposed large-scale analysis confirmed the previous study. The proposed molecular subtypes were also noted to be akin to that of TCGA (Fig. 1.4A) (The Cancer Genome Atlas Research Network, 2011). However, the subtyping schemes from these published studies did not show a one-to-one match with our proposed

classification (Fig. 1.4A; see the mutual relationships among Epi-A or Epi-B; C2, C3 or C4; Immunoreactive or Differentiated). In addition, the Stem-B/C6 subtype, which comprised most of the non-serous tumours, was identified from the analyses of multi-histotype ovarian cancers by both AOCS (Tothill et al, 2008) and us but not by TCGA in their analysis of only high-grade serous ovarian adenocarcinomas (Fig. 1.4A) (The Cancer Genome Atlas Research Network, 2011). The overwhelming number of serous tumours in the collection (n = 1,274) might have caused the classification of most of the biologically distinct non-serous histotypes into the same molecular subtype (Stem-B) (Fig. 1.4B). Intriguingly, some of the serous tumours were also classified into the Stem-B subtype (Fig. 1.4B), implying the presence of a unique less serous subgroup within serous carcinoma. This notion was supported by the fact that serous samples of Stem-B subtype have significantly lower expression level of *WT1* gene, a marker for serous adenocarcinoma of the ovary (Lawrenson & Gayther, 2009; Tan et al, 2013). Overall, our proposed EOC classification is predominantly a combination of discrimination by histotype and the molecular subtypes defined by AOCS (Tothill et al, 2008) and TCGA (The Cancer Genome Atlas Research Network, 2011), but also reveal novel biological features. For consistency, the proposed molecular classification will be widely used in this thesis.

1.2.4 Clinical relevance of proposed epithelial ovarian carcinoma subtypes

The proposed subtypes have also been correlated with various clinicopathological parameters so as to ascertain their clinical relevance. Indeed, significant correlation was found between the proposed subtype and patient outcome, with Epi-A, Epi-B and Stem-B subtypes showing better prognosis in the Kaplan-Meier analysis, while Mes and Stem-A tumours were linked with poorer outcomes (Fig. 1.5A). Even when only high-grade serous carcinomas are analysed, the proposed subtypes also showed similar significant distinctions in survival in Kaplan-Meier curves (Fig. 1.5B). On closer examination, the poor prognosis Stem-A tumours can also be found at stages 1 and 2 having poorer outcomes than those of other subtypes (Fig. 1.6A), and were also found to be enriched in older patients (Fig. 1.6B). On the other hand, the other poor prognosis subtype – Mes, included more advanced staged and metastasised tumours (Fig. 1.6C). In the univariate and multivariate Cox regression analyses, both Stem-A and Epi-B subtypes are identified as prognostic factors that are independent of multiple clinical parameters and status (Table 1.1).

Pathway analysis also revealed clear distinctions in the enrichment of the gene expression signatures for various pathways (Fig. 1.7). Through the application of single sample gene set enrichment analysis (ss-GSEA) on 1,538 samples using 6,898 gene sets, 207 gene sets were found to be subtype-specific (Subramanian et al, 2005). For instance, Mes tumours correlated with *Metastases* and *TGFβ-related* pathways, consistent with their link with epithelial-mesenchymal transition (EMT) and metastasis (Fig. 1.7) (Maruyama

et al, 2000; Yin et al, 1999). In comparison, *chromatin remodelling* gene sets were highly enriched in the Stem-A subtype (Fig. 1.7). Overall, the proposed expression-based subtyping scheme is able to dissect EOC heterogeneity into subgroups with similar biological properties and clinical relevance.

1.2.5 Predictive model for proposed molecular subtype classification

A predictive framework based on a Binary Regression (BinReg) model was also developed as a potential diagnostic tool for quantitative gene expression-based subgroup assignment (Tan et al, 2013). The predictive capability of the model was demonstrated to be comparable with those reported in previous studies for multiple breast cancer cohorts (Calza et al, 2006; Haibe-Kains et al, 2012). In addition, extensive validation exercises were carried out, affirming the accuracy and robustness of the model (Tan et al, 2013). However, details of the model and the validations performed are beyond the scope of this thesis, and will not be discussed further.

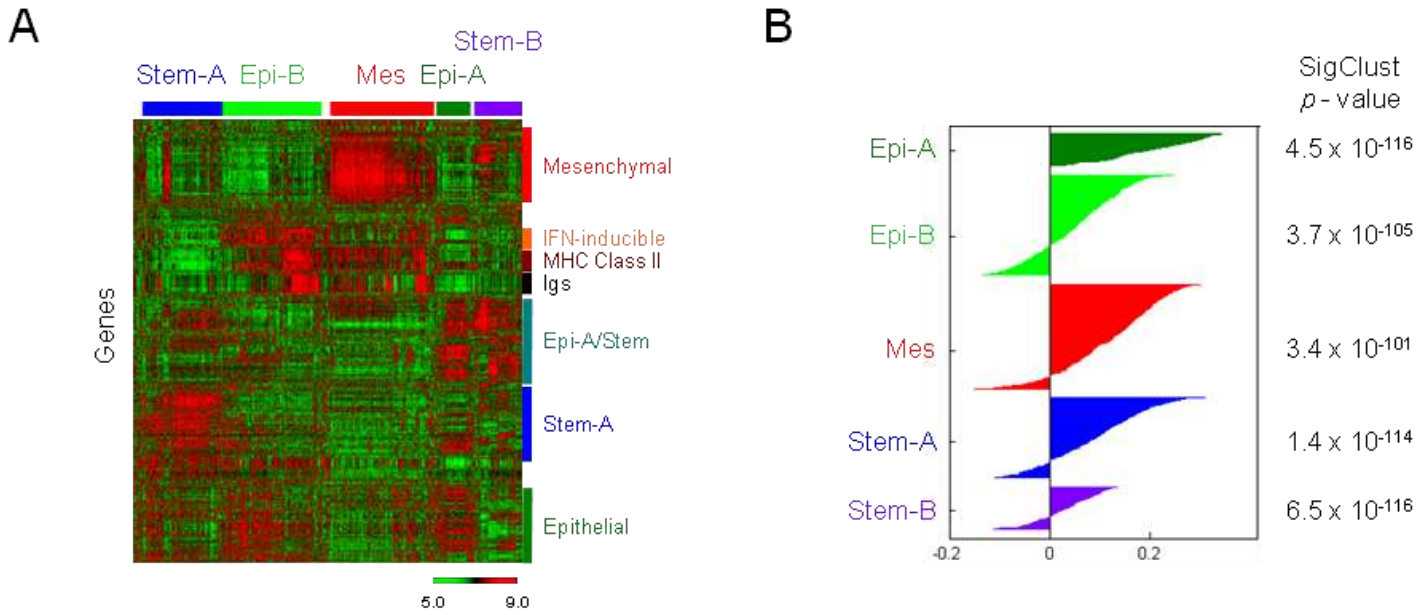

Figure 1.3 Proposed molecular classification of epithelial ovarian carcinoma.
A. Gene expression heatmap for the five tumour clusters (red = high; green = low expression). Consensus clustering of 1,538 samples identified five subtypes, designated by the associated gene components. Note the similarities between Epi-A/Stem-B subtype tumours, between Epi-A/Epi-B subtypes for epithelial genes, and the expression pattern of Epi-A/Stem genes. B. Silhouette plot. Note the large proportion of clinical samples with positive silhouette width (SW) values, suggestive of tumour similarity within each subtype. SigClust (Liu et al, 2008) *p*-values indicative of significance of clustering are shown to the right of the silhouette plot. Tan et al (2013).

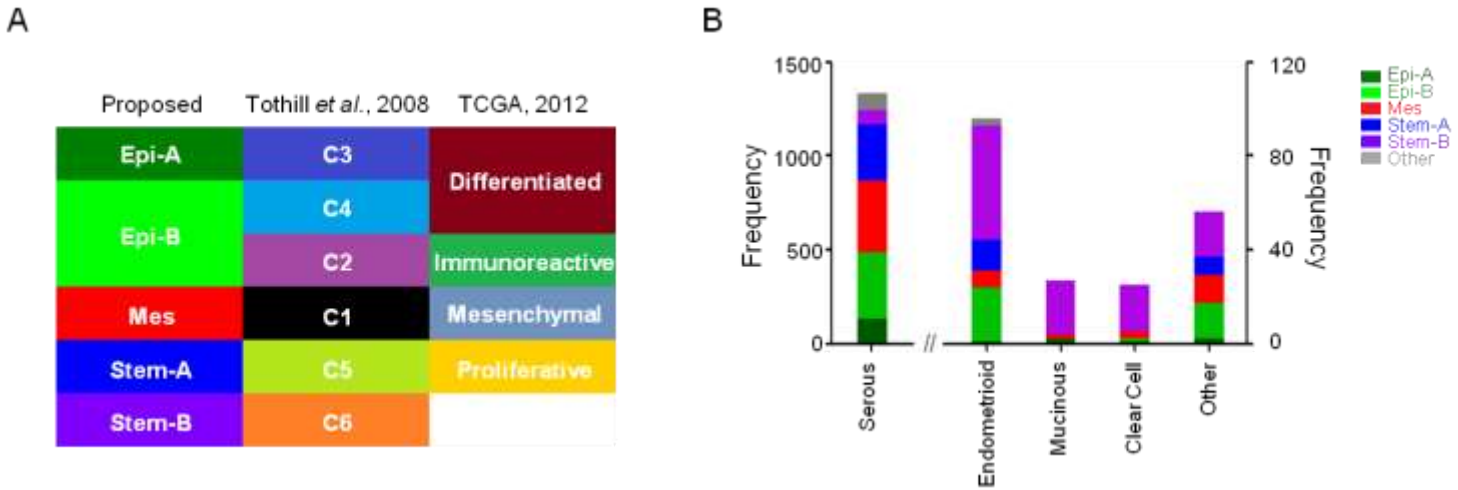

Figure 1.4 Comparison of proposed classification with published schemes and the distribution of proposed subtypes in each histotype.

A. Comparison of the proposed molecular subtype with previously published subtyping schemes for EOC by AOCS (Tothill et al, 2008) and TCGA (The Cancer Genome Atlas Research Network, 2011). Note that Epi-B subtype carries an immunoreactive and a differentiated component, and also that TCGA molecular subtyping lacks Stem-B/C6 population. B. Subtype distribution by histologies. Note the large proportion of clinical samples classified as Stem-B in non-serous histotypes (Endometrioid, Mucinous and Clear Cell), as compared to that of serous histotype. Tan et al (2013).

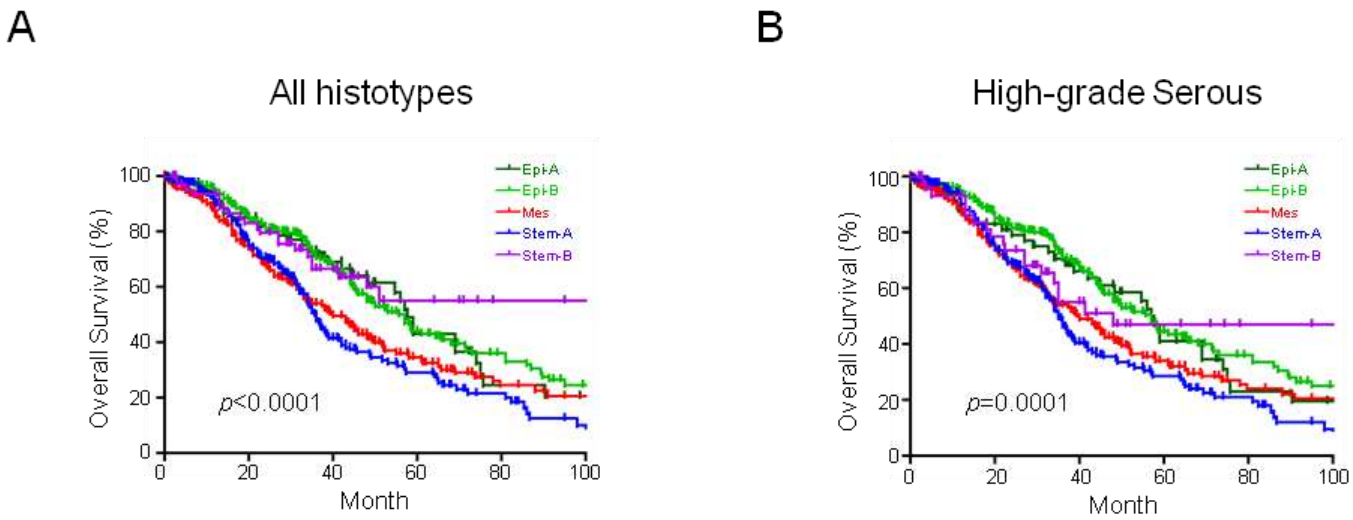

Figure 1.5 Correlation of proposed subtypes with overall survival.
A. Kaplan-Meier survival analysis for each subtype. Among data for 1,538 patient samples, survival information for 978 samples was available (Epi-A: 80, Epi-B: 264, Mes: 284, Stem-A: 220, Stem-B: 61 and others: 69 samples) and used for the Kaplan-Meier analysis. B. Prognostic feature of subtypes in high-grade serous ovarian EOC only. A total of 863 samples in this category were analysed (Epi-A; 63, Epi-B; 258, Mes; 280, Stem-A; 217, and Stem-B; 45 samples). Note that the proposed molecular classification further dissects heterogeneity of high-grade serous EOCs in patient prognosis. Tan et al (2013).

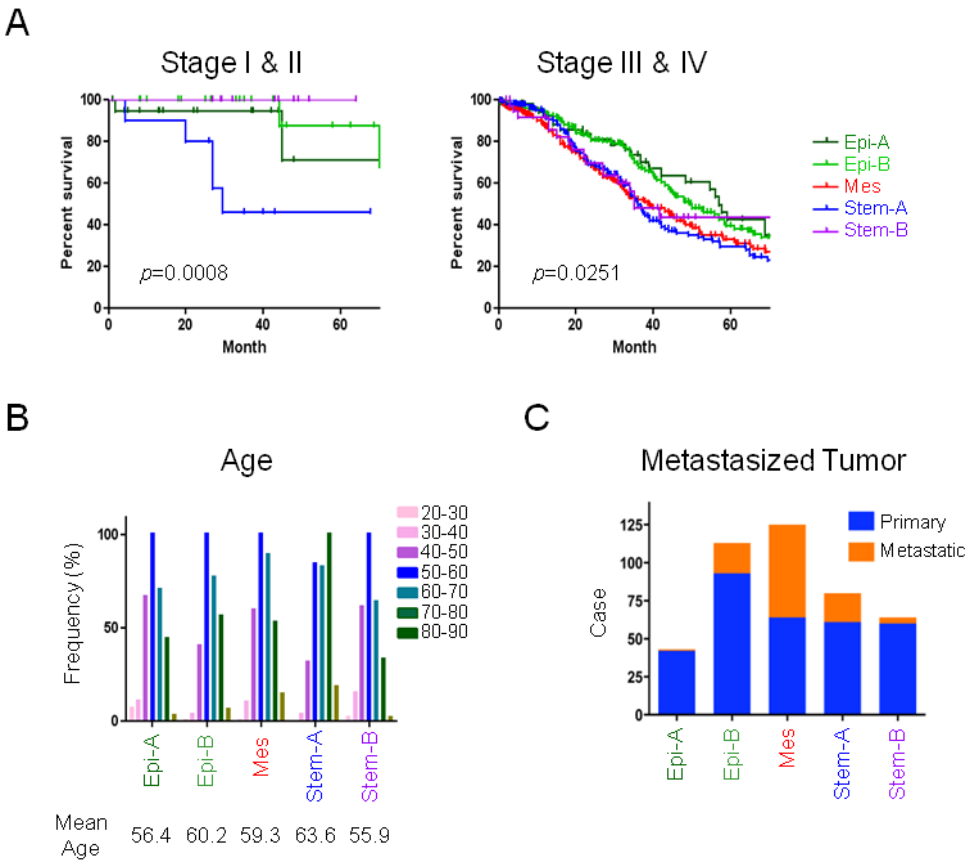

Figure 1.6 Clinicopathological characterisation of proposed molecular subtypes.

A. Kaplan-Meier survival analyses stratified by clinical stage. Note that patients with stage I or II Stem-A ovarian carcinomas have worse outcome, with statistical significance. Epi-A and Epi-B subtypes show better prognoses overall, but Stem-B cancers are no longer benign at advanced stages. B and C. Histograms showing the relationship between expression subtypes with age distribution (B, where the mean age in years is shown underneath) and primary or metastasised tumours (C). Definition of metastasised tumour follows the original description in the literature (Anglesio et al, 2008; Bowen et al, 2009; Tone et al, 2008; Tothill et al, 2008). Tan et al (2013).

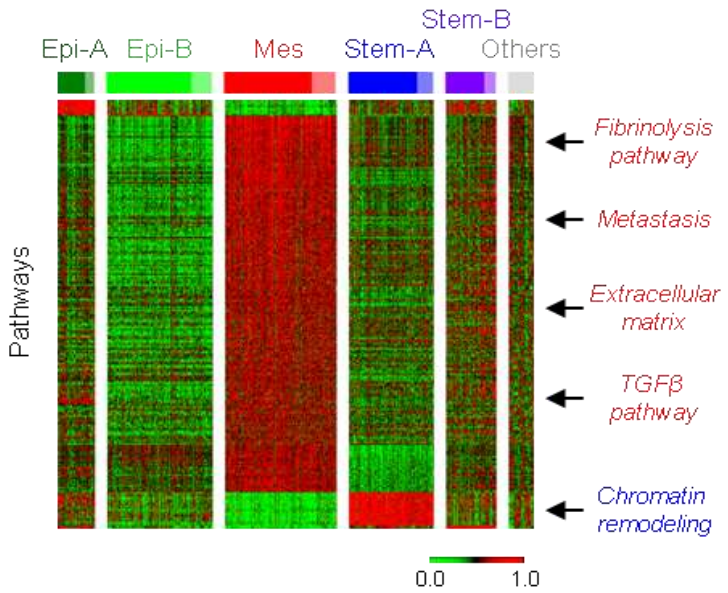

Figure 1.7 Subtype-specific pathway enrichment.
Heatmap shows subtype-specific single sample gene set enrichment analysis (ss-GSEA) scores (false discovery rate (FDR) in significance analysis of microarrays (SAM) q = 0%, receiver operation curve (ROC) >0.85) for 1,538 ovarian cancer samples. Red = high; green = low enrichment scores. Gene sets are aligned in descending value of ROC. Samples are aligned by subtype classification and silhouette width (SW) (Fig. 1.3B). Deep colour = positive SW (core samples); pale colour = samples classified, but negative SW. "Others" indicates the unclassified samples not grouped in any of the five subtypes in the initial CC analysis in Fig. 1.3A. Arrows indicate positions of selected pathways. Tan et al (2013).

1.2.6 Representative cell lines as model for the proposed molecular subtypes

The availability of the proposed classification scheme to dissect the complexity of EOC pave the way for further work into the identification of relevant molecular targets, that will lead to the development of precision medicine for EOC. However, a major challenge is to identify cell lines that reflect the relevant underlying tumour biology (Chin et al, 2011). Expression studies of cultured breast cancer cell lines have shown that *in vitro* cells retain subtype characteristics corresponding to those of their *in vivo* counterparts, indicating that matching breast cancer cell lines by expression data could represent *in vivo* tumours (Gatza et al, 2010; Neve et al, 2006; Perou et al, 2000). Hence, cell lines corresponding to each proposed EOC subtype could be used for *in vitro* modelling.

By performing two rounds of consensus clustering on the expression microarray data of 142 cultured EOC cell lines, we identified representative cell lines for each proposed subtypes (Fig. 1.8A) (Tan et al, 2013). The robustness of the classification was unambiguously supported by similarity matrices, as well as the positive silhouette width values (Rousseeuw, 1987) with significant *p*-value by SigClust (Fig. 1.8A) (Liu et al, 2008). Furthermore, a high correlation between clinical tumour subtype and cell line subtype was demonstrated in the Spearman correlation map analysis (Fig. 1.8B; average spearman *rho* = 0.80), demonstrating a high level of similarity between EOC cell lines and tumour transcriptomic expression patterns.

Similar to clinical samples, pathway analysis on the cell lines data also revealed clear distinctions in the enrichment of the gene expression signatures for various pathways (Fig. 1.9). As expected, Epi-A cell lines were characterised by cell adhesion-related gene sets, reflecting enrichment of epithelial cell markers. Notably, 33 cell line subtype-specific gene sets were shared with tumours, indicating similarity between cell lines and tumours in the pattern of pathway enrichment. Overlapped gene sets include the enrichment of *fibrinolysis pathway* and *chromatin modification* in the Mes and Stem-A subtypes, respectively (Fig. 1.9). Additionally, the proposed molecular subtypes were shown to have significant correlation with *in vitro* phenotypes, such as population doubling time and anchorage-independent cell growth potential (Fig. 1.10). Representative cell lines of the better prognosis Epi-A and Epi-B subtypes have longer population doubling times and decreased colony-forming ability, which may reflect the less-aggressive behaviour of clinical tumours (Fig. 1.10).

Intriguingly, we also identified representative cell lines for the C1/Mes subtype, which is known to be driven by stromal elements (Tan et al, 2013; Tothill et al, 2008). Though stromal elements are not part of any cell line model, stromal-related gene sets were found to be specifically enriched in our Mes tumours (Fig. 1.7), as well as in Mes representative cell lines (Fig. 1.9) (Tan et al, 2013). In addition, Mes tumours are not only characterised by stromal gene expression signature, but also predominantly expressed fibroblastic/mesenchymal genes, such as *VCAM1*, *ZEB1*, *TWIST1*, and extracellular matrix genes, including collagen and *FN1* (Fig. 1.3A) (Tan et al, 2013). Expression of these genes are also enhanced in Mes representative cell

lines (Fig. 1.8A) (Tan et al, 2013). Therefore, even though subtype-representative cell lines are admittedly not the perfect *in vitro* models for clinical tumour subtypes, these cell lines are thus far, the most representative models readily available for molecular subtype study.

At the same time, it should be noted that a recent study identified several commonly used ovarian cancer cell lines as poor models of high-grade serous ovarian cancer, and consequently, forced a significant re-evaluation of many of the cell lines used in ovarian cancer research (Domcke et al, 2013). Unfortunately, these important findings were only published in 2013, and thus, were impossible to be factored into this thesis.

With the availability of a classification scheme to dissect the heterogeneity in EOC, as well as representative cell line models, the first part of this thesis strives to identify functionally relevant targets for the proposed subtypes, which hopefully will lay the foundation for developing therapeutics that could be matched with the characteristics of individual patients.

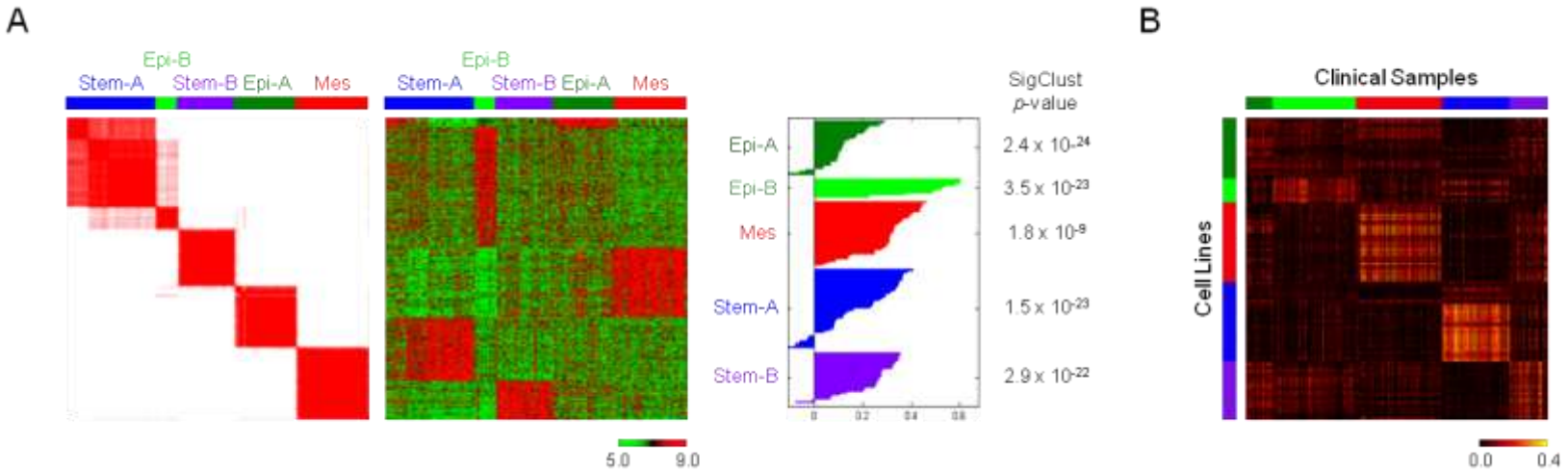

Figure 1.8 Identification of representative cell lines for proposed molecular subtype.
A. EOC cell line classification. Left panel. Consensus clustering matrix of 142 EOC cell lines. Red = high; white = low similarity. Middle panel. Gene expression heatmap of EOC cell lines. Red = high; green = low expression. Right panel. Silhouette analysis for each proposed subtype. Column to the right of silhouette plot is the SigClust (Liu et al, 2008) *p*-value indicative of cluster significance for each subtype. B. Heatmap of Spearman correlation *Rho* of gene expression between clinical tumour subtype (n = 1,538) and EOC cell line subtype (n = 142). Yellow indicates a perfect correlation (*Rho* = 1) whereas black indicates no correlation (*Rho* = 0). Tan et al (2013).

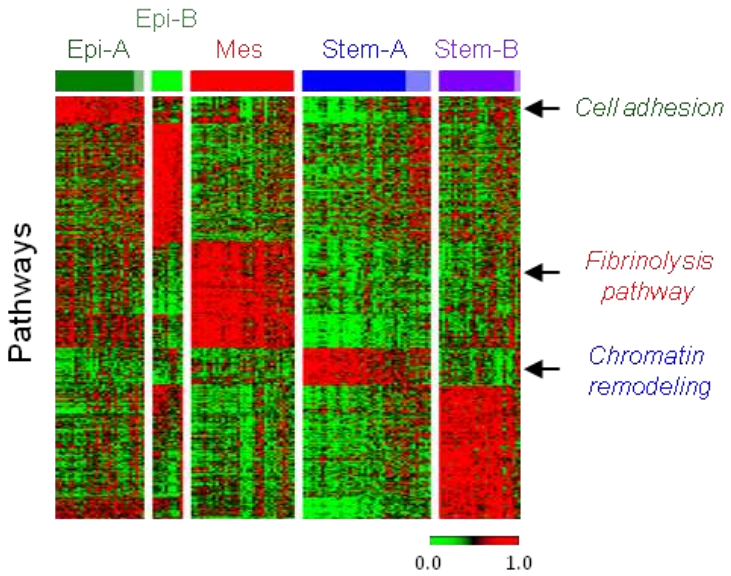

Figure 1.9 Cell line subtype-specific pathway enrichment.
Heatmap shows subtype-specific single sample gene set enrichment analysis (ss-GSEA) scores (false discovery rate (FDR) in significance analysis of microarrays (SAM) q = 0%, receiver operation curve (ROC) >0.85) for 142 cultured EOC cell lines. Red = high; green = low enrichment scores. Gene sets are aligned in descending value of ROC. Samples are aligned by subtype classification and silhouette width (SW) (Fig. 1.8A). Deep colour = positive SW (core samples); pale colour = samples classified, but negative SW. Arrows indicate positions of selected pathways. Tan et al (2013).

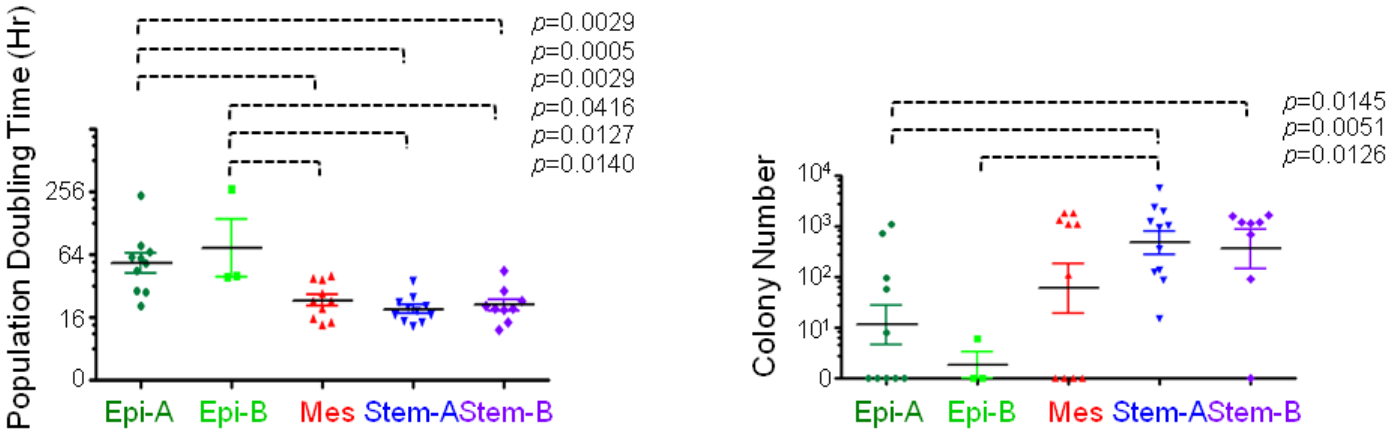

Figure 1.10 Characterisation of *in vitro* phenotypes of representative cell lines.
Dot plots show the population doubling time of representative cell lines as measured by the MTS assay (Left panel) (Matsumura et al, 2011) and the anchorage-independent cell growth ability for each representative cell line as measured by the methylcellulose assay (Right panel) (Mori et al, 2009). Log_{10}-transformed colony number is shown. *p*-values were computed by Mann-Whitney *U*-test. Tan et al (2013).

1.3 Platinum resistance in epithelial ovarian carcinoma

1.3.1 Overview of the platinum-based chemotherapy

The first member of a class of platinum-containing anti-cancer drugs, *cis*-diamminedichloroplatinum(II), best known as cisplatin or CDDP, was first described by Michele Peyrone in 1845. For a long time, it was known as Peyrone's salt until its cytotoxic and antiproliferative property was discovered serendipitously in 1965, by Barnett Rosenberg. At that time, Barnett Rosenberg was investigating the involvement of electric field in cell division when he noticed that bacterial cell growth was inhibited by a soluble platinum complex (cisplatin) discharged during electrolysis from the platinum electrodes. Subsequently, it was found to be effective at regressing tumours in rats (Rosenberg et al, 1969), leading to the approval by the FDA in 1978 for the treatment of testicular and bladder cancer. In testicular cancer, cisplatin is particularly effective, with an overall cure rate of more than 95% (Kartalou & Essigmann, 2001). Presently, cisplatin is employed against a wide range of solid malignancies, including ovarian, colorectal, lung, and head and neck cancers.

However, the treatment is limited by its high toxicity and effects on kidneys (nephrotoxicity), peripheral nerves (neurotoxicity) and the inner ear (ototoxicity) (Kelland, 2007). Much effort has been made in designing new platinum drugs that could lessen or remove the severe side effects of cisplatin, while retaining its anticancer properties. A major breakthrough in this regard was achieved in the mid-1980s, with the introduction of carboplatin (Harrap, 1985). In contrast to cisplatin, carboplatin does not displays nephrotoxicity and neurotoxicity, but instead frequently leads to reversible thrombocytopenia

(Kelland, 2007). The active form of carboplatin is identical to that of cisplatin, except that carboplatin requires higher concentration to exert similar effects and has slower rate of adduct formation (Knox et al, 1986). Though the potency of carboplatin is reduced, numerous randomised clinical trials reported comparable survival rates between cisplatin and carboplatin regimens (Aabo et al, 1998). As a result, carboplatin was granted FDA approval in 1989, and is now widely accepted as one of the standards in treating ovarian cancer.

Apart from high toxicity, the clinical usefulness of cisplatin in ovarian cancer is also limited by the high incidence of acquired and intrinsic resistance of cells to the drug. As mentioned in the earlier section, the majority of the ovarian cancer patients experience initial therapeutic success with platinum-based chemotherapy, while only approximately 20% of patients have platinum-refractory disease (Cannistra, 2004). Unfortunately, a large fraction of the originally sensitive tumours eventually develops resistance against platinum-based therapies (Vaughan et al, 2011). Of note, most cisplatin resistant tumours also fail to respond to carboplatin (Galluzzi et al, 2012). Numerous attempts were thus made to develop new, improved platinum drugs to overcome chemoresistance, and so far, only oxaliplatin has been approved by the FDA for the treatment of colorectal cancer (Kelland, 2007). However, cisplatin and oxaliplatin induces disparate recognition and processing events, and exerts anticancer activity on contrasting range of tumours (Chaney et al, 2005; Rixe et al, 1996). For instance, colorectal cancer which was initially acknowledged to be insensitive to platinum drugs, was found to be responsive to oxaliplatin-based regimen (Goldberg et al, 2004; Rothenberg et al, 2003).

In recent years, the development of platinum(IV) carboxylate prodrugs have been encouraging. A prominent example is satraplatin, which is the first orally administered platinum drug under active clinical investigation (Kelland, 2007). Platinum(IV) carboxylates contain cisplatin or carboplatin conjugated with symmetric bioactive axial groups, which could potentially be any chemical moiety of choice (Wang & Lippard, 2005). In fact, platinum(IV) carboxylates with enzyme inhibitors and moieties that can potentiate cisplatin activities have been reported (Ang et al, 2005; Barnes et al, 2004). Notably, the potential of platinum(IV) carboxylates is further expanded by the recent development of a new class of asymmetric platinum(IV) carboxylates, which can contain two different functional axial groups (Chin et al, 2012). In their study, Chin et al (2012) combined both hydrophilic and lipophilic ligands onto the same cisplatin template, leading to novel platinum(IV) carboxylates with better aqueous solubility and are also equally efficacious against *in vitro* cancer cells as cisplatin. Though platinum(IV) carboxylates offer unlimited number of exciting possibilities, none have yet been shown to provide significant advantage over cisplatin and carboplatin (Galluzzi et al, 2012).

Overall, the main limitation to the effectiveness of cisplatin in the battle against solid neoplasms is the high incidence of chemoresistance. Accordingly, circumventing platinum resistance remains one of the main research goals in the ovarian cancer field.

1.3.2 Mode of action of cisplatin

It has been suggested prominently in the past that cisplatin exerts its anticancer effects via the formation of platinum-DNA adducts, which in turn, leads to the inhibition of DNA replication, cell cycle arrest and/or apoptosis (Kartalou & Essigmann, 2001; Michalke, 2010). In concordance with this hypothesis, platinum adduct levels in blood cells of cancer patients was found to be directly correlated with clinical response (Reed et al, 1986).

For cisplatin to avidly bind to DNA, it has to be intracellularly activated by a series of aquation reactions to form a positively charged aquated species. Besides DNA, these highly reactive molecules also react with a variety of cytoplasmic substrates, particularly with endogenous nucleophiles, including reduced glutathione, methionine, metallothioneins and sulphur-containing proteins (Galluzzi et al, 2012; Michalke, 2010). Such bindings will deplete the reduced species and offset the redox balance of the cell, making the cell more susceptible to oxidative stress, but at the same time, these reduced species can also serve as a sequester and prevent the interaction of aquated cisplatin with DNA (Koberle et al, 2010).

In the nucleus, aquated cisplatin leads to the formation of inter- and intra-strand platinum-DNA adducts cause distortion in the DNA and impedes cellular processes, such as replication and transcription (Mello et al, 1995; Uchida et al, 1986). If the extent of the damage is limited, the cell may induce cell cycle arrest and attempt to re-establish DNA integrity through DNA repair pathways, such as nucleotide excision repair (NER) and mismatch repair (MMR) system (Furuta et al, 2002; Kunkel & Erie, 2005). Generally, the DNA

damage will be beyond repair and this activates signalling cascades that ultimately leads to apoptosis. However, multiple signalling pathways that control cell growth, differentiation and stress responses, have been implicated as the linking pathway(s) between platinum-DNA binding and apoptosis (Kelland, 2007). Moreover, attempts to decipher the relative contribution of these pathways are further complicated by contrasting reports in the literature (Galluzzi et al, 2012).

Taken together, the effectiveness of platinum drugs to form platinum-DNA adducts seems to be dependent on the availability of platinum to interact with DNA, as well as the downstream signalling cascade to elicit cell cycle arrest and/or cell death (Kelland, 2007). Though adduct formation is well-characterised to be the major mode of action of cisplatin, it should also be noted that cisplatin-induced apoptosis can also occur independently of DNA damage (Berndtsson et al, 2007; Mandic et al, 2003). All these imply that the antineoplastic effect of cisplatin can be mediated by multiple mechanisms and the alterations in any of these mechanisms can lead to cancer cells presenting a platinum resistance phenotype. A simple graphical illustration of the mode of action of cisplatin is shown in Figure 1.11.

1.3.3 Mechanisms of cisplatin resistance

To date, several mechanisms of cisplatin resistance have been described, and can be broadly classified into two main categories: (1) mechanisms that prevent formation of platinum-DNA adducts and (2)

mechanisms that prevent the activation of cisplatin-induced apoptosis following adducts formation (Galluzzi et al, 2012; Kelland, 2007).

The first category can be mediated through the modulation of intracellular accumulation of cisplatin, as well as the increased removal of platinum-induced DNA lesions by repair pathways. For instance, aquated cisplatin can be subjected to increased efflux from the cells, due to the upregulation of membrane transporters, such as the ATP-binding cassette (ABC) family of plasma membrane transporters (Liedert et al, 2003; Yamasaki et al, 2011) and the copper-extruding P-type ATPases (Nakayama et al, 2002). Intracellular accumulation of cisplatin can also be reduced through the downregulation of cisplatin uptake (Ishida et al, 2002), as well as increased expression of cisplatin sequester proteins, such as glutathione and metallothioneins (Chen & Kuo, 2010; Kasahara et al, 1991). Alternatively, resistance can be acquired through the increased ability of DNA repair pathways to remove adducts (Kelland, 2007) and the increased tolerance of DNA polymerases to bypass adducts (Hoffmann et al, 1995). In fact, expression of *ERCC1*, a critical gene within the NER repair pathway is found to be negatively correlated with cellular sensitivity to cisplatin (Li et al, 2000). The importance of DNA repair pathways is further exemplified by testicular cancers, whose low DNA repair capability contribute to their hypersensivitiy to cisplatin (Koberle et al, 1999). Overall, these mechanisms serve to reduce platinum-DNA adducts, and in so doing, prevent the activation of signalling cascades leading to apoptosis.

For the second category, a plethora of alterations, including defects in the signalling cascades that elicit apoptosis, defects in the apoptotic machinery itself, as well as the enhancements of pro-survival pathways, can prevent the occurrence of cisplatin-induced apoptosis (Galluzzi et al, 2012). Several dozens of proteins, including TP53, pro- and anti-apoptotic members of the BCL-2 protein family, caspase-inhibitory proteins, and many others are involved in the regulation and execution of apoptosis, and most of them have been shown to be modulator of response to cisplatin (Gadducci et al, 2002; Han et al, 2003; Nakamura et al, 2004). Moreover, platinum resistance needs not necessarily to be acquired through alterations in pathways directly engaged by cisplatin. Indeed, genes modulations that render cells less sensitive to cell death signals (prosurvival) have also been found to be associated with cisplatin resistance (Deng et al, 2009; Hu & Friedman, 2010).

It must be noted that the mechanisms listed above is by no means exhaustive. Combination of these mechanisms and also many other undescribed mechanisms may be responsible for the acquired and intrinsic platinum resistance of cancers, reflecting the multi-factorial nature of cisplatin resistance. In view of these, combination therapies of cisplatin with drugs targeting these mechanisms may be a feasible strategy in circumventing platinum resistance.

In the context of ovarian cancers, translation of the increased understanding of cisplatin resistance mechanisms into clinical practice is still lacking (Vaughan et al, 2011), and the optimal combination chemotherapies that can restore cisplatin sensitivity to therapeutic useful levels remain

undetermined (Sandler et al, 2006). The challenge is further compounded by the notion that most of these mechanisms modulate cisplatin response in a very restricted number of settings, and are likely to be context-dependent (Galluzzi et al, 2012). Moreover, most cisplatin-resistance studies are based on targeted gene approach, with few genome-wide functional studies. Hence, in the second part of the thesis, we propose using a genome-wide knockdown approach to identify functionally relevant molecular targets that could be used to sensitise EOC to platinum-based drug.

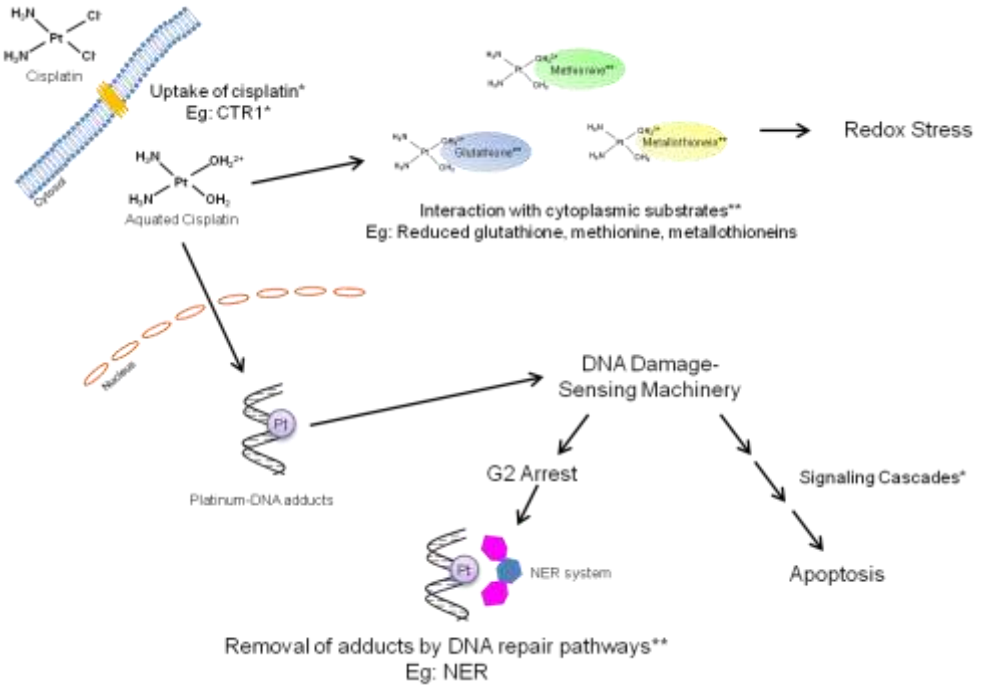

Figure 1.11 Mode of action of cisplatin.
Cells can uptake cisplatin through transmembrane protein, such as the copper transporter 1 (CTR1). Intracellular cisplatin is aquated and form positively charged aquated species that can react with nucleophilic sites on intracellular macromolecules. In the cytosol, it binds with cytoplasmic substrates, such as reduced glutathione, methionine and metallothioneins. Such bindings deplete the reduced species and sustain the generation of reactive oxygen species. In the nucleus, the reaction with DNA yields inter- and intra-strand platinum-DNA adducts that impedes cellular processes, such as replication and transcription. Adducts cause distortion in DNA that can be recognised by DNA damage-sensing machinery. If damage is limited, the cell may induce cell cycle arrest and remove adducts through DNA repair pathways, such as nucleotide excision repair (NER). Otherwise, the cell activates signalling cascades that ultimately leads to apoptosis. Multiple signalling pathways link cisplatin-induced DNA damage and apoptosis. Cisplatin resistance can be mediated through the downregulation (*) and upregulation (**) of these pathways.

1.4 Hypothesis and objective of the thesis

Despite extensive research in ovarian cancer, in particular epithelial ovarian carcinomas (EOC), the disease remains the most lethal gynaecologic malignancy. For the past few decades, improvements in the 5-year relative survival are at best, modest. The possible reasons for these low survival rates are the high incidence of chemoresistance found with EOC and a lack of consideration of the high degree of heterogeneity of EOC in the current standard of care. Accordingly, the thesis is divided into two parts in an attempt to address these two concerns.

EOC, like most cancers, is hallmarked by a high degree of heterogeneity, but it is still widely treated as a single disease entity. To address this heterogeneity, our group recently proposed a classification scheme based on transcriptional profiles to dissect EOC into five molecular subtypes. These subtypes exhibited significantly distinct clinicopathological characteristics, deregulated pathways and rates of overall survival. Hence, the proposed classification scheme confers new opportunities to devise effective therapeutic strategies, specific for each of the multiple subtypes. Therefore, for the first part of the thesis, we aim to identify subtype-specific targets, with particular focus on the poor prognosis Stem-A subtype. Such targets could be utilised for future therapy, and hopefully contribute to the improvement of targeted therapeutic regimens for EOC patients. The specific aims are as follows:

1. To identify Stem-A subtype-specific growth-promoting genes and validate the subtype specificity of these genes on at least 5 representative cell lines of each subtype.

2. To identify the pathway that mediate cell growth and survival in Stem-A subtype and demonstrate the subtype specificity effect of drug inhibitors specific to the pathway.

For the second part of the thesis, we attempt to improve patient survival via circumventing platinum resistance of EOC. Since the approval of cisplatin by the FDA in 1978, platinum-based therapy has been the standard of care for EOC patients, and majority of them respond well to the initial treatment. Unfortunately, a large fraction of the tumours eventually acquire resistance to cisplatin, leading to relapse and treatment failure. Hence, the clinical usefulness of cisplatin in EOC is limited by the high incidence of platinum-resistance. Extensive research has been carried out on strategies for circumventing platinum resistance, but as of now, none has been introduced into clinical practice. Therefore, for the second part, we intent to utilise a genome-wide knockdown approach, so as to identify target genes that can be used to enhance the sensitivity of resistant cells to cisplatin. The specific aims are as follows:

1. To identify cisplatin resistance candidate genes through the use of genome-wide knockdown approach.

2. To test whether drug inhibitors specific to these genes are able to sensitise various cell lines to cisplatin.

CHAPTER 2

MATERIALS AND METHODS

2.1 Materials

2.1.1 Reagents

The pooled library of shRNA-expressing lentiviruses (TRC1.0, #CSTVRS), pLKO.1-puro shRNA expressing vectors, lentiviral packaging mix (#SHP001), polybrene (hexadimethrine bromide, #H9268), puromycin (#P9620), dimethyl sulfoxide (DMSO, #D2650), radioimmunoprecipitation assay (RIPA) buffer (#R0278), paclitaxel (#T7402), vincristine (#V8879), vinorelbine (#V2264) and cisplatin (#C2210000) were purchased from Sigma Aldrich (St Louis, MA). SL0101 (#S560000) was purchased from Toronto Research Chemicals (Toronto, Canada). ChIP-Seq sample preparation kit (#IP-102-1001), and multiplexing index 6 and index 12 primers (#PE-400-1001) were purchased from Illumina (San Diego, CA). KOD Plus ver. 2 polymerase (#KOD-211) was purchased from Toyobo (Japan). Roswell Park Memorial Institute (RPMI) 1640 medium (#23400), Dulbecco's Modified Eagle Medium (DMEM, #12800), PureLink genomic DNA kits (#K1820-01), 10% Novex tris-borate-EDTA (TBE) gel (#EC6275BOX) and ProLong Gold Antifade reagent (#P36930) were purchased from Invitrogen (Carlsbad, CA). Fetal bovine serum (#S1810-500) was purchased from Biowest (Nuaillé, France). QIAQuick PCR Purification Kit (#28106), RNeasy Kit (#74104) and Omniscript RT Kit (#205111) were purchased from Qiagen (Hilden,

Germany). SYBR Green PCR Master Mix (#4309155) was purchased from Applied Biosystems (Foster City, CA).

All siRNA reagents used in the present study (Dharmacon SMART pool siGENOME siRNA; Dharmacon SMART pool ON-TARGET*plus* siRNA) and their transfection reagents (DF1, T-2001; DF2, T-2002, DF3, T-2003; DF4, T-2004) were purchased from Thermo Scientific (Lafayette, CO). CellTiter 96 AQueous Non-Radioactive Cell Proliferation Assay (#G5430) was purchased from Promega (Fitchburg, WI). Affymetrix Human Exon 1.0 ST arrays were purchased from Affymetrix (Santa Clara, CA).

The EB3-GFP expressing plasmid was a gift from Prof. Michael Sheetz and Dr. Pascale Monzo of the Mechanobiology Institute of Singapore. X-tremeGene HP DNA transfection reagent (#06-366-236-001) and FuGene6 (#11 988 387 001) were purchased from Roche Applied Science (Basel, Switzerland). Protease inhibitor cocktail (#539134) was purchased from Calbiochem (Boston, MA). Pierce BCA protein assay (#23225) was purchased from Thermo Scientific (Rockford, IL). Immobilon-FL Transfer membrane (#IPFL00010) was purchased from Merck Millipore (Billerica, MA). Antibodies directed against PARP (#9542) and Caspase-3 (#9662) were purchased from Cell Signaling (Danvers, MA), antibody against pericentrin (#ab4448) was from Abcam (Cambridge, MA), while those against beta-actin (#A1978) and alpha-tubulin (#T6074) were purchased from Sigma Aldrich. The secondary antibodies for western blotting: secondary IRDye 800CW conjugated goat anti-rabbit (#926-32211) and IRDye 680 conjugated goat anti-

mouse antibodies (#926-32220) were purchased from LI-COR Biosciences (Lincoln, NE), whereas those for immunofluorescence analysis: Cy2 conjugated donkey anti-rabbit IgG (H&L) (#611-711-127) and Cy3.5 conjugated donkey anti-mouse IgG (H&L) antibodies (#610-712-124) were from Rockland (Gilbertsville, PA).

2.1.2 Cell lines

Twenty-three ovarian cancer cell lines (OVCA429, OVCAR-8, OVCA433, PEO1, ovary1847, HEY, HeyA8, HeyC2, SKOV-3, A2780, CH1, PA-1, SKOV-4, SKOV-6, OVCAR-3, DOV 13, OVCA432, OVCA420, RMG-II, JHOS-2, IGROV-1, TOV-112D, OVCAR-10) were gifts from Dr. Noriomi Matsumura of Kyoto University, Kyoto, Japan. Other cell line, such as HEK-293 (#CRL-1573) was obtained from American Type Culture Collection (Manassas, VA). All ovarian cancer cell lines were cultured in RPMI 1640 medium, while HEK-293 was cultured in DMEM. All media were supplemented with 10% foetal bovine serum. All cell lines were maintained at 37 °C in a humidified incubator containing 5% CO_2.

2.2 Genome-wide RNAi screen for subtype-specific growth determinants

2.2.1 Lentiviral library infection

Fourteen ovarian cancer cell lines representing Epi-A, Mes or Stem-A subtype were infected with the pooled library of shRNA-expressing lentiviruses (80,000 clones targeting 16,000 genes per library; Sigma Aldrich).

These cell lines were chosen based on the silhouette width for the subtype signature (Table 3.1), so as to have “more representative” cell lines for a given subtype. To ensure the highest probability of having single shRNA integration into the host genome in each cell, cells were infected at a multiplicity of interest (MOI) of 0.3 (Luo et al, 2008). Under selection pressure from puromycin (5 μg/ml; Sigma Aldrich), infected cells were allowed to propagate for ~14 days (~4 or 5 passages).

2.2.2 shRNA retrieval by PCR of the genomic DNA

At the endpoint of the incubation, genomic DNA was harvested from the resulting cells by PureLink Genomic DNA kits (Invitrogen), following the manufacturer’s recommendations. The integrated shRNA sequences were retrieved from the genomic DNA (100 ng) by PCR amplification using vector primers (shRNA Forward Primer: 5'-atcttgtggaaaggacgaaac-3' and shRNA Reverse Primer: 5'-tactgccatttgtctcgaggt-3') with KOD Plus ver. 2 polymerase (Toyobo). The PCR amplification conditions were as follow: 28-32 cycles of 98°C for 10 sec, 56°C for 30 sec, and 68°C for 1 min. Products were purified with QIAQuick PCR Purification Kit (Qiagen), following the manufacturer’s recommendations.

2.2.3 Next-generation sequencing analysis to count copy number of individual shRNAs

Amplified DNA (20 ng) from PCR was used to construct a sequencing library using a ChIP-Seq sample preparation kit (Illumina). The two sample-multiplexing sequencing method was used individually, with multiplexing

index 6 and index 12 primers for each sample (Illumina). Constructed libraries were subjected to a final size-selection step on a 10% Novex TBE gel (Invitrogen). DNA fragments of 205 bp were excised, recovered and quantified following Illumina's qPCR quantification protocol and guides. Quantified libraries were then sequenced on the Genome Analyzer IIx (Illumina) using the multiplexing single-end sequencing protocol at a length of 58 + 7 bp (#PE-400-2002, Illumina). Image analysis and base calls were performed using the default settings. After stripping off the PCR primer sequences, reads were then aligned to the shRNA library using Bowtie with the specified settings: --solexa1.3-quals –n 0 –l 5 -v 0 -k 1 -m 1 --best –strata -y –nomaqround. The data are made available on Gene Expression Omnibus (GEO), with the accession of GSE45420. Concordance in the shRNA copy numbers among replicates was statistically evaluated by Spearman Correlation test.

2.2.4 Statistical identification of subtype-specific growth determinants

Using reads with a perfect match to the reference sequences (Sigma Aldrich), copy number was counted and normalised by total number of reads in a sample. RNAi gene enrichment ranking (RIGER) was used to find phenotype-specific, functionally relevant genes from the scale-normalised copy number count data (Luo et al, 2008). Among 80,000 hairpins included in the library, next-generation sequencing analyses detected 60,002 and 65,533 shRNA hairpins in two independent screenings and 57,168 hairpins were intersected in both results. We compiled and subsequently standardised these

two datasets by ComBat (Johnson et al, 2007). Binary comparisons were performed on the three subtypes (e.g. Epi-A subtype versus the others). We adopted the signal-to-ratio as the metric for ranking hairpins, 1000 as the number of permutations, and Kolmogorov-Smirnov in the RIGER settings. The false discovery rate was computed using the Benjamini and Hochberg procedure. Genes were considered significant at $q < 0.005$ in Fig. 3.5 or $q < 0.03$ for the subsequent validation study (Section 2.3).

2.3 Validation of functional determinants in cell growth of Stem-A cell lines

From the genome-wide RNAi screen (Section 2.2), 135 top hit genes ($q < 0.03$) were selected as Stem-A-specific growth-promoting genes for further validation using siRNAs. The validation experiments were performed via a process consisting of four steps (Fig. 3.7). Dharmacon SMART pool siGENOME siRNA (1st and 2nd steps) and Dharmacon SMART pool ON-TARGET*plus* siRNA (3rd and 4th steps) formats (Thermo Scientific) were used to examine the effect of gene knockdown on the cell growth of ovarian cancer cell lines (Fig. 3.7). We used two negative controls (siGENOME Non-Targeting Pools #1 and #2) for Dharmacon SMART pool siGENOME siRNA transfection, and one negative control (ON-TARGET*plus* Non-Targeting Pool) for Dharmacon SMART pool ON-TARGET*plus* siRNA transfection. PA-1 (1st, 2nd and 3rd steps) and CH1, A2780 and OVCAR-3 (4th step) were used as representative cell line(s) for the Stem-A subtype. As reference(s) for

the subtype, HeyA8 (1st step), HeyA8 and OVCA433 (2nd and 3rd steps), OVCA429, PEO1, ovary1847, SKOV-3 and HEY (4th step) were used (Fig. 3.7). The reverse transfection method (Ziauddin & Sabatini, 2001) was used to transfect the cells with each individual siRNA per well in a 96-well format. The optimal transfection conditions of each cell line are shown in Table 2.1. The optimal conditions were previously determined, such that reverse transfection of *siGAPDH* into the cells at these conditions would cause the reduction of GAPDH activity by more than 80%. Assays were performed in quadruplicate. After 96 hour incubation, an MTS assay was used to measure cell growth using a CellTiter 96 AQueous Non-Radioactive Cell Proliferation Assay (Promega), following the manufacturer's recommendations. Genes were identified as Stem-A-specific growth-promoting genes when their down-regulation caused ≥ 20% growth suppression on the Stem-A cell line (Student's *t*-test, $p < 0.001$), and showed ≥ 20% more growth suppression on the Stem-A line than on the reference cell lines. For the fourth step of the validation process, differences in growth suppression between Stem-A and non-Stem-A cell lines were statistically evaluated by Mann Whitney *U*-test in GraphPad Prism.

Table 2.1 siRNA reverse transfection conditions for ovarian cancer cell lines.

Cell Line	Subtype	Seeding Density	Transfection Reagent	Volume of Transfection Reagent
PA-1	Stem-A	1200 cells/well	DF2	0.22 µl
CH1	Stem-A	1800 cells/well	DF4	0.17 µl
A2780	Stem-A	2000 cells/well	DF1	0.16 µl
OVCAR-3	Stem-A	4000 cells/well	DF3	0.20 µl
HeyA8	Mes	800 cells/well	DF4	0.08 µl
ovary1847	Mes	2500 cells/well	DF2	0.12 µl
SKOV-3	Mes	2500 cells/well	DF2	0.12 µl
HEY	Mes	1000 cells/well	DF4	0.08 µl
OVCA433	Epi-A	2500 cells/well	DF1	0.30 µl
OVCA429	Epi-A	1500 cells/well	DF4	0.22 µl
PEO1	Epi-A	4000 cells/well	DF4	0.24 µl

2.4 Ovarian tumour gene expression data derived from publicly available databases

Ovarian tumour gene expression datasets were downloaded from multiple data repositories: Gene Expression Omnibus (GEO), Array Express, Expression Project for Oncology (ExpO), and The Cancer Genome Atlas (TCGA) in February 2010. Microarray data on Affymetrix U133A or U133Plus2 platforms were collected, with no limit on patient race, pre-treatment history or medical conditions, or on the stages, grades, and histology of the disease. Altogether, 1,538 ovarian tumour samples were assembled, of which, 1,142 samples were identified as core samples, based on their positive

silhouette width values for the subtype signature (Fig. 1.3B) (Tan et al, 2013). Note that ComBat was performed on the compiled expression data to remove batch effect while conserving meaningful variation (Tan et al, 2013).

Of these datasets, only expression data from GSE3149 (Bild et al, 2006) and TCGA (The Cancer Genome Atlas Research Network, 2011) have accompanying information regarding the patients' clinical response to chemotherapy. Most patients in these datasets received platinum-based chemotherapy and had their clinical responses assessed per Response Evaluation Criteria in Solid Tumor (RECIST) (Kang et al, 2012).

2.5 Expression data of cultured cell lines

Microarray analyses for the gene expression of 142 ovarian cancer cell lines were previously assembled from four independent datasets: Duke University, Kyoto University, National University of Singapore and Lawrence Berkeley National Laboratory (Tan et al, 2013). Of these samples, 129 samples were identified as core samples, based on their positive silhouette width values for the subtype signature (Fig. 1.8A) (Tan et al, 2013).

2.6 Pathway analysis for Stem-A-specific gene knockdowns

Dharmacon SMART pool ON-TARGET*plus* siRNA (Thermo Scientific) was used for the individual silencing of validated Stem-A-specific growth-promoting genes—*TUBGCP4* and *NAT10*—in OVCA433 (Epi-A), HeyA8 (Mes), and PA-1 (Stem-A), with ON-TARGET*plus* Non-Targeting

Pool (Thermo Scientific) as a negative control. siRNA reverse transfections were performed in triplicate, in a 6-well plate, as recommended: OVCA433, 32,000 cells with 3.0 μl of DF1; HEYA8, 19,000 cells with 0.7 μl of DF4; PA1, 18,000 cells with 2.5 μl of DF2. After 96 hour incubation, RNA were extracted, as recommended (RNeasy Mini Kit, Qiagen), and used for Affymetrix Human Exon 1.0 ST arrays (Affymetrix). There were a total of 9 expression samples.

Single sample-Gene set enrichment analysis (ss-GSEA) was performed to compute enrichment scores to the expression data (Molecular Signature Database, MSigDB version 3.0; 6,769 gene sets) (Subramanian et al, 2005). The ss-GSEA score fold-change of each individual gene knockdown clones were then computed by taking the difference of ss-GSEA scores between knockdown clones and the mean of the negative control. For each gene silencing, gene sets with standard deviation of <0.1 and maximum absolute fold change of > 0.3 across OVCA433, HeyA8 and PA-1 were denoted as commonly altered gene sets. These gene sets are shown in Appendix II. In addition, comparison of PA-1 against OVCA433 and HeyA8 was performed to identify pathways specifically down-regulated in PA-1 in each individual gene knockdown experiment. Gene sets with Significance Analysis of Microarrays (SAM; FDR q < 2.5%), Receiver Operation Curve (ROC >0.9) and showed at least 20% reduction in ss-GSEA score relative to negative control were selected as PA-1 (Stem-A) specific down-regulated gene sets. These gene sets are shown in Appendix III.

2.7 Stem-A-specific enrichment of microtubule/tubulin-related gene sets

A total of 19 microtubule/tubulin-related gene sets were collected from MSigDB version 3.0 (Table 4.1). Enrichment scores for each gene set were computed using ss-GSEA to estimate the pathway activity in 1,142 core samples of ovarian clinical tumours and 129 core samples of cell lines samples. Differences in pathway activity between Stem-A and non-Stem-A subgroups were statistically evaluated by Mann Whitney *U*-test.

2.8 Measurement of cell line drug sensitivity

Eighteen ovarian cancer cell lines (12 non-Stem-A: OVCA433, OVCA429, OVCAR-8, PEO1, OVCA432, OVCA420, HeyA8, HEY, HeyC2, SKOV-3, ovary1847 and DOV 13; 6 Stem-A: PA-1, CH1, A2780, OVCAR-3, SKOV-4 and SKOV-6) were tested for their sensitivity to paclitaxel, vincristine and vinorelbine, as described previously (Bild et al, 2006). Cells were seeded in 96-well plates at an optimal density, which was determined for each cell line to ensure that it reached 80% confluence by the end of the assay. Following an overnight incubation, cells were treated with nine concentrations of each drug (2-fold dilution series over a 128-fold concentration range) for 48 hour. The percentage of the cell population responding to the drug relative to the negative controls was measured using a CellTiter 96 AQueous Non-Radioactive Cell Proliferation Assay, following the manufacturer's recommendations (Promega). Dose-response curves were plotted using GraphPad Prism, to derive a growth inhibitory concentration of 50% (GI50;

drug concentration for 50% growth inhibitory effects on cells) for each cell line in at least three independent experiments of triplicates. Mann-Whitney U-test of GraphPad Prism was used to statistically evaluate the averaged GI50s between non-Stem-A and Stem-A cell lines.

Note that the procedure described above was also used for the measurement of cisplatin sensitivity of OVCA433 cells, but with slight modification: cells were cultured with increasing concentrations of cisplatin for 72 hour, instead of 48 hour. In addition, ten ovarian cancer cell lines (OVCA433, OVCA429, RMG-II, OVCAR8, JHOS-2, PA-1, CH1, IGROV-1, TOV-112D and OVCAR-10) were tested for their sensitivity to cisplatin, in the presence or absence of SL0101 (Toronto Research Chemicals). For this assay, cells treated with nine different concentrations of cisplatin were additionally treated with 40 μM SL0101 or its vehicle control (0.04% DMSO). After 72 hour incubation, MTS assay was similarly performed to measure the effect of the drug combination on cell growth, which was subsequently used to plot dose-response curves in GraphPad Prism. Cisplatin GI50 values of SL0101-treated cells or vehicle-treated cells were then determined from the dose-response curves. Assays were repeated in at least three independent experiments. For each cell line, differences in cisplatin GI50 values between SL0101 treatment and vehicle control were statistically evaluated using Student's *t*-test.

2.9 Western blotting analysis

Total cell lysates were prepared by direct lysis with RIPA buffer (Sigma Aldrich), supplemented with protease inhibitor cocktail (Calbiochem). Protein concentrations were determined using Pierce BCA protein assay (Thermo Scientific). Electrophoresis of the cell lysates were carried out with a BioRad Mini Protean II apparatus and transferred onto Immobilon-FL transfer membranes (Merck Millipore) with a BioRad Mini Trans-Blot apparatus, following the manufacturer's recommendations. Membranes were immunoblotted with primary antibodies directed against PARP (Cell Signaling), Caspase-3 (Cell Signaling) or β-actin (Sigma Aldrich), followed by immunoblotting with secondary IRDye 800CW conjugated goat anti-rabbit or IRDye 680 conjugated goat anti-mouse antibodies (LI-COR Biosciences). The western blots were scanned using an Odyssey Infrared Imaging System from LI-COR Biosciences.

2.10 Live-cell imaging of EB3-GFP comets

Ovarian cancer cell lines—OVCA433 (Epi-A), HeyA8 (Mes) and A2780 (Stem-A)—were seeded on glass coverslips at low density, to ensure that the cells would only reach 30% confluence after overnight incubation. EB3-GFP expressing plasmid was then transfected into the cells using X-tremeGene HP DNA transfection reagent (Roche Applied Science), according to the manufacturer's recommendations. At 24 hour post-transfection, time-lapse images of EB3-GFP comets were taken using Olympus total internal reflection fluorescence (TIRF)-iLas^2 microscope system with 1 s time interval,

200 ms exposure time and 60X TIRF objective lens. For each cell line, at least 180 EB3-RFP comets from 6 independent cells were manually tracked using the Fiji software (Schindelin et al, 2012).

2.11 Immunofluorescence analysis

Ovarian cancer cell lines—OVCA433 (Epi-A), HeyA8 (Mes) and A2780 (Stem-A)—were seeded on glass coverslips at a density, such that cells would reach 50% confluence after overnight incubation. Cells were then fixed with cold methanol for 5 mins at -20°C, and blocked in 0.5% BSA/0.1% Triton X in PBS for 10 min at room temperature. After which, cells were incubated with primary antibodies directed against pericentrin (Abcam) and alpha-tubulin (Sigma Aldrich), followed by incubating with secondary Cy2 conjugated donkey anti-rabbit IgG (H&L) and Cy3.5 conjugated donkey anti-mouse IgG (H&L) antibodies (Rockland). DNA staining was then performed by incubating the cells with DAPI in PBS for 5 min at room temperature. The glass coverslips were mounted on glass slides with ProLong Gold Antifade reagent (Invitrogen). Images were taken using Olympus cell^TIRF Illuminator, and analysed using the Fiji software (Schindelin et al, 2012).

2.12 Genome-wide RNAi screen for cisplatin resistance candidate genes

OVCA433 cells were infected with the pooled library of shRNA-expressing lentiviruses (80,000 clones targeting 16,000 genes per library;

Sigma Aldrich) at a MOI of 0.3 (Luo et al, 2008), selected with puromycin (5 μg/ml) and plated into two populations at a seeding density ratio of 2:1. The smaller population was left untreated, while the larger population was cultured in 11 μM cisplatin. After 5 days in culture, shRNA inserts were retrieved from the surviving cells in the untreated and treated populations following the procedure described in Section 2.2.2. Copy numbers of individual shRNA were determined through the next-generation sequencing analysis, as described in Section 2.2.3. Concordance in the shRNA copy numbers among replicates was statistically evaluated by Spearman Correlation test.

Using reads with a perfect match to the reference sequences (Sigma Aldrich), copy number was counted and normalised by total number of reads in a sample. RIGER analysis was then performed on the scale-normalised copy number count data to find shRNAs relatively amplified or depleted in the cisplatin-treated population (Luo et al, 2008), and thereby identify genes that are functionally relevant to cisplatin sensitivity. We adopted the signal-to-ratio as the metric for ranking hairpins, 1000 as the number of permutations, and Kolmogorov-Smirnov in the RIGER settings. The false discovery rate was computed using the Benjamini and Hochberg procedure. Genes were considered significant at $q < 0.005$ in Fig. 5.2 and in the subsequent validation study (Section 2.13).

2.13 Validation of functional determinants in cisplatin sensitivity

2.13.1 Custom siRNA library as a second screen for cisplatin resistance candidate genes

The validation experiments were performed via a two steps process (Fig. 5.3). For the first step, a custom siRNA library based on the Dharmacon SMART pool siGENOME siRNA format (Thermo Scientific), was used to target the 96 top hit cisplatin resistance candidate genes from the genome-wide RNAi screen ($q < 0.005$; Section 2.12). All siRNAs, including the two negative control siRNAs (siGENOME Non-Targeting Pools #1 and #2, Thermo Scientific) were individually seeded by the manufacturer in 96-well plates. siRNA transfections were performed by introducing OVCA433 cells (1500 cells/well) and DF1 (0.3 μl) into each siRNA-containing well. Each siRNA transfections were performed in eight replicates, which were split into two populations at 24 hour post-transfection. One population was left untreated, while the other population were cultured in 20 μM cisplatin. After 72 hour in culture, effects of siRNAs on cell viability in the presence or absence of cisplatin were measured by MTS assay using CellTiter 96 AQueous Non-Radioactive Cell Proliferation Assay (Promega). Each siRNA was assigned a viability ratio calculated as mean viability in cisplatin divided by mean viability in the absence of cisplatin. The viability ratios were determined in three independent experiments. Following which, differences between the viability ratios of each siRNA and those of negative control siRNAs, were statistically evaluated using Student's *t*-test. Genes, which upon siRNA silencing, further reduce cell viability in the presence of cisplatin

(Student's *t*-test, cut-off *p*-value of 0.05), were retained for the second step of the validation process.

2.13.2 Validation of cisplatin resistance candidate genes by shRNAs

For the second step of the validation process (Fig. 5.3), stable integrants expressing shRNAs that target the 16 genes identified from the second screen ($p < 0.05$; Section 2.13.1), were used to ascertain whether inhibition of these genes sensitised cells to cisplatin. To establish stable integrants, lentiviruses were first generated by co-transfecting pLKO.1-puro shRNA expressing vector and Lentiviral Packaging Mix (Sigma Aldrich) into HEK-293 cells using FuGene6 (Roche Applied Science), following the manufacturer's recommendations. Virus supernatants were harvested at 36 hour after transfection and used to infect OVCA433 cells in the presence of polybrene (8 μg/ml; Sigma Aldrich). Stable integrants were then established through puromycin selection (5 μg/ml; Sigma Aldrich), and subsequently tested for their sensitivity to cisplatin, as described in Section 2.8. Stable integrant established from shRNA that targets Luciferase (shLuciferase), was used as a negative control. Differences between the cisplatin GI50 values of each stable integrant and those of shLuciferase were statistically evaluated using Student's *t*-test.

2.13.3 Measurement of shRNA knockdown efficiency by quantitative RT-PCR

To measure the knockdown efficiency of shRNAs, quantitative RT-PCR was performed on the stable integrants established in Section 2.13.2. Total RNA was isolated from cultured cells using RNeasy Kit (Qiagen), according to the manufacturer's recommendations. RNA was reverse-transcribed using Omniscript RT Kit (Qiagen), according to the manufacturer's instructions. qPCR was then performed on 7000 Real-Time PCR system (Applied Biosystems), using SYBR Green PCR Master Mix (Applied Biosystems) and primers specific to the target genes, following the recommended condition of holding at 95°C for 10 min, followed by 40 cycles of 98°C for 5 sec and 72°C for 1 min. Primers were designed using Primer3 software (http://frodo.wi.mit.edu/primer3/) and are listed in Table 2.2. The expression levels of target genes were determined based on standard curves, with *GAPDH* as the endogenous quantitative control. For each stable integrant, the shRNA knockdown efficiency was computed by normalising the target gene expression level in stable integrant with that in negative control (shLuciferase).

Table 2.2 Primers used for quantitative RT-PCR.

Gene Name	Primer	Sequence	Length (nt)	Tm (°C)	Amplicon (nt)
MLH1	Forward	tccatccggaagcagtacat	20	60	101
	Reverse	tgttccacagtccacttcca	20	60	
CATSPER3	Forward	gaccttgagccacactgacc	20	60	169
	Reverse	gggcaagtcttccagcatta	20	60	
TNPO3	Forward	cttgccctacagatgccttc	20	60	167
	Reverse	ataatttctgtgcgccgatt	20	60	
KCNN1	Forward	gctaacacgcttaccgacct	20	60	120
	Reverse	atccaagcggctttccag	18	60	
RIT2	Forward	ggtgctggtgggtaacaaaa	20	58	112
	Reverse	ggctgcagaggtctcaaaaa	20	58	
RPS6KA1	Forward	tcccaccaggacctacagc	19	58	110
	Reverse	gccaggatggatgactcg	18	57	
CYB5R3	Forward	gagcatgcagattggagaca	20	60	139
	Reverse	gatcatgcccacagacttca	20	60	
SLC22A6	Forward	tgttcggctaccttgcagac	20	58	116
	Reverse	gcagtagatggggaagttgg	20	57	
TNPO2	Forward	tggcagacttcatcaaaca	19	61	94
	Reverse	gcgatggtggtgatgagaat	20	61	
KCNH3	Forward	ttcctttatgggccagacac	20	60	132
	Reverse	atccaggagacaccagaacg	20	60	
ABCC3	Forward	gctcttcactgtggtcatcct	21	59	220
	Reverse	ctggttggcatccaccttag	20	60	
SLC23A2	Forward	gccagcatcatcgagtctatt	21	60	128
	Reverse	tgccatcaagaacacaggag	20	60	
ART4	Forward	ggtcaactggaacctgagcaca	22	59	114
	Reverse	tgatgacactggtcaaaaaggagagaga	28	58	
MRPL3	Forward	tggctctgtacctggacataaa	22	59	134
	Reverse	ttctggcagttcctcttcatc	21	59	
AKAP13	Forward	attcctggagacggttgc	18	60	123
	Reverse	ggatcctgtgctgtcatcatt	21	60	
PODXL	Forward	accgataccccaaaacacct	20	60	102
	Reverse	ggacgagctgcttctcactc	20	60	
GAPDH	Forward	gacagtcagccgcatcttct	20	60	127
	Reverse	ttaaaagcagccctggtgac	20	60	

CHAPTER 3

GENOME-WIDE FUNCTIONAL SCREEN FOR SUBTYPE-SPECIFIC GROWTH-PROMOTING GENES

3.1 Introduction

Despite recent drug development and numerous clinical trials, epithelial ovarian cancer (EOC) remains the deadliest of all gynaecologic cancers. For the past 30 years, there were limited improvements in the overall mortality rates (Siegel et al, 2013), and advanced stage EOC remains associated with low 5-year survival rates (Howlader et al, 2013). The standard chemotherapy for EOC has yet to progress beyond platinum-based therapy that was introduced in the late 1970s (Vaughan et al, 2011). Thus, there is still significant unmet need for women who have been diagnosed with ovarian cancer and new therapeutic strategies should be implemented for ovarian cancer patients.

Paramount to the development of new drugs with higher efficacy is the realization of the fact that EOC represents a collection of molecularly distinct diseases and exhibit extensive heterogeneity (Bast et al, 2009; Coleman et al, 2013; Gomez-Raposo et al, 2010). Thus, standardised chemotherapy regimens should not be identical to all EOC patients. In recognition of this fact, world leaders in ovarian cancer field have been advocating for a major shift in clinical trial design from all-inclusive Phase III trials to subtype-specific

(randomised) Phase II trials that are based on sound scientific rationale (Vaughan et al, 2011). Accordingly, clinical trials are being designed to exploit the specific pathway aberrations associated with histotypes, such as low-grade serous, clear cell and endometrioid ovarian carcinoma (Coleman et al, 2013). For example, low-grade serous ovarian carcinoma, which has a high incidence of RAS pathway mutations (Singer et al, 2003), is currently being investigated in relation to response to the MEK inhibitor, MEK162 (http://www.clinicaltrials.gov/ct/show/NCT01849874).

Besides tumour histopathology, the heterogeneity of EOC can be defined through high throughput molecular techniques. Rather than evaluating one factor or small panels of factors at a time, such techniques allow comprehensive assessment of complex biological samples at the DNA, RNA and protein levels. Of these techniques, gene expression profiling has been the most developed, and is now widely used by multiple groups in their search for molecular-phenotypic correlations (Denkert et al, 2009; Mok et al, 2009). Major efforts have been made by The Cancer Genome Atlas (TCGA) and the Australian Ovarian Cancer Study (AOCS) to extensively characterize EOC. Through analysis of genomic profiles from multiple tumour samples, they demonstrated the existence of recurrent subtypes defined by transcriptional patterns (The Cancer Genome Atlas Research Network, 2011; Tothill et al, 2008). However, analysis of 285 serous and endometrioid EOC by AOCS identified six molecular subtypes (Tothill et al, 2008), whereas TCGA reported four molecular subtypes in their analysis of 489 high-grade serous EOC (The Cancer Genome Atlas Research Network, 2011). These differences are likely to arise because of varied histotype presentation, samples sizes and

analytical criteria. Using a much larger collection of ovarian tumour gene expression data, our group recently identified five molecular subtypes (Epi-A, Epi-B, Mes, Stem-A and Stem-B) (Fig. 1.3A) that exhibited distinct clinicopathological characteristics and rates of overall survival (Figs 1.5 and 1.6) (Tan et al, 2013). In addition, our group was also able to identify representative ovarian cancer cell lines for each molecular subtypes (Fig. 1.8A) (Tan et al, 2013). Though the cell lines may be divergent from their ancestral tumour and not wholly representative of the full diversity of ovarian cancer, the cell line classification represents a foundation for the development of personalised therapy.

Personalised therapy refers to the matching of patients to appropriate therapy according to the biological features of the tumour and pharmacogenomics. With the increased emphasis on targeted treatments and precision medicine, molecular profiling is starting to influence cancer management, from prognostic classification to predicting the most efficacious treatment. Several clinical trials are being designed to evaluate the extent to which patients matched to therapeutic regimens by their molecular profiles can improve clinical outcome. A prominent example is the large, non-randomised trial, named WINTHER, in which all patients enrolled are assigned to a rational personalised therapeutic regimen based on the RNA profiles of their tumours (http://www.clinicaltrials.gov/ct/show/NCT01856296). In fact, personalised cancer therapies have already been used with success among others for chronic myelogenous leukemia, ER- or Her2-positive breast cancer and EGFR-mutated lung cancer (Quintas-Cardama et al, 2009; Rosell et al, 2010; Yaziji et al, 2004).

In personalised therapy, it is critical that the drugs target critical pathways that are required for cancer cell viability, and have to be highly selective to a particular group of patients rather than broadly cytotoxic (Berns & Bernards, 2012). However, other than the standard platinum-taxane based regimen, there are little alternative therapeutic options for EOC. Consequently, for our proposed EOC classification scheme to be useful, it requires the parallel identification of molecular targets, which could be used to develop therapeutic options relevant for each molecular subtype.

The recent success in suppressing the growth of cultured lung cancer cells with activating *EGFR* mutations by siRNA (Sordella et al, 2004) unveiled the sensitivity of RNA interference- (RNAi) based approaches in distinguishing drivers of tumour growth. As such, short duplex RNAs (siRNAs) and vector encoded short hairpin RNAs (shRNAs) libraries that cover almost the entire or subsets of the human genome have been generated to uncover genes that play a causal role in specific cancer phenotypes. Thus, one approach for the identification of specific targets for EOC subtypes is the use of such RNAi libraries to perform a genome-wide, systematic, functional assessment of genes for their contribution to each molecular subtype.

Depending on the biological system and the choice of the RNAi reagent, the RNAi-based screen can be performed in arrayed or pooled format. The arrayed screen format involves the introduction of individual siRNAs or shRNAs into cultured cells, and can be used for the isolation of key regulators of cancer cell growth or other more diverse and complex phenotypes, such as DNA content, cell shape and protein localisation (Berns & Bernards, 2012).

However, single-well screen of the entire genome requires very large number of plates, a logistically complex and expensive procedure. In contrast, the pooled screening approach with shRNAs is primarily used to screen for cell growth phenotypes. Pools of shRNA-expressing vectors are introduced into cultured cells by transfection or infection such that a typical cell is subjected to only one integration event of an shRNA-expressing genome into the host. Cells are then allowed to proliferate for a period of time to permit the amplification or depletion of hairpins accordingly. Although the vast majority of shRNAs have minimal effects on cell proliferation and/or viability, an shRNA that silences the expression of a critical gene will be relatively depleted. Conversely, the relative amplification of a shRNA suggests that it targets a gene with an inhibitory role in cell growth. These integrated hairpins are then subsequently retrieved from the genomic DNA by PCR amplification, and the abundance of individual shRNA sequence can be measured with microarray hybridisation (Luo et al, 2008). Recently, next-generation sequencing (NGS) technology emerged as an alternative to microarray-based approach, and in comparison, NGS offers better sensitivity and unlimited dynamic range (Sims et al, 2011).

Notably, large-scale genetic studies using RNAi libraries have enabled the unbiased identification of genes responsible for proliferation and viability, tumorigenicity, adhesion, migration and drug sensitivity in human cancer cell lines (Bajrami et al, 2013; Huang et al, 2008; Kolfschoten et al, 2005; Luo et al, 2008; Smolen et al, 2010), as well as in mouse models (Meacham et al, 2009; Zender et al, 2008). For instance, the successful application of a pooled shRNA library led to the discovery of *PAX8* as having a more essential role in

proliferation and survival in ovarian cancer cell lines than in cell lines from other tissues (Cheung et al, 2011). Furthermore, *TBK1* was identified as a synthetic lethal partner of oncogenic *KRAS* in an earlier report using arrayed shRNA library (Barbie et al, 2009). Despite these successes, RNAi technology has not been used to identify subtype-specific growth-promoting genes, particularly in the context of ovarian cancer.

Here, we performed a genome-wide loss-of-function screen to identify molecular targets crucial for cell growth in a selected subtype (Stem-A). Upon extensive validation of the top hits, *TUBGCP4* and *NAT10* were identified as Stem-A-specific essential genes that can be used as potential therapeutic targets in EOC. Together with the proposed EOC molecular classification described in Introduction, the results presented in Chapter 3 and 4 were previously published in EMBO Molecular Medicine (Tan et al, 2013).

3.2 Results

3.2.1 Genome-wide functional screen for subtype-specific growth-promoting genes

Genes essential to each molecular subtype were investigated via genome-wide screens using the pooled The RNAi Consortium (TRC) lentiviral shRNA library (Moffat et al, 2006; Root et al, 2006), with the presumption that tumours within the same subtype would share molecular mechanisms for their growth (proliferation and/or survival). The genome-wide functional screen was performed on 14 ovarian cancer cell lines, representing Epi-A, Mes and Stem-A subtypes, that differ profoundly in gene expression

and clinical properties (Figs. 1.3A and 1.5A) (4 Epi-A: OVCA429, OVCAR-8, OVCA433, PEO1; 5 Mes: ovary1847, HEY, HeyA8, HeyC2, SKOV-3; and 5 Stem-A: A2780, CH1, PA-1, SKOV-4, SKOV-6). These 14 cell lines were selected based on their high silhouette width values for the subtype, acknowledging that PA-1 is a teratocarcinoma cell line (Table 3.1; Fig. 1.8A). Silhouette is a graphical aid for the identification of representative members of each cluster, wherein members with positive silhouette width values indicate higher similarity to members of their own cluster than to any members of other clusters, and vice versa for those with negative values (Rousseeuw, 1987). Thus, the selection of cell lines with high silhouette width values allows screening with the more representative cell lines for a given subtype.

The TRC library contains 80,000 lentivirally expressing short hairpin RNAs (shRNAs), with 4 or more independent shRNAs targeting each of 16,000 human genes. In addition, each lentiviral vector encodes each shRNA expression cassette with the puromycin resistance gene, allowing the use of puromycin to isolate stable integrants.

The experimental strategy of the screen is shown in Fig. 3.1. The cell lines were infected with the shRNA pools at a multiplicity of infection (MOI) of 0.3, to ensure the highest probability of having single shRNA integration into the host genome in each cell (Luo et al, 2008). Under puromycin pressure, infected cells were allowed to propagate for ~14 days, whereby cells expressing shRNAs that silence genes that are required for and known to suppress the cell growth were depleted from and enriched in the culture, respectively. Hence, the abundance of each shRNA (shRNA copy number)

reflects the effect of each shRNA on cell proliferation or viability. At the endpoint of the incubation, the genomic DNA was harvested from the resulting cells and integrated shRNA sequences were retrieved from the genome by PCR amplification using vector primers. PCR amplified DNAs were sequenced using highly parallel next generation sequencing and reads with perfect match to reference sequences that are provided by Sigma were used to retrieve the copy number of each shRNA for each cell line sample. Comparison of the shRNA copy numbers among cell lines from the three subtypes (Epi-A, Mes and Stem-A) consequently reveals the subtype-specific depletion or enrichment of cells expressing a given shRNA.

To define subtype essential genes, RNAi gene enrichment ranking (RIGER) analysis was used to identify genes that have more than one independent shRNAs specifically depleted or amplified in a given subtype (Luo et al, 2008). RIGER takes into account all independent shRNAs targeting each gene in its analysis, and from there, calculates a normalised enrichment score (NES) for each gene with respect to the molecular subtypes or any other specific classifications. This analysis provides increased power to the screen, and compensates for any variation in gene silencing efficacy and possible 'off-targets' effects of each shRNA.

Table 3.1 Description of ovarian cancer cell lines used.

Cell Line	Subtype	Silhouette width	Histology	Original Repository	Source	Reference	*TP53* Status
A2780	Stem-A	0.41	Undifferentiated	ECACC, #93112519	Kyoto U.	(Eva et al, 1982)	Wild-type
CH1	Stem-A	0.35	Papillary cystadenocarcinoma	--	Kyoto U.	(Hills et al, 1989)	Wild-type
HEY	Mes	0.46	Serous	--	Kyoto U.	(Buick et al, 1985)	Wild-type
HeyA8	Mes	0.44	Serous	--	Kyoto U.	(Mills et al, 1990)	Wild-type
HeyC2	Mes	0.44	Serous	--	Kyoto U.	(Mills et al, 1990)	Wild-type
ovary1847	Mes	0.26	Serous	--	Kyoto U.	(Eva et al, 1982)	T125-K132 deletion
OVCA429	Epi-A	0.28	Serous	--	Kyoto U.	(Bast et al, 1981)	Wild-type
OVCA433	Epi-A	0.22	Papillary serous cystadenocarcinoma	--	Kyoto U.	(Bast et al, 1981)	Wild-type
OVCAR-3	Stem-A	0.14	Poorly differentiated papillary adenocarcinoma	ATCC, #HTB-161	Kyoto U.	(Hamilton et al, 1983)	R248Q
OVCAR-8	Epi-A	0.12	Undifferentiated	NCI-Frederick	Kyoto U.	(Schilder et al, 1990)	L43 deletion
PA-1	Stem-A	0.35	Teratocarcinoma	ATCC, #CRL-1572	Kyoto U.	(Zeuthen et al, 1980)	Wild-type
PEO1	Epi-A	0.22	Poorly differentiated serous adenocarcinoma	CRT	Kyoto U.	(Wolf et al, 1987)	G244D
SKOV-3	Mes	0.36	Serous	ATCC, #HTB-77	Kyoto U.	(Buick et al, 1985)	Y126C
SKOV-4	Stem-A	0.29	--	--	Kyoto U.	--	R273C
SKOV-6	Stem-A	0.34	--	--	Kyoto U.	--	R273C

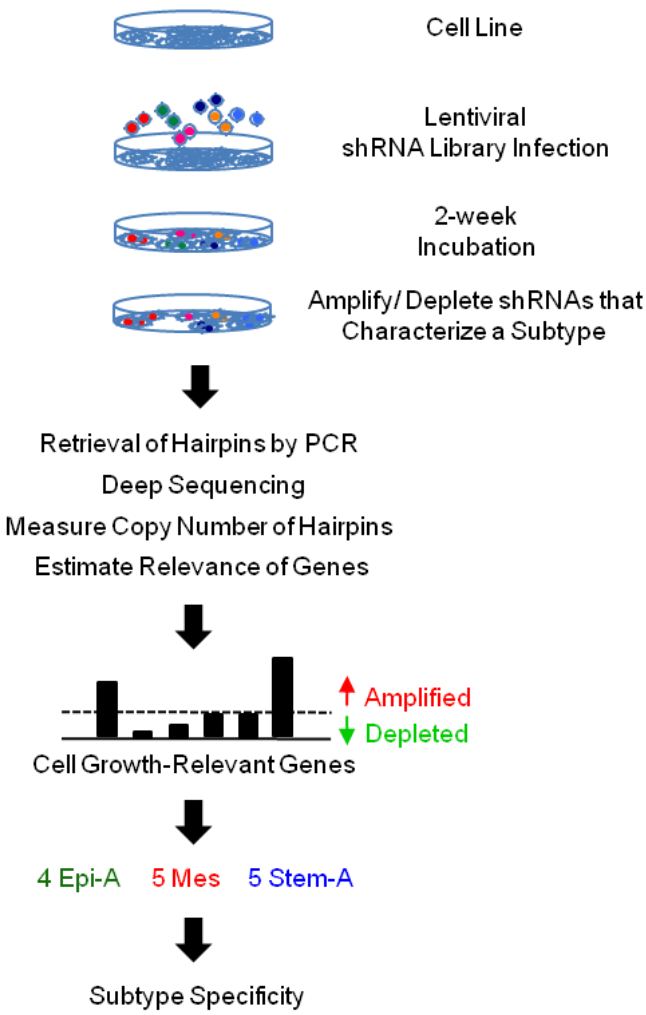

Figure 3.1 Experimental strategy of the genome-wide functional screen for subtype-specific growth-promoting genes.
Schematic showing identification of functionally relevant genes for cell growth in a subtype-specific manner. Genome-wide collection of shRNA vectors are introduced into the cell lines in a pooled format. shRNAs that target growth-promoting genes will become depleted, while those that target growth suppressive genes are enriched. Copy numbers of shRNAs are retrieved by PCR amplification and subsequent sequencing approach. Subtype-specific depleted and amplified shRNAs can be identified by comparing the shRNA copy numbers among cell lines from the three subtypes (Epi-A, Mes and Stem-A). Tan et al (2013).

3.2.2 Assessing the reliability of the genome-wide functional screen

Two independent screens were performed to ensure reproducibility. The initial assay was designed to determine concordance among four experimental replicates of a single cell line per subtype (OVCA433, HeyA8 and PA-1 was used to represent Epi-A, Mes and Stem-A subtypes, respectively). Spearman correlations revealed tight correlations among the quadruplicates in the screen (Fig. 3.2). The second screen was performed in the aforementioned 14 cell lines with the aim to detect differences across subtypes as well as concordance among different cell lines within a subtype. Fig. 3.3 illustrates highly distinctive genome-wide patterns in the copy number of subtype-specific shRNAs that were depleted or amplified. Since the screenings detected similarity in subtype-specific depletions or amplifications of hairpins, datasets from both independent screens were combined and used to identify subtype-specific growth-promoting genes. Though the correlations among the quadruplicates and different cell lines within a subtype may not be perfect, these observations demonstrate the capability of the system to identify shRNAs with differential role in proliferation in a subtype-specific manner.

Next, to further assess the reliability of the shRNA screen, RIGER analysis was performed to identify genes that correlated with the *TP53* status of the 14 cell lines (Table 3.1). *TP53* is a well-known tumour suppressor gene that plays a crucial role in preventing tumour development and progression through transcriptional dependent and independent mechanisms. Downstream genes of TP53 include genes involved in the induction of cell cycle arrest or apoptosis after DNA damage, the maintenance of genomic stability, and the inhibition of angiogenesis (Nakamura, 2004). As such, the suppression of

TP53 should confer selective growth advantage to *TP53* wild-type cells (Nakamura, 2004). Indeed, the systematic functional screening showed that *TP53* is among the top ranked genes associated with *TP53* genotype of the cultured cell lines. The copy numbers of all four *TP53*-targeting hairpins were specifically higher in *TP53* wild-type cell lines than in mutant cell lines (Fig. 3.4), indicating that *TP53* suppression specifically increased the cell growth of wild-type cells. Subsequently, RIGER analysis was applied to identify genes specifically relevant for cell growth in a molecular subtype.

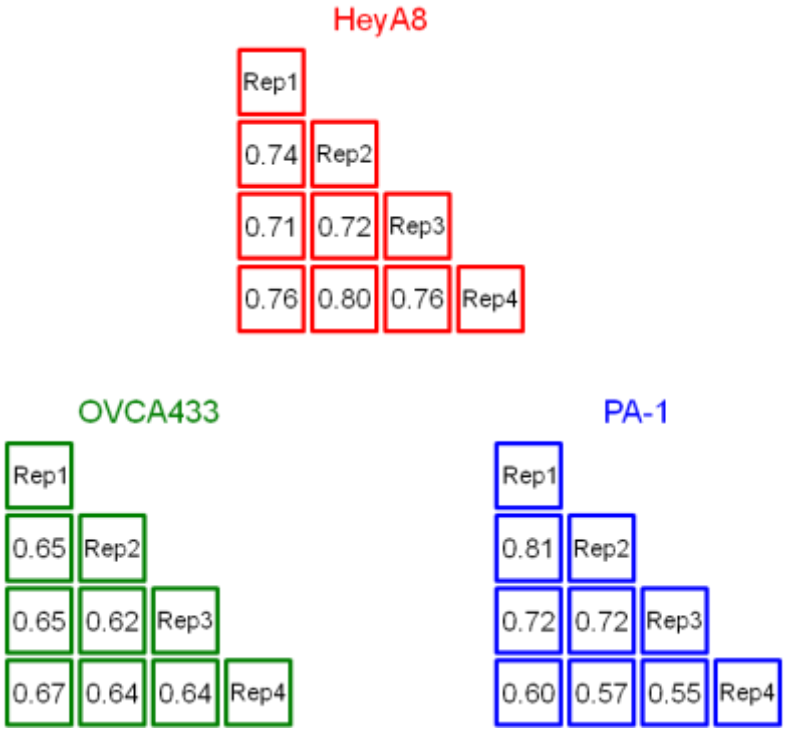

Figure 3.2 Correlation among replicates in the initial genome-wide screen. Pair-wise comparisons of normalised read counts from quadruplicates of shRNA sequences amplified from genomic DNA of HeyA8, OVCA433 and PA-1 in the initial genome-wide functional screen. Numbers indicate spearman correlation *rho* between replicates. Abbreviations: Rep; Replicate.

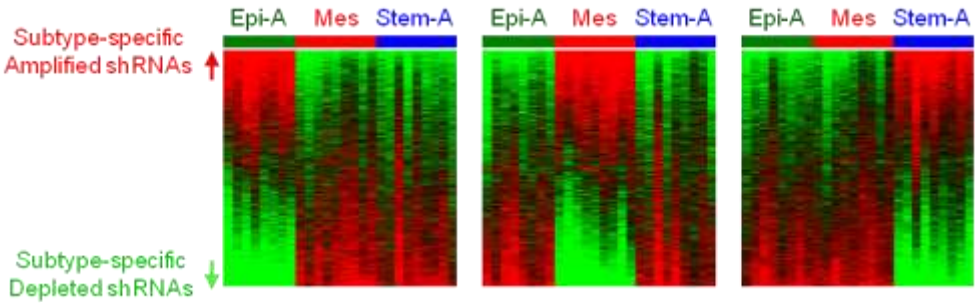

Figure 3.3 Genome-wide patterns of shRNA copy number across different subtypes.
Heatmaps of centred and normalised copy numbers of all shRNAs (57,168 hairpins) retrieved from the 14 cell lines via next-generation sequencing analysis. The results are compiled from two independent screens. Quadruplicates of three cell lines (OVCA433; Epi-A, HeyA8; Mes and PA-1; Stem-A) were assayed in the initial screen, while the other screen regarded one experimental replicate of 14 different cell lines (Table 3.1). The cell lines were sorted according to their subtypes (Epi-A, Mes then Stem-A), whereas the shRNA copy numbers were sorted according to hairpin score in the RIGER analysis (Luo et al, 2008). Note that a clear genome-wide distinctive pattern of hairpins across subtypes was detected. Red = higher; green = lower copy number counts. Tan et al (2013).

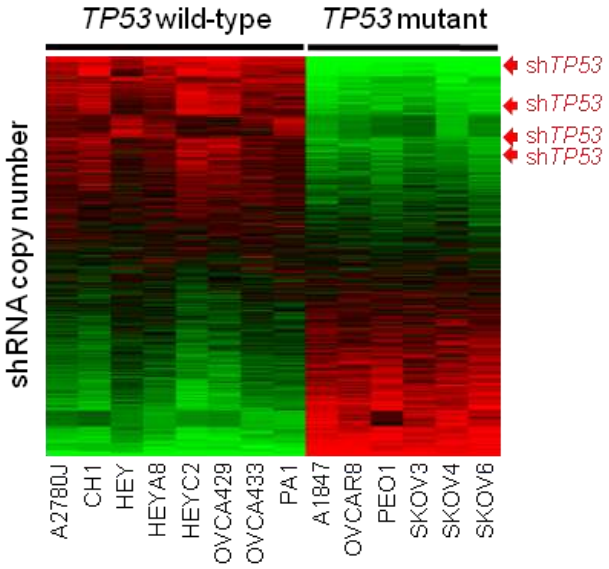

Figure 3.4 Correlation of shRNAs with cell lines *TP53* status.
Heatmap of centred and normalised copy numbers of all shRNAs (57,168 hairpins) retrieved from the 14 cell lines via next-generation sequencing analysis. RIGER analysis (Luo et al, 2008) was performed to identify genes that correlated with the *TP53* status. The cell lines were sorted according to *TP53* wild-type and mutant (Table 3.1), whereas the shRNA copy numbers were sorted according to hairpin score in the RIGER analysis. Red arrows indicate positions of independent shRNAs targeting *TP53*. Note that the copy numbers of all four *TP53*-targeting hairpins were relatively higher in cells with wild-type *TP53*. Red = higher; green = lower copy number counts.

3.2.3 Identification of subtype-specific growth-promoting genes

The primary aim of the screens was to identify genes that, when inhibited, would render growth suppression on a certain molecular subtype. Through RIGER analysis, we identified depleted shRNAs targeting 77 genes for Epi-A, 85 genes for Mes, and 88 genes for Stem-A subtypes (Fig. 3.5), with high significance in subtype enrichment ($q < 0.005$) and Hairpin Score (> 0.2). These genes are potentially involved in growth promotion of the cells in a given subtype (Appendix I). Conversely, amplified hairpins targeting 43 genes for Epi-A, 72 genes for Mes, and 44 genes for Stem-A (Fig. 3.5) that may have a suppressive effect on cell growth of the given subtype under conventional culture conditions were identified (Appendix I). The effect size was reasonably large (Cohen, 1988; Monk et al, 2012; Syrjanen & Syrjanen, 2013): the mean effect sizes of depleted hairpins were Epi-A = -0.9098; Mes = -0.7681 and Stem-A = -0.7818, and those of amplified hairpins were Epi-A = 0.8128, Mes = 0.8282 and Stem-A = 0.7486 (Fig. 3.6; Appendix I). For most of the growth-related functional genes, the abundance of shRNAs did not show significant correlation to gene expression, implying that the functional relevance of the genes was independent of their expression levels.

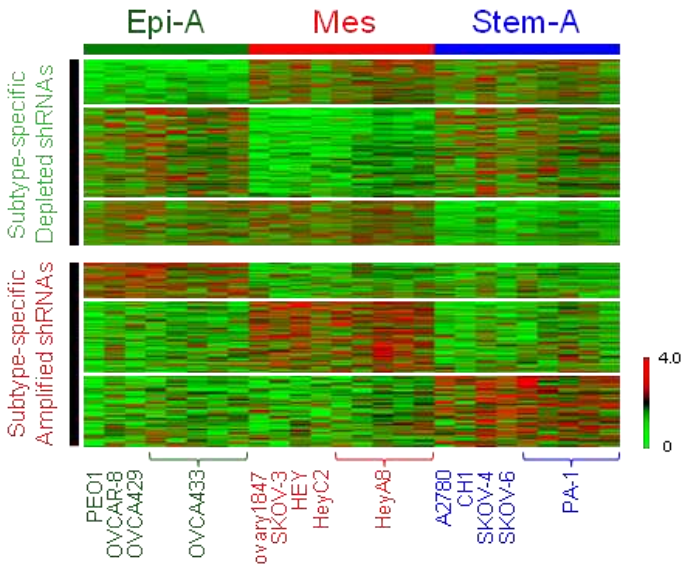

Figure 3.5 RIGER analysis of shRNA screen identifying subtype-specific functional relevance genes.

Gene centred and normalized heatmap, compiled from two independent screens, shows hairpins selectively depleted or amplified in each subtype. The quadruplicates of three cell lines (OVCA433; Epi-A, HeyA8; Mes and PA-1; Stem-A) were assayed in the initial screen, while the second screen used one experimental replicate of 14 different cell lines (Table 3.1). The copy number of each hairpin was counted and normalized against the total number of reads in a sample and then rendered to RIGER analysis, with which binary comparisons were performed for each subtype to obtain subtype-specific cell growth determinant genes (e.g. Epi-A subtype versus the others) (Luo et al, 2008). Top panel. Subtype-specific depleted hairpins in Epi-A, followed by Mes and Stem-A subtypes. Each row represents shRNA hairpin copy number and is sorted according to the hairpin score identified in RIGER (Luo et al, 2008). Only hairpin scores ≥ 0.2 and genes significantly enriched in a subtype ($q < 0.005$) are shown. Bottom panel. Subtype-specific amplified hairpins arranged as in the top panel. Red = higher; green = lower copy number counts. Tan et al (2013).

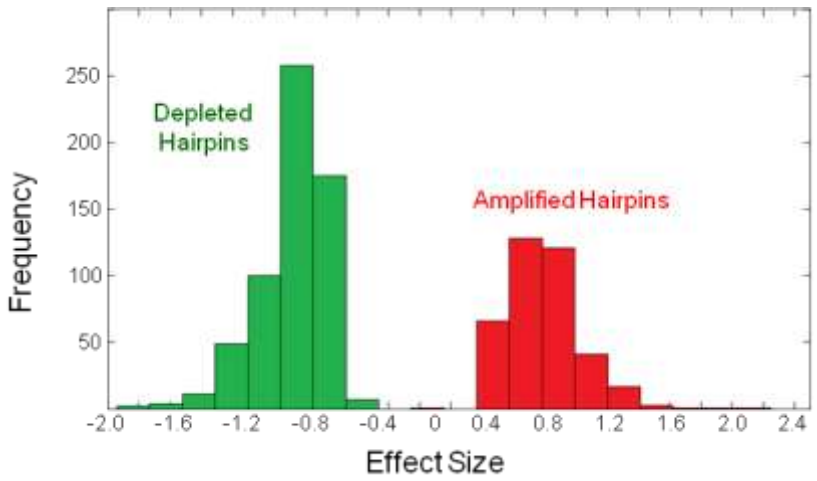

Figure 3.6 Effect size distribution of subtype-specific amplified or depleted hairpins.
Effect-size distribution of the subtype-specific amplified or depleted hairpins from the three binary comparisons in RIGER analysis. *x*-axis is the effect size, *y*-axis is the frequency. Green = subtype-specific depleted hairpins; subtype-specific amplified hairpins. Tan et al (2013).

3.2.4 Validation of subtype-specific growth-promoting genes

To validate the effects of the genes identified from the screens, we focused on the Stem-A subtype (given its worse clinical outcome; Fig. 1.5A) and targeted individual genes with siRNA (Fig. 3.7A). In addition, only growth-promoting genes (i.e. gene targets of depleted shRNAs) were subjected for validation, as most pharmacological agents inhibit rather activate protein function. Accordingly, 135 genes depleted in Stem-A subtype were chosen based on a less stringent *q*-value cut-off of 0.03 from RIGER analysis (note that a more stringent *q*-value was used in Fig. 3.5; Table 3.2).

The validation of these 135 genes was performed in a process that consisted of four steps (Fig. 3.7B) in order to identify siRNAs that inhibited growth on Stem-A cells but had a minimal effect on other cells. Genes were individually silenced in ovarian cancer cell lines in 96-well format through the reverse transfection method (Ziauddin & Sabatini, 2001), whereby the cells, siRNAs and optimal transfection reagent were all added to the wells at the same time (see Materials and Methods section 2.3 for additional details). The effect of siRNA on cell growth was then measured with the MTS assay after 96-hour incubation (Fig. 3.7A). For all four steps of validation, Stem-A-specific essential genes were identified as positive hits based on the following comparisons using Student *t*-tests: 1) comparison between the growth inhibitory effect of silencing the gene of interest with that of the siRNA negative controls in the Stem-A cells; and 2) comparison between the effect on Stem-A cells with that on the references for the subtype (i.e. non-Stem-A cells) (Fig. 3.7B). Significance thresholds for the two comparisons were as follows: 1) $\geq$ 20% growth suppression in Stem-A cell with $p < 0.001$ in a

Student's *t*-test comparing negative control with the gene of interest, and 2) ≥ 20% growth suppression in Stem-A cell(s) as compared with the reference cell line(s).

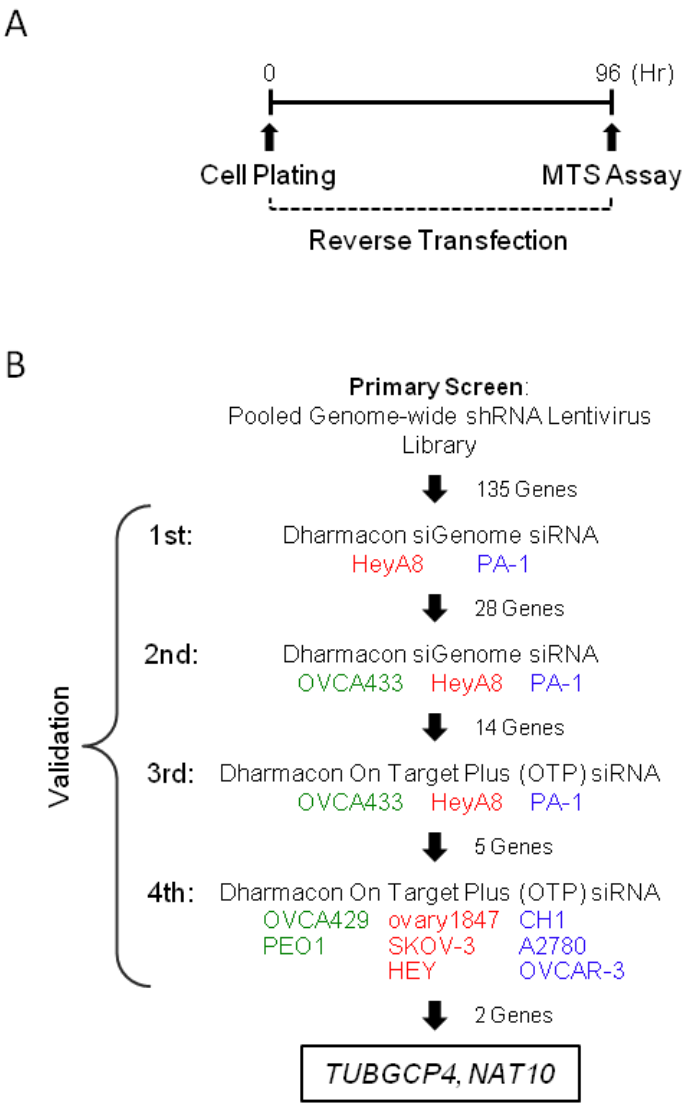

Figure 3.7 Schematics of subtype-specific functional relevance genes validation.
A. Timeline of assay performed for the siRNA validation experiment. B. Schematic of siRNA experiments validating the identified Stem-A-specific growth-promoting genes. This analysis led to the identification of two functionally relevant genes specific to Stem-A: *TUBGCP4* and *NAT10*. Green = Epi-A; red = Mes; blue = Stem-A subtype. Tan et al (2013).

In the first step of validation, experiments were only performed in PA-1 (Stem-A) and HeyA8 (Mes) cells, and 28 genes were found to be selective for PA-1 cell growth (Table 3.2). In the second step, we examined the effect of these 28 genes in PA-1 (Stem-A), HeyA8 (Mes) and OVCA433 (Epi-A), and further confirmed the growth suppressive effect of 14 of these 28 genes (Table 3.2). For the third step, the platform was switched from "siGenome" to "On-Target Plus siRNA" to further validate our observations using different sets of target sequences in the genes as well as to reduce possible off-target effects. After this step, five genes (*TUBGCP4, NAT10, GTF3C1, BLOC1S1* and *LRRC59*) were validated as PA-1-relevant genes (Fig. 3.8; Table 3.2). Importantly, PA-1 (Stem-A) cells showed cleavage of Caspase-3 and PARP after treatment with si*TUBGCP4*, si*NAT10*, si*GTF3C1* or si*LRRC59*, indicating activation of apoptosis in these cells (Fig. 3.8). On the contrary, cleavage of Caspase-3 and PARP was not detected in non-Stem-A cells (HeyA8 and OVCA433) (Fig. 3.9).

Finally, as the fourth step of the validation process, the experiments were conducted with use of additional non-Stem-A (Mes: ovary1847, SKOV-3 and HEY; Epi-A: OVCA429 and PEO1) and Stem-A (CH1, A2780 and OVCAR-3) cell lines to ensure its reproducibility and to exclude any possible impact of PA-1 cells being derived from a different cell-of-origin (teratocarcinoma), even though it had the highest silhouette width of the Stem-A cell lines. *TUBGCP4* or *NAT10* siRNA treatment reproducibly resulted in a statistically significant reduction in cell growth for the Stem-A cell lines, whereas cell growth for non-Stem-A cell lines was minimally affected (Fig. 3.10; Table 3.2). These multiple stages of rigorous validation confirmed the

dependence of Stem-A cell lines on *TUBGCP4* and *NAT10* in cell growth and ensured that this effect was not limited to PA-1 cells. Silencing of the other three genes (*GTF3C1*, *BLOC1S1* and *LRRC59*), albeit not statistically significant, also exhibited a tendency toward differential toxicity in Stem-A cells (Fig. 3.10). These observations demonstrate that subtype classification based on gene expression is indeed mirrored by patterns of functional genetic determinants of cell viability. Moreover, the validated genes can provide us with an insight into the molecular mechanisms of Stem-A tumour growth.

Table 3.2 List of Stem-A-selective growth-promoting genes identified for validation.

Subtype	Step	No. of Genes	Genes
Stem-A	Candidates identified by shRNA screen	135	*ACAB, ACER3, ACVR2A, ATIC, BAI2, BEX1, BLOC1S1, C12orf10, C16orf71, C2CD2, CA8, CAB39L, CAP2, CASC1, CCL3L1, CDKL3, CHD9, CHPT1, CRELD1, CTTNBP2, CUL7, DBNDD1, DDX11, DGKB, ECSIT, EGFR, EIF2S3, EPN2, ETFA, ETV2, FAM32A, FIGNL1, FLCN, FOXRED2, FRS2, GNPDA1, GOLIM4, GORASP2, GP1BB, GPSM2, GRIK5, GRWD1, GTF3C1, GUF1, HAX1, HIF3A, HIPK2, HIST1H2AI, HIST1H4J, HMGN2, HNRNPUL1, HS3ST4, INTS12, IQCC, ISCU, JUP, KIAA1012, KIAA1772, KIF2C, KLHL2, KREMEN2, LANCL1, LCMT1, LIPT1, LMNB2, LRRC59, MAD2L1, MAR6, MAZ, MED17, MINPP1, MRPS14, MTHFD2L, NAALAD2, NAB2, NANOG, NAT10, NCAM2, NONO, NPY, NQO2, NUP210, NXPH4, OR2T4, OR5T3, OXCT1, PBX2, PCOLCE2, PIAS4, PIR, PNPLA4, POLR2J, PPP1R10, PPP1R3C, PRDX4, PRKD3, PTPRD, QRICH1, RAB33B, REEP1, RFC3, RNF4, ROBO1, RPL3L, SERTAD3, SFRS2, SMUG1, SNRPN, SSRP1, SSX2IP, TBCC, TEX14, TFAM, TMEM121, TNFRSF4, TRAF5, TRPM8, TSPYL2, TTC3, TTLL7, TUBGCP4, UBB, UBL5, UNC119, PGCP, UTP14A, WNT10B, ZFP2, ZFR, ZNF35, ZNF573, ZNF652, ZNF770, ZNF804A, ZZZ3*
	Candidates identified by validation step 1	28	*ACVR2A, BAI2, BLOC1S1, C16orf71, C2CD2, CA8, CCL3L1, CHPT1, GP1BB, GTF3C1, HIF3A, HIST1H2AI, ISCU, KLHL2, LRRC59, NANOG, NAT10, NONO, PIAS4, PIR, QRICH1, SFRS2, TEX14, TMEM121, TRPM8, TUBGCP4, UBL5, WNT10B*
	Candidates identified by validation step 2	14	*QRICH1, CHPT1, LRRC59, CA8, NONO, TUBGCP4, BLOC1S1, KLHL2, HIST1H2AI, TMEM121, GP1BB, TEX14, GTF3C1, NAT10*
	Candidates identified by validation step 3	5	*LRRC59, TUBGCP4, BLOC1S1, GTF3C1, NAT10*
	Candidates verified in 11 Ovarian Cell Lines (7 non-Stem-A VS 4 Stem-A)	2	*TUBGCP4, NAT10*

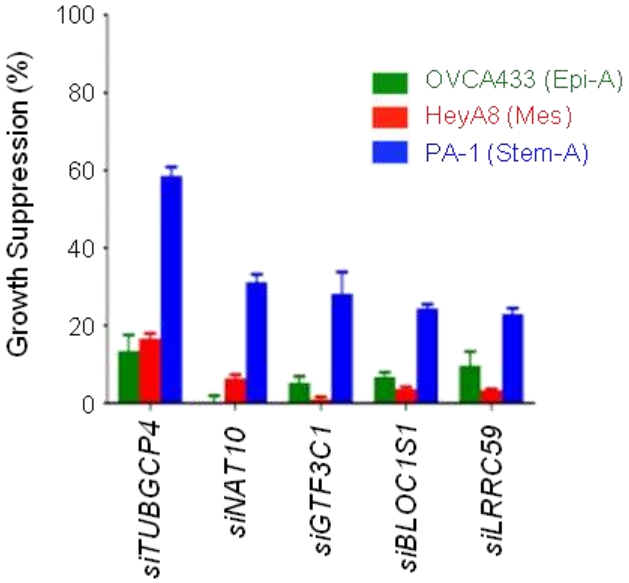

Figure 3.8 Validation of PA-1 (Stem-A) functional relevance genes.
Validation of subtype-selective effect of the genes on cell growth by siRNAs. Effect of gene knockdown on cell growth (bar plots) as a percentage ratio of growth suppression, normalized against the negative controls. Error bar indicates the SEM of three independent quadruplicate experiments. Stem-A-selective growth suppression effect is shown for the inhibition of the five validated PA-1 (Stem-A)-specific growth-promoting genes in OVCA433, HeyA8 and PA-1, respectively. Green = OVCA433 (Epi-A); red = HeyA8 (Mes); blue = PA-1 (Stem-A). Tan et al (2013).

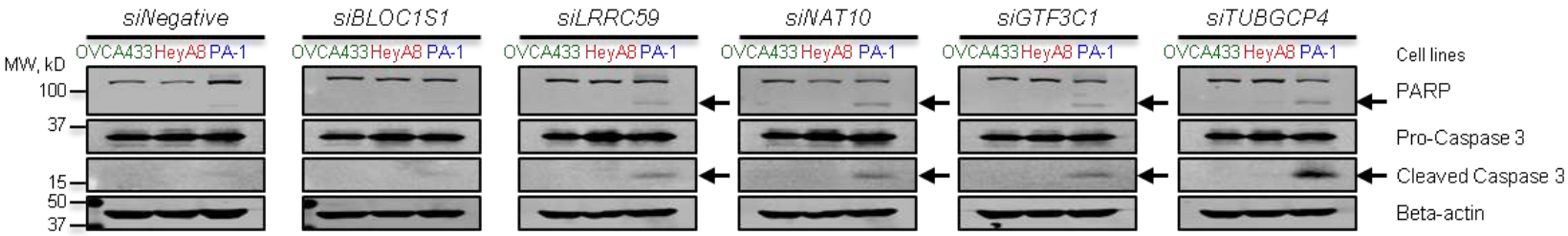

Figure 3.9 Detection of apoptotic activity initiated by the five PA-1 (Stem-A) functional relevance gene knockdowns.
The five PA-1 selective genes were silenced individually by siRNA in OVCA433 (Epi-A), HeyA8 (Mes) and PA-1 (Stem-A) and examined for the presence of apoptotic activity by immunoblotting for cleaved PARP and Caspase 3. Arrows indicate cleavage of PARP and Caspase 3. Suppression of *LRRC59, NAT10, GTF3C1 and TUBGCP4* was linked with the induction of apoptosis only in PA-1 cells, albeit a slight apoptotic response was also detected using the siRNA negative control in PA-1. Green = Epi-A cell line; red = Mes cell line; blue = Stem-A cell line. Tan et al (2013).

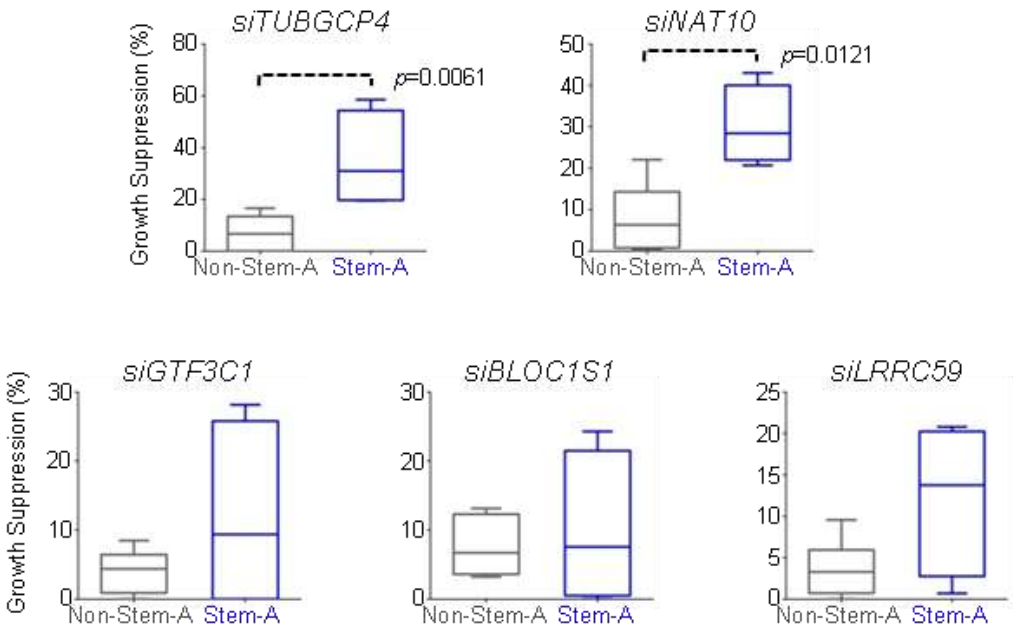

Figure 3.10 Effect of silencing PA-1 (Stem-A) selective genes on cell growth in other ovarian cancer cell lines.
The five PA-1-selective genes were silenced individually by siRNA in non-Stem-A (OVCA433, OVCA429, PEO1, HeyA8, ovary1847, SKOV-3 and HEY) and Stem-A (PA-1, CH1, A2780 and OVCAR-3) cell lines in three independent quadruplicate experiments, and examined for their effect on cell growth relative to the negative control. Averaged percentages of growth suppression in each group are shown as a box plot and were statistically evaluated using Mann-Whitney *U*-test with GraphPad Prism. Bottom, middle and top lines of each box represent the 25th percentile, median and 75th percentile, respectively, and whiskers extend to the most extreme values of the group. Inhibition with si*TUBGCP4* or si*NAT10* significantly suppressed cell growth of Stem-A cell lines as compared to non-Stem-A cell lines. Grey = non-Stem-A cell lines; blue = Stem-A cell lines. Tan et al (2013).

3.3 Discussion

The consensus clustering of a large collection of epithelial ovarian carcinoma (EOC) samples presented previously by our group identified five molecular subtypes (Epi-A, Epi-B, Mes, Stem-A and Stem-B) that exhibited distinct clinicopathological characteristics and rates of overall survival (Tan et al, 2013). As a complement to the proposed classification scheme, we performed an unbiased genome-wide RNAi screen for genes that modulate cell growth (proliferation and/or viability) in a subtype-specific manner and illustrated that subtype-matched cell lines have distinct vulnerabilities. In particular, *TUBGCP4* and *NAT10* were proven as specific growth-promoting genes for the poor-prognosis Stem-A subtype. These results offer possible opportunities in developing therapeutic strategies that could be matched with the characteristics of individual patients.

The functional screen reported here confers opportunities to recognize molecular vulnerabilities as well as particular drug sensitivities relevant for each molecular subtypes of EOC. In the current era of molecular targeted therapies, there has been an increased appreciation of the importance of individual diversity in cancer biology (De Palma & Hanahan, 2012; Vaughan et al, 2011). This comes with a shift in clinical trials design from all-inclusive Phase III trials to subgroup-specific Phase II trials (Vaughan et al, 2011), so as to connect particular patient subgroups to therapies with the highest likelihood of benefit. Of note, such concept is only useful when therapeutic alternatives are available. Thus far, therapeutic options for EOC are rather limited and no studies have been able to reveal molecular subtype-specific dependencies in EOC. It is thus our intention to uncover subtype-specific targets, and for the

first time, we utilised the pooled shRNA library, in combination with next-generation sequencing technology as the detection platform (Sims et al, 2011), to identify key subtype-specific regulators of cancer cell proliferation and/or survival. Importantly, we have demonstrated that specific growth determinants can be distinguished amongst the ovarian cancer subtypes at the genome-wide as well as gene level. This observation supports the potential for subtype-specific therapeutic options in treating ovarian carcinoma and reinforces the clinical importance of the classification scheme proposed previously (Tan et al, 2013).

As an initial approach, we elected to explore essential genes belonging to the poor prognosis Stem-A subtype of EOC. Our results showed that Stem-A cell lines exhibit selective sensitivity to the suppression of *TUBGCP4* and *NAT10*. On the other hand, the silencing of these genes had minimal growth suppression effect on non-Stem-A cell lines, and thus, suggesting that new therapeutics targeting these genes could prove useful in the therapy of Stem-A EOC tumours.

The relevance of such subtype-specific targets has been exemplified by oestrogen receptor 1 (*ESR1*) for luminal-subtype breast cancers; these cancers share not only clinical features such as prognosis and the response to hormonotherapy, but also the pattern of gene expression (Sorlie et al, 2001). *ESR1* has been used not only for diagnosis but also as a molecular target to treat cancer patients with this subtype (Chia et al, 2012; Howell, 2013). In another example, associations of epidermal growth factor receptor (*EGFR*) mutations and echinoderm microtubule associated protein like 4 - anaplastic

lymphoma kinase (*EML4-ALK*) translocations in non-small cell lung cancer (NSCLC) patients with improved response to EGFR (gefitinib, erlotinib and afatinib) and ALK (crizotinib) tyrosine kinase inhibitors, respectively (Gaughan & Costa, 2011) are paving the way for individualised care of NSCLCs. In fact, poly (ADP) ribose polymerase (PARP) inhibitors, such as olaparib, have been shown in several clinical trials to exhibit selective toxicity to EOC tumours with *BRCA1*/*2* germline mutations (Farmer et al, 2005; Fong et al, 2009). Most recently, cyclin E1 (*CCNE1)* over-expressing ovarian cancer cell lines were found to be selectively sensitive to *BRCA1* gene suppression, suggesting that inhibition of *BRCA1* represents a potential therapeutic approach for *CCNE1*-amplified EOC tumours (Etemadmoghadam et al, 2013). Similarly, we hoped that our findings will help in the improvement of therapeutic regimens for EOC patients.

It should be pointed out that the functional screen was conducted using ovarian cancer cell lines, which were assigned to unique ovarian tumour subtypes by expression data (Tan et al, 2013). We acknowledge that cell lines may be divergent from their ancestral tumour and not wholly representative of the full diversity of EOC. For instance, tumour-associated non-epithelial cells, such as blood vessels, fibroblasts and inflammatory cells are not recapitulated in the cell line model. Nonetheless, the subtype-representative cell line models were previously identified based on their similarity in transcriptional profile with their primary tumour counterparts (Tan et al, 2013). These similarities were illustrated by the spearman correlation map in gene expression (Fig. 1.8B; average spearman *rho* = 0.80), as well as by the shared subtype-specific gene sets enrichment in tumours and cell lines (Figs. 1.7 and 1.9). While the

correlations between primary tumour subtypes and cell line subtypes are admittedly not perfect, subtype-representative cell lines are thus far, the most representative models readily available for molecular subtype study. In fact, subtype-matched cultured breast cancer cell lines have been used by several groups to represent their *in vivo* counterparts (Gatza et al, 2010; Neve et al, 2006; Perou et al, 2000). Subsequent integration of our findings with the transcriptional, copy number, structural or epigenomic analyses of cancer genomes by The Cancer Genome Atlas (TCGA) and other such efforts would further validate the clinical relevance of our two Stem-A candidate genes; *TUBGCP4* and *NAT10* (Garay & Gray, 2012).

Towards the end of this thesis, Domcke *et al*. (2013) published an important study, in which they compared the genomic profiles of high-grade serous ovarian cancer (HGSOC) samples in TCGA with those of human ovarian cancer cell lines in Broad-Novartis Cancer Cell Line Encyclopedia (CCLE) and then, ranked the cell lines according to their suitability as HGSOC models. Based on their ranking, majority of the ovarian serous cell lines utilised (Table 3.1), as representative models for our proposed molecular subtypes of epithelial ovarian carcinoma (EOC), were listed as 'bad' cell line models of HGSOC (Domcke et al, 2013). However, it is also clear that these cell lines share common transcriptional signatures with their corresponding EOC molecular subtypes; in particular, those of serous carcinoma (Tan et al, 2013). Nevertheless, it is true that the lack of good HGSOC models could have an impact on the results. To exclude this possible impact, further verification using cell lines that are highly representative of the EOC molecular subtypes and are also good models of HGSOC, is still required.

Interestingly, the biological functions of both TUBGCP4 and NAT10 are associated with microtubules. TUBGCP4 (tubulin, gamma complex associated protein 4) is a component of the gamma-tubulin ring complex (γTuRC), which is involved in the nucleation of microtubules from centrosome, chromatin and spindle microtubules (Fava et al, 1999; Goshima et al, 2008; Guillet et al, 2011; Moritz et al, 1995). Of note, TUBGCP4 is evolutionarily conserved (Fava et al, 1999), implying that it performs functions that confer selective advantage. Depletion of the gene ortholog leads to the reduction of γTuRC in sucrose gradients, as well as an increase in the frequency of chromosome mis-segregation in the filamentous fungi *Aspergillus nidulans*, thus suggesting that TUBGCP4 has a role in the assembly or stability of the ring complex and in ensuring the fidelity of chromosomal segregation (Xiong & Oakley, 2009). Even so, TUBGCP4 has been shown to be non-essential for viability in yeast and in *Drosophila melanogaster* (Anders et al, 2006; Verollet et al, 2006), and also non-critical for the correct organization of cytoplasmic microtubules in *Aspergillus nidulans* (Xiong & Oakley, 2009). This is perhaps less puzzling in light of recent findings that the sub-complex of γTuRC, gamma-tubulin sub-complex (γTuSC) forms ring structure even in the absence of other γTuRC components and nucleates microtubules from the centrosome, albeit at a much lower efficiency (Kollman et al, 2010; Oegema et al, 1999). Conversely, microtubule nucleation from non-centrosomal sites, such as within the mitotic spindle, depends largely on γTuRC-specific components, which includes TUBGCP4 (Kollman et al, 2011; Verollet et al, 2006). NAT10 (N-acetyltransferase 10), on the other hand, is a protein with lysine acetyltransferase activity, and thus

far, has been implicated in diverse processes, including telomerase activity, cell survival, cell cytokinesis and nuclear architecture (Larrieu et al, 2014; Liu et al, 2007; Lv et al, 2003; Shen et al, 2009). Briefly, NAT10 was first identified as an activator of telomerase activity through the transactivation of the hTERT promoter (Lv et al, 2003). In addition, NAT10 was found to be involved in DNA damage response and enhanced cell survival in the presence of genotoxic agents (Liu et al, 2007). Recent reports showed that the knockdown of NAT10 led to morphological changes in nuclear shape and also induced defective cytokinesis (Larrieu et al, 2014; Shen et al, 2009). Notably, NAT10 is known to acetylate α-tubulin, and in turn regulates microtubule stability (Perdiz et al, 2011; Shen et al, 2009). Inhibition of its acetyltransferase activity by the specific chemical inhibitor, Remodelin, indeed caused reorganisation of the microtubule network (Larrieu et al, 2014). Given that both genes are associated with microtubules, it may be worth examining microtubule-related pathways in Stem-A EOC tumours and/or cell lines. Such pathway analysis could possibly allow us to move from targeting individual genes to pathway-targeted therapeutic approach.

Generally, our findings add on to those of previous studies that used pooled shRNA libraries in loss-of-function studies to identify essential genes in specific human cancer cell lines in the context of synthetic lethality (Bajrami et al, 2013; Luo et al, 2008; Scholl et al, 2009) and lineage-specificity (Cheung et al, 2011). However, a major issue to date remains the off-target effects of siRNAs and shRNAs, resulting in the inhibition of genes that are not the intended target (Ashworth & Bernards, 2010). As such, it is commonly accepted that extensive validation of hits identified is required for

any RNAi-based screens. Another critical consideration for pooled shRNA screening is the extent to which each shRNA construct is accurately and sufficiently represented during the hairpin retrieval by PCR amplification (Sims et al, 2011; Strezoska et al, 2012). PCR amplification has been demonstrated to be a substantial source of data variability, and so, optimisation of amplification conditions would help to avoid introduction of bias (Strezoska et al, 2012). Besides PCR optimisation, location of PCR primers away from the stem of hairpin also substantially improved the uniformity of PCR amplification, compared to primers that amplify the hairpin stem (Strezoska et al, 2012). Accordingly, data reproducibility could be improved by the use of pooled barcoded-shRNA libraries, in which each independent shRNA is tagged with a unique barcode sequence. Unfortunately, such libraries were not available to us at the time of our screening, which possibly account for our less than perfect correlations among the technical replicates. At the same time, we also cannot eliminate the possibility that other factors were missed in our screen.

In addition, a major shortcoming of RNAi screens is the current lack of standardisation, and thus, making it difficult for individual laboratories to compare their data (Berns & Bernards, 2012). Attempts to integrate the results from our screen with that of another published screen using the same shRNA library (Cheung et al, 2011) were not feasible because of the differences in experimental design and detection platforms. Even so, the power of RNAi screens in discovering underlying relationships between genotype and essential genes should not be discounted, and can be a valuable tool to extend the realm of molecular targets in cancer.

CHAPTER 4

MICROTUBULES AS TARGETS IN STEM-A EPITHELIAL OVARIAN CARCINOMA TUMOURS

4.1 Introduction

As mentioned in Section 1.1.5, epithelial ovarian carcinoma (EOC) is hallmarked by a high degree of heterogeneity that arises as a consequence of varied somatic mutations and epigenetic changes acquired during the process of tumorigenesis and tumour progression. In addition, genomic characterization of EOC has revealed the existence of molecular subtypes that are associated with distinct clinicopathological characteristics (Tan et al, 2013; The Cancer Genome Atlas Research Network, 2011; Tothill et al, 2008). As a result, world-leading ovarian cancer researchers and clinician scientists have been advocating for the need to recognise EOC as a series of molecularly and etiologically distinct diseases (Bast et al, 2009; Vaughan et al, 2011). This realisation has opened the frontier of personalised cancer medicine for EOC, where the unique biology and genetics of a patient's tumour is incorporated into the decisions on optimal treatment strategies. However, therapeutic options for EOC have yet to progress beyond the standard platinum-taxane based chemotherapy.

To improve current therapeutic options, extensive efforts have been made in surveying EOC for actionable genomic and epigenomic events. In some instances, molecular-based knowledge gained from these genome-wide analytical approaches has already an impact on developing personalised

therapies. For instance, the discovery that many high-grade serous ovarian carcinomas are *BRCA1* or *BRCA2* defective (Press et al, 2008) has prompted the investigation into the efficacy of PARP inhibitors towards such tumours (Banerjee et al, 2010; Farmer et al, 2005). Studies have shown that the loss of PARP-1 function (a critical DNA damage sensor protein in base excision repair pathway) results in the generation of DNA lesions that are normally repaired by the homologous recombination DNA repair pathway (Farmer et al, 2005). Since both BRCA1 and BRCA2 proteins are part of the homologous recombination pathway, PARP inhibitors are, thus, selectively lethal to *BRCA1/2* defective cells (Banerjee et al, 2010). Indeed, a Phase I study of the orally active PARP inhibitor, olaparib, reported that only *BRCA1/2* mutation carriers were associated with objective anti-tumour activity (Fong et al, 2009). These promising results as well as those of other randomised Phase II studies (Audeh et al, 2010; Ledermann et al, 2012) provided preliminary vindication of using PARP inhibitors against *BRCA1/2* defective advanced ovarian cancer.

Adding on to these findings, our group recently reported the identification of two subtype-specific growth-promoting genes (*TUBGCP4* and *NAT10*) that hopefully could be used as therapeutic targets for our proposed poor-prognosis Stem-A subtype (Tan et al, 2013). In addition, the association of both genes to microtubule suggests that it may be worth investigating the relevance of microtubule-targeted agents to Stem-A EOC tumours.

Such microtubule-targeted agents comprise of chemically diverse compounds, such as taxanes, epothilones, vinca alkaloids, halichondrins,

maytansinoids and colchicine-site binding agents, which bind to tubulin and/or microtubule, and alter microtubule polymerisation and dynamics in diverse ways (Dumontet & Jordan, 2010). Given the importance of microtubules in cell proliferation, such alterations induce mitotic arrest, and thus, mediate anti-tumour activity. Unsurprisingly, these agents have been part of the pharmacopoeia of anticancer therapy for decades, where they are often incorporated in combination chemotherapy regimens for a broad range of solid tumours and haematological malignancies (Dimitroulis & Stathopoulos, 2005; Gridelli et al, 2005; Markman, 2008). Even so, extensive research is still being devoted to understanding the role of the extremely diverse microtubule-targeted agents in different cancer cells and also the mechanisms of resistance to these agents (Dumontet & Jordan, 2010). Hopefully, our investigation of their clinical relevance to Stem-A EOC tumours may lead to a better understanding and utilisation of microtubule-targeted agents in anticancer therapy in EOC.

In this chapter, the clinical relevance of the Stem-A specific growth-promoting genes, *TUBGCP4* and *NAT10*, and their associated pathway(s) were evaluated using the expression data of clinical tumours and cell lines. Next, expression microarray analyses were performed to identify pathways affected by the Stem-A specific growth-promoting genes. Finally, we evaluated the relevance of the various microtubule-targeted agents to Stem-A ovarian cancer cell lines, and linked the subtype with tubulin polymerisation inhibitory drugs.

4.2 Results

4.2.1 Analysis of *TUBGCP4* and *NAT10* expression in ovarian tumours and cell lines expression data

Genome-wide transcriptional analysis of the expressed mRNAs has been widely used to search for molecular-phenotypic correlations in cancer research, with the presumption that correlatively up- and down-regulated gene transcripts are hinting of their respective roles as cancer driver and suppressor genes. And so, to integrate our findings in Chapter 3 with the transcriptional analyses of cancer genomes, we examined the expression level of the two Stem-A specific growth-promoting genes, *TUBGCP4* and *NAT10* in publicly available datasets. For this purpose, we utilised the expression data from the core samples of ovarian clinical tumours (n = 1,142) and ovarian cancer cell lines (n = 129), which were identified in our proposed molecular subtyping to be "more representative" for a given subtype (Figs. 1.3B and 1.8A) (Tan et al, 2013). To eliminate any possible technical differences inherent among the different collection sites, the strong batch-effect among the independent datasets was removed by ComBat (Fig. 1.1).

On average, the expression level of both *TUBGCP4* and *NAT10* is significantly, but only slightly higher in Stem-A clinical tumours than in non-Stem-A clinical tumours (Figs. 4.1A and 4.1B). In ovarian cancer cell lines, similar findings were observed for *TUBGCP4* (Fig. 4.1C), but no significant enrichment of *NAT10* was observed (Fig. 4.1D). Though these observations suggest the relevance of *TUBGCP4* and *NAT10* in Stem-A EOC tumours, the differences in expression were modest. Moreover, drugs that can alter the

function of these two proteins are currently not available, and thus, we should also focus our attention on their associated pathway(s).

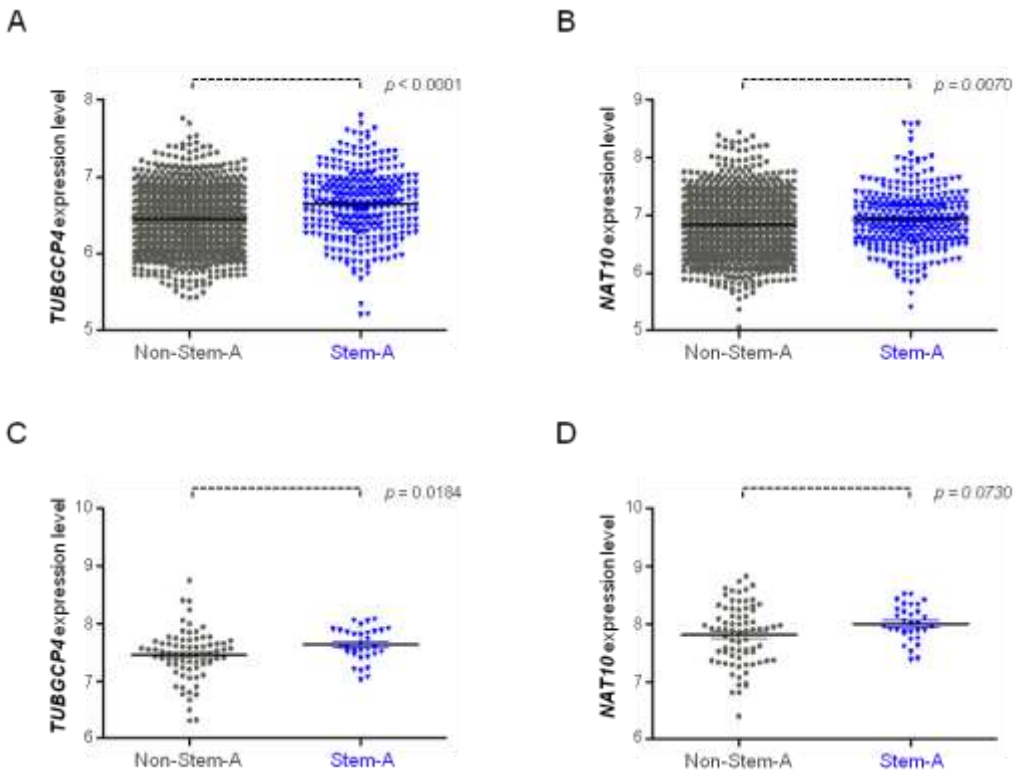

Figure 4.1 Comparison of Stem-A specific genes expression in non-Stem-A and Stem-A subgroups of ovarian cancer.
Expression level of the two Stem-A specific growth-promoting genes, *TUBGCP4* and *NAT10* were examined in 1,142 core samples of ovarian clinical tumours (A and B) and 129 core samples of cell lines samples (C and D). Differences in the gene expression between non-Stem-A and Stem-A subgroups were statistically evaluated with Mann-Whitney U-test in Graphpad Prism. Grey = non-Stem-A subgroup; blue = Stem-A subgroup.

4.2.2 Identification of pathways that mediate effects of Stem-A specific genes

Identification of *TUBGCP4* and *NAT10* as Stem-A specific genes prompted us to explore the mechanisms, through which the growth-promoting effects are mediated in Stem-A subtype (Figs. 3.10 and 4.2). Each of the Stem-A specific genes was silenced by siRNAs in 3 ovarian cancer cell lines, representing Epi-A, Mes and Stem-A subtypes (Epi-A: OVCA433; Mes: HeyA8; and Stem-A: PA-1). Following which, changes in the transcriptome resulting from the gene silencing were analysed to identify which pathways were affected.

Quantitative analyses confirmed that all siRNA transfection experiments produced significant and appropriate knockdown of these two genes with 71.0 ~ 92.6 (median 84.8) % efficacy (Fig. 4.3). Using 6,769 gene sets that were downloaded from Molecular Signature Database (MSigDB) version 3.0 (Subramanian et al, 2005), single sample gene set enrichment analysis (ss-GSEA) was utilised to compute enrichment scores for all samples (Verhaak et al, 2010). The enrichment score indicates the degree of enrichment of genes in a gene set as compared to those genes outside the gene set (Verhaak et al, 2010), and thus, reflects the activity of the associated pathway in a sample. As such, changes in enrichment scores reveal the effect of gene silencing on a pathway. From this pathway analysis, we detected 425 gene sets to be commonly altered across the three cell lines (Fig. 4.4; Appendix II). As one of the components required for microtubule nucleation (Fava et al, 1999), gene targeting of *TUBGCP4* resulted in down-regulation of the "Microtubule" gene set in the transcriptome (Fig. 4.4), indicating that this

approach can connect a gene with a pathway as expected from the biological function of the gene.

We next focused on differential pathway alterations as a consequence of gene silencing among the three cell lines. The pathway analysis revealed several PA-1 specific down-regulation gene sets with notable enrichment in metabolism-related gene sets (Fig. 4.5). To better identify pathways that link these two genes with PA-1 growth promotion, we surveyed for PA-1-specific down-regulated gene sets that overlapped with the ones that were distinctly enriched in the cell lines expression data of Stem-A subtype (Fig. 1.9). In total, 91 gene sets were found overlapped, and of these, 23 gene sets recurred between the two genes (Fig. 4.5; Appendix III). Unfortunately, apart from the recurrence of some mitochondria-related pathways such as “Mitochondria Membrane” and “Heme Biosynthetic Process”, no other notable regulatory pathways were found.

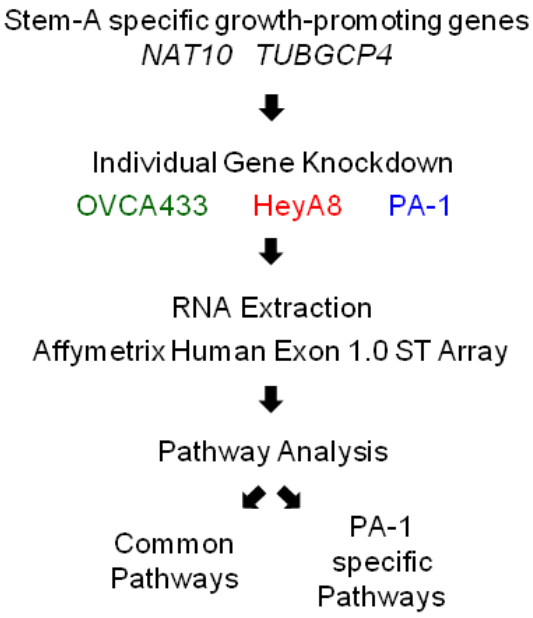

Figure 4.2 Experimental strategy for the identification of pathways affected by silencing Stem-A specific genes.
A schematic of the experiment to identify pathways linked to the growth-promoting effects of Stem-A specific genes, *TUBGCP4* and *NAT10*. Genes were individually silenced in OVCA433 (Epi-A), HeyA8 (Mes) and PA-1 (Stem-A) by siRNAs. Changes in mRNA transcription were measured by expression microarray, and subsequently subjected to pathway analysis to identify common and PA-1 specific altered pathways. Green = OVCA433 (Epi-A), Red = HeyA8 (Mes), Blue = PA-1 (Stem-A).

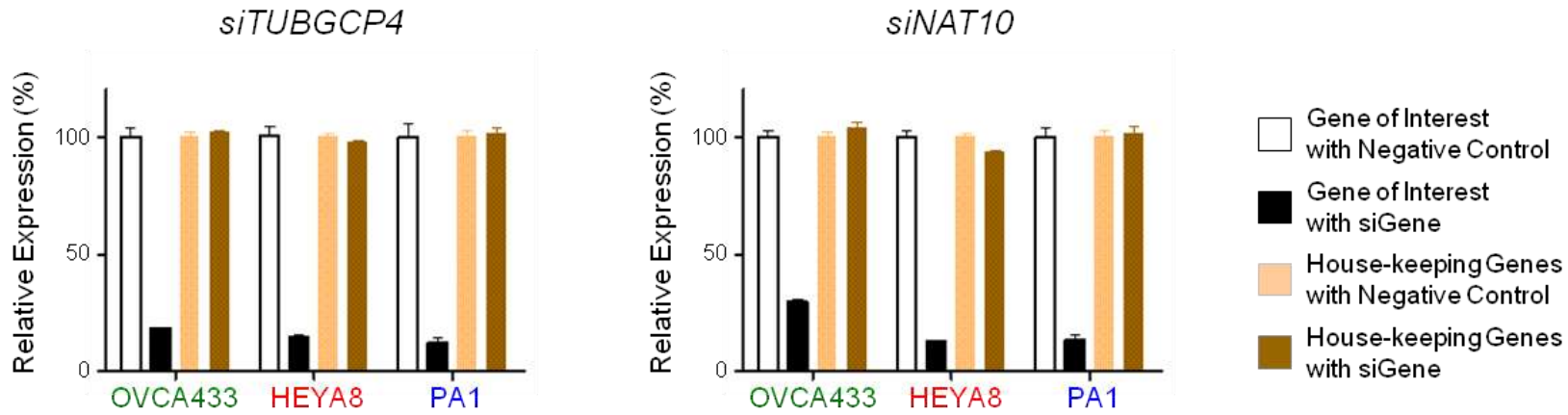

Figure 4.3 Quantitative analysis of Stem-A specific genes silencing by siRNAs.
Effect of silencing each of the two Stem-A specific genes on the relative gene expression in the three cell lines (OVCA433, HeyA8 and PA-1). Bar plots indicate the expression of genes of interest with Non-Targeting siRNA (negative control) (white bar) and siRNA targeting the gene of interest (si"Gene"; black bar), and the averaged expression of house-keeping genes (*ACTB, B2M, GAPDH, HPRT1, PGK1, PGK2, PPP1CA, RPL13A, TBP, TFRC*) with Non-Targeting siRNA (negative control) (pink bar) and siRNA targeting the gene of interest (brown bar). Error bar indicates SEM of three independent triplicate experiments. Green = OVCA433 (Epi-A), Red = HeyA8 (Mes), Blue = PA-1 (Stem-A). Tan et al (2013).

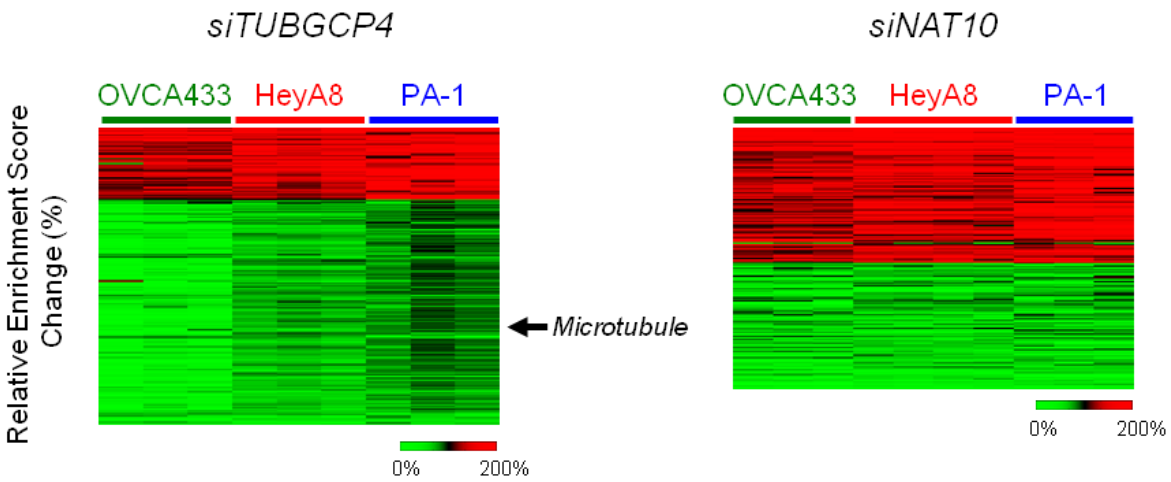

Figure 4.4 Common altered pathways arisen from individual Stem-A specific growth-promoting genes knockdown.
Common pathways in response to knockdown of the two Stem-A specific genes, *TUBGCP4* (Left panel) and *NAT10* (Right panel). Heatmaps show the relative change in ss-GSEA enrichment scores (si"Gene" versus siNon-Targeting negative control). Position of the *Microtubule* gene set is indicated to the right. List of commonly altered pathways can be found in Appendix II. Red = increased activity; green = decreased activity. The bar on top of the heatmap indicates triplicates or quadruplicates of OVCA433, HeyA8 and PA-1 cells. Green = OVCA433 (Epi-A), Red = HeyA8 (Mes), Blue = PA-1 (Stem-A). Tan et al (2013).

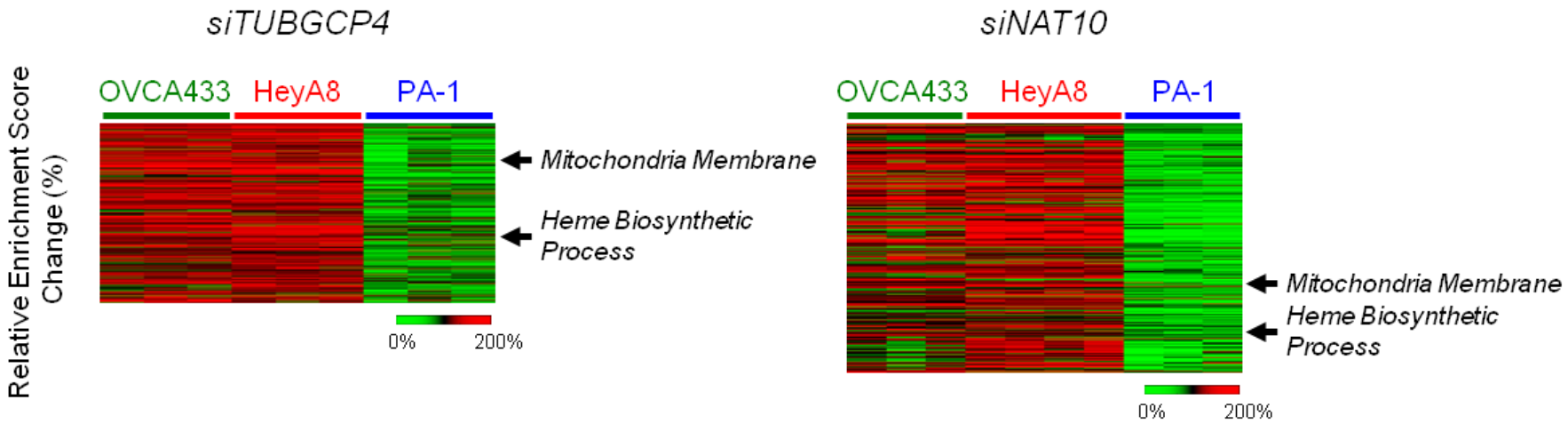

Figure 4.5 PA-1 specific altered pathways arisen from individual Stem-A specific growth-promoting genes knockdown. PA-1 specific down-regulated pathways in response to knockdown of the two Stem-A specific genes, *TUBGCP4* (Left panel) and *NAT10* (Right panel). Heatmaps show the relative change in pathway activities of ss-GSEA enrichment scores (si"Gene" versus siNon-Targeting negative control). Positions of the recurrent gene sets, *Mitochondria membrane* and *Heme biosynthetic process* are indicated to the right. List of PA-1 specific down-regulated pathways that were also distinctly enriched in the cell lines expression data of Stem-A subtype can be found in Appendix III. Red = increased activity; green = decreased activity. The bar on top of the heatmap indicates triplicates or quadruplicates of OVCA433, HeyA8 and PA-1 cells. Green = OVCA433 (Epi-A), Red = HeyA8 (Mes), Blue = PA-1 (Stem-A).

4.2.3 Analysis of microtubule/tubulin-related pathway activity in ovarian tumours and cell lines

As mentioned in Section 3.3, TUBGCP4 is a component of γ-tubulin ring complex that is involved in the nucleation of tubulin dimers in the cell (Fava et al, 1999; Goshima et al, 2008; Guillet et al, 2011; Moritz et al, 1995), while NAT10 is reported as a possible acetyl transferase of γ-tubulin that may be involved in the stabilisation of microtubules (Hubbert et al, 2002; Shen et al, 2009). In addition, silencing of the Stem-A specific gene, *TUBGCP4* also resulted in a down-regulation of the *Microtubule* gene set in the transcriptome across Epi-A, Mes and Stem-A cell lines (Fig. 4.4; Appendix II). As such, the selective effect of si*TUBGCP4* or si*NAT10* on Stem-A cell lines (Fig. 3.10) may suggest that pathways related to microtubules may be significantly relevant to Stem-A subtype as compared to other subtypes.

To investigate this possibility, we compiled all microtubule/tubulin-related gene sets (n = 19; Table 4.1) from Molecular Signature Database version 3.0 (Subramanian et al, 2005) and utilised them for ss-GSEA on ovarian clinical tumours and cell lines expression data. Again, the ss-GSEA was performed to estimate the activity of a gene set in a sample (Verhaak et al, 2010). Comparison of the ss-GSEA enrichment scores between Stem-A and non-Stem-A subgroups of clinical tumours, as well as cell lines revealed higher activity of microtubule/tubulin-related pathways in Stem-A than that in non-Stem-A subgroups ($p = 6.6\text{x}10^{-67}$ and $p = 2.1\text{x}10^{-6}$ by Mann-Whitney U-test, respectively; Fig. 4.6; Table 4.1). Of note, in our previous analysis of subtype-specific pathway enrichment, microtubule/tubulin-related gene sets were also found to be distinctly enriched in the Stem-A subtype (Figs. 1.7 and

1.9). Taken together, these observations suggested the possible importance of microtubule activity to Stem-A cells.

Table 4.1 Microtubule/tubulin-related gene sets.

		Stem-A vs Rest, Mann Whitney *p* - value	
Index	**Gene set**	**Clinical Sample**	**Cell Line**
1	BETA_TUBULIN_BINDING	5.2×10^{-17}	0.0242
2	TUBULIN_BINDING	3.0×10^{-54}	1.1×10^{-06}
3	MICROTUBULE	2.0×10^{-51}	8.6×10^{-05}
4	MICROTUBULE_ASSOCIATED_COMPLEX	1.8×10^{-63}	0.0043
5	MICROTUBULE_BASED_MOVEMENT	2.2×10^{-53}	8.4×10^{-06}
6	MICROTUBULE_BASED_PROCESS	4.0×10^{-34}	0.0003
7	MICROTUBULE_BINDING	1.7×10^{-49}	2.2×10^{-06}
8	MICROTUBULE_CYTOSKELETON	3.3×10^{-67}	0.0004
9	MICROTUBULE_CYTOSKELETON_ORGANIZATION_AND_BIOGENESIS	6.6×10^{-42}	0.0079
10	MICROTUBULE_MOTOR_ACTIVITY	8.8×10^{-49}	5×10^{-07}
11	MICROTUBULE_ORGANIZING_CENTER	2.6×10^{-45}	0.0003
12	MICROTUBULE_ORGANIZING_CENTER_ORGANIZATION_AND_BIOGENESIS	1.3×10^{-36}	3.4×10^{-05}
13	MICROTUBULE_ORGANIZING_CENTER_PART	3.0×10^{-36}	3.0×10^{-06}
14	MICROTUBULE_POLYMERIZATION_OR_DEPOLYMERIZATION	9.4×10^{-44}	9.9×10^{-07}
15	BIOCARTA_AKAPCENTROSOME_PATHWAY	2.2×10^{-19}	0.0022
16	CENTROSOME	1.7×10^{-43}	0.0005
17	CENTROSOME_CYCLE	2.4×10^{-19}	0.9382
18	CENTROSOME_ORGANIZATION_AND_BIOGENESIS	1.5×10^{-30}	2.6×10^{-05}
19	KINETOCHORE	1.3×10^{-35}	0.0003

Enrichment score difference is significant at $p < 0.05$ and is highlighted in red.

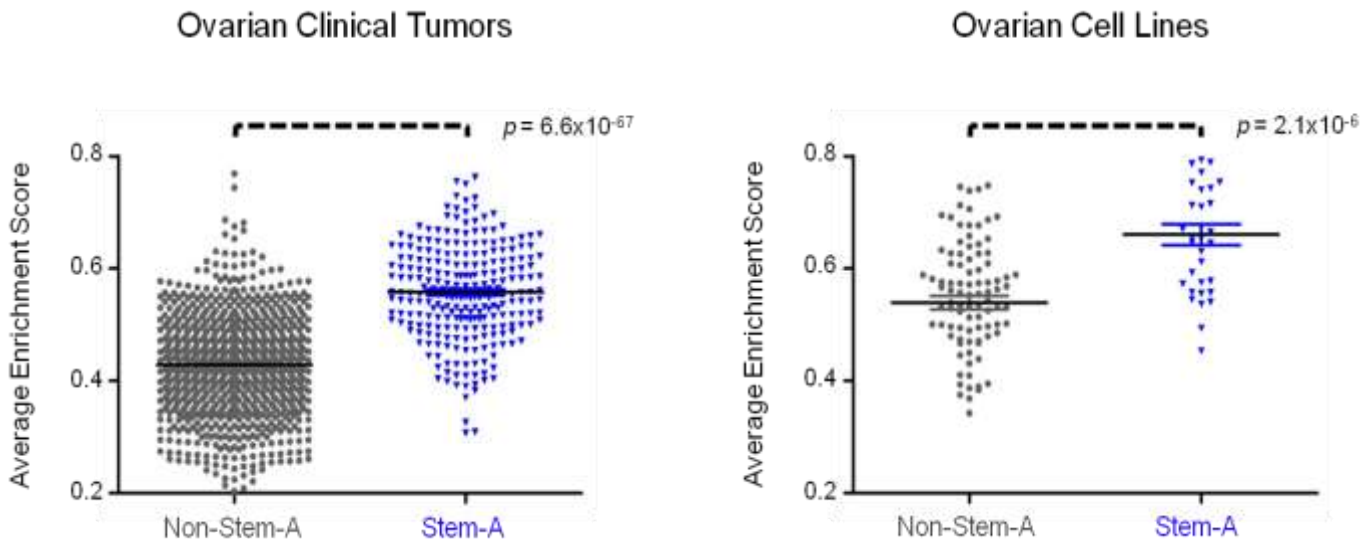

Figure 4.6 Comparison of microtubule/tubulin-related pathways in non-Stem-A and Stem-A subgroups of ovarian cancer. Estimated microtubule activity in non-Stem-A and Stem-A subgroups of ovarian cancer. Microtubule activity in 1,142 core samples of ovarian clinical tumours (Left panel) and 129 core samples of cell lines samples (Right panel) was estimated based on the average single sample gene set enrichment analysis (ss-GSEA) enrichment score of 19 microtubule/tubulin-related gene sets (Table 4.1) acquired from GSEA databases. Differences in microtubule activity between non-Stem-A and Stem-A subgroups were statistically evaluated with Mann-Whitney U-test in Graphpad Prism. Grey = non-Stem-A subgroup; blue = Stem-A subgroup. Tan et al (2013).

4.2.4 Investigation of the susceptibility of Stem-A cells to microtubule-targeted agents

The dependencies of Stem-A cell lines to genes associated with microtubules— *TUBGCP4* and *NAT10* (Fig. 3.10), as well as the comparatively high microtubule activity in Stem-A tumours and cell lines (Fig. 4.6), may suggest that the Stem-A cells are more susceptible to mitotic inhibition than cells of other subtypes. These findings prompted us to examine the *in vitro* sensitivity of Stem-A cells to microtubule-targeted agents such as paclitaxel, vincristine and vinorelbine. For this purpose, a panel of 18 ovarian cancer cell lines (12 non-Stem-A: OVCA433, OVCA429, OVCAR-8, PEO1, OVCA432, OVCA420, HeyA8, HEY, HeyC2, SKOV-3, ovary1847 and DOV 13; 6 Stem-A: PA-1, CH1, A2780, OVCAR-3, SKOV-4 and SKOV-6) was assayed for their growth inhibitory concentration of 50% (GI50; drug concentration for 50% growth inhibitory effects on cells) in at least three independent experiments. The Stem-A cell lines were found to be more sensitive to inhibitors of tubulin polymerisation, vincristine and vinorelbine (Lobert et al, 1996), than non-Stem-A cell lines (Figs. 4.7B and 4.7C). In contrast, paclitaxel, a drug that stabilizes microtubules (Manfredi & Horwitz, 1984), resulted in no significant distinction between the two subgroups (Fig. 4.7A).

The results were further confirmed by western blot analysis, whereby cells were treated with increasing concentrations of vincristine for 48-hours, and subsequently, immunoblotted for the presence of apoptotic activity (cleavage of PARP and Caspase 3). As expected, 48-hour vincristine treatment caused apoptosis in Stem-A cell lines at 1.2 nM (Fig. 4.8), whereas minimal or

no apoptosis was observed in non-Stem-A cell lines, even at 10 nM concentration (Fig. 4.8). Therefore, these findings provided evidence that drugs targeting tubulin polymerisation may be useful in treating patients with Stem-A EOC with poor clinical outcomes.

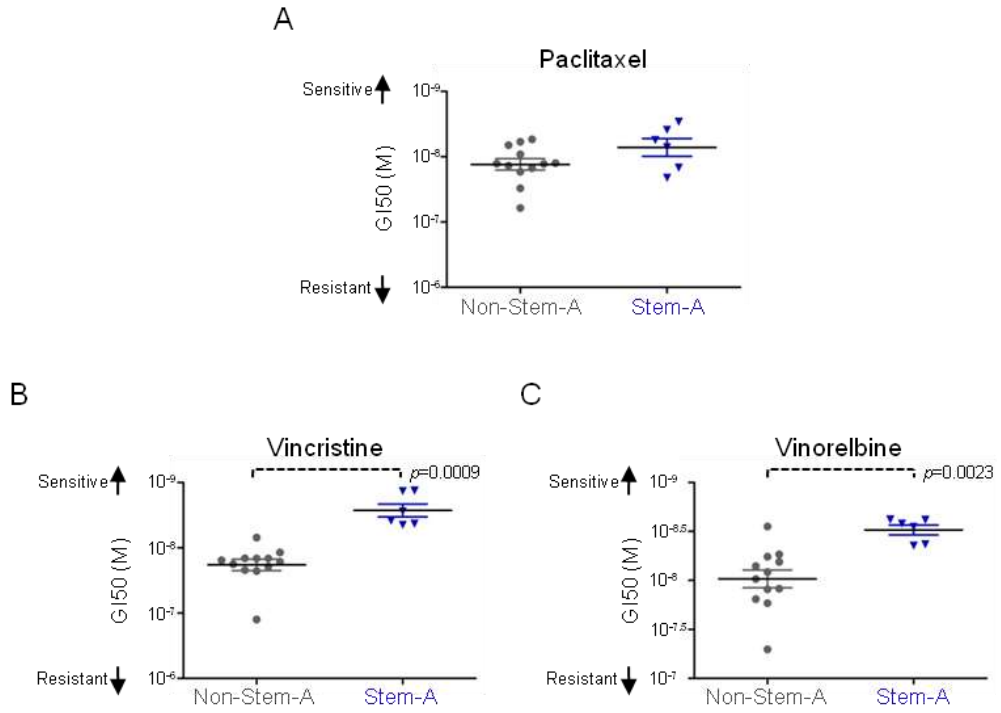

Figure 4.7 Susceptibility of Stem-A cells to microtubule assembly inhibitors.
Specificity of microtubule-targeted agents sensitivity in ovarian cancer cell lines. A panel of 18 ovarian cancer cell lines was classified into non-Stem-A (OVCA433, OVCA429, OVCAR-8, PEO1, OVCA432, OVCA420, HeyA8, HEY, HeyC2, SKOV-3, ovary1847 and DOV 13) or Stem-A (PA-1, CH1, A2780, OVCAR-3, SKOV-4 and SKOV-6) groups and analysed for their sensitivity to paclitaxel (A), vincristine (B) and vinorelbine (C). GI50 values were calculated with the results from cell proliferation assays for each cell type in three independent triplicate experiments, and the mean GI50s are shown as dot plots. A non-parametric Mann-Whitney U-test in Graphpad Prism was used to evaluate the results statistically. A higher value along the y-axis indicates increased sensitivity to the drugs. Stem-A cell lines were significantly more sensitive to vincristine and vinorelbine, but not to paclitaxel. Grey = non-Stem-A subgroup; blue = Stem-A subgroup. Tan et al (2013).

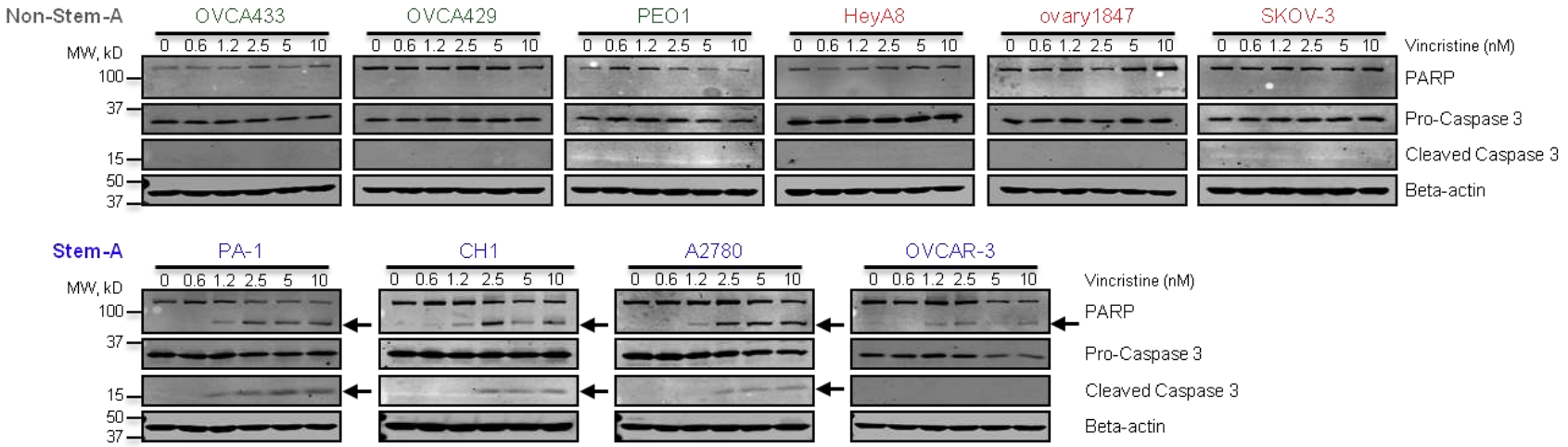

Figure 4.8 Western blot analysis of Stem-A cells sensitivity to microtubule assembly inhibitors.
Detection of apoptotic activity upon vincristine treatment. Six non-Stem-A (Upper panel) and four Stem-A (Lower panel) cell lines were subjected to increasing concentrations of vincristine (0 to 10 nM) for 48 h. The presence of apoptotic activity was determined by immunoblotting for cleaved PARP and Caspase 3, as indicated by arrows. Induction of apoptotic activity was only detected in Stem-A cell lines. Grey = non-Stem-A subgroup; blue = Stem-A subgroup. Tan et al (2013).

4.2.5 Correlation of Stem-A specific dependency with properties of Stem-A cell lines

All, if not most, microtubule-targeted agents are anti-mitotic agents that inhibit cell proliferation by binding to microtubules and suppressing microtubule dynamics (Dumontet & Jordan, 2010). And so, modifications of tubulin-microtubule complex that influence drug binding or the effects of drug binding, as well as alterations that perturb microtubule dynamics are likely to influence sensitivity to microtubule-targeted agents (Dumontet & Jordan, 2010; Gan et al, 2010). Thus, we sought to understand how the vulnerabilities of Stem-A cell lines to tubulin polymerisation inhibitory drugs (Figs. 4.7B and 4.7C) relate to various properties, such as the intrinsic dynamics of microtubules and microtubule structure.

To examine the intrinsic microtubule dynamics, we transfected EB3-RFP expressing plasmid into 3 ovarian cancer cell lines, representing Epi-A, Mes and Stem-A subtypes (Epi-A: OVCA433; Mes: HeyA8; and Stem-A: A2780). The expressed microtubule plus end binding fusion protein, EB3-RFP accumulated at the ends of growing microtubules, and served as a marker for visualising microtubule growth in live cells (Stepanova et al, 2003). Time-lapse images were acquired by total internal reflection fluorescence (TIRF) microscope, from which the movements of the RFP-fused protein along each individual microtubule were manually tracked. The results showed no significant differences in the average velocity of RFP-fused protein movements among the 3 cell lines (Figs. 4.9A and 4.9B), indicating that the susceptibility of Stem-A cells to tubulin polymerisation inhibitory drugs is probably not influenced by the intrinsic dynamics of microtubules.

We next investigated the integrity of microtubule and centrosome by immunofluorescent staining with alpha-tubulin and pericentrin antibodies, respectively. As an initial approach, only 3 ovarian cancer cell lines were examined (Epi-A: OVCA433; Mes: HeyA8; and Stem-A: A2780). In general, we did not observe any differences in microtubule structure or distribution among the 3 cell lines (Fig. 4.10). Conversely, abnormally-shaped or large centrosomes were observed in the Stem-A representative cell line, A2780, but not in the other 2 non-Stem-A cell lines (Fig. 4.10). These preliminary observations suggested a possible association between tubulin polymerisation inhibitory drugs sensitivity and centrosome abnormalities, but more studies will be needed to establish this association.

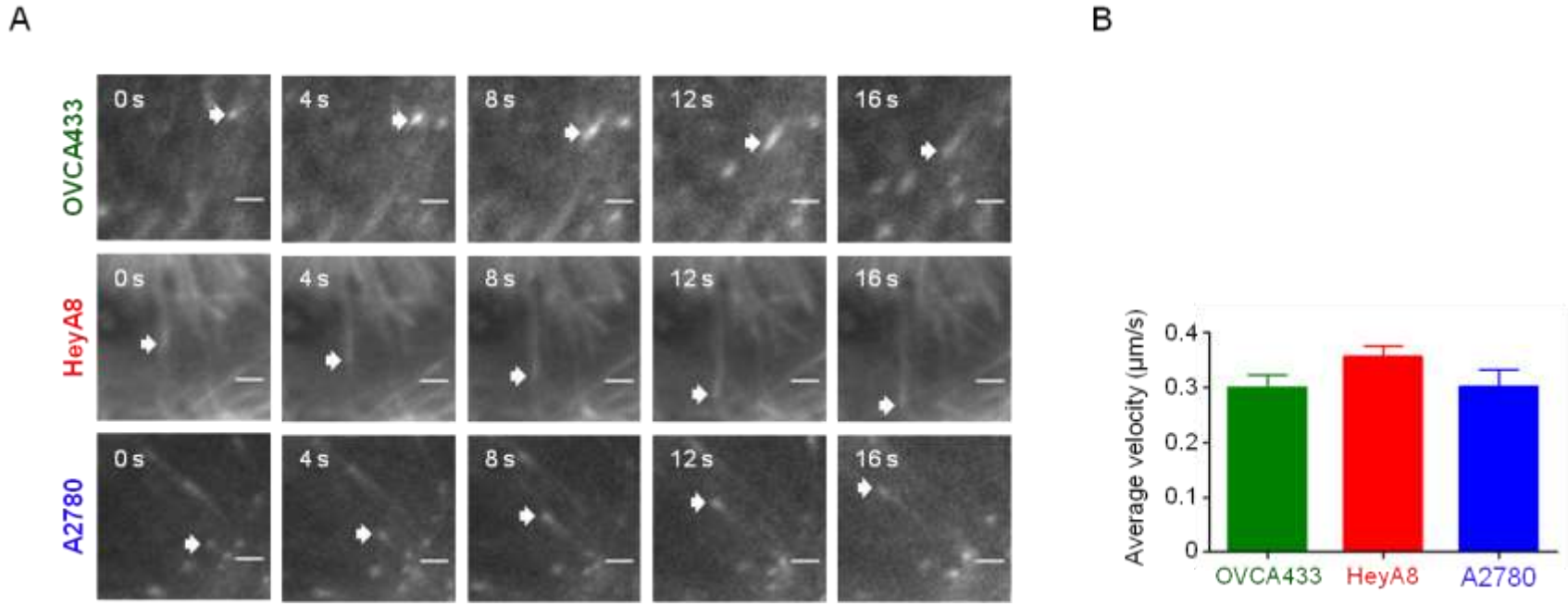

Figure 4.9 Analysis of microtubule dynamics in ovarian cancer cell lines.
A. Representative time-lapse sequences of EB3-RFP comets in OVCA433 (Epi-A; Top panels), HeyA8 (Mes; Middle panels) and A2780 (Stem-A; Bottom panels) cell lines. Cells expressing EB3-RFP, a plus end microtubule marker, were imaged with total internal reflection fluorescence (TIRF) microscope, at a 1 s time interval. Arrows indicate positions of marked EB3-RFP comets. Scale bars, 2µm. B. Quantifications of microtubule dynamics. The life history of at least 180 EB3-RFP comets (extracted from 6 independent cells) was manually tracked to determine the dynamic parameters for each cell lines. Bar plots indicate average velocity of EB3-RFP comets movements. Error bar represents the SEM of three independent experiments. No significant differences in microtubule dynamics was observed among the 3 cell lines. Green = OVCA433 (Epi-A); red = HeyA8 (Mes); blue = A2780 (Stem-A).

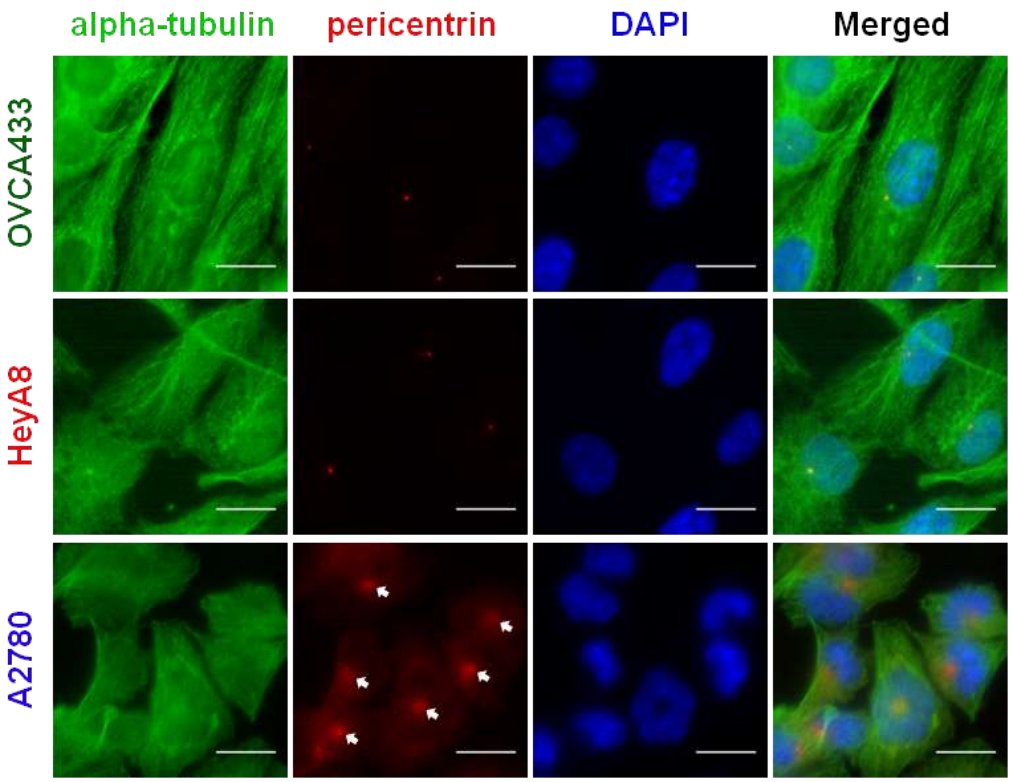

Figure 4.10 Immunofluorescence analysis of microtubule and centrosome integrity in ovarian cancer cell lines.
Representative immunofluorescence images for microtubule and centrosome in OVCA433 (Epi-A; Top panels), HeyA8 (Mes; Middle panels) and A2780 (Stem-A; Bottom panels) cell lines. Cells were fixed and immunostained with antibodies against α-tubulin (green) and pericentrin (red). DNA staining was performed with DAPI (blue). Images were taken using a laser scanning confocal microscope. Centrosome abnormalities were only observed in A2780 (Stem-A) cells, as indicated by arrows. Scale bars, 20μm.

4.3 Discussion

In the previous chapter, we identified *TUBGCP4* and *NAT10* in an unbiased genome-wide RNAi screen for genes that modulate proliferation and/or survival in a subtype-specific manner. In addition, the interrogation of these Stem-A specific genes across multiple ovarian cancer cell lines provided further evidences of the subtype-specific dependence. Therefore, we proceeded to evaluate the relevance of these genes and their associated pathway in ovarian clinical tumours. In particular, the poor-prognosis Stem-A subtype was found to exhibit elevated microtubule activity. Upon further investigation, Stem-A representative cell lines were found to be significantly more sensitive to several tubulin polymerisation inhibitor drugs, such as vincristine and vinorelbine than cell lines of other subtypes. Hopefully, these findings offer possible opportunities to improve therapeutics for epithelial ovarian carcinoma (EOC).

With the development of genome-wide analysis tools, bewilderingly large numbers of different epigenomic and genomic aberrations, which can be targeted for therapeutic benefit, are now being discovered. Such findings offer unprecedented opportunities for accelerating improvement of cancer therapeutics, but at the same time, presents a significant challenge for therapy development. It is not financially or logistically feasible to develop therapies targeting all these aberrations and also carry out clinical trials for them. This is especially true for EOC given the relatively low prevalence of the disease. Hence, a few criteria have been proposed to evaluate targets for cancer therapy development.

An ideal therapeutic target would be a driver protein or pathway that is uniquely up-regulated in target tumour with poor clinical outcomes (Garay & Gray, 2012). In addition, the target should also be druggable (Garay & Gray, 2012). Indeed, our present data provide evidence that *TUBGCP4* and *NAT10* are functionally relevant to the poor-prognosis Stem-A subtype (Chapter 3). Integrated analysis of the functional dependencies and the transcriptional profiles of ovarian clinical tumours revealed significant up-regulation of *TUBGCP4* and *NAT10* in the Stem-A subtype. However, it should be pointed out that the differences in expression were not convincingly high, and together with the lack of readily available specific drug inhibitors, *TUBGCP4* and *NAT10* are unlikely to be prioritised for therapy development. Therefore, in the next step, we switched from targeting individual genes to targeting pathway(s) that mediate the effects of *TUBGCP4* and *NAT10*.

In the integrated genomic analyses of high-grade serous ovarian carcinoma, the high frequency of de-regulated RB1 and PI3K/RAS signalling pathways were found to be driven by a diverse array of low prevalence genomic and epigenomic aberrations that vary between patients (The Cancer Genome Atlas Research Network, 2011). These observations indicate that pathway-targeted therapeutics could be a powerful alternative to target tumours or tumour subtypes. Unfortunately, attempts to identify effector pathway(s) of *TUBGCP4* and *NAT10* through the genome-wide transcriptional analysis were unsuccessful. On the other hand, the association of *TUBGCP4* and *NAT10* with microtubules prompted us to examine the microtubule/tubulin-related pathway, and we indeed found significantly high microtubule activity in the Stem-A subtype. Of note, Stem-A representative

cell lines were found to be specifically more susceptible to tubulin polymerisation inhibitory drugs, vincristine and vinorelbine, but not to the tubulin stabilising drugs, paclitaxel.

Both vincristine and vinorelbine are well-established chemotherapeutic agents that block cell proliferation by inhibiting microtubule assembly through its interaction with microtubule ends (Lobert et al, 1996). On the other hand, paclitaxel enhance microtubule polymerisation by binding to the inside surface of microtubule (Desai & Mitchison, 1997). As such, their diverse mechanisms of action could possibly account for their differential responses in EOC subtypes. In fact, these drugs have been approved for different cancer types. Paclitaxel is primarily employed in solid cancers, such as breast, ovarian and gastro-oesophageal, while vincristine and vinorelbine are most often used for haematological malignancies, such as lymphomas and leukaemia (Stanton et al, 2011).

Further investigations on cellular properties found a Stem-A cell line with centrosomal abnormalities, suggesting a possible association with tubulin polymerisation inhibitory drugs sensitivity. Centrosomal abnormalities have been identified in many different tumours, including ovarian carcinoma, and their prominence often correlates with poor clinical outcome (Chan, 2011; Nigg, 2006). However, it remains unclear whether these abnormalities can account for the Stem-A susceptibility to vincristine and vinorelbine, and also whether these abnormalities can also be found in other Stem-A cells. Hence, it should be noted that these findings are, at best preliminary, and more work is needed.

So far, the molecular mechanisms linking *TUBGCP4* or *NAT10* with Stem-A growth remains to be elucidated. Nevertheless, the susceptibility to vincristine and vinorelbine underscores the possible importance of tubulin polymerisation in Stem-A cells. However, they are not standard chemotherapeutic reagents for the treatment of EOC, unlike paclitaxel (Armstrong et al, 2006; McGuire et al, 1996). The molecules implicated in the tubulin polymerisation pathway may provide us with a potential platform to more effectively target Stem-A ovarian cancer, and hopefully improve the survival of these patients.

CHAPTER 5

GENOME-WIDE FUNCTIONAL SCREEN FOR CISPLATIN RESISTANCE CANDIDATE GENES

5.1 Introduction

Although therapeutic strategies that could be matched with the characteristics of individual patients are promising, progression free survival of epithelial ovarian carcinoma (EOC) could also be improved by circumventing platinum resistance. Hence, in this second part of the thesis, we attempt to address the critical issue of chemoresistance in EOC.

Platinum derivatives, such as cisplatin and carboplatin, play a central role as a first-line treatment option in EOC, and are usually administered together with taxanes. Although EOC is a relatively chemosensitive disease, approximately 20% of patients present platinum-refractory disease (Cannistra, 2004). Moreover, a large fraction of the patients who initially experience therapeutic success, suffer from relapse within a window of months to years, and the relapsed tumours typically acquire resistance to platinum (Coleman et al, 2013; Vaughan et al, 2011). Thus, intrinsic and acquired platinum resistance are among the major reasons for the low survival of EOC, and overcoming platinum resistance will allow patients to achieve more durable response to therapy.

Previous studies have classified the mechanisms of cisplatin resistance into two main categories: the first, prevention of platinum-DNA adducts

formation and the second, impairment in activation of apoptotic response following adducts formation (Galluzzi et al, 2012). The former category can be mediated through decreased uptake, increased detoxification and export of platinum and elevated DNA repair, while the latter category can occur as a consequence of defective apoptotic signal transduction and activation of pro-survival pathways. At present, this knowledge is yet to be translated into clinical practice (Vaughan et al, 2011). Hence, circumventing platinum resistance remains a critical goal for ovarian cancer therapeutics.

One approach for the identification of novel combination therapies that can circumvent platinum resistance is the use of a genome-wide RNAi screen. Such RNAi screens have proven to be a powerful approach in identifying both drug resistance mechanisms and enhancers of drugs activity, from which strategies to counter resistance can be developed (Berns & Bernards, 2012). The use of these screens to identify novel drug enhancers has been exemplified by the discovery that suppression of *ATP6V0D2*, a subunit of the vacuolar ATPase led to enhanced sensitivity of non-small cell lung cancer (NSCLC) cell lines to paclitaxel (Whitehurst et al, 2007). In particular, treatment of NSCLC lines with a vacuolar ATPase inhibitor, RTA203 in combination with paclitaxel revealed a significant collaborative impact on viability (Whitehurst et al, 2007). Moreover, the genome-wide RNAi screen that we presented in Chapter 3 also illustrated the strong predictive power of such screens for identification of potential therapeutic targets.

Therefore, in this chapter, we performed a genome-wide loss-of-function screen to identify molecular targets that, when inhibited, would

enhance the sensitivity of cells to cisplatin. Following extensive validation of the top hits, we identified six genes, including *ABCC3, KCNH3, KCNN1, MLH1, MRPL3* and *RPS6KA1* as cisplatin resistance candidate genes. In addition, combination of a RPS6KA1 specific inhibitor, SL0101 with cisplatin was shown to render cells more sensitive to cisplatin.

5.2 Results

5.2.1 Genome-wide functional screen for cisplatin resistance candidate genes

Similar to our screen for subtype-specific growth-promoting genes (Chapter 3), genes relevant to cisplatin resistance were also investigated via genome-wide screens using the pooled The RNAi Consortium (TRC) lentiviral shRNA library (Moffat et al, 2006; Root et al, 2006). Compared to the functional screen in Chapter 3, the screen presented herein was designed to identify gene targets that upon suppression by shRNA further reduce cell viability as otherwise expected at a sub-lethal cisplatin concentration. Such genes are likely to be involved in cisplatin resistance mechanisms, and can be targeted to increase the cisplatin sensitivity of resistant cells. Hence, these genes will be denoted as cisplatin resistance candidate genes.

Growth inhibitory concentration of 50% (GI50; drug concentration for 50% growth inhibitory effects on cells) of cisplatin for a panel of 46 ovarian cancer cell lines spanned a wide range of concentrations, from 0.38 μM to 41.43 μM (Matsumura et al, 2011). Given its high GI50 value (22.58 μM;

median GI50 is 9.29 μM) and ease of handling, the cell line, OVCA433 was selected from this panel for the genome-wide functional screen.

The TRC library, as described in Section 3.2.1, contains 80,000 lentivirally expressing shRNAs, with 4 or more independent shRNAs targeting each of 16,000 human genes. In addition, each lentiviral vector encodes each shRNA expression cassette with the puromycin resistance gene, allowing the use of puromycin to isolate stable integrants.

The experimental strategy for this screen is shown in Fig. 5.1. OVCA433 cells were infected with the shRNA pools at a multiplicity of infection (MOI) of 0.3, to ensure the highest probability of having single shRNA integration into the host genome in each cell (Luo et al, 2008). Puromycin was then used to select for the presence of shRNA vectors. After selection, infected cells were split into two populations at a ratio of 1:2, of which the former population was left untreated and used as reference, while the latter population was treated with 11 μM cisplatin. This cisplatin dosage was previously known to inhibit OVCA433 cell growth by 50% after 5 days of culture, thus implying that the number of cells expressing shRNAs that are of no relevance to cisplatin would be the same in both populations. In particular, shRNAs that silence genes involved in cisplatin resistance mechanism(s), would upon cisplatin treatment, further limit the growth or viability of the cells into which they were introduced, resulting in the relative depletion of such shRNAs. Conversely, relative amplification of shRNAs suggests that they target genes that help to mediate the anticancer effect of cisplatin. Such genes will be denoted as cisplatin sensitizing genes. Therefore, by comparing

the abundance of each shRNA (shRNA copy number) in the cisplatin treatment population to that in the reference population, we can identify shRNAs that decreased or increased cell growth or viability in the presence of cisplatin, but to ignore shRNAs that were inherently toxic and have no synergistic relationship with cisplatin.

At the endpoint of the incubation, the genomic DNA was harvested from the resulting cells and integrated shRNA sequences were retrieved from the genome by PCR amplification using vector primers. PCR amplified DNAs were sequenced using highly parallel next generation sequencing and reads with perfect match to reference sequences that are provided by Sigma, were used to retrieve the copy number of each shRNA for each population. Comparison of the shRNA copy numbers between the two populations consequently reveals the relevance of each shRNA to cisplatin.

To define genes relevant to cisplatin, RNAi gene enrichment ranking (RIGER) analysis was used to identify genes that have more than one independent shRNAs relatively depleted or amplified in the cisplatin treatment population (Luo et al, 2008). RIGER takes into account all independent shRNAs targeting each gene in its analysis, and from there, calculates a normalised enrichment score (NES) for each gene. This analysis provides increased power to the screen, and compensates for any variation in gene silencing efficacy and possible ‘off-targets’ effects of each shRNA.

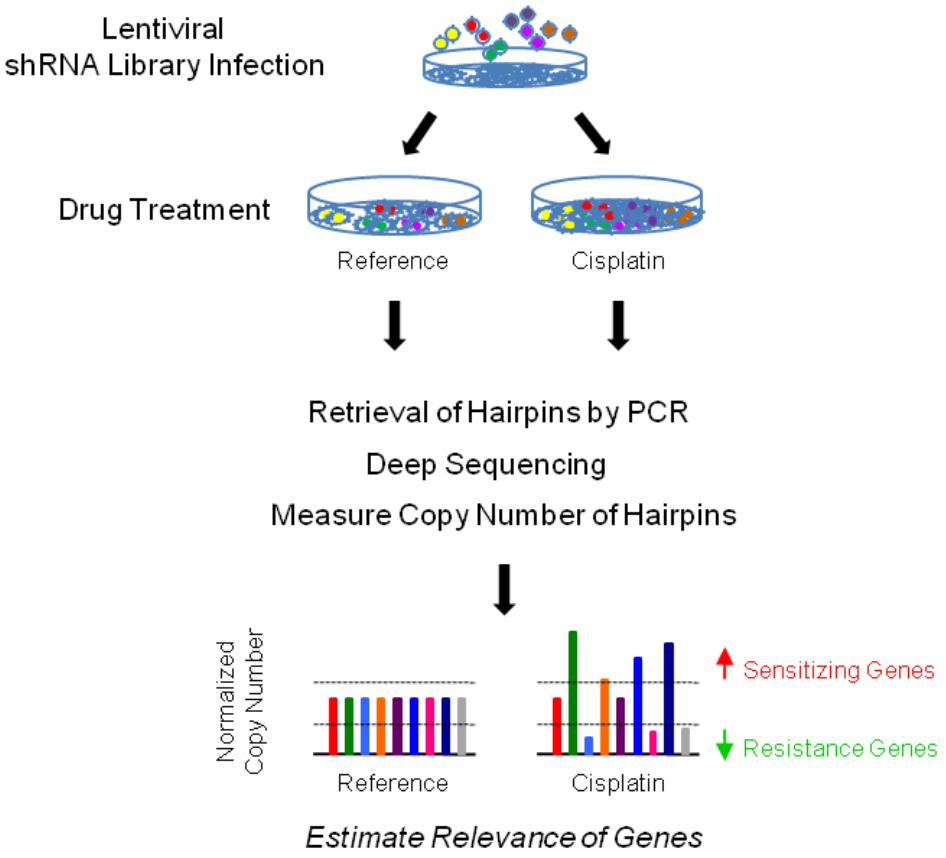

Figure 5.1 Experimental strategy of the genome-wide functional screen for cisplatin resistance candidate genes.
Schematic design showing the identification of genes with relevance to cisplatin. Genome-wide collection of shRNA vectors are introduced into OVCA433 cells in a pooled format. Infected cells were split into two populations: Reference and Cisplatin treatment. shRNAs that increase sensitivity of OVCA433 to cisplatin (Resistance genes) will be relatively depleted, while those that decrease cisplatin sensitivity (Sensitizing genes) are relatively amplified. Copy numbers of shRNAs are retrieved by PCR amplification and subsequent sequencing approach. Depleted and amplified shRNAs can be identified by comparing the shRNA copy numbers from both populations.

5.2.2 Identification of cisplatin resistance candidate genes

The primary aim of the screen presented herein was to identify genes that, when inhibited, would render OVCA433 cells more sensitive to cisplatin. Figure 5.2 showed the abundance of the shRNA vectors in both the reference and cisplatin treatment cell populations. To determine the concordance among the technical replicates, we employed spearman correlation analysis in the reference (Spearman *rho* = 0.6059) and the cisplatin treatment populations (Spearman *rho* = 0.6551). Similar to our previous screen (Section 3.2.2), the concordance was not perfect; this approach would need further improvement. Nevertheless, distinct differences in the shRNA copy numbers can still be observed between the two cell populations.

Through RIGER analysis, we identified relatively depleted shRNAs targeting 96 genes (Fig. 5.2; Appendix IV), with high significance ($q < 0.005$) and Hairpin Score (> 0.5). These indicated that shRNA silencing of these genes decreased cell viability in the presence of cisplatin. It is possible that these genes are involved in cisplatin resistance mechanisms, and are thus, denoted as cisplatin resistance candidate genes. Conversely, relatively amplified hairpins targeting 78 genes (Fig. 5.2; Appendix IV) that may be involved in cisplatin response were identified. Viability of cisplatin-treated cells increased when these genes were silenced, implying that their increased abundance might augment the sensitivity of OVCA433 to cisplatin. These genes are thus, denoted as cisplatin sensitizing genes.

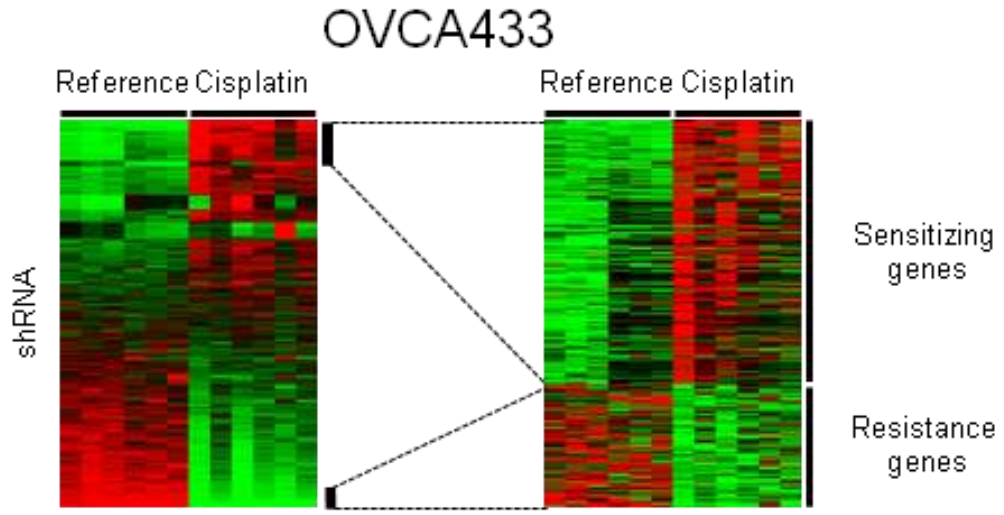

Figure 5.2 RIGER analysis of shRNA screen identifying cisplatin resistance candidate genes.
Heatmaps of centred and normalised copy numbers of all shRNAs retrieved after next-generation sequencing analysis (Left panel) and shRNAs with high significance ($q < 0.005$) and hairpin Score (> 0.5) in RIGER analysis (Right panel). Each row represents shRNA hairpin copy number and is sorted according to the hairpin score identified in RIGER (Luo et al, 2008). Red = higher; green = lower copy number counts.

5.2.3 Validation of cisplatin resistance candidate genes

The cisplatin resistance genes and the sensitizing candidate genes identified from our genome-wide screen (Fig. 5.2) are both potential targets for therapy. However, it is more difficult to develop therapies that enhance the function of a sensitizing gene than it is to suppress the activity of a cisplatin resistance candidate gene. In addition, most pharmacological agents inhibit rather than activate protein function. Therefore, we elected to focus on the cisplatin resistance candidate genes, of which 96 genes were chosen based on the *q*-value cut-off of 0.005 from RIGER analysis (Fig. 5.2).

To confirm that inhibition of these genes indeed sensitises cells to cisplatin, we performed the validation in a process that consisted of two steps (Fig. 5.3). First, we performed a second screen on OVCA433 cells using siRNAs, targeting each of the 96 cisplatin resistance candidate genes (Fig. 5.4A). Specifically, genes were individually silenced by siRNAs in 96-well format through the reverse transfection method (Ziauddin & Sabatini, 2001). Transfections were performed in octuplicate for quadruplicate analysis in the presence and the absence of cisplatin. A 72-hour exposure to 20 μM cisplatin was used as a sub-lethal dose that should only inhibit OVCA433 cell growth by approximately 50%. Cell viability was subsequently measured with the MTS assay after 72-hour cisplatin treatment (Fig. 5.4A). Each siRNA was assigned a viability ratio calculated as mean viability in cisplatin divided by mean viability in the absence of cisplatin. Cisplatin resistance candidate genes were identified as positive hits based on the *p*-value cut-off of 0.05 in a Student's *t*-test analysis comparing the viability ratio of silencing the gene of interest with that of the siRNA negative controls. Thus, in this second screen,

silencing of 16 genes was found to increase the sensitivity of OVCA433 cells to cisplatin (Fig. 5.4B; Table 5.1).

Finally, for the next step of the validation process (Fig. 5.3), we switched from siRNA to shRNA to further validate our observations using different sets of target sequences in the genes as well as to reduce possible off-target effects. OVCA433 cells were lentivirally transduced with individual shRNAs to establish stable integrants for each of the 16 genes identified from the second screen (Fig. 5.4B). Stable integrant established from shRNA targeting Luciferase (shLuciferase) was used as a negative control. These stable integrants were exposed to a range of doses of cisplatin, and assessed for viability after 3 days. Six of the stable integrants showed a shift in their dose-response curves (Fig. 5.5A-F), indicating that the expression of shRNAs targeting *ABCC3, KCNH3, KCNN1, MLH1, MRPL3* and *RPS6KA1*, sensitised OVCA433 cells to cisplatin. Indeed, GI50 values for these six stable integrants were at least twice lower than that of the shLuciferase control (Fig. 5.6A). The reliability of these six shRNAs to reduce expression of their respective genes was confirmed by quantitative RT-PCR analysis (Fig. 5.6B). Overall, these multiple stages of validation confirmed that silencing of *ABCC3, KCNH3, KCNN1*, *MLH1*, *MRPL3* and *RPS6KA1* rendered OVCA433 cells more sensitive to cisplatin.

Moreover, in the absence of cisplatin, expression of shRNAs targeting these six genes caused no more than 15% reduction in cell viability as compared to the negative control (shLuciferase) (Fig. 5.7), and also did not lead to changes in cell morphology. These observations suggested that the

increase in cisplatin sensitivity is unlikely to be indirectly caused by the effects of gene silencing on cell health.

Our finding of a member of the ATP binding cassette (ABC) transporter superfamily, *ABCC3* as a cisplatin resistance candidate gene is consistent with earlier reports which demonstrated their contributions to chemoresistance through the efflux of anticancer drugs from cancer cells (Borst et al, 2000; Gottesman et al, 2002; Januchowski et al, 2013). However, the discovery of six genes with seemingly diverse biological functions reflects the multi-factorial nature of cisplatin resistance (Coleman et al, 2013). Since all experiments were conducted in a single cell line, OVCA433, we have no idea whether the inhibition of these six genes can also render other ovarian cancer cell lines more sensitive to cisplatin, and thus, raising the possibility that the relevance of these genes to cisplatin resistance could be cell line-specific. As such, investigation of these genes in other cell lines is required.

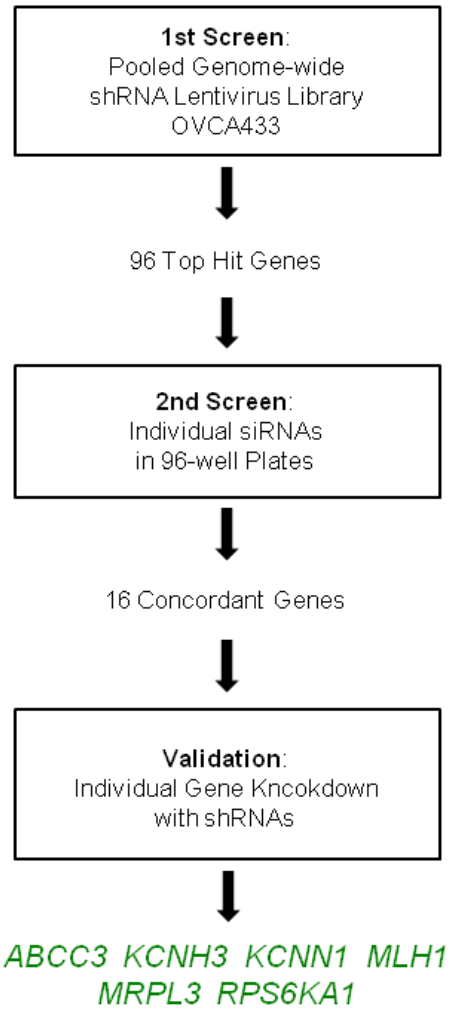

Figure 5.3 Schematics of cisplatin resistance candidate genes validation. Schematic of experiments validating the cisplatin resistance candidate genes identified from the genome-wide functional screen. This analysis led to the identification of six genes involved in the cisplatin resistance of OVCA433 cells: *ABCC3*, *KCNH3*, *KCNN1*, *MLH1*, *MRPL3* and *RPS6KA1*.

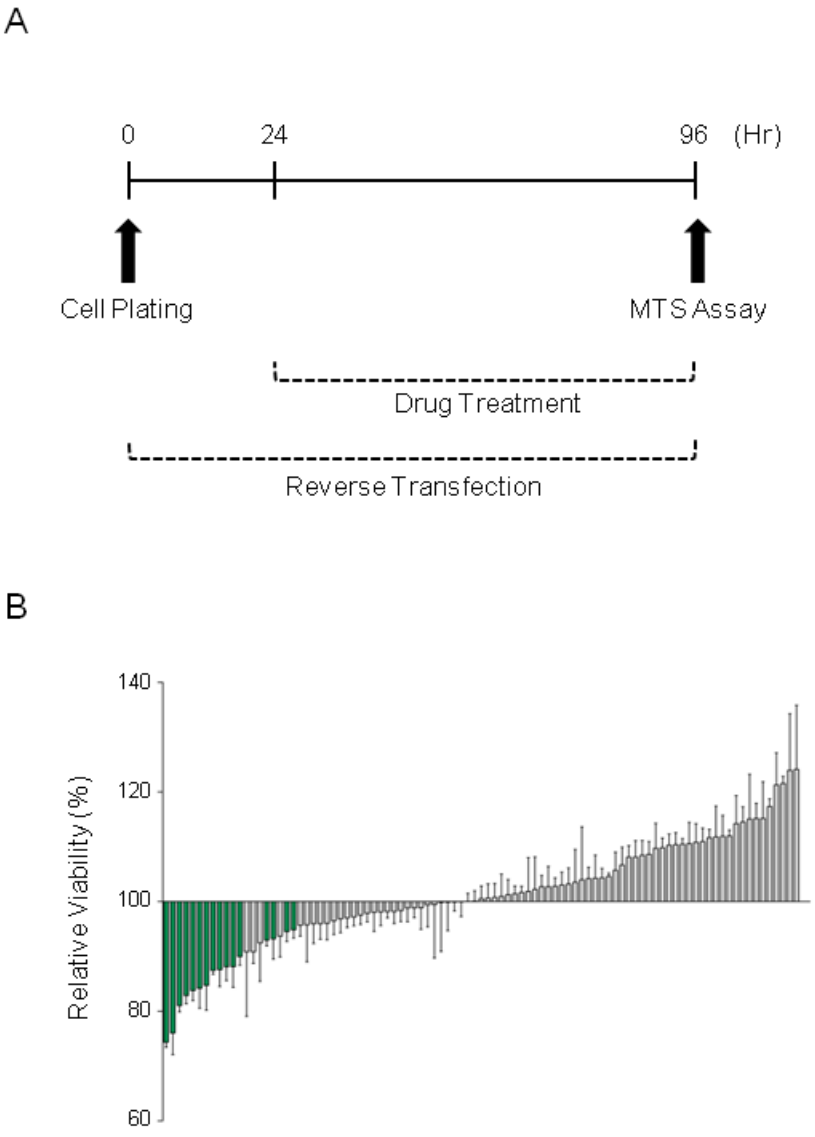

Figure 5.4 Second screen for cisplatin resistance candidate genes using siRNAs.

A. Timeline of assay performed for the second screen. B. Effects of individual siRNAs on the cisplatin sensitivity of OVCA433 cells. 96 cisplatin resistance candidate genes (Fig. 5.2) were silenced individually by siRNAs, and exposed to the presence and the absence of cisplatin. Each siRNA was assigned a viability ratio calculated as mean viability in cisplatin divided by mean viability in the absence of cisplatin. Bar plot indicates the viability ratio of siRNA relative to that of negative control siRNAs. Error bar indicates the SEM of three independent quadruplicate experiments. siRNAs with statistically significant relative viability (p-value < 0.05) in Student's t-test were shown as green. The second screen identified 16 siRNAs that enhanced the sensitivity of OVCA433 to cisplatin.

Table 5.1 List of cisplatin resistance candidate genes identified for validation.

Step	No. of Genes	Genes
Candidates identified by shRNA screen	96	*SLC5A1, RB1, PABPC4, SLC6A13, ANAPC11, SLC22A6, CAV3, AKR1B10, KCND1, ATP6V0A1, SLC22A1, TNFRSF8, NF2, TBL3, KCNN1, CLDN14, EXOC3, HIST1H4F, RIT2, RPS6KA1, MLH1, CATSPER3, VTI1A, KRTHA1, AP1M1, RPL7L1, XRCC4, SLC6A17, TNPO3, SLC23A2, CTAG2, CYB5R3, SLC27A5, ZNF510, FKSG30, MRPL3, LOC393062, SPTBN4, DUOX2, KIFC3, SLC5A12, ABCC3, MR1, VKORC1, RAB3GAP2, PPL, SLCO4C1, PEX5, SLC35E2, SLCO2A1, BIN1, ATP6V0D2, TRPC3, ATP6V0A2, CLCN1, AKAP8, KCNJ3, ST3GAL6, SLC35B1, RBM15, CKAP1, ZNF694, SLC25A17, ZNF546, ATP1B3, SCN4A, CKS1B, TRPV3, DUOX1, TPCN2, WDR57, HIST1H4B, KCNH3, CACNA2D1, INCENP, NMRAL1, AKAP13, TMEM16A, CBR1, DPP10, MYO15A, TNPO2, GPC3, ZNF418, SLC26A4, ACE, ART4, PODXL, SARS2, ARL6, AOF1, NDST3, SLC25A18, KCNN4, SSX9, PKIG*
Candidates identified by second screen	16	*MLH1, CATSPER3, TNPO3, KCNN1, RIT2, RPS6KA1, CYB5R3, SLC22A6, TNPO2, KCNH3, ABCC3, SLC23A2, ART4, MRPL3, AKAP13, PODXL*
Candidates identified by shRNA validation	6	*MLH1, RPS6KA1, KCNH3, KCNN1, MRPL3, ABCC3*

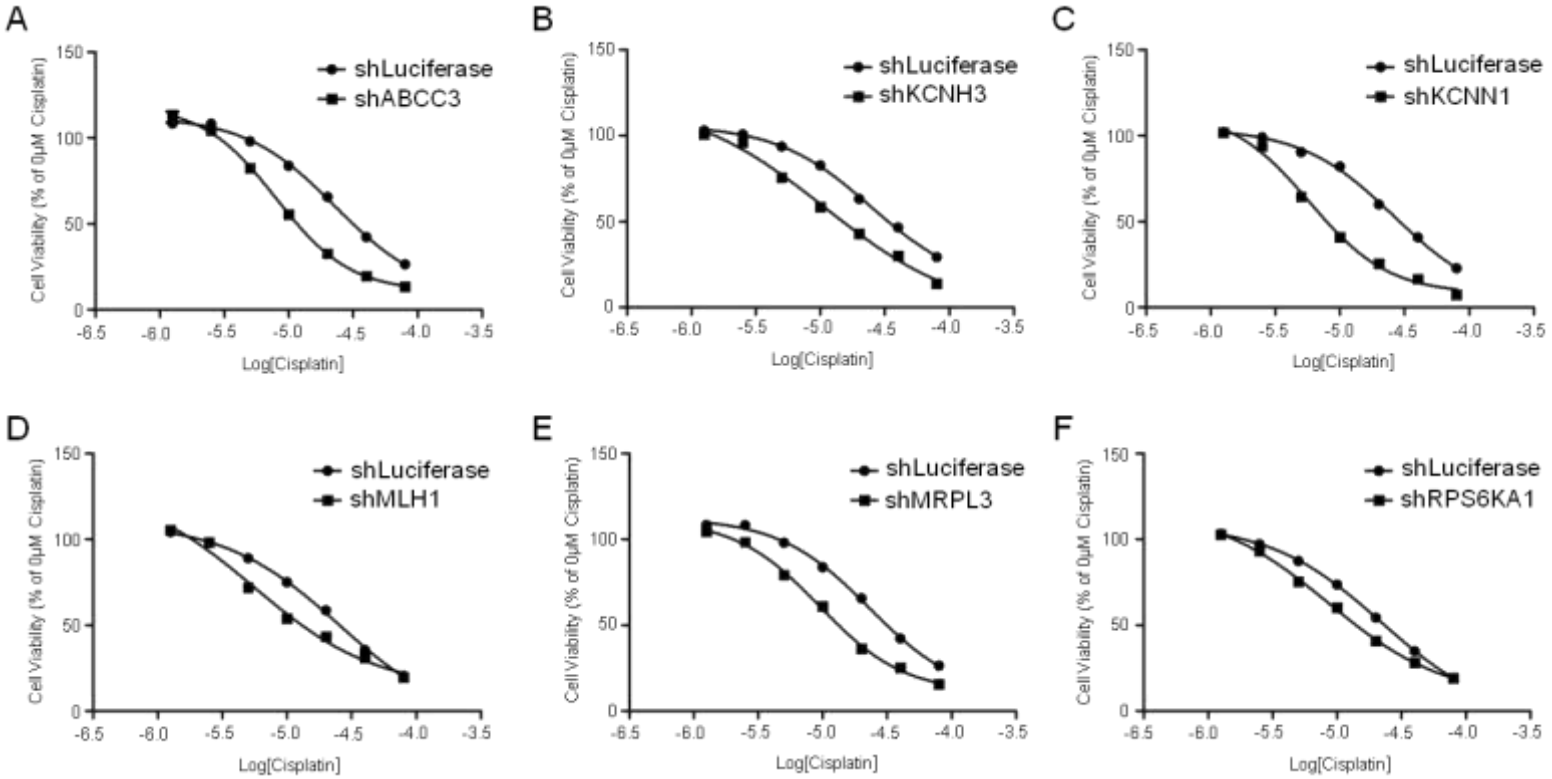

Figure 5.5 Dose-response curves of stable integrants expressing shRNAs against cisplatin resistance candidate genes. Stable integrants of OVCA433 established from shRNAs targeting *ABCC3* (A), *KCNH3* (B), *KCNN1* (C), *MLH1* (D), *MRPL3* (E) and *RPS6KA1* (F) were exposed to a range of cisplatin concentrations, and assessed for viability after 3 days. All six shRNAs, in comparison to control shRNA targeting luciferase, sensitised OVCA433 cells to cisplatin. Representative dose-response curves of three independent experiments are shown.

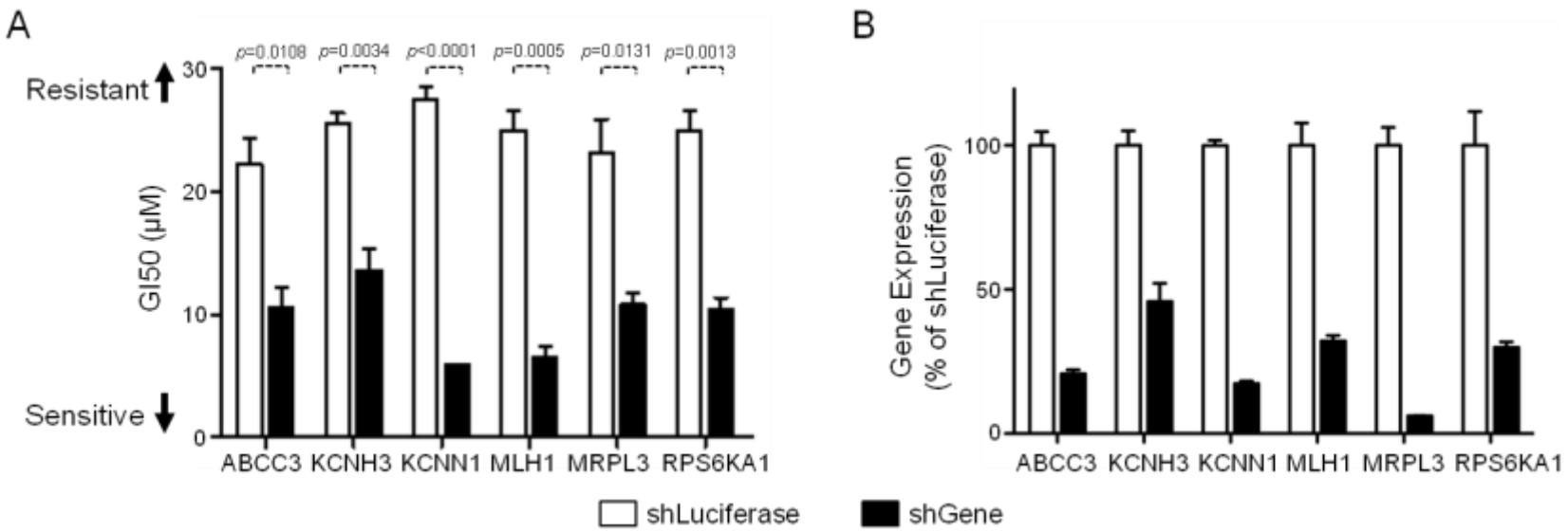

Figure 5.6 Effect of silencing cisplatin resistance candidate genes on cisplatin sensitivity.
A. Assessment of cisplatin sensitivity of stable integrants expressing shRNAs against *ABCC3, KCNH3, KCNN1, MLH1, MRPL3* and *RPS6KA1*. Averaged GI50 values of cisplatin for each stable integrants are shown as a bar plot and were statistically evaluated using Student's t-test. Error bar indicates SEM of three independent triplicate experiments. A higher value along the y-axis indicates decreased sensitivity to cisplatin. All six stable integrants were significantly more sensitive to cisplatin than control. White bar = control shRNA targeting luciferase (shLuciferase), Black bar = shRNA targeting gene of interest (sh"Gene"). B. Quantitative analysis of cisplatin resistance candidate genes silencing by shRNAs. Bar plots indicate the expression of genes of interest with control shRNA targeting luciferase (shLuciferase; white bar) and shRNA targeting the gene of interest (sh"Gene"; black bar). Error bar indicates SEM of three independent triplicate experiments.

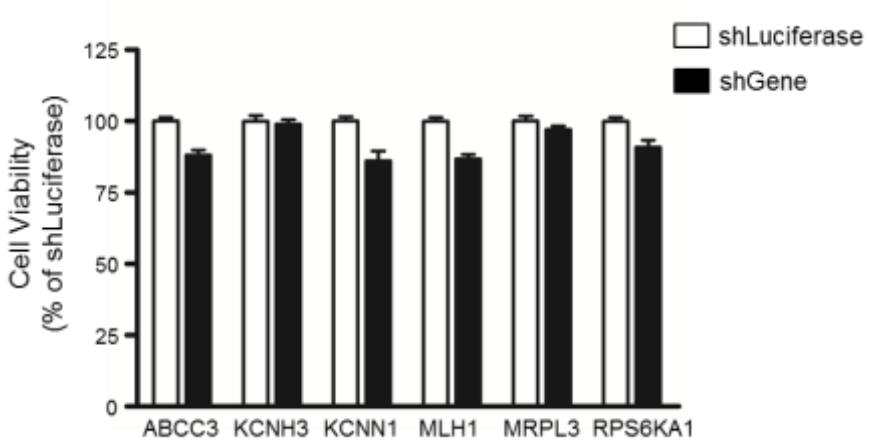

Figure 5.7 Effect of gene silencing on cell health.
Assessment of cell viability of stable integrants expressing shRNAs against *ABCC3, KCNH3, KCNN1, MLH1, MRPL3* and *RPS6KA1*. Bar plots indicate the cell viability of stable integrants (sh"Gene"; black bar), normalised against the negative control (shLuciferase; white bar). Error bar indicates SEM of three independent triplicate experiments. In the absence of cisplatin, none of the six stable integrants showed more than 15% reduction in cell viability.

5.2.4 RPS6KA1 as a target in cisplatin resistance

The availability of a specific RPS6KA1 inhibitor, SL0101 prompted us to further validate the relevance of RPS6KA1 to cisplatin resistance across multiple ovarian cancer cell lines. SL0101 is a flavonoid glycoside (kaempferol 3-O-(3”,4”-di-O-acetyl-α-L-rhamnopyranoside)) which was isolated from the extract of the tropical plant *Forsteronia refracta* (Smith et al, 2005). Its ability to inhibit RPS6KA1 kinase activity was initially discovered through a high throughput ELISA screen (Smith et al, 2005). Subsequent *in vitro* kinase assays with a panel of 71 protein kinases demonstrated the specificity of SL0101 to RPS6KA1, as well as to another member of the p90 ribosomal S6 kinase (RSK) family, RPS6KA3 (Bain et al, 2007). Conversely, AURKB and PIM3 were inhibited with slightly lower potency and other protein kinases in the panel were unaffected (Bain et al, 2007). The interaction of SL0101 with RSK was further shown by the crystallographic model of SL0101 in complex with the amino-terminal kinase domain of RPS6KA3 (Utepbergenov et al, 2012). Of note, SL0101 was proven to be an effective RPS6KA1 inhibitor in intact cells (Smith et al, 2005). Moreover, MCF-7 cells that are dependent on the RSK pathway were found to be susceptible to growth inhibition by SL0101, in accordance with its function as a RSK-specific inhibitor (Smith et al, 2005). Taken together, SL0101 can be a useful tool for analysing the role of RPS6KA1 in cisplatin resistance.

Accordingly, the GI50 values of cisplatin for a panel of 10 ovarian cancer cell lines (OVCA433, OVCA429, RMG-II, OVCAR8, JHOS-2, PA-1, CH1, IGROV-1, TOV-112D and OVCAR-10) was determined in the presence of vehicle or 40 μM SL0101. Though SL0101 exhibited high affinity for

RPS6KA1 in *in vitro* kinase assay (Smith et al, 2007), it was observed that such high concentration of SL0101 is required to elicit phenotypic responses of intact cells to SL0101-induced RSK inhibition (Smith et al, 2005). Inhibition of RPS6KA1 kinase activity by SL0101 indeed sensitised 5 cell lines in the panel, including OVCA433 to cisplatin (Fig. 5.8A). Moreover, the reduction in GI50 values for SL0101-treated OVCA433 cells was comparable with our previous findings using RPS6KA1-specific shRNA (Figs. 5.6A and 5.8A). These results confirmed RPS6KA1 as a cisplatin resistance candidate gene and showed that its relevance to cisplatin resistance was not limited to OVCA433 cells. At the same time, the fact that only 5 out of 10 cell lines showed reduction in their GI50 values (Figs 5.8A and 5.8B), suggested that the relevance of RPS6KA1 to cisplatin resistance is likely to be context-dependent, which is consistent with the multi-factorial nature of cisplatin resistance (Galluzzi et al, 2012).

Intriguingly, the 5 sensitized cell lines were previously identified to be representative of our proposed Epi-A subtype, whereas other cell lines in the panel that did not show increase in cisplatin sensitivity (Fig. 5.8B) were representatives of the proposed Stem-A subtype (Tan et al, 2013). In view of these observations, it is tempting to speculate that the role of RPS6KA1 is dependent on the molecular subtype status of the cells. At present, the relevance of the proposed molecular classification of EOC in circumventing cisplatin resistance remains to be determined.

Next, we sought to assess the validity of our *in vitro* findings by extending our study to clinical ovarian tumour samples. We took advantage of

ovarian tumour gene expression data that have accompanying information about the patients' clinical response to chemotherapy (GSE3149 and TCGA) (Bild et al, 2006; The Cancer Genome Atlas Research Network, 2011). Most patients in these data sets received standard platinum-based chemotherapy with carboplatin, another platinum drug that has an equivalent mode of action as cisplatin (Knox et al, 1986). Based on Response Evaluation Criteria In Solid Tumour (RECIST), clinical samples were first subdivided into two populations; those with complete response (CR) and those with partial response (PR), stable disease or progressive disease (non-responder; NR). Following which, the average expression of RPS6KA1 was compared between the two populations. We found that the average level of RPS6KA1 in partial/non-responders is significantly higher than the expression level in complete-responders (Fig. 5.9), suggesting the possible role of RPS6KA1 in rendering patients to respond poorly to platinum-based chemotherapy. However, we are also aware that RPS6KA1 is unlikely to be the main reason for poor clinical response to chemotherapy, as shown by the modest difference in its average expression between the two patient populations (Fig. 5.9), as well as the modest increase in cisplatin sensitivity of ovarian cancer cell lines by SL0101-induced RPS6KA1 inhibition (Fig. 5.8A).

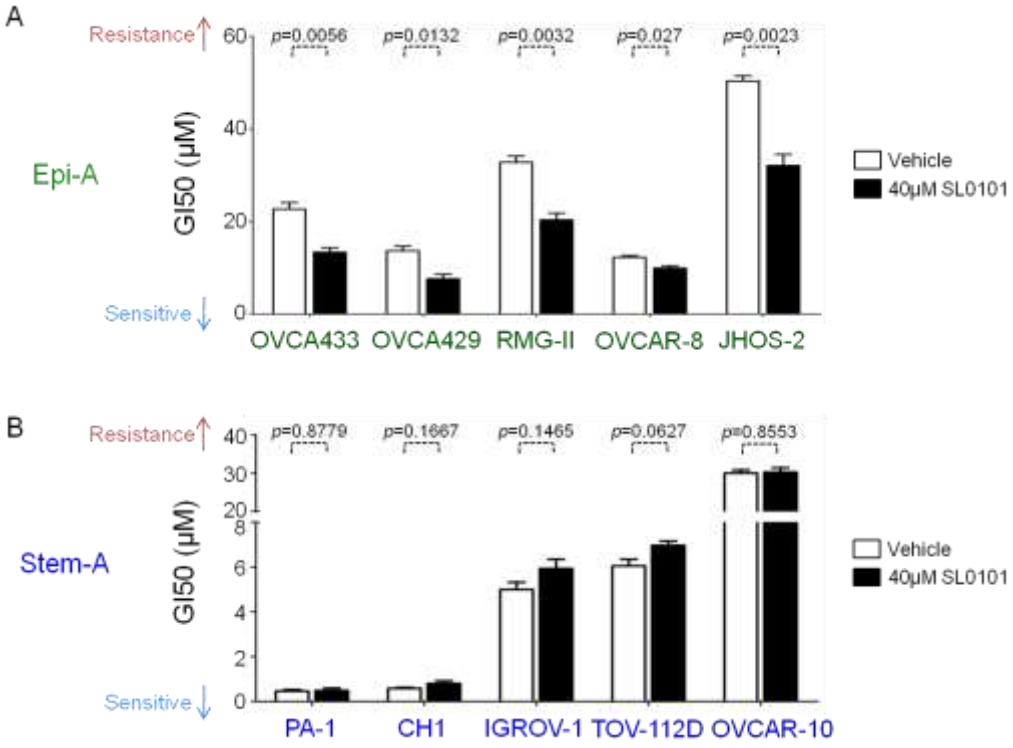

Figure 5.8 Effect of RPS6KA1-specific inhibitor, SL0101 on cisplatin sensitivity.

A panel of 10 ovarian cancer cell lines (OVCA433, OVCA429, RMG-II, OVCAR8, JHOS-2, PA-1, CH1, IGROV-1, TOV-112D and OVCAR-10) was treated with increasing concentration of cisplatin for 72 hour in the presence of vehicle or 40 μM SL0101. GI50 values of cisplatin were then determined using Graphpad Prism, and shown as mean ± SE of three independent triplicate experiments. Effect of SL0101 on GI50 values of cisplatin was statistically evaluated using Student's t-test. A higher value along the y-axis indicates decreased sensitivity to cisplatin. SL0101 treatment rendered cell lines that are representative of Epi-A subtype (A) to be more sensitive to cisplatin, whereas Stem-A cell lines (B) showed no significant change in cisplatin sensitivity. White bar = vehicle, Black bar = 40 μM SL0101 treatment.

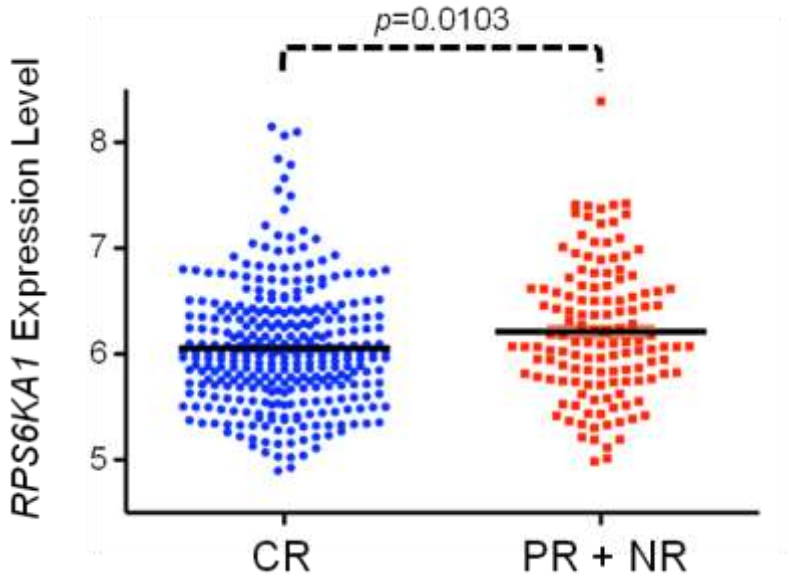

Figure 5.9 Relevance of *RPS6KA1* expression in clinical response to standard chemotherapy.
Dot plot of *RPS6KA1* expression retrieved from clinical ovarian tumour samples that have accompanying information about the patients' clinical response to chemotherapy (GSE3149 and TCGA) (Bild et al, 2006; The Cancer Genome Atlas Research Network, 2011). Classification of samples was based on Response Evaluation Criteria In Solid Tumour (RECIST): blue = complete response (CR); red = partial response (PR), stable disease and progressive disease (non-responder; NR). Differences in *RPS6KA1* expression was statistically evaluated with Mann-Whitney U-test in Graphpad Prism. Partial/Non-responders had significantly higher expression of *RPS6KA1* than complete responders.

5.3 Discussion

In this second part of the thesis, we took advantage of the genome-wide pooled shRNA library to perform an unbiased screen for genes that modulate the cisplatin sensitivity of a resistant cell line, OVCA433. Inhibition of six genes, *ABCC3, KCNH3, KCNN1, MLH1, MRPL3* and *RPS6KA1* were found to enhance the activity of cisplatin in OVCA433 cells. In particular, combination treatment of cisplatin with a RPS6KA1-specific inhibitor, SL0101 rendered Epi-A representative cell lines, including OVCA433, more sensitive to cisplatin. These results revealed the value of targeting RPS6KA1 in countering cisplatin resistance, and further investigation of its function may lead to increased understanding of cisplatin resistance mechanisms. On the other hand, cisplatin sensitivities of Stem-A representative cell lines were unaffected by SL0101 treatment.

Platinum resistance is a major obstacle in the treatment of EOC. EOC can be intrinsically resistant to or rapidly acquire resistance to platinum-based chemotherapy, leading to therapeutic failure (Cannistra, 2004; Coleman et al, 2013; Vaughan et al, 2011). Thus, circumventing platinum resistance is one of the main research goals in the ovarian cancer field. Combination chemotherapy strategies targeting resistance mechanisms have been proposed to have the best chance in significant chemosensitisation (Galluzzi et al, 2012). So far, multiple mechanisms have been described (see Section 1.3.3 for details), but which of these mechanisms should be preferentially targeted remains to be determined. Hence, the unbiased functional screen represented herein confers opportunities to recognise combination strategies relevant for

all or subsets of EOC patients (Ashworth & Bernards, 2010; Berns & Bernards, 2012).

As an initial approach, we utilised a cisplatin resistant cell line, OVCA433 to identify enhancers of cisplatin activity. The cell line was established by Bast *et al.* (1981) from a patient with serous papillary cystadenocarcinoma, and so far, has been used as a model of HGSOC by at least five publications (Cai & Xu, 2013; Creighton et al, 2010; Liu et al, 2010; Rauh-Adelmann et al, 2000; Yang et al, 2010). However, due to the lack of the DNA copy-number profile for OVCA433 in the CCLE database, the suitability of OVCA433 as a HGSOC model cannot be verified (Domcke et al, 2013).

Nevertheless, we uncovered six cisplatin resistance candidate genes—*ABCC3, KCNH3, KCNN1, MLH1, MRPL3* and *RPS6KA1*—from the screen. These genes may not only be useful in future chemosensitisation strategies, but also in development of new predictive and prognostic biomarkers of clinical response to platinum drugs. Even so, further investigation is required to examine their clinical relevance.

RPS6KA1 is a member of the p90 ribosomal S6 kinase (RSK) family, which are downstream effectors of the RAS-mitogen-activated protein kinase (MAPK) signalling cascade (Anjum & Blenis, 2008). The structure of RPS6KA1 consists of two non-identical kinase domains (Jones et al, 1988). The carboxyl-terminal kinase domain contains a docking site for extracellular signal-regulated kinase-1/-2 (ERK1/2) (Gavin & Nebreda, 1999) while the amino-terminal kinase domain is responsible for the phosphorylation of many

cytosolic and nuclear targets (Leighton et al, 1995). Substrates of RPS6KA1 include transcription factors, such as cyclic AMP response element-binding protein (CREB), serum response factor (SRF), oestrogen receptor 1 (ESR1) and nuclear factor-κB (NF-κB) (Anjum & Blenis, 2008; Frodin & Gammeltoft, 1999), as well as kinases, such as tumour suppressor death-associated protein kinase (DAPK), BUB1 mitotic checkpoint serine/threonine kinase and membrane-associated tyrosine- and threonine-specific CDC2-inhibitory kinase 1 (PKMYT1) (Anjum et al, 2005; Palmer et al, 1998; Schwab et al, 2001). The functions of these substrates associate RPS6KA1 with diverse cellular processes, including transcriptional regulation, cell cycle regulation and cell survival. In fact, RPS6KA1 has been implicated in several cancers, including breast and lung cancer as driver of proliferation and metastasis (Doehn et al, 2009; Lara et al, 2011; Smith et al, 2005). Though RPS6KA1 has yet to be directly associated with platinum resistance, inhibition of its activators, ERK1/2 has been reported to sensitise ovarian cancer cell lines to cisplatin (Hayakawa et al, 1999; Lee et al, 2007). On the other hand, there are also reports demonstrating that ERK1/2 activation potentiates platinum-induced apoptosis in ovarian cancer cell lines (Gupta et al, 2013; Nonaka et al, 2012). These conflicting reports illustrated that the roles of ERK1/2 in the cellular response to cisplatin is likely to depend on the individual cellular context (Wang & Lippard, 2005). Similarly, we found that inhibition of RPS6KA1 activity by the small molecule inhibitor, SL0101 led to differential changes in the cisplatin sensitivities of ovarian cancer cell lines. Despite so, the value of targeting RPS6KA1 or its associated pathway in chemosensitisation strategies may worth further investigation. In addition,

development of a predictive framework that could align such strategies to appropriate patients will be beneficial. Preliminary observations suggested that the proposed molecular classification of EOC presented in Section 1.2.3 may be useful for this purpose.

ABCC3 is a member of the ATP binding cassette (ABC) transporter superfamily that is known to mediate multidrug resistance (Gottesman et al, 2002). Like other members of its family, ABCC3 is also an organic anion transporter with broad drug specificity, and is able to confer resistance to anticancer drugs, such as etoposide, teniposide, methotrexate, cisplatin and doxorubicin (Gottesman et al, 2002; Januchowski et al, 2013; Kool et al, 1999; Szakacs et al, 2006). Currently, agents that can modulate ABCC3 function are not known, as much focus has instead been given to other members of the family, ABCB1, ABCC1 and ABCG2 (Szakacs et al, 2006). However, clinical trials evaluating the inhibition of these ABC transporters have met with little success, as the inhibitors often have pharmacokinetic interactions with other drugs and are associated with adverse side-effects (Szakacs et al, 2006). Even so, researchers remain optimistic that multidrug resistance mediated by ABC transporters can one day be vanquished (Gottesman et al, 2002; Saneja et al, 2014; Szakacs et al, 2006).

Both KCNN1 and KCNH3 are potassium channels that are involved in the regulation of potassium ion concentration. Though both genes have not been implicated in platinum resistance, changes in extracellular potassium ion concentration have been shown to influence the intracellular accumulation of cisplatin, which in turn, affects the formation of platinum-DNA adducts

(Andrews et al, 1991; Gately & Howell, 1993). It remains to be determined whether inhibition of KCNN1 and KCNH3 also modulate the intracellular accumulation of cisplatin.

MRPL3 is a ribosomal protein that is exclusively found in mitochondria (Gruschke et al, 2010). Recent reports have associated MRPL3 with mitochondrial cardiomyopathy (Galmiche et al, 2011) and common familial colorectal cancer (Gylfe et al, 2013), but none showed its involvement in platinum resistance. As a result, we have no clue how inhibition of MRPL3 sensitises OVCA433 cells to cisplatin.

Lastly, MLH1 is a component of the DNA mismatch repair (MMR) process that is normally responsible for the recognition and repair of erroneous insertions and deletions by DNA replication and recombination (Kunkel & Erie, 2005). It is widely described that the MMR system is able to detect but fail to repair platinum-induced DNA damage, and thus, lead to the induction of cell cycle arrest and apoptosis (Vaisman et al, 1998). In fact, components of MMR system, including MLH1 are often found to be mutated or under-expressed in cells selected for cisplatin resistance (Aebi et al, 1996; Drummond et al, 1996; Strathdee et al, 1999). Moreover, higher number of relapsed ovarian tumours had *MLH1* promoter methylation, as compared to matched chemo-naïve tumours (Gifford et al, 2004). Unfortunately, this is contrary to our findings, where silencing of *MLH1* rendered OVCA433 cells more sensitive to cisplatin. On the other hand, compelling data showing the relationship between MMR pathway and cisplatin-induced cytotoxicity in clinical settings have yet to be reported (Galluzzi et al, 2012; Wang &

Lippard, 2005). For instance, immuno-histochemical staining for MLH1 in ovarian tumours revealed no association between MLH1 expression and overall survival (Samimi et al, 2000). Hence, doubts over the contributions of defective MMR pathway to cisplatin resistance remain, and more in-depth studies are still required.

It should be pointed out that the aforementioned genes are by no means the principal cause of cisplatin resistance. Though shRNA silencing of each of the six genes resulted in significant decrease in GI50 values of cisplatin, cisplatin sensitivities were only increased by two-fold. Moreover, these genes are functionally diverse, with no clear connection among them. Taken together, these findings reinforced the notion that not one mechanism can solely explain for the presence of a platinum resistance phenotype (Galluzzi et al, 2012; Kartalou & Essigmann, 2001). As such, any future combination chemotherapy strategies will have to target platinum resistance at multiple levels (Galluzzi et al, 2012). Additionally, we are also aware that cell lines may be divergent from their ancestral tumours and the extent to which the data presented herein mirror the situation in human tumours is still uncertain.

Nevertheless, our study can serve as an initial screen for modulators of cisplatin sensitivity that could be used to better understand cisplatin resistance and facilitate the development of strategies for circumventing resistance. Given the heterogeneity of EOC and the multi-factorial nature of platinum resistance, the low survival of EOC patients could be improved by tailoring appropriate chemosensitisation strategies to individual platinum-refractory patients.

CHAPTER 6

GENERAL DISCUSSION AND FUTURE WORK

6.1 General discussion

The increased awareness of a high degree of heterogeneity in EOC cries out for an urgent need to replace current standard of care with treatments specifically designed for the different histological or molecular subtypes of EOC (Vaughan et al, 2011). Unfortunately, aside from the classical platinum/taxane-based chemotherapy, gyne-oncologists have limited access to other therapeutic options. Thus, the challenge is to develop a classification scheme that can define EOC into molecularly homogeneous subgroups, with each benefiting from novel therapeutic strategies.

In a previous study, we reported the identification of five molecular subtypes (Epi-A, Epi-B, Mes, Stem-A and Stem-B) that exhibited distinct clinicopathological characteristics (Tan et al, 2013). This classification scheme is in good agreement with other classification schemes published by TCGA (The Cancer Genome Atlas Research Network, 2011) and AOCS (Tothill et al, 2008), yet reveals novel biological features.

As a complementary approach, the first part of the study conducted an unbiased RNAi-based genetic screen for genes that are essential for each molecular subtype. In particular, the screen demonstrated that specific growth determinants can be distinguished amongst the molecular subtypes, thus supporting the feasibility of developing subtype-specific therapeutics for EOC.

Subsequent validation experiments confirmed *TUBGCP4* and *NAT10* to be functionally relevant for the cell growth of the poor-prognosis Stem-A subtype. At present, the molecular mechanisms accounting for the preferential growth suppression of Stem-A cells by *TUBGCP4* or *NAT10* knockdown are unknown. Since both genes are associated with microtubules, one would expect that pathways related to microtubules may somehow be relevant to the Stem-A subtype. Indeed, our present data provide evidence that the Stem-A subtype exhibits gene signatures associated with microtubule dynamics and are sensitive to drugs interfering with tubulin polymerisation, such as vincristine and vinorelbine. These findings underscore the possible importance of tubulin polymerisation in Stem-A cells. Thus, further studies on the molecules implicated in tubulin polymerisation may allow a deeper understanding of the differences amongst the molecular subtypes, and in turn, facilitate the development of driver-/mechanism-targeted therapies or drugs combinations of higher efficacy in Stem-A tumours.

To date, a few targeted therapies have already been incorporated into the standard of care of other cancers, such as chronic myeloid leukemia (CML), breast and NSCLC (Ma & Adjei, 2009). A classic example is the specific inhibitor of BCR-ABL tyrosine kinase, imatinib for CML (Druker et al, 2006). In fact, PARP inhibitors, such as olaparib have already been proposed to be effective against EOC with defective homologous recombination repair pathway (BRCA-like) (Banerjee et al, 2010; Fong et al, 2009). Thus, it is hoped that relative successes of targeted therapies obtained in other cancers would also occur for EOC.

On the other hand, the clinical usefulness of platinum-based drugs in treating EOC is limited by the high incidence of chemoresistance, and thus, circumventing platinum resistance is also a critical goal in the ovarian cancer research field. In this context, the unbiased RNAi-based genetic screen performed in the second part of the thesis, identified *ABCC3, KCNH3, KCNN1, MLH1, MRPL3* and *RPS6KA1* as genes that can modulate the sensitivity of ovarian cancer cell line to cisplatin. These findings suggest that these genes could possibly be involved in the cisplatin resistance mechanisms of ovarian cancer cell lines. Although studies showing the relevance of these genes to the platinum resistance in established tumours are necessary, these genes may represent potential targets for chemosensitisation strategies.

However, given the multi-factorial nature of platinum resistance, it is highly likely that a particular resistance mechanism may only be relevant in a restricted number of settings (Galluzzi et al, 2012). Thus, there is also the need to identify patients that would benefit from particular chemosensitisation strategies. This notion is also evident in the present study, where the combinatorial treatment of cisplatin and a RPS6KA1-specific inhibitor, SL0101 only rendered Epi-A representative cell lines, but not Stem-A representative cell lines more sensitive to cisplatin. Although the influence of the molecular subtype status on SL0101-induced chemosensitisation remains to be determined, it is clear that the role of RPS6KA1 in cisplatin resistance is dependent on the individual cellular content. Taken together, the challenges are to identify promising candidates that should be modulated for optimal chemosensitisation, as well as to discover predictive biomarkers that would allow patient stratification.

More generally, the present study illustrates the usefulness of RNAi-based genetic screens in identifying subtype-specific regulators of cancer cell proliferation and/or survival, as well as regulators of cisplatin sensitivity. Together with other studies (Bajrami et al, 2013; Barbie et al, 2009; Berns et al, 2007; Cheung et al, 2011; Lam et al, 2008; Luo et al, 2008), we showed that RNAi-based genetic screen is a feasible strategy to systematically identify key players involved in cancer progression and drug responsiveness, and also identify potential targets for therapeutic intervention. Although we only assessed a single phenotype (cell viability), the approach may be extended to other phenotypes, and thus, provides insights into a wide range of biological processes in mammalian cells.

However, RNAi-based genetic screens are still in need of further improvements. For instance, the methodology outlined in the thesis can be further improved through thorough optimisation of conditions for virus transduction and PCR amplification. Current RNAi reagents can be enhanced to provide more efficient suppression of the intended targets, while lowering possibility of off-targets effects. In addition, the genetic screens have to be standardised by the scientific community, so as to ensure reliable and reproducible data (Berns & Bernards, 2012). Such efforts would give researchers high confidence in the biological significance of hit genes, and ultimately, deliver truly effective therapeutic regimens.

6.2 Future work

Though findings from the present study suggest possible therapeutic approaches for EOC, further studies are still needed before such approaches can become clinically applicable. Therefore, in the following paragraphs, we shall discuss some of these future works.

The susceptibility of Stem-A cells to tubulin polymerisation inhibitor drugs, as shown in the first part of the thesis (Chapter 4), is a potential platform for Stem-A-specific therapeutics. This finding may be further examined to elucidate the mechanisms by which tubulin polymerisation regulate the viability of Stem-A cells, with focus on ascertaining the molecule(s) involved and how to exploit them for therapy development. List of genes implicated in the tubulin polymerisation pathway would have to be curated from literature reviews, and then systematically examined for their relevance to Stem-A cell growth. The gene list may include those involved in microtubule nucleation, dynamics and interaction with chromosomes or cellular organelles. In fact, some of them have already been proposed as potential therapeutic targets in cancer cells (Dumontet & Jordan, 2010). In addition, substantial efforts are still being devoted to the identification and evaluation of new microtubule-targeted agents that are insensitive to resistance mechanisms, increase tumour selectivity or have reduced toxicity (Bailly et al, 2003; Hamel et al, 1999; Kita et al, 2013; Romagnoli et al, 2013). Thus, examination of these new agents in regard to their relevance to Stem-A cells, might allow us to further validate our findings and more effectively target Stem-A ovarian cancer.

However, a crucial challenge facing the use of subtype-specific therapeutics is the paucity of biomarkers to identify patients who are most likely to benefit from particular targeted therapies. A predictive model based on BinReg was previously reported by us as a potential diagnostic tool for subtype assignment (Tan et al, 2013), but that will require the use of genome-wide expression arrays on every cancer specimen. Moreover, it will be a financial burden on the patients. Hence, it would be worth exploring the feasibility of characterising each subtype with a small subset of genes or immunohistochemistry of selected biomarkers.

Next, in the second part of the thesis, we uncovered six genes—*ABCC3, KCNH3, KCNN1, MLH1, MRPL3* and *RPS6KA1*—as possible targets for chemosensitisation strategies. Though inhibitions of these genes were found to enhance cisplatin sensitivity, their involvement in resistance mechanisms remains to be precisely determined. Thus, the mechanisms by which these genes modulate cisplatin sensitivity would be investigated and any positive findings will lead to increased understanding of cisplatin resistance. This knowledge will not only provide us with new insights for developing improved therapeutic strategies for circumventing platinum resistance, but also for the discovery of prognostic and predictive biomarkers.

REFERENCES

Aabo K, Adams M, Adnitt P, Alberts DS, Athanazziou A, Barley V, Bell DR, Bianchi U, Bolis G, Brady MF, Brodovsky HS, Bruckner H, Buyse M, Canetta R, Chylak V, Cohen CJ, Colombo N, Conte PF, Crowther D, Edmonson JH, Gennatas C, Gilbey E, Gore M, Guthrie D, Yeap BY, et al. (1998) Chemotherapy in advanced ovarian cancer: four systematic meta-analyses of individual patient data from 37 randomized trials. Advanced Ovarian Cancer Trialists' Group. *Br J Cancer* **78:** 1479-1487

Aarnio M, Sankila R, Pukkala E, Salovaara R, Aaltonen LA, de la Chapelle A, Peltomaki P, Mecklin JP, Jarvinen HJ (1999) Cancer risk in mutation carriers of DNA-mismatch-repair genes. *Int J Cancer* **81:** 214-218

Aebi S, Kurdi-Haidar B, Gordon R, Cenni B, Zheng H, Fink D, Christen RD, Boland CR, Koi M, Fishel R, Howell SB (1996) Loss of DNA mismatch repair in acquired resistance to cisplatin. *Cancer Res* **56:** 3087-3090

Ahmed N, Thompson EW, Quinn MA (2007) Epithelial-mesenchymal interconversions in normal ovarian surface epithelium and ovarian carcinomas: an exception to the norm. *J Cell Physiol* **213:** 581-588

Alizadeh AA, Eisen MB, Davis RE, Ma C, Lossos IS, Rosenwald A, Boldrick JC, Sabet H, Tran T, Yu X, Powell JI, Yang L, Marti GE, Moore T, Hudson J, Jr., Lu L, Lewis DB, Tibshirani R, Sherlock G, Chan WC, Greiner TC, Weisenburger DD, Armitage JO, Warnke R, Levy R, Wilson W, Grever MR, Byrd JC, Botstein D, Brown PO, Staudt LM (2000) Distinct types of diffuse large B-cell lymphoma identified by gene expression profiling. *Nature* **403:** 503-511

Anders A, Lourenco PC, Sawin KE (2006) Noncore components of the fission yeast gamma-tubulin complex. *Mol Biol Cell* **17:** 5075-5093

Andrews PA, Mann SC, Huynh HH, Albright KD (1991) Role of the Na+, K(+)-adenosine triphosphatase in the accumulation of cis-diamminedichloroplatinum(II) in human ovarian carcinoma cells. *Cancer Res* **51:** 3677-3681

Ang WH, Khalaila I, Allardyce CS, Juillerat-Jeanneret L, Dyson PJ (2005) Rational design of platinum(IV) compounds to overcome glutathione-S-transferase mediated drug resistance. *J Am Chem Soc* **127:** 1382-1383

Anglesio MS, Arnold JM, George J, Tinker AV, Tothill R, Waddell N, Simms L, Locandro B, Fereday S, Traficante N, Russell P, Sharma R, Birrer MJ, deFazio A, Chenevix-Trench G, Bowtell DD (2008) Mutation of ERBB2 provides a novel alternative mechanism for the ubiquitous activation of RAS-MAPK in ovarian serous low malignant potential tumors. *Mol Cancer Res* **6:** 1678-1690

Anjum R, Blenis J (2008) The RSK family of kinases: emerging roles in cellular signalling. *Nat Rev Mol Cell Biol* **9:** 747-758

Anjum R, Roux PP, Ballif BA, Gygi SP, Blenis J (2005) The tumor suppressor DAP kinase is a target of RSK-mediated survival signaling. *Curr Biol* **15:** 1762-1767

Armstrong DK, Bundy B, Wenzel L, Huang HQ, Baergen R, Lele S, Copeland LJ, Walker JL, Burger RA (2006) Intraperitoneal cisplatin and paclitaxel in ovarian cancer. *N Engl J Med* **354:** 34-43

Ashworth A, Bernards R (2010) Using functional genetics to understand breast cancer biology. *Cold Spring Harb Perspect Biol* **2:** a003327

Audeh MW, Carmichael J, Penson RT, Friedlander M, Powell B, Bell-McGuinn KM, Scott C, Weitzel JN, Oaknin A, Loman N, Lu K, Schmutzler RK, Matulonis U, Wickens M, Tutt A (2010) Oral poly(ADP-ribose) polymerase inhibitor olaparib in patients with BRCA1 or BRCA2 mutations and recurrent ovarian cancer: a proof-of-concept trial. *Lancet* **376:** 245-251

Auersperg N, Edelson MI, Mok SC, Johnson SW, Hamilton TC (1998) The biology of ovarian cancer. *Semin Oncol* **25:** 281-304

Auersperg N, Wong AS, Choi KC, Kang SK, Leung PC (2001) Ovarian surface epithelium: biology, endocrinology, and pathology. *Endocr Rev* **22:** 255-288

Auner V, Kriegshauser G, Tong D, Horvat R, Reinthaller A, Mustea A, Zeillinger R (2009) KRAS mutation analysis in ovarian samples using a high sensitivity biochip assay. *BMC Cancer* **9:** 111

Bailly C, Bal C, Barbier P, Combes S, Finet JP, Hildebrand MP, Peyrot V, Wattez N (2003) Synthesis and biological evaluation of 4-arylcoumarin analogues of combretastatins. *J Med Chem* **46:** 5437-5444

Bain J, Plater L, Elliott M, Shpiro N, Hastie CJ, McLauchlan H, Klevernic I, Arthur JS, Alessi DR, Cohen P (2007) The selectivity of protein kinase inhibitors: a further update. *Biochem J* **408:** 297-315

Bajrami I, Frankum JR, Konde A, Miller RE, Rehman FL, Brough R, Campbell J, Sims D, Rafiq R, Hooper S, Chen L, Kozarewa I, Assiotis I, Fenwick K, Natrajan R, Lord CJ, Ashworth A (2013) Genome-wide profiling of genetic synthetic lethality identifies CDK12 as a novel determinant of PARP1/2 inhibitor sensitivity. *Cancer Res*

Banerjee S, Kaye SB, Ashworth A (2010) Making the best of PARP inhibitors in ovarian cancer. *Nat Rev Clin Oncol* **7:** 508-519

Barbie DA, Tamayo P, Boehm JS, Kim SY, Moody SE, Dunn IF, Schinzel AC, Sandy P, Meylan E, Scholl C, Frohling S, Chan EM, Sos ML, Michel K, Mermel C, Silver SJ, Weir BA, Reiling JH, Sheng Q, Gupta PB, Wadlow RC, Le H, Hoersch S, Wittner BS, Ramaswamy S, Livingston DM, Sabatini DM, Meyerson M, Thomas RK, Lander ES, Mesirov JP, Root DE, Gilliland DG, Jacks T, Hahn WC (2009) Systematic RNA interference reveals that oncogenic KRAS-driven cancers require TBK1. *Nature* **462:** 108-112

Barnes KR, Kutikov A, Lippard SJ (2004) Synthesis, characterization, and cytotoxicity of a series of estrogen-tethered platinum(IV) complexes. *Chem Biol* **11:** 557-564

Bast RC, Jr., Feeney M, Lazarus H, Nadler LM, Colvin RB, Knapp RC (1981) Reactivity of a monoclonal antibody with human ovarian carcinoma. *J Clin Invest* **68:** 1331-1337

Bast RC, Jr., Hennessy B, Mills GB (2009) The biology of ovarian cancer: new opportunities for translation. *Nat Rev Cancer* **9:** 415-428

Berchuck A, Schildkraut JM, Pearce CL, Chenevix-Trench G, Pharoah PD (2008) Role of genetic polymorphisms in ovarian cancer susceptibility: development of an international ovarian cancer association consortium. In *Ovarian cancer state of the art and future directions in translational research* Coukos G, Berchuck A, Ozols RF (eds), pp 53-67. New York, NY: Springer,

Berndtsson M, Hagg M, Panaretakis T, Havelka AM, Shoshan MC, Linder S (2007) Acute apoptosis by cisplatin requires induction of reactive oxygen species but is not associated with damage to nuclear DNA. *Int J Cancer* **120:** 175-180

Berns K, Bernards R (2012) Understanding resistance to targeted cancer drugs through loss of function genetic screens. *Drug Resist Updat* **15:** 268-275

Berns K, Horlings HM, Hennessy BT, Madiredjo M, Hijmans EM, Beelen K, Linn SC, Gonzalez-Angulo AM, Stemke-Hale K, Hauptmann M, Beijersbergen RL, Mills GB, van de Vijver MJ, Bernards R (2007) A functional genetic approach identifies the PI3K pathway as a major determinant of trastuzumab resistance in breast cancer. *Cancer Cell* **12:** 395-402

Bild AH, Yao G, Chang JT, Wang Q, Potti A, Chasse D, Joshi MB, Harpole D, Lancaster JM, Berchuck A, Olson JA, Jr., Marks JR, Dressman HK, West M, Nevins JR (2006) Oncogenic pathway signatures in human cancers as a guide to targeted therapies. *Nature* **439:** 353-357

Bookman MA, Brady MF, McGuire WP, Harper PG, Alberts DS, Friedlander M, Colombo N, Fowler JM, Argenta PA, De Geest K, Mutch DG, Burger RA, Swart AM, Trimble EL, Accario-Winslow C, Roth LM (2009) Evaluation of new platinum-based treatment regimens in advanced-stage ovarian cancer: a Phase III Trial of the Gynecologic Cancer Intergroup. *J Clin Oncol* **27:** 1419-1425

Borst P, Evers R, Kool M, Wijnholds J (2000) A family of drug transporters: the multidrug resistance-associated proteins. *J Natl Cancer Inst* **92:** 1295-1302

Bowen NJ, Walker LD, Matyunina LV, Logani S, Totten KA, Benigno BB, McDonald JF (2009) Gene expression profiling supports the hypothesis that human ovarian surface epithelia are multipotent and capable of serving as ovarian cancer initiating cells. *BMC Med Genomics* **2:** 71

Bowtell DD (2010) The genesis and evolution of high-grade serous ovarian cancer. *Nat Rev Cancer* **10:** 803-808

Boyd J, Rubin SC (1997) Hereditary ovarian cancer: molecular genetics and clinical implications. *Gynecol Oncol* **64:** 196-206

Brown PO, Palmer C (2009) The preclinical natural history of serous ovarian cancer: defining the target for early detection. *PLoS Med* **6:** e1000114

Buick RN, Pullano R, Trent JM (1985) Comparative properties of five human ovarian adenocarcinoma cell lines. *Cancer Res* **45:** 3668-3676

Buys SS, Partridge E, Black A, Johnson CC, Lamerato L, Isaacs C, Reding DJ, Greenlee RT, Yokochi LA, Kessel B, Crawford ED, Church TR, Andriole GL, Weissfeld JL, Fouad MN, Chia D, O'Brien B, Ragard LR, Clapp JD, Rathmell JM, Riley TL, Hartge P, Pinsky PF, Zhu CS, Izmirlian G, Kramer BS, Miller AB, Xu JL, Prorok PC, Gohagan JK, Berg CD (2011) Effect of screening on ovarian cancer mortality: the Prostate, Lung, Colorectal and Ovarian (PLCO) Cancer Screening Randomized Controlled Trial. *JAMA* **305:** 2295-2303

Cai H, Xu Y (2013) The role of LPA and YAP signaling in long-term migration of human ovarian cancer cells. *Cell Commun Signal* **11:** 31

Calza S, Hall P, Auer G, Bjohle J, Klaar S, Kronenwett U, Liu ET, Miller L, Ploner A, Smeds J, Bergh J, Pawitan Y (2006) Intrinsic molecular signature of breast cancer in a population-based cohort of 412 patients. *Breast Cancer Res* **8:** R34

Canevari S, Raspagliesi F, Lorusso D (2013) Bevacizumab treatment and quality of life in advanced ovarian cancer. *Future Oncol* **9:** 951-954

Cannistra SA (2004) Cancer of the ovary. *N Engl J Med* **351:** 2519-2529

Catasus L, Bussaglia E, Rodrguez I, Gallardo A, Pons C, Irving JA, Prat J (2004) Molecular genetic alterations in endometrioid carcinomas of the ovary: similar frequency of beta-catenin abnormalities but lower rate of microsatellite instability and PTEN alterations than in uterine endometrioid carcinomas. *Hum Pathol* **35:** 1360-1368

Chambers AF, Groom AC, MacDonald IC (2002) Dissemination and growth of cancer cells in metastatic sites. *Nat Rev Cancer* **2:** 563-572

Chan JY (2011) A clinical overview of centrosome amplification in human cancers. *Int J Biol Sci* **7:** 1122-1144

Chaney SG, Campbell SL, Bassett E, Wu Y (2005) Recognition and processing of cisplatin- and oxaliplatin-DNA adducts. *Crit Rev Oncol Hematol* **53:** 3-11

Chen C, Grennan K, Badner J, Zhang D, Gershon E, Jin L, Liu C (2011) Removing batch effects in analysis of expression microarray data: an evaluation of six batch adjustment methods. *PLoS One* **6:** e17238

Chen HH, Kuo MT (2010) Role of glutathione in the regulation of Cisplatin resistance in cancer chemotherapy. *Met Based Drugs* **2010**

Chen S, Iversen ES, Friebel T, Finkelstein D, Weber BL, Eisen A, Peterson LE, Schildkraut JM, Isaacs C, Peshkin BN, Corio C, Leondaridis L, Tomlinson G, Dutson D, Kerber R, Amos CI, Strong LC, Berry DA, Euhus DM, Parmigiani G (2006) Characterization of BRCA1 and BRCA2 mutations in a large United States sample. *J Clin Oncol* **24:** 863-871

Cheng W, Liu J, Yoshida H, Rosen D, Naora H (2005) Lineage infidelity of epithelial ovarian cancers is controlled by HOX genes that specify regional identity in the reproductive tract. *Nat Med* **11:** 531-537

Cheung HW, Cowley GS, Weir BA, Boehm JS, Rusin S, Scott JA, East A, Ali LD, Lizotte PH, Wong TC, Jiang G, Hsiao J, Mermel CH, Getz G, Barretina J, Gopal S, Tamayo P, Gould J, Tsherniak A, Stransky N, Luo B, Ren Y, Drapkin R, Bhatia SN, Mesirov JP, Garraway LA, Meyerson M, Lander ES, Root DE, Hahn WC (2011) Systematic investigation of genetic vulnerabilities across cancer cell lines reveals lineage-specific dependencies in ovarian cancer. *Proc Natl Acad Sci U S A* **108:** 12372-12377

Chia SK, Bramwell VH, Tu D, Shepherd LE, Jiang S, Vickery T, Mardis E, Leung S, Ung K, Pritchard KI, Parker JS, Bernard PS, Perou CM, Ellis MJ, Nielsen TO (2012) A 50-gene intrinsic subtype classifier for prognosis and prediction of benefit from adjuvant tamoxifen. *Clin Cancer Res* **18:** 4465-4472

Chin CF, Tian Q, Setyawati MI, Fang W, Tan ES, Leong DT, Ang WH (2012) Tuning the activity of platinum(IV) anticancer complexes through asymmetric acylation. *J Med Chem* **55:** 7571-7582

Chin L, Hahn WC, Getz G, Meyerson M (2011) Making sense of cancer genomic data. *Genes Dev* **25:** 534-555

Clarke-Pearson DL (2009) Clinical practice. Screening for ovarian cancer. *N Engl J Med* **361:** 170-177

Cohen J (1988) *Statistical power analysis for the behavioral sciences (2 ed.)*: Lawrence Erlbaum Associates.

Coleman RL, Monk BJ, Sood AK, Herzog TJ (2013) Latest research and treatment of advanced-stage epithelial ovarian cancer. *Nat Rev Clin Oncol* **10:** 211-224

Collisson EA, Sadanandam A, Olson P, Gibb WJ, Truitt M, Gu S, Cooc J, Weinkle J, Kim GE, Jakkula L, Feiler HS, Ko AH, Olshen AB, Danenberg KL, Tempero MA, Spellman PT, Hanahan D, Gray JW (2011) Subtypes of pancreatic ductal adenocarcinoma and their differing responses to therapy. *Nat Med* **17:** 500-503

Colombo N, Peiretti M, Garbi A, Carinelli S, Marini C, Sessa C, Group EGW (2012) Non-epithelial ovarian cancer: ESMO Clinical Practice Guidelines for diagnosis, treatment and follow-up. *Ann Oncol* **23 Suppl 7:** vii20-26

Cramer DW, Liberman RF, Titus-Ernstoff L, Welch WR, Greenberg ER, Baron JA, Harlow BL (1999) Genital talc exposure and risk of ovarian cancer. *Int J Cancer* **81:** 351-356

Creighton CJ, Fountain MD, Yu Z, Nagaraja AK, Zhu H, Khan M, Olokpa E, Zariff A, Gunaratne PH, Matzuk MM, Anderson ML (2010) Molecular profiling uncovers a p53-associated role for microRNA-31 in inhibiting the proliferation of serous ovarian carcinomas and other cancers. *Cancer Res* **70:** 1906-1915

De Palma M, Hanahan D (2012) The biology of personalized cancer medicine: facing individual complexities underlying hallmark capabilities. *Mol Oncol* **6:** 111-127

Deavers MT, Malpica A, Liu J, Broaddus R, Silva EG (2003) Ovarian sex cord-stromal tumors: an immunohistochemical study including a comparison of calretinin and inhibin. *Mod Pathol* **16:** 584-590

Deng X, Ewton DZ, Friedman E (2009) Mirk/Dyrk1B maintains the viability of quiescent pancreatic cancer cells by reducing levels of reactive oxygen species. *Cancer Res* **69:** 3317-3324

Denkert C, Budczies J, Darb-Esfahani S, Gyorffy B, Sehouli J, Konsgen D, Zeillinger R, Weichert W, Noske A, Buckendahl AC, Muller BM, Dietel M, Lage H (2009) A prognostic gene expression index in ovarian cancer - validation across different independent data sets. *J Pathol* **218:** 273-280

Desai A, Mitchison TJ (1997) Microtubule polymerization dynamics. *Annu Rev Cell Dev Biol* **13:** 83-117

Dimitroulis J, Stathopoulos GP (2005) Evolution of non-small cell lung cancer chemotherapy (Review). *Oncol Rep* **13:** 923-930

Doehn U, Hauge C, Frank SR, Jensen CJ, Duda K, Nielsen JV, Cohen MS, Johansen JV, Winther BR, Lund LR, Winther O, Taunton J, Hansen SH, Frodin M (2009) RSK is a principal effector of the RAS-ERK pathway for eliciting a coordinate promotile/invasive gene program and phenotype in epithelial cells. *Mol Cell* **35:** 511-522

Domcke S, Sinha R, Levine DA, Sander C, Schultz N (2013) Evaluating cell lines as tumour models by comparison of genomic profiles. *Nat Commun* **4:** 2126

Downs L, Boente MP (2003) Germ Cell Tumors. In *Atlas of clinical oncology, Ovarian cancer*, Ozols RF, American Cancer Society. (eds), 16, pp ix, 246 p. Hamilton, Ont. ; Lewiston, NY: BC Decker

Druker BJ, Guilhot F, O'Brien SG, Gathmann I, Kantarjian H, Gattermann N, Deininger MW, Silver RT, Goldman JM, Stone RM, Cervantes F, Hochhaus A, Powell BL, Gabrilove JL, Rousselot P, Reiffers J, Cornelissen JJ, Hughes T, Agis H, Fischer T, Verhoef G, Shepherd J, Saglio G, Gratwohl A, Nielsen JL, Radich JP, Simonsson B, Taylor K, Baccarani M, So C, Letvak L, Larson RA (2006) Five-year follow-up of patients receiving imatinib for chronic myeloid leukemia. *N Engl J Med* **355:** 2408-2417

Druker BJ, Talpaz M, Resta DJ, Peng B, Buchdunger E, Ford JM, Lydon NB, Kantarjian H, Capdeville R, Ohno-Jones S, Sawyers CL (2001) Efficacy and safety of a specific inhibitor of the BCR-ABL tyrosine kinase in chronic myeloid leukemia. *N Engl J Med* **344:** 1031-1037

Drummond JT, Anthoney A, Brown R, Modrich P (1996) Cisplatin and adriamycin resistance are associated with MutLalpha and mismatch repair deficiency in an ovarian tumor cell line. *J Biol Chem* **271:** 19645-19648

du Bois A, Luck HJ, Meier W, Adams HP, Mobus V, Costa S, Bauknecht T, Richter B, Warm M, Schroder W, Olbricht S, Nitz U, Jackisch C, Emons G, Wagner U, Kuhn W, Pfisterer J (2003) A randomized clinical trial of cisplatin/paclitaxel versus carboplatin/paclitaxel as first-line treatment of ovarian cancer. *J Natl Cancer Inst* **95:** 1320-1329

du Bois A, Reuss A, Pujade-Lauraine E, Harter P, Ray-Coquard I, Pfisterer J (2009) Role of surgical outcome as prognostic factor in advanced epithelial ovarian cancer: a combined exploratory analysis of 3 prospectively randomized phase 3 multicenter trials: by the Arbeitsgemeinschaft Gynaekologische Onkologie Studiengruppe Ovarialkarzinom (AGO-OVAR) and the Groupe d'Investigateurs Nationaux Pour les Etudes des Cancers de l'Ovaire (GINECO). *Cancer* **115:** 1234-1244

Dubeau L (2008) The cell of origin of ovarian epithelial tumours. *Lancet Oncol* **9:** 1191-1197

Dumontet C, Jordan MA (2010) Microtubule-binding agents: a dynamic field of cancer therapeutics. *Nat Rev Drug Discov* **9:** 790-803

Eisenkop SM, Friedman RL, Wang HJ (1998) Complete cytoreductive surgery is feasible and maximizes survival in patients with advanced epithelial ovarian cancer: a prospective study. *Gynecol Oncol* **69:** 103-108

Etemadmoghadam D, Weir BA, Au-Yeung G, Alsop K, Mitchell G, George J, Davis S, D'Andrea AD, Simpson K, Hahn WC, Bowtell DD (2013) Synthetic lethality between CCNE1 amplification and loss of BRCA1. *Proc Natl Acad Sci U S A* **110:** 19489-19494

Eva A, Robbins KC, Andersen PR, Srinivasan A, Tronick SR, Reddy EP, Ellmore NW, Galen AT, Lautenberger JA, Papas TS, Westin EH, Wong-Staal F, Gallo RC, Aaronson SA (1982) Cellular genes analogous to retroviral onc genes are transcribed in human tumour cells. *Nature* **295:** 116-119

Farmer H, McCabe N, Lord CJ, Tutt AN, Johnson DA, Richardson TB, Santarosa M, Dillon KJ, Hickson I, Knights C, Martin NM, Jackson SP, Smith GC, Ashworth A (2005) Targeting the DNA repair defect in BRCA mutant cells as a therapeutic strategy. *Nature* **434:** 917-921

Fathalla MF (1971) Incessant ovulation--a factor in ovarian neoplasia? *Lancet* **2:** 163

Fava F, Raynaud-Messina B, Leung-Tack J, Mazzolini L, Li M, Guillemot JC, Cachot D, Tollon Y, Ferrara P, Wright M (1999) Human 76p: A new member of the gamma-tubulin-associated protein family. *J Cell Biol* **147:** 857-868

Feeley KM, Wells M (2001) Precursor lesions of ovarian epithelial malignancy. *Histopathology* **38:** 87-95

Fodde R (2009) The stem of cancer. *Cancer Cell* **15:** 87-89

Fong PC, Boss DS, Yap TA, Tutt A, Wu P, Mergui-Roelvink M, Mortimer P, Swaisland H, Lau A, O'Connor MJ, Ashworth A, Carmichael J, Kaye SB, Schellens JH, de Bono JS (2009) Inhibition of poly(ADP-ribose) polymerase in tumors from BRCA mutation carriers. *N Engl J Med* **361:** 123-134

Fox N, Mathers N (1997) Empowering research: statistical power in general practice research. *Fam Pract* **14:** 324-329

Frodin M, Gammeltoft S (1999) Role and regulation of 90 kDa ribosomal S6 kinase (RSK) in signal transduction. *Mol Cell Endocrinol* **151:** 65-77

Furuta T, Ueda T, Aune G, Sarasin A, Kraemer KH, Pommier Y (2002) Transcription-coupled nucleotide excision repair as a determinant of cisplatin sensitivity of human cells. *Cancer Res* **62:** 4899-4902

Gadducci A, Cosio S, Muraca S, Genazzani AR (2002) Molecular mechanisms of apoptosis and chemosensitivity to platinum and paclitaxel in ovarian cancer: biological data and clinical implications. *Eur J Gynaecol Oncol* **23:** 390-396

Gadducci A, Guerrieri ME, Genazzani AR (2012) New insights on the pathogenesis of ovarian carcinoma: molecular basis and clinical implications. *Gynecol Endocrinol* **28:** 582-586

Galluzzi L, Senovilla L, Vitale I, Michels J, Martins I, Kepp O, Castedo M, Kroemer G (2012) Molecular mechanisms of cisplatin resistance. *Oncogene* **31:** 1869-1883

Galmiche L, Serre V, Beinat M, Assouline Z, Lebre AS, Chretien D, Nietschke P, Benes V, Boddaert N, Sidi D, Brunelle F, Rio M, Munnich A, Rotig A (2011) Exome sequencing identifies MRPL3 mutation in mitochondrial cardiomyopathy. *Hum Mutat* **32:** 1225-1231

Gan PP, McCarroll JA, Po'uha ST, Kamath K, Jordan MA, Kavallaris M (2010) Microtubule dynamics, mitotic arrest, and apoptosis: drug-induced differential effects of betaIII-tubulin. *Mol Cancer Ther* **9:** 1339-1348

Garay JP, Gray JW (2012) Omics and therapy - a basis for precision medicine. *Mol Oncol* **6:** 128-139

Gately DP, Howell SB (1993) Cellular accumulation of the anticancer agent cisplatin: a review. *Br J Cancer* **67:** 1171-1176

Gatza ML, Lucas JE, Barry WT, Kim JW, Wang Q, Crawford MD, Datto MB, Kelley M, Mathey-Prevot B, Potti A, Nevins JR (2010) A pathway-based classification of human breast cancer. *Proc Natl Acad Sci U S A* **107:** 6994-6999

Gaughan EM, Costa DB (2011) Genotype-driven therapies for non-small cell lung cancer: focus on EGFR, KRAS and ALK gene abnormalities. *Ther Adv Med Oncol* **3:** 113-125

Gavin AC, Nebreda AR (1999) A MAP kinase docking site is required for phosphorylation and activation of p90(rsk)/MAPKAP kinase-1. *Curr Biol* **9:** 281-284

Gershenson DM, Del Junco G, Copeland LJ, Rutledge FN (1984) Mixed germ cell tumors of the ovary. *Obstet Gynecol* **64:** 200-206

Gifford G, Paul J, Vasey PA, Kaye SB, Brown R (2004) The acquisition of hMLH1 methylation in plasma DNA after chemotherapy predicts poor survival for ovarian cancer patients. *Clin Cancer Res* **10:** 4420-4426

Gilks CB, Prat J (2009) Ovarian carcinoma pathology and genetics: recent advances. *Hum Pathol* **40:** 1213-1223

Goldberg RM, Sargent DJ, Morton RF, Fuchs CS, Ramanathan RK, Williamson SK, Findlay BP, Pitot HC, Alberts SR (2004) A randomized controlled trial of fluorouracil plus leucovorin, irinotecan, and oxaliplatin combinations in patients with previously untreated metastatic colorectal cancer. *J Clin Oncol* **22:** 23-30

Gomez-Raposo C, Mendiola M, Barriuso J, Hardisson D, Redondo A (2010) Molecular characterization of ovarian cancer by gene-expression profiling. *Gynecol Oncol* **118:** 88-92

Goodman MT, Howe HL, Tung KH, Hotes J, Miller BA, Coughlin SS, Chen VW (2003) Incidence of ovarian cancer by race and ethnicity in the United States, 1992-1997. *Cancer* **97:** 2676-2685

Gore M, du Bois A, Vergote I (2006) Intraperitoneal chemotherapy in ovarian cancer remains experimental. *J Clin Oncol* **24:** 4528-4530

Goshima G, Mayer M, Zhang N, Stuurman N, Vale RD (2008) Augmin: a protein complex required for centrosome-independent microtubule generation within the spindle. *J Cell Biol* **181:** 421-429

Gottesman MM, Fojo T, Bates SE (2002) Multidrug resistance in cancer: role of ATP-dependent transporters. *Nat Rev Cancer* **2:** 48-58

Green A, Purdie D, Bain C, Siskind V, Russell P, Quinn M, Ward B (1997) Tubal sterilisation, hysterectomy and decreased risk of ovarian cancer. Survey of Women's Health Study Group. *Int J Cancer* **71:** 948-951

Gridelli C, Aapro M, Ardizzoni A, Balducci L, De Marinis F, Kelly K, Le Chevalier T, Manegold C, Perrone F, Rosell R, Shepherd F, De Petris L, Di Maio M, Langer C (2005) Treatment of advanced non-small-cell lung cancer in the elderly: results of an international expert panel. *J Clin Oncol* **23:** 3125-3137

Gruschke S, Grone K, Heublein M, Holz S, Israel L, Imhof A, Herrmann JM, Ott M (2010) Proteins at the polypeptide tunnel exit of the yeast mitochondrial ribosome. *J Biol Chem* **285:** 19022-19028

Guillet V, Knibiehler M, Gregory-Pauron L, Remy MH, Chemin C, Raynaud-Messina B, Bon C, Kollman JM, Agard DA, Merdes A, Mourey L (2011) Crystal structure of gamma-tubulin complex protein GCP4 provides insight into microtubule nucleation. *Nat Struct Mol Biol* **18:** 915-919

Gupta GP, Massague J (2006) Cancer metastasis: building a framework. *Cell* **127:** 679-695

Gupta N, Xu Z, El-Sehemy A, Steed H, Fu Y (2013) Notch3 induces epithelial-mesenchymal transition and attenuates carboplatin-induced apoptosis in ovarian cancer cells. *Gynecol Oncol* **130:** 200-206

Gylfe AE, Katainen R, Kondelin J, Tanskanen T, Cajuso T, Hanninen U, Taipale J, Taipale M, Renkonen-Sinisalo L, Jarvinen H, Mecklin JP, Kilpivaara O, Pitkanen E, Vahteristo P, Tuupanen S, Karhu A, Aaltonen LA (2013) Eleven candidate susceptibility genes for common familial colorectal cancer. *PLoS Genet* **9:** e1003876

Haibe-Kains B, Desmedt C, Loi S, Culhane AC, Bontempi G, Quackenbush J, Sotiriou C (2012) A three-gene model to robustly identify breast cancer molecular subtypes. *J Natl Cancer Inst* **104:** 311-325

Hamel E, Sackett DL, Vourloumis D, Nicolaou KC (1999) The coral-derived natural products eleutherobin and sarcodictyins A and B: effects on the assembly of purified tubulin with and without microtubule-associated proteins and binding at the polymer taxoid site. *Biochemistry* **38:** 5490-5498

Hamilton TC, Young RC, McKoy WM, Grotzinger KR, Green JA, Chu EW, Whang-Peng J, Rogan AM, Green WR, Ozols RF (1983) Characterization of a

human ovarian carcinoma cell line (NIH:OVCAR-3) with androgen and estrogen receptors. *Cancer Res* **43:** 5379-5389

Han JY, Hong EK, Choi BG, Park JN, Kim KW, Kang JH, Jin JY, Park SY, Hong YS, Lee KS (2003) Death receptor 5 and Bcl-2 protein expression as predictors of tumor response to gemcitabine and cisplatin in patients with advanced non-small-cell lung cancer. *Med Oncol* **20:** 355-362

Hanahan D, Weinberg RA (2011) Hallmarks of cancer: the next generation. *Cell* **144:** 646-674

Hankinson SE, Colditz GA, Hunter DJ, Willett WC, Stampfer MJ, Rosner B, Hennekens CH, Speizer FE (1995) A prospective study of reproductive factors and risk of epithelial ovarian cancer. *Cancer* **76:** 284-290

Hankinson SE, Hunter DJ, Colditz GA, Willett WC, Stampfer MJ, Rosner B, Hennekens CH, Speizer FE (1993) Tubal ligation, hysterectomy, and risk of ovarian cancer. A prospective study. *JAMA* **270:** 2813-2818

Harrap KR (1985) Preclinical studies identifying carboplatin as a viable cisplatin alternative. *Cancer Treat Rev* **12 Suppl A:** 21-33

Hayakawa J, Ohmichi M, Kurachi H, Ikegami H, Kimura A, Matsuoka T, Jikihara H, Mercola D, Murata Y (1999) Inhibition of extracellular signal-regulated protein kinase or c-Jun N-terminal protein kinase cascade, differentially activated by cisplatin, sensitizes human ovarian cancer cell line. *J Biol Chem* **274:** 31648-31654

Helland A, Anglesio MS, George J, Cowin PA, Johnstone CN, House CM, Sheppard KE, Etemadmoghadam D, Melnyk N, Rustgi AK, Phillips WA, Johnsen H, Holm R, Kristensen GB, Birrer MJ, Pearson RB, Borresen-Dale AL, Huntsman DG, deFazio A, Creighton CJ, Smyth GK, Bowtell DD (2011) Deregulation of MYCN, LIN28B and LET7 in a molecular subtype of aggressive high-grade serous ovarian cancers. *PLoS One* **6:** e18064

Hendrix ND, Wu R, Kuick R, Schwartz DR, Fearon ER, Cho KR (2006) Fibroblast growth factor 9 has oncogenic activity and is a downstream target of Wnt signaling in ovarian endometrioid adenocarcinomas. *Cancer Res* **66:** 1354-1362

Herzog TJ, Pothuri B (2006) Ovarian cancer: a focus on management of recurrent disease. *Nat Clin Pract Oncol* **3:** 604-611

Hills CA, Kelland LR, Abel G, Siracky J, Wilson AP, Harrap KR (1989) Biological properties of ten human ovarian carcinoma cell lines: calibration in vitro against four platinum complexes. *Br J Cancer* **59:** 527-534

Hoffmann JS, Pillaire MJ, Maga G, Podust V, Hubscher U, Villani G (1995) DNA polymerase beta bypasses in vitro a single d(GpG)-cisplatin adduct placed on codon 13 of the HRAS gene. *Proc Natl Acad Sci U S A* **92:** 5356-5360

Hogdall EV, Christensen L, Kjaer SK, Blaakaer J, Bock JE, Glud E, Norgaard-Pedersen B, Hogdall CK (2003) Distribution of HER-2 overexpression in ovarian carcinoma tissue and its prognostic value in patients with ovarian carcinoma: from the Danish MALOVA Ovarian Cancer Study. *Cancer* **98:** 66-73

Holschneider CH, Berek JS (2000) Ovarian cancer: epidemiology, biology, and prognostic factors. *Semin Surg Oncol* **19:** 3-10

Hoskins WJ, McGuire WP, Brady MF, Homesley HD, Creasman WT, Berman M, Ball H, Berek JS (1994) The effect of diameter of largest residual disease on survival after primary cytoreductive surgery in patients with suboptimal residual epithelial ovarian carcinoma. *Am J Obstet Gynecol* **170:** 974-979; discussion 979-980

Howell SJ (2013) Advances in the treatment of luminal breast cancer. *Curr Opin Obstet Gynecol* **25:** 49-54

Howlader N, Noone AM, Krapcho M, Garshell J, Neyman N, Altekruse SF, Kosary CL, Yu M, Ruhl J, Tatalovich Z, Cho H, Mariotto A, Lewis DR, Chen HS, Feuer EJ, Cronin KA. (2013) SEER Cancer Statistics Review, 1975-2010, National Cancer Institute. Bethesda, MD, http://seer.cancer.gov/csr/1975_2010/, based on November 2012 SEER data submission, posted to the SEER web site, April 2013.

Hsu DS, Balakumaran BS, Acharya CR, Vlahovic V, Walters KS, Garman K, Anders C, Riedel RF, Lancaster J, Harpole D, Dressman HK, Nevins JR, Febbo PG, Potti A (2007) Pharmacogenomic strategies provide a rational approach to the treatment of cisplatin-resistant patients with advanced cancer. *J Clin Oncol* **25:** 4350-4357

Hu J, Friedman E (2010) Depleting Mirk Kinase Increases Cisplatin Toxicity in Ovarian Cancer Cells. *Genes Cancer* **1:** 803-811

Huang X, Wang JY, Lu X (2008) Systems analysis of quantitative shRNA-library screens identifies regulators of cell adhesion. *BMC Syst Biol* **2:** 49

Hubbert C, Guardiola A, Shao R, Kawaguchi Y, Ito A, Nixon A, Yoshida M, Wang XF, Yao TP (2002) HDAC6 is a microtubule-associated deacetylase. *Nature* **417:** 455-458

Iorio E, Ricci A, Bagnoli M, Pisanu ME, Castellano G, Di Vito M, Venturini E, Glunde K, Bhujwalla ZM, Mezzanzanica D, Canevari S, Podo F (2010) Activation of phosphatidylcholine cycle enzymes in human epithelial ovarian cancer cells. *Cancer Res* **70:** 2126-2135

Ishida S, Lee J, Thiele DJ, Herskowitz I (2002) Uptake of the anticancer drug cisplatin mediated by the copper transporter Ctr1 in yeast and mammals. *Proc Natl Acad Sci U S A* **99:** 14298-14302

Januchowski R, Zawierucha P, Andrzejewska M, Rucinski M, Zabel M (2013) Microarray-based detection and expression analysis of ABC and SLC transporters in drug-resistant ovarian cancer cell lines. *Biomed Pharmacother* **67:** 240-245

Jemal A, Bray F, Center MM, Ferlay J, Ward E, Forman D (2011) Global cancer statistics. *CA Cancer J Clin* **61:** 69-90

Jochumsen KM, Tan Q, Hogdall EV, Hogdall C, Kjaer SK, Blaakaer J, Kruse TA, Mogensen O (2009) Gene expression profiles as prognostic markers in women with ovarian cancer. *Int J Gynecol Cancer* **19:** 1205-1213

Jochumsen KM, Tan Q, Holund B, Kruse TA, Mogensen O (2007) Gene expression in epithelial ovarian cancer: a study of intratumor heterogeneity. *Int J Gynecol Cancer* **17:** 979-985

Johnson CC, Kessel B, Riley TL, Ragard LR, Williams CR, Xu JL, Buys SS (2008) The epidemiology of CA-125 in women without evidence of ovarian cancer in the Prostate, Lung, Colorectal and Ovarian Cancer (PLCO) Screening Trial. *Gynecol Oncol* **110:** 383-389

Johnson WE, Li C, Rabinovic A (2007) Adjusting batch effects in microarray expression data using empirical Bayes methods. *Biostatistics* **8:** 118-127

Jones SW, Erikson E, Blenis J, Maller JL, Erikson RL (1988) A Xenopus ribosomal protein S6 kinase has two apparent kinase domains that are each similar to distinct protein kinases. *Proc Natl Acad Sci U S A* **85:** 3377-3381

Judson PL, Boente MP (2003) Ovarian Sex Cord-Stromal Tumors. In *Atlas of clinical oncology, Ovarian cancer*, Ozols RF, American Cancer Society. (eds), 17, pp ix, 246 p. Hamilton, Ont. ; Lewiston, NY: BC Decker

Kang J, D'Andrea AD, Kozono D (2012) A DNA repair pathway-focused score for prediction of outcomes in ovarian cancer treated with platinum-based chemotherapy. *J Natl Cancer Inst* **104:** 670-681

Kartalou M, Essigmann JM (2001) Mechanisms of resistance to cisplatin. *Mutat Res* **478:** 23-43

Kasahara K, Fujiwara Y, Nishio K, Ohmori T, Sugimoto Y, Komiya K, Matsuda T, Saijo N (1991) Metallothionein content correlates with the sensitivity of human small cell lung cancer cell lines to cisplatin. *Cancer Res* **51:** 3237-3242

Katsumata N, Yasuda M, Takahashi F, Isonishi S, Jobo T, Aoki D, Tsuda H, Sugiyama T, Kodama S, Kimura E, Ochiai K, Noda K (2009) Dose-dense paclitaxel once a week in combination with carboplatin every 3 weeks for advanced ovarian cancer: a phase 3, open-label, randomised controlled trial. *Lancet* **374:** 1331-1338

Kelland L (2007) The resurgence of platinum-based cancer chemotherapy. *Nat Rev Cancer* **7:** 573-584

Kigawa J (2013) New strategy for overcoming resistance to chemotherapy of ovarian cancer. *Yonago Acta Med* **56:** 43-50

Kita M, Hirayama Y, Yoneda K, Yamagishi K, Chinen T, Usui T, Sumiya E, Uesugi M, Kigoshi H (2013) Inhibition of microtubule assembly by a complex of actin and antitumor macrolide aplyronine A. *J Am Chem Soc* **135:** 18089-18095

Knox RJ, Friedlos F, Lydall DA, Roberts JJ (1986) Mechanism of cytotoxicity of anticancer platinum drugs: evidence that cis-diamminedichloroplatinum(II) and cis-diammine-(1,1-cyclobutanedicarboxylato)platinum(II) differ only in the kinetics of their interaction with DNA. *Cancer Res* **46:** 1972-1979

Koberle B, Masters JR, Hartley JA, Wood RD (1999) Defective repair of cisplatin-induced DNA damage caused by reduced XPA protein in testicular germ cell tumours. *Curr Biol* **9:** 273-276

Koberle B, Tomicic MT, Usanova S, Kaina B (2010) Cisplatin resistance: preclinical findings and clinical implications. *Biochim Biophys Acta* **1806:** 172-182

Kolfschoten IG, van Leeuwen B, Berns K, Mullenders J, Beijersbergen RL, Bernards R, Voorhoeve PM, Agami R (2005) A genetic screen identifies PITX1 as a suppressor of RAS activity and tumorigenicity. *Cell* **121:** 849-858

Kollman JM, Merdes A, Mourey L, Agard DA (2011) Microtubule nucleation by gamma-tubulin complexes. *Nat Rev Mol Cell Biol* **12:** 709-721

Kollman JM, Polka JK, Zelter A, Davis TN, Agard DA (2010) Microtubule nucleating gamma-TuSC assembles structures with 13-fold microtubule-like symmetry. *Nature* **466:** 879-882

Kool M, van der Linden M, de Haas M, Scheffer GL, de Vree JM, Smith AJ, Jansen G, Peters GJ, Ponne N, Scheper RJ, Elferink RP, Baas F, Borst P (1999) MRP3, an organic anion transporter able to transport anti-cancer drugs. *Proc Natl Acad Sci U S A* **96:** 6914-6919

Koulouris CR, Penson RT (2009) Ovarian stromal and germ cell tumors. *Semin Oncol* **36:** 126-136

Kunkel TA, Erie DA (2005) DNA mismatch repair. *Annu Rev Biochem* **74:** 681-710

Kuo KT, Guan B, Feng Y, Mao TL, Chen X, Jinawath N, Wang Y, Kurman RJ, Shih Ie M, Wang TL (2009) Analysis of DNA copy number alterations in ovarian serous tumors identifies new molecular genetic changes in low-grade and high-grade carcinomas. *Cancer Res* **69:** 4036-4042

Kurman RJ, Shih IM (2010) The origin and pathogenesis of epithelial ovarian cancer: a proposed unifying theory. *Am J Surg Pathol* **34:** 433-443

La Vecchia C, Decarli A, Negri E, Parazzini F, Gentile A, Cecchetti G, Fasoli M, Franceschi S (1987) Dietary factors and the risk of epithelial ovarian cancer. *J Natl Cancer Inst* **79:** 663-669

Lam LT, Davis RE, Ngo VN, Lenz G, Wright G, Xu W, Zhao H, Yu X, Dang L, Staudt LM (2008) Compensatory IKKalpha activation of classical NF-kappaB signaling during IKKbeta inhibition identified by an RNA interference sensitization screen. *Proc Natl Acad Sci U S A* **105:** 20798-20803

Lara R, Mauri FA, Taylor H, Derua R, Shia A, Gray C, Nicols A, Shiner RJ, Schofield E, Bates PA, Waelkens E, Dallman M, Lamb J, Zicha D, Downward J, Seckl MJ, Pardo OE (2011) An siRNA screen identifies RSK1 as a key modulator of lung cancer metastasis. *Oncogene* **30:** 3513-3521

Larrieu D, Britton S, Demir M, Rodriguez R, Jackson SP (2014) Chemical inhibition of NAT10 corrects defects of laminopathic cells. *Science* **344:** 527-532

Lawrenson K, Gayther SA (2009) Ovarian cancer: a clinical challenge that needs some basic answers. *PLoS Med* **6:** e25

Ledermann J, Harter P, Gourley C, Friedlander M, Vergote I, Rustin G, Scott C, Meier W, Shapira-Frommer R, Safra T, Matei D, Macpherson E, Watkins C, Carmichael J, Matulonis U (2012) Olaparib maintenance therapy in platinum-sensitive relapsed ovarian cancer. *N Engl J Med* **366:** 1382-1392

Lee S, Yoon S, Kim DH (2007) A high nuclear basal level of ERK2 phosphorylation contributes to the resistance of cisplatin-resistant human ovarian cancer cells. *Gynecol Oncol* **104:** 338-344

Leighton IA, Dalby KN, Caudwell FB, Cohen PT, Cohen P (1995) Comparison of the specificities of p70 S6 kinase and MAPKAP kinase-1 identifies a relatively specific substrate for p70 S6 kinase: the N-terminal kinase domain of MAPKAP kinase-1 is essential for peptide phosphorylation. *FEBS Lett* **375:** 289-293

Lengyel E (2010) Ovarian cancer development and metastasis. *Am J Pathol* **177:** 1053-1064

Li Q, Yu JJ, Mu C, Yunmbam MK, Slavsky D, Cross CL, Bostick-Bruton F, Reed E (2000) Association between the level of ERCC-1 expression and the repair of cisplatin-induced DNA damage in human ovarian cancer cells. *Anticancer Res* **20:** 645-652

Liedert B, Materna V, Schadendorf D, Thomale J, Lage H (2003) Overexpression of cMOAT (MRP2/ABCC2) is associated with decreased formation of platinum-DNA adducts and decreased G2-arrest in melanoma cells resistant to cisplatin. *J Invest Dermatol* **121:** 172-176

Liu G, Yang G, Chang B, Mercado-Uribe I, Huang M, Zheng J, Bast RC, Lin SH, Liu J (2010) Stanniocalcin 1 and ovarian tumorigenesis. *J Natl Cancer Inst* **102:** 812-827

Liu H, Ling Y, Gong Y, Sun Y, Hou L, Zhang B (2007) DNA damage induces N-acetyltransferase NAT10 gene expression through transcriptional activation. *Mol Cell Biochem* **300:** 249-258

Liu Y, Hayes DN, Nobel A, Marron JS (2008) Statistical Significance of Clustering for High-Dimension, Low-Sample Size Data. *Journal of the American Statistical Association* **103:** 1281-1293

Lobert S, Vulevic B, Correia JJ (1996) Interaction of vinca alkaloids with tubulin: a comparison of vinblastine, vincristine, and vinorelbine. *Biochemistry* **35:** 6806-6814

Lowe KA, Chia VM, Taylor A, O'Malley C, Kelsh M, Mohamed M, Mowat FS, Goff B (2013) An international assessment of ovarian cancer incidence and mortality. *Gynecol Oncol* **130:** 107-114

Luo B, Cheung HW, Subramanian A, Sharifnia T, Okamoto M, Yang X, Hinkle G, Boehm JS, Beroukhim R, Weir BA, Mermel C, Barbie DA, Awad T, Zhou X, Nguyen T, Piqani B, Li C, Golub TR, Meyerson M, Hacohen N, Hahn WC, Lander ES, Sabatini DM, Root DE (2008) Highly parallel identification of essential genes in cancer cells. *Proc Natl Acad Sci U S A* **105:** 20380-20385

Lv J, Liu H, Wang Q, Tang Z, Hou L, Zhang B (2003) Molecular cloning of a novel human gene encoding histone acetyltransferase-like protein involved in transcriptional activation of hTERT. *Biochem Biophys Res Commun* **311:** 506-513

Ma WW, Adjei AA (2009) Novel agents on the horizon for cancer therapy. *CA Cancer J Clin* **59:** 111-137

Mandic A, Hansson J, Linder S, Shoshan MC (2003) Cisplatin induces endoplasmic reticulum stress and nucleus-independent apoptotic signaling. *J Biol Chem* **278:** 9100-9106

Manfredi JJ, Horwitz SB (1984) Taxol: an antimitotic agent with a new mechanism of action. *Pharmacol Ther* **25:** 83-125

Markman M (2008) Antineoplastic agents in the management of ovarian cancer: current status and emerging therapeutic strategies. *Trends Pharmacol Sci* **29:** 515-519

Maruyama K, Ochiai A, Akimoto S, Nakamura S, Baba S, Moriya Y, Hirohashi S (2000) Cytoplasmic beta-catenin accumulation as a predictor of hematogenous metastasis in human colorectal cancer. *Oncology* **59:** 302-309

Matei D, Brown J, Frazier L (2013) Updates in the management of ovarian germ cell tumors. *Am Soc Clin Oncol Educ Book* **2013:** 210-216

Matsumura N, Huang Z, Mori S, Baba T, Fujii S, Konishi I, Iversen ES, Berchuck A, Murphy SK (2011) Epigenetic suppression of the TGF-beta pathway revealed by transcriptome profiling in ovarian cancer. *Genome Res* **21:** 74-82

McGuire WP, Hoskins WJ, Brady MF, Kucera PR, Partridge EE, Look KY, Clarke-Pearson DL, Davidson M (1996) Cyclophosphamide and cisplatin compared with paclitaxel and cisplatin in patients with stage III and stage IV ovarian cancer. *N Engl J Med* **334:** 1-6

Meacham CE, Ho EE, Dubrovsky E, Gertler FB, Hemann MT (2009) In vivo RNAi screening identifies regulators of actin dynamics as key determinants of lymphoma progression. *Nat Genet* **41:** 1133-1137

Mello JA, Lippard SJ, Essigmann JM (1995) DNA adducts of cis-diamminedichloroplatinum(II) and its trans isomer inhibit RNA polymerase II differentially in vivo. *Biochemistry* **34:** 14783-14791

Michalke B (2010) Platinum speciation used for elucidating activation or inhibition of Pt-containing anti-cancer drugs. *J Trace Elem Med Biol* **24:** 69-77

Mills GB, May C, Hill M, Campbell S, Shaw P, Marks A (1990) Ascitic fluid from human ovarian cancer patients contains growth factors necessary for intraperitoneal growth of human ovarian adenocarcinoma cells. *J Clin Invest* **86:** 851-855

Mink PJ, Folsom AR, Sellers TA, Kushi LH (1996) Physical activity, waist-to-hip ratio, and other risk factors for ovarian cancer: a follow-up study of older women. *Epidemiology* **7:** 38-45

Miracle-McMahill HL, Calle EE, Kosinski AS, Rodriguez C, Wingo PA, Thun MJ, Heath CW, Jr. (1997) Tubal ligation and fatal ovarian cancer in a large prospective cohort study. *Am J Epidemiol* **145:** 349-357

Moffat J, Grueneberg DA, Yang X, Kim SY, Kloepfer AM, Hinkle G, Piqani B, Eisenhaure TM, Luo B, Grenier JK, Carpenter AE, Foo SY, Stewart SA, Stockwell BR, Hacohen N, Hahn WC, Lander ES, Sabatini DM, Root DE (2006) A lentiviral RNAi library for human and mouse genes applied to an arrayed viral high-content screen. *Cell* **124:** 1283-1298

Mok SC, Bonome T, Vathipadiekal V, Bell A, Johnson ME, Wong KK, Park DC, Hao K, Yip DK, Donninger H, Ozbun L, Samimi G, Brady J, Randonovich M, Pise-Masison CA, Barrett JC, Wong WH, Welch WR, Berkowitz RS, Birrer MJ (2009) A gene signature predictive for outcome in advanced ovarian cancer identifies a survival factor: microfibril-associated glycoprotein 2. *Cancer Cell* **16:** 521-532

Monk BJ, Huang HQ, Burger RA, Mannel RS, Homesley HD, Fowler J, Greer BE, Boente M, Liang SX, Wenzel L (2012) Patient reported outcomes of a randomized, placebo-controlled trial of bevacizumab in the front-line treatment of ovarian cancer: A Gynecologic Oncology Group Study. *Gynecol Oncol*

Mori S, Chang JT, Andrechek ER, Matsumura N, Baba T, Yao G, Kim JW, Gatza M, Murphy S, Nevins JR (2009) Anchorage-independent cell growth signature identifies tumors with metastatic potential. *Oncogene* **28:** 2796-2805

Moritz M, Braunfeld MB, Sedat JW, Alberts B, Agard DA (1995) Microtubule nucleation by gamma-tubulin-containing rings in the centrosome. *Nature* **378:** 638-640

Nakamura M, Tsuji N, Asanuma K, Kobayashi D, Yagihashi A, Hirata K, Torigoe T, Sato N, Watanabe N (2004) Survivin as a predictor of cis-diamminedichloroplatinum sensitivity in gastric cancer patients. *Cancer Sci* **95:** 44-51

Nakamura Y (2004) Isolation of p53-target genes and their functional analysis. *Cancer Sci* **95:** 7-11

Nakayama K, Kanzaki A, Ogawa K, Miyazaki K, Neamati N, Takebayashi Y (2002) Copper-transporting P-type adenosine triphosphatase (ATP7B) as a cisplatin based chemoresistance marker in ovarian carcinoma: comparative analysis with expression of MDR1, MRP1, MRP2, LRP and BCRP. *Int J Cancer* **101:** 488-495

Neve RM, Chin K, Fridlyand J, Yeh J, Baehner FL, Fevr T, Clark L, Bayani N, Coppe JP, Tong F, Speed T, Spellman PT, DeVries S, Lapuk A, Wang NJ, Kuo WL, Stilwell JL, Pinkel D, Albertson DG, Waldman FM, McCormick F,

Dickson RB, Johnson MD, Lippman M, Ethier S, Gazdar A, Gray JW (2006) A collection of breast cancer cell lines for the study of functionally distinct cancer subtypes. *Cancer Cell* **10:** 515-527

Nigg EA (2006) Origins and consequences of centrosome aberrations in human cancers. *Int J Cancer* **119:** 2717-2723

Nonaka M, Itamochi H, Kawaguchi W, Kudoh A, Sato S, Uegaki K, Naniwa J, Sato S, Shimada M, Oishi T, Terakawa N, Kigawa J, Harada T (2012) Activation of the mitogen-activated protein kinase kinase/extracellular signal-regulated kinase pathway overcomes cisplatin resistance in ovarian carcinoma cells. *Int J Gynecol Cancer* **22:** 922-929

O'Shannessy DJ, Jackson SM, Twine NC, Hoffman BE, Dezso Z, Agoulnik SI, Somers EB (2013) Gene expression analyses support fallopian tube epithelium as the cell of origin of epithelial ovarian cancer. *Int J Mol Sci* **14:** 13687-13703

Oegema K, Wiese C, Martin OC, Milligan RA, Iwamatsu A, Mitchison TJ, Zheng Y (1999) Characterization of two related Drosophila gamma-tubulin complexes that differ in their ability to nucleate microtubules. *J Cell Biol* **144:** 721-733

Palmer A, Gavin AC, Nebreda AR (1998) A link between MAP kinase and p34(cdc2)/cyclin B during oocyte maturation: p90(rsk) phosphorylates and inactivates the p34(cdc2) inhibitory kinase Myt1. *EMBO J* **17:** 5037-5047

Partridge E, Kreimer AR, Greenlee RT, Williams C, Xu JL, Church TR, Kessel B, Johnson CC, Weissfeld JL, Isaacs C, Andriole GL, Ogden S, Ragard LR, Buys SS (2009) Results from four rounds of ovarian cancer screening in a randomized trial. *Obstet Gynecol* **113:** 775-782

Pejovic T, Pande NT, Mori M, Mhawech-Fauceglia P, Harrington C, Mongoue-Tchokote S, Dim D, Andrews C, Beck A, Tarumi Y, Djilas J, Cappuccini F, Caballero O, Huang J, Levy S, Tsiamouri A, Cain J, Bagby GC, Strausberg RL, Simpson AJ, Odunsi KO (2009) Expression profiling of the ovarian surface kinome reveals candidate genes for early neoplastic changes. *Transl Oncol* **2:** 341-349

Perdiz D, Mackeh R, Pous C, Baillet A (2011) The ins and outs of tubulin acetylation: more than just a post-translational modification? *Cell Signal* **23:** 763-771

Perou CM, Sorlie T, Eisen MB, van de Rijn M, Jeffrey SS, Rees CA, Pollack JR, Ross DT, Johnsen H, Akslen LA, Fluge O, Pergamenschikov A, Williams C, Zhu SX, Lonning PE, Borresen-Dale AL, Brown PO, Botstein D (2000) Molecular portraits of human breast tumours. *Nature* **406:** 747-752

Perren TJ, Swart AM, Pfisterer J, Ledermann JA, Pujade-Lauraine E, Kristensen G, Carey MS, Beale P, Cervantes A, Kurzeder C, du Bois A, Sehouli J, Kimmig R, Stahle A, Collinson F, Essapen S, Gourley C, Lortholary A, Selle F, Mirza MR, Leminen A, Plante M, Stark D, Qian W, Parmar MK, Oza AM (2011) A phase 3 trial of bevacizumab in ovarian cancer. *N Engl J Med* **365:** 2484-2496

Pettersson F, Fotiou S, Einhorn N, Silfversward C (1985) Cohort study of the long-term effect of irradiation for carcinoma of the uterine cervix. Second primary malignancies in the pelvic organs in women irradiated for cervical carcinoma at Radiumhemmet 1914-1965. *Acta Radiol Oncol* **24:** 145-151

Piccart MJ, Bertelsen K, James K, Cassidy J, Mangioni C, Simonsen E, Stuart G, Kaye S, Vergote I, Blom R, Grimshaw R, Atkinson RJ, Swenerton KD, Trope C, Nardi M, Kaern J, Tumolo S, Timmers P, Roy JA, Lhoas F, Lindvall B, Bacon M, Birt A, Andersen JE, Zee B, Paul J, Baron B, Pecorelli S (2000) Randomized intergroup trial of cisplatin-paclitaxel versus cisplatin-cyclophosphamide in women with advanced epithelial ovarian cancer: three-year results. *J Natl Cancer Inst* **92:** 699-708

Press JZ, De Luca A, Boyd N, Young S, Troussard A, Ridge Y, Kaurah P, Kalloger SE, Blood KA, Smith M, Spellman PT, Wang Y, Miller DM, Horsman D, Faham M, Gilks CB, Gray J, Huntsman DG (2008) Ovarian carcinomas with genetic and epigenetic BRCA1 loss have distinct molecular abnormalities. *BMC Cancer* **8:** 17

Purdie DM, Bain CJ, Siskind V, Webb PM, Green AC (2003) Ovulation and risk of epithelial ovarian cancer. *Int J Cancer* **104:** 228-232

Quintas-Cardama A, Kantarjian H, Cortes J (2009) Imatinib and beyond--exploring the full potential of targeted therapy for CML. *Nat Rev Clin Oncol* **6:** 535-543

Quirk JT, Natarajan N (2005) Ovarian cancer incidence in the United States, 1992-1999. *Gynecol Oncol* **97:** 519-523

Rauh-Adelmann C, Lau KM, Sabeti N, Long JP, Mok SC, Ho SM (2000) Altered expression of BRCA1, BRCA2, and a newly identified BRCA2 exon

12 deletion variant in malignant human ovarian, prostate, and breast cancer cell lines. *Mol Carcinog* **28:** 236-246

Reed E, Yuspa SH, Zwelling LA, Ozols RF, Poirier MC (1986) Quantitation of cis-diamminedichloroplatinum II (cisplatin)-DNA-intrastrand adducts in testicular and ovarian cancer patients receiving cisplatin chemotherapy. *J Clin Invest* **77:** 545-550

Rice MS, Murphy MA, Vitonis AF, Cramer DW, Titus LJ, Tworoger SS, Terry KL (2013) Tubal ligation, hysterectomy, and epithelial ovarian cancer in the New England case-control study. *Int J Cancer*

Riman T, Dickman PW, Nilsson S, Correia N, Nordlinder H, Magnusson CM, Persson IR (2002) Risk factors for invasive epithelial ovarian cancer: results from a Swedish case-control study. *Am J Epidemiol* **156:** 363-373

Risch HA, Marrett LD, Howe GR (1994) Parity, contraception, infertility, and the risk of epithelial ovarian cancer. *Am J Epidemiol* **140:** 585-597

Rixe O, Ortuzar W, Alvarez M, Parker R, Reed E, Paull K, Fojo T (1996) Oxaliplatin, tetraplatin, cisplatin, and carboplatin: spectrum of activity in drug-resistant cell lines and in the cell lines of the National Cancer Institute's Anticancer Drug Screen panel. *Biochem Pharmacol* **52:** 1855-1865

Rodriguez GC, Nagarsheth NP, Lee KL, Bentley RC, Walmer DK, Cline M, Whitaker RS, Isner P, Berchuck A, Dodge RK, Hughes CL (2002) Progestin-induced apoptosis in the Macaque ovarian epithelium: differential regulation of transforming growth factor-beta. *J Natl Cancer Inst* **94:** 50-60

Roland KB, Rodriguez JL, Patterson JR, Trivers KF (2013) A literature review of the social and psychological needs of ovarian cancer survivors. *Psychooncology*

Romagnoli R, Baraldi PG, Lopez-Cara C, Salvador MK, Preti D, Tabrizi MA, Balzarini J, Nussbaumer P, Bassetto M, Brancale A, Fu XH, Yang G, Li J, Zhang SZ, Hamel E, Bortolozzi R, Basso G, Viola G (2013) Design, synthesis and biological evaluation of 3,5-disubstituted 2-amino thiophene derivatives as a novel class of antitumor agents. *Bioorg Med Chem*

Root DE, Hacohen N, Hahn WC, Lander ES, Sabatini DM (2006) Genome-scale loss-of-function screening with a lentiviral RNAi library. *Nat Methods* **3:** 715-719

Rosell R, Viteri S, Molina MA, Benlloch S, Taron M (2010) Epidermal growth factor receptor tyrosine kinase inhibitors as first-line treatment in advanced nonsmall-cell lung cancer. *Curr Opin Oncol* **22:** 112-120

Rosenberg B, VanCamp L, Trosko JE, Mansour VH (1969) Platinum compounds: a new class of potent antitumour agents. *Nature* **222:** 385-386

Rothenberg ML, Oza AM, Bigelow RH, Berlin JD, Marshall JL, Ramanathan RK, Hart LL, Gupta S, Garay CA, Burger BG, Le Bail N, Haller DG (2003) Superiority of oxaliplatin and fluorouracil-leucovorin compared with either therapy alone in patients with progressive colorectal cancer after irinotecan and fluorouracil-leucovorin: interim results of a phase III trial. *J Clin Oncol* **21:** 2059-2069

Rousseeuw PJ (1987) Silhouettes: a graphical aid to the intepretation and validation of cluster analysis. *J Comput Appl Math* **20:** 53-65

Runnebaum IB, Stickeler E (2001) Epidemiological and molecular aspects of ovarian cancer risk. *J Cancer Res Clin Oncol* **127:** 73-79

Sabatier R, Finetti P, Cervera N, Birnbaum D, Bertucci F (2009) Gene expression profiling and prediction of clinical outcome in ovarian cancer. *Crit Rev Oncol Hematol* **72:** 98-109

Samimi G, Fink D, Varki NM, Husain A, Hoskins WJ, Alberts DS, Howell SB (2000) Analysis of MLH1 and MSH2 expression in ovarian cancer before and after platinum drug-based chemotherapy. *Clin Cancer Res* **6:** 1415-1421

Sandler A, Gray R, Perry MC, Brahmer J, Schiller JH, Dowlati A, Lilenbaum R, Johnson DH (2006) Paclitaxel-carboplatin alone or with bevacizumab for non-small-cell lung cancer. *N Engl J Med* **355:** 2542-2550

Saneja A, Khare V, Alam N, Dubey RD, Gupta PN (2014) Advances in P-glycoprotein-based approaches for delivering anticancer drugs: pharmacokinetic perspective and clinical relevance. *Expert Opin Drug Deliv* **11:** 121-138

Sawyers CL, Abate-Shen C, Anderson KC, Barker A, Baselga J, Berger NA, Foti M, Jemal A, Lawrence TS, Li CI, Mardis ER, Neumann PJ, Pardoll DM, Prendergast GC, Reed JC, Weiner GJ (2013) Cancer Progress Report 2013. *Clin Cancer Res*

Schiff PB, Fant J, Horwitz SB (1979) Promotion of microtubule assembly in vitro by taxol. *Nature* **277:** 665-667

Schilder RJ, Hall L, Monks A, Handel LM, Fornace AJ, Jr., Ozols RF, Fojo AT, Hamilton TC (1990) Metallothionein gene expression and resistance to cisplatin in human ovarian cancer. *Int J Cancer* **45:** 416-422

Schindelin J, Arganda-Carreras I, Frise E, Kaynig V, Longair M, Pietzsch T, Preibisch S, Rueden C, Saalfeld S, Schmid B, Tinevez JY, White DJ, Hartenstein V, Eliceiri K, Tomancak P, Cardona A (2012) Fiji: an open-source platform for biological-image analysis. *Nat Methods* **9:** 676-682

Schlesselman JJ (1995) Net effect of oral contraceptive use on the risk of cancer in women in the United States. *Obstet Gynecol* **85:** 793-801

Scholl C, Frohling S, Dunn IF, Schinzel AC, Barbie DA, Kim SY, Silver SJ, Tamayo P, Wadlow RC, Ramaswamy S, Dohner K, Bullinger L, Sandy P, Boehm JS, Root DE, Jacks T, Hahn WC, Gilliland DG (2009) Synthetic lethal interaction between oncogenic KRAS dependency and STK33 suppression in human cancer cells. *Cell* **137:** 821-834

Schorge JO, Modesitt SC, Coleman RL, Cohn DE, Kauff ND, Duska LR, Herzog TJ (2010) SGO White Paper on ovarian cancer: etiology, screening and surveillance. *Gynecol Oncol* **119:** 7-17

Schwab MS, Roberts BT, Gross SD, Tunquist BJ, Taieb FE, Lewellyn AL, Maller JL (2001) Bub1 is activated by the protein kinase p90(Rsk) during Xenopus oocyte maturation. *Curr Biol* **11:** 141-150

Shen Q, Zheng X, McNutt MA, Guang L, Sun Y, Wang J, Gong Y, Hou L, Zhang B (2009) NAT10, a nucleolar protein, localizes to the midbody and regulates cytokinesis and acetylation of microtubules. *Exp Cell Res* **315:** 1653-1667

Shih Ie M, Kurman RJ (2004) Ovarian tumorigenesis: a proposed model based on morphological and molecular genetic analysis. *Am J Pathol* **164:** 1511-1518

Siegel R, Naishadham D, Jemal A (2013) Cancer statistics, 2013. *CA Cancer J Clin* **63:** 11-30

Sims D, Mendes-Pereira AM, Frankum J, Burgess D, Cerone MA, Lombardelli C, Mitsopoulos C, Hakas J, Murugaesu N, Isacke CM, Fenwick

K, Assiotis I, Kozarewa I, Zvelebil M, Ashworth A, Lord CJ (2011) High-throughput RNA interference screening using pooled shRNA libraries and next generation sequencing. *Genome Biol* **12:** R104

Singer G, Oldt R, 3rd, Cohen Y, Wang BG, Sidransky D, Kurman RJ, Shih Ie M (2003) Mutations in BRAF and KRAS characterize the development of low-grade ovarian serous carcinoma. *J Natl Cancer Inst* **95:** 484-486

Singer G, Stohr R, Cope L, Dehari R, Hartmann A, Cao DF, Wang TL, Kurman RJ, Shih Ie M (2005) Patterns of p53 mutations separate ovarian serous borderline tumors and low- and high-grade carcinomas and provide support for a new model of ovarian carcinogenesis: a mutational analysis with immunohistochemical correlation. *Am J Surg Pathol* **29:** 218-224

Slamon DJ, Leyland-Jones B, Shak S, Fuchs H, Paton V, Bajamonde A, Fleming T, Eiermann W, Wolter J, Pegram M, Baselga J, Norton L (2001) Use of chemotherapy plus a monoclonal antibody against HER2 for metastatic breast cancer that overexpresses HER2. *N Engl J Med* **344:** 783-792

Smith JA, Maloney DJ, Hecht SM, Lannigan DA (2007) Structural basis for the activity of the RSK-specific inhibitor, SL0101. *Bioorg Med Chem* **15:** 5018-5034

Smith JA, Poteet-Smith CE, Xu Y, Errington TM, Hecht SM, Lannigan DA (2005) Identification of the first specific inhibitor of p90 ribosomal S6 kinase (RSK) reveals an unexpected role for RSK in cancer cell proliferation. *Cancer Res* **65:** 1027-1034

Smolen GA, Zhang J, Zubrowski MJ, Edelman EJ, Luo B, Yu M, Ng LW, Scherber CM, Schott BJ, Ramaswamy S, Irimia D, Root DE, Haber DA (2010) A genome-wide RNAi screen identifies multiple RSK-dependent regulators of cell migration. *Genes Dev* **24:** 2654-2665

Sordella R, Bell DW, Haber DA, Settleman J (2004) Gefitinib-sensitizing EGFR mutations in lung cancer activate anti-apoptotic pathways. *Science* **305:** 1163-1167

Sorlie T, Perou CM, Tibshirani R, Aas T, Geisler S, Johnsen H, Hastie T, Eisen MB, van de Rijn M, Jeffrey SS, Thorsen T, Quist H, Matese JC, Brown PO, Botstein D, Lonning PE, Borresen-Dale AL (2001) Gene expression patterns of breast carcinomas distinguish tumor subclasses with clinical implications. *Proc Natl Acad Sci U S A* **98:** 10869-10874

Stanton RA, Gernert KM, Nettles JH, Aneja R (2011) Drugs that target dynamic microtubules: a new molecular perspective. *Med Res Rev* **31:** 443-481

Stark D, Nankivell M, Pujade-Lauraine E, Kristensen G, Elit L, Stockler M, Hilpert F, Cervantes A, Brown J, Lanceley A, Velikova G, Sabate E, Pfisterer J, Carey MS, Beale P, Qian W, Swart AM, Oza A, Perren T (2013) Standard chemotherapy with or without bevacizumab in advanced ovarian cancer: quality-of-life outcomes from the International Collaboration on Ovarian Neoplasms (ICON7) phase 3 randomised trial. *Lancet Oncol* **14:** 236-243

Stepanova T, Slemmer J, Hoogenraad CC, Lansbergen G, Dortland B, De Zeeuw CI, Grosveld F, van Cappellen G, Akhmanova A, Galjart N (2003) Visualization of microtubule growth in cultured neurons via the use of EB3-GFP (end-binding protein 3-green fluorescent protein). *J Neurosci* **23:** 2655-2664

Strathdee G, MacKean MJ, Illand M, Brown R (1999) A role for methylation of the hMLH1 promoter in loss of hMLH1 expression and drug resistance in ovarian cancer. *Oncogene* **18:** 2335-2341

Strezoska Z, Licon A, Haimes J, Spayd KJ, Patel KM, Sullivan K, Jastrzebski K, Simpson KJ, Leake D, van Brabant Smith A, Vermeulen A (2012) Optimized PCR conditions and increased shRNA fold representation improve reproducibility of pooled shRNA screens. *PLoS One* **7:** e42341

Sturgeon CM, Duffy MJ, Stenman UH, Lilja H, Brunner N, Chan DW, Babaian R, Bast RC, Jr., Dowell B, Esteva FJ, Haglund C, Harbeck N, Hayes DF, Holten-Andersen M, Klee GG, Lamerz R, Looijenga LH, Molina R, Nielsen HJ, Rittenhouse H, Semjonow A, Shih Ie M, Sibley P, Soletormos G, Stephan C, Sokoll L, Hoffman BR, Diamandis EP (2008) National Academy of Clinical Biochemistry laboratory medicine practice guidelines for use of tumor markers in testicular, prostate, colorectal, breast, and ovarian cancers. *Clin Chem* **54:** e11-79

Subramanian A, Tamayo P, Mootha VK, Mukherjee S, Ebert BL, Gillette MA, Paulovich A, Pomeroy SL, Golub TR, Lander ES, Mesirov JP (2005) Gene set enrichment analysis: a knowledge-based approach for interpreting genome-wide expression profiles. *Proc Natl Acad Sci U S A* **102:** 15545-15550

Syrjanen K, Syrjanen S (2013) Detection of human papillomavirus in sinonasal papillomas: Systematic review and meta-analysis. *Laryngoscope* **123:** 181-192

Szabo CI, King MC (1997) Population genetics of BRCA1 and BRCA2. *Am J Hum Genet* **60:** 1013-1020

Szakacs G, Paterson JK, Ludwig JA, Booth-Genthe C, Gottesman MM (2006) Targeting multidrug resistance in cancer. *Nat Rev Drug Discov* **5:** 219-234

Takano M, Kikuchi Y, Yaegashi N, Kuzuya K, Ueki M, Tsuda H, Suzuki M, Kigawa J, Takeuchi S, Tsuda H, Moriya T, Sugiyama T (2006) Clear cell carcinoma of the ovary: a retrospective multicentre experience of 254 patients with complete surgical staging. *Br J Cancer* **94:** 1369-1374

Tan DS, Iravani M, McCluggage WG, Lambros MB, Milanezi F, Mackay A, Gourley C, Geyer FC, Vatcheva R, Millar J, Thomas K, Natrajan R, Savage K, Fenwick K, Williams A, Jameson C, El-Bahrawy M, Gore ME, Gabra H, Kaye SB, Ashworth A, Reis-Filho JS (2011) Genomic analysis reveals the molecular heterogeneity of ovarian clear cell carcinomas. *Clin Cancer Res* **17:** 1521-1534

Tan TZ, Miow QH, Huang RY, Wong MK, Ye J, Lau JA, Wu MC, Bin Abdul Hadi LH, Soong R, Choolani M, Davidson B, Nesland JM, Wang LZ, Matsumura N, Mandai M, Konishi I, Goh BC, Chang JT, Thiery JP, Mori S (2013) Functional genomics identifies five distinct molecular subtypes with clinical relevance and pathways for growth control in epithelial ovarian cancer. *EMBO Mol Med* **5:** 1051-1066

The Cancer Genome Atlas Research Network (2011) Integrated genomic analyses of ovarian carcinoma. *Nature* **474:** 609-615

The Cancer Genome Atlas Research Network (2012) Comprehensive molecular portraits of human breast tumours. *Nature* **490:** 61-70

Thiery JP, Acloque H, Huang RY, Nieto MA (2009) Epithelial-mesenchymal transitions in development and disease. *Cell* **139:** 871-890

Tone AA, Begley H, Sharma M, Murphy J, Rosen B, Brown TJ, Shaw PA (2008) Gene expression profiles of luteal phase fallopian tube epithelium from BRCA mutation carriers resemble high-grade serous carcinoma. *Clin Cancer Res* **14:** 4067-4078

Tothill RW, Tinker AV, George J, Brown R, Fox SB, Lade S, Johnson DS, Trivett MK, Etemadmoghadam D, Locandro B, Traficante N, Fereday S, Hung JA, Chiew YE, Haviv I, Gertig D, DeFazio A, Bowtell DD (2008) Novel molecular subtypes of serous and endometrioid ovarian cancer linked to clinical outcome. *Clin Cancer Res* **14:** 5198-5208

Tung CS, Mok SC, Tsang YT, Zu Z, Song H, Liu J, Deavers MT, Malpica A, Wolf JK, Lu KH, Gershenson DM, Wong KK (2009) PAX2 expression in low malignant potential ovarian tumors and low-grade ovarian serous carcinomas. *Mod Pathol* **22:** 1243-1250

Uchida K, Tanaka Y, Nishimura T, Hashimoto Y, Watanabe T, Harada I (1986) Effect of serum on inhibition of DNA synthesis in leukemia cells by cis- and trans-(Pt (NH3) 2C1(2)). *Biochem Biophys Res Commun* **138:** 631-637

Utepbergenov D, Derewenda U, Olekhnovich N, Szukalska G, Banerjee B, Hilinski MK, Lannigan DA, Stukenberg PT, Derewenda ZS (2012) Insights into the inhibition of the p90 ribosomal S6 kinase (RSK) by the flavonol glycoside SL0101 from the 1.5 A crystal structure of the N-terminal domain of RSK2 with bound inhibitor. *Biochemistry* **51:** 6499-6510

Vaisman A, Varchenko M, Umar A, Kunkel TA, Risinger JI, Barrett JC, Hamilton TC, Chaney SG (1998) The role of hMLH1, hMSH3, and hMSH6 defects in cisplatin and oxaliplatin resistance: correlation with replicative bypass of platinum-DNA adducts. *Cancer Res* **58:** 3579-3585

Vaughan S, Coward JI, Bast RC, Jr., Berchuck A, Berek JS, Brenton JD, Coukos G, Crum CC, Drapkin R, Etemadmoghadam D, Friedlander M, Gabra H, Kaye SB, Lord CJ, Lengyel E, Levine DA, McNeish IA, Menon U, Mills GB, Nephew KP, Oza AM, Sood AK, Stronach EA, Walczak H, Bowtell DD, Balkwill FR (2011) Rethinking ovarian cancer: recommendations for improving outcomes. *Nat Rev Cancer* **11:** 719-725

Vella N, Aiello M, Russo AE, Scalisi A, Spandidos DA, Toffoli G, Sorio R, Libra M, Stivala F (2011) 'Genetic profiling' and ovarian cancer therapy (review). *Mol Med Rep* **4:** 771-777

Verhaak RG, Hoadley KA, Purdom E, Wang V, Qi Y, Wilkerson MD, Miller CR, Ding L, Golub T, Mesirov JP, Alexe G, Lawrence M, O'Kelly M, Tamayo P, Weir BA, Gabriel S, Winckler W, Gupta S, Jakkula L, Feiler HS, Hodgson JG, James CD, Sarkaria JN, Brennan C, Kahn A, Spellman PT, Wilson RK, Speed TP, Gray JW, Meyerson M, Getz G, Perou CM, Hayes DN (2010) Integrated genomic analysis identifies clinically relevant subtypes of glioblastoma characterized by abnormalities in PDGFRA, IDH1, EGFR, and NF1. *Cancer Cell* **17:** 98-110

Verhaak RG, Tamayo P, Yang JY, Hubbard D, Zhang H, Creighton CJ, Fereday S, Lawrence M, Carter SL, Mermel CH, Kostic AD, Etemadmoghadam D, Saksena G, Cibulskis K, Duraisamy S, Levanon K,

Sougnez C, Tsherniak A, Gomez S, Onofrio R, Gabriel S, Chin L, Zhang N, Spellman PT, Zhang Y, Akbani R, Hoadley KA, Kahn A, Kobel M, Huntsman D, Soslow RA, Defazio A, Birrer MJ, Gray JW, Weinstein JN, Bowtell DD, Drapkin R, Mesirov JP, Getz G, Levine DA, Meyerson M (2013) Prognostically relevant gene signatures of high-grade serous ovarian carcinoma. *J Clin Invest* **123:** 517-525

Verollet C, Colombie N, Daubon T, Bourbon HM, Wright M, Raynaud-Messina B (2006) Drosophila melanogaster gamma-TuRC is dispensable for targeting gamma-tubulin to the centrosome and microtubule nucleation. *J Cell Biol* **172:** 517-528

Wang D, Lippard SJ (2005) Cellular processing of platinum anticancer drugs. *Nat Rev Drug Discov* **4:** 307-320

Whitehurst AW, Bodemann BO, Cardenas J, Ferguson D, Girard L, Peyton M, Minna JD, Michnoff C, Hao W, Roth MG, Xie XJ, White MA (2007) Synthetic lethal screen identification of chemosensitizer loci in cancer cells. *Nature* **446:** 815-819

Wolf CR, Hayward IP, Lawrie SS, Buckton K, McIntyre MA, Adams DJ, Lewis AD, Scott AR, Smyth JF (1987) Cellular heterogeneity and drug resistance in two ovarian adenocarcinoma cell lines derived from a single patient. *Int J Cancer* **39:** 695-702

Xiong Y, Oakley BR (2009) In vivo analysis of the functions of gamma-tubulin-complex proteins. *J Cell Sci* **122:** 4218-4227

Yamasaki M, Makino T, Masuzawa T, Kurokawa Y, Miyata H, Takiguchi S, Nakajima K, Fujiwara Y, Matsuura N, Mori M, Doki Y (2011) Role of multidrug resistance protein 2 (MRP2) in chemoresistance and clinical outcome in oesophageal squamous cell carcinoma. *Br J Cancer* **104:** 707-713

Yang G, Chang B, Yang F, Guo X, Cai KQ, Xiao XS, Wang H, Sen S, Hung MC, Mills GB, Chang S, Multani AS, Mercado-Uribe I, Liu J (2010) Aurora kinase A promotes ovarian tumorigenesis through dysregulation of the cell cycle and suppression of BRCA2. *Clin Cancer Res* **16:** 3171-3181

Yaziji H, Goldstein LC, Barry TS, Werling R, Hwang H, Ellis GK, Gralow JR, Livingston RB, Gown AM (2004) HER-2 testing in breast cancer using parallel tissue-based methods. *JAMA* **291:** 1972-1977

Yin JJ, Selander K, Chirgwin JM, Dallas M, Grubbs BG, Wieser R, Massague J, Mundy GR, Guise TA (1999) TGF-beta signaling blockade inhibits PTHrP

secretion by breast cancer cells and bone metastases development. *J Clin Invest* **103:** 197-206

Zender L, Xue W, Zuber J, Semighini CP, Krasnitz A, Ma B, Zender P, Kubicka S, Luk JM, Schirmacher P, McCombie WR, Wigler M, Hicks J, Hannon GJ, Powers S, Lowe SW (2008) An oncogenomics-based in vivo RNAi screen identifies tumor suppressors in liver cancer. *Cell* **135:** 852-864

Zeuthen J, Norgaard JO, Avner P, Fellous M, Wartiovaara J, Vaheri A, Rosen A, Giovanella BC (1980) Characterization of a human ovarian teratocarcinoma-derived cell line. *Int J Cancer* **25:** 19-32

Ziauddin J, Sabatini DM (2001) Microarrays of cells expressing defined cDNAs. *Nature* **411:** 107-110

Zorn KK, Bonome T, Gangi L, Chandramouli GV, Awtrey CS, Gardner GJ, Barrett JC, Boyd J, Birrer MJ (2005) Gene expression profiles of serous, endometrioid, and clear cell subtypes of ovarian and endometrial cancer. *Clin Cancer Res* **11:** 6422-6430

Appendix I. The genes for subtype-specific depleted and amplified shRNAs.

Index	Gene	NES	False Discovery Rate *q*-value	Hairpin ID	Hairpin score	Effect size	Subtype	Depleted/ Amplified
1	*RNF2*	1.88	0	TRCN0000033698,TRCN0000033695,TRCN0000033694	0.59, 0.56, 0.43	-0.98, -1.12, -0.86	Epi-A	Depleted
2	*AQP12A*	1.82	0.0001	TRCN0000060249,TRCN0000060252	0.85, 0.47	-1.55, -0.86	Epi-A	Depleted
3	*ZNF673*	1.81	0.0002	TRCN0000018204,TRCN0000018203,TRCN0000018205	0.46, 0.45, 0.44	-0.79, -0.84, -0.75	Epi-A	Depleted
4	*LIX1L*	1.8	0.0004	TRCN0000135165,TRCN0000138619	0.65, 0.46	-1.05, -0.74	Epi-A	Depleted
5	*SH3TC1*	1.8	0.0004	TRCN0000062609,TRCN0000062608	0.51, 0.46	-0.92, -0.93	Epi-A	Depleted
6	*CD160*	1.79	0.0014	TRCN0000057578,TRCN0000057581,TRCN0000057580	0.60, 0.45, 0.35	-1.12, -0.85, -0.67	Epi-A	Depleted
7	*LIN7A*	1.79	0.0005	TRCN0000116868,TRCN0000116871	0.64, 0.49	-1.24, -0.97	Epi-A	Depleted
8	*NIP7*	1.79	0.0014	TRCN0000145541,TRCN0000139190,TRCN0000144658 ,TRCN0000122000	0.80, 0.70, 0.34, 0.34	-1.23, -1.13, -0.55, -0.57	Epi-A	Depleted
9	*FAM26E*	1.78	0.0007	TRCN0000122216,TRCN0000142408	0.58, 0.48	-1.03, -0.82	Epi-A	Depleted
10	*MRAS*	1.78	0.0014	TRCN0000036992,TRCN0000036990	0.70, 0.51	-1.34, -1.02	Epi-A	Depleted
11	*RBM14*	1.78	0.0007	TRCN0000072693,TRCN0000072694,TRCN0000072695	0.59, 0.45, 0.42	-0.87, -0.89, -0.78	Epi-A	Depleted
12	*SPON1*	1.78	0.0016	TRCN0000116980,TRCN0000116979,TRCN0000116977	0.73, 0.65, 0.60	-1.15, -1.22, -1.13	Epi-A	Depleted
13	*C9orf98*	1.77	0.0023	TRCN0000078681,TRCN0000078678,TRCN0000078682	0.57, 0.47, 0.38	-0.97, -0.91, -0.75	Epi-A	Depleted
14	*ERVWE1*	1.77	0.0021	TRCN0000062273,TRCN0000062277,TRCN0000062276	0.62, 0.51, 0.35	-1.21, -0.86, -0.63	Epi-A	Depleted
15	*LEP*	1.77	0.002	TRCN0000058357,TRCN0000058355,TRCN0000058353 ,TRCN0000058354	0.66, 0.40, 0.39, 0.34	-1.11, -0.78, -0.70, -0.67	Epi-A	Depleted
16	*NCAM1*	1.77	0.0008	TRCN0000073460,TRCN0000073462	0.62, 0.41	-0.91, -0.79	Epi-A	Depleted

Appendix I. The genes for subtype-specific depleted and amplified shRNAs. (continued)

Index	Gene	NES	*False Discovery Rate q*-value	Hairpin ID	Hairpin score	Effect size	Subtype	Depleted/ Amplified
17	*CARS*	1.76	0.0008	TRCN0000045755,TRCN0000045757,TRCN0000045753	0.72, 0.46, 0.40	-1.19, -0.79, -0.66	Epi-A	Depleted
18	*HELB*	1.76	0.0008	TRCN0000152487,TRCN0000152488	0.47, 0.46	-0.79, -0.77	Epi-A	Depleted
19	*PDE4D*	1.75	0.0028	TRCN0000048835,TRCN0000048837,TRCN0000048836	0.85, 0.33, 0.31	-1.46, -0.62, -0.62	Epi-A	Depleted
20	*RAB1B*	1.75	0.0009	TRCN0000047216,TRCN0000047217	0.56, 0.53	-1.10, -0.91	Epi-A	Depleted
21	*STAG3L1*	1.75	0.003	TRCN0000062692,TRCN0000062691,TRCN0000062689	0.64, 0.62, 0.47	-1.13, -1.13, -0.75	Epi-A	Depleted
22	*XRCC6*	1.75	0.0033	TRCN0000039612,TRCN0000039608,TRCN0000010371	0.93, 0.62, 0.37	-1.66, -1.17, -0.72	Epi-A	Depleted
23	*DLAT*	1.74	0.0033	TRCN0000035922	1.06	-1.93	Epi-A	Depleted
24	*KIAA0196*	1.74	0.0034	TRCN0000128435,TRCN0000129923,TRCN0000128018	0.77, 0.48, 0.44	-1.27, -0.77, -0.87	Epi-A	Depleted
25	*RNF34*	1.74	0.0033	TRCN0000033950,TRCN0000033952,TRCN0000033953	0.47, 0.44, 0.41	-0.93, -0.85, -0.72	Epi-A	Depleted
26	*SNX31*	1.74	0.0033	TRCN0000135764,TRCN0000136843,TRCN0000135498	0.63, 0.48, 0.44	-1.00, -0.81, -0.85	Epi-A	Depleted
27	*C7orf58*	1.73	0.0036	TRCN0000136490,TRCN0000137513,TRCN0000137019	0.80, 0.54, 0.46	-1.17, -0.89, -0.72	Epi-A	Depleted
28	*COX10*	1.73	0.0015	TRCN0000034557,TRCN0000034558	0.67, 0.40	-1.28, -0.60	Epi-A	Depleted
29	*FBLN1*	1.73	0.0036	TRCN0000055677,TRCN0000055673,TRCN0000055675	0.77, 0.57, 0.42	-1.26, -1.02, -0.84	Epi-A	Depleted
30	*HEY2*	1.73	0.0015	TRCN0000020252,TRCN0000020253,TRCN0000020251	0.44, 0.37, 0.37	-0.86, -0.67, -0.63	Epi-A	Depleted
31	*SCLY*	1.73	0.0039	TRCN0000078291,TRCN0000078289	0.87, 0.57	-1.58, -0.96	Epi-A	Depleted

Appendix I. The genes for subtype-specific depleted and amplified shRNAs. (continued)

Index	Gene	NES	*False Discovery Rate q*-value	Hairpin ID	Hairpin score	Effect size	Subtype	Depleted/ Amplified
32	*C13orf27*	1.72	0.0018	TRCN0000072335,TRCN0000072333	0.55, 0.37	-0.83, -0.61	Epi-A	Depleted
33	*CRLF3*	1.72	0.004	TRCN0000063378,TRCN0000063380,TRCN0000063379 ,TRCN0000063381	0.68, 0.44, 0.35, 0.26	-1.16, -0.86, -0.70, -0.52	Epi-A	Depleted
34	*LRRC36*	1.72	0.0017	TRCN0000128589,TRCN0000146913,TRCN0000129364	0.66, 0.47, 0.38	-1.22, -0.91, -0.64	Epi-A	Depleted
35	*OR4D9*	1.72	0.004	TRCN0000061034,TRCN0000061036,TRCN0000061037	0.62, 0.56, 0.42	-1.17, -0.96, -0.80	Epi-A	Depleted
36	*TTK*	1.72	0.0048	TRCN0000006358,TRCN0000006356	0.48, 0.38	-0.83, -0.63	Epi-A	Depleted
37	*GRID1*	1.71	0.0048	TRCN0000063035,TRCN0000063036	0.53, 0.28	-1.01, -0.56	Epi-A	Depleted
38	*DCTN1*	1.7	0.0024	TRCN0000063971,TRCN0000063968	0.53, 0.46	-0.89, -0.74	Epi-A	Depleted
39	*LMNB1*	1.7	0.0024	TRCN0000029270,TRCN0000029271,TRCN0000029269 ,TRCN0000029272	0.45, 0.36, 0.35, 0.33	-0.74, -0.73, -0.58, -0.64	Epi-A	Depleted
40	*MRGPRF*	1.7	0.0024	TRCN0000011771,TRCN0000011770	0.35, 0.35	-0.59, -0.62	Epi-A	Depleted
41	*SEMA6B*	1.7	0.0024	TRCN0000061039,TRCN0000061041,TRCN0000061038	0.80, 0.57, 0.36	-1.23, -0.96, -0.59	Epi-A	Depleted
42	*NCAPD3*	1.69	0.0026	TRCN0000062184,TRCN0000062185,TRCN0000062186	0.66, 0.50, 0.38	-1.20, -0.99, -0.69	Epi-A	Depleted
43	*TMEM38A*	1.69	0.0027	TRCN0000127540,TRCN0000129632	0.41, 0.35	-0.67, -0.59	Epi-A	Depleted
44	*WDR72*	1.69	0.0002	TRCN0000137006,TRCN0000134128	0.84, 0.69	-1.47, -1.15	Epi-A	Depleted
45	*KCNS1*	1.68	0.0031	TRCN0000044214	0.59	-1.17	Epi-A	Depleted
46	*LASS6*	1.68	0.0031	TRCN0000128857,TRCN0000128836	0.52, 0.46	-1.02, -0.73	Epi-A	Depleted
47	*NRCAM*	1.68	0.0002	TRCN0000123083,TRCN0000123082,TRCN0000123081	0.67, 0.50, 0.48	-1.08, -0.84, -0.93	Epi-A	Depleted
48	*PCDHGA2*	1.68	0.0031	TRCN0000053813,TRCN0000053814,TRCN0000053816	0.47, 0.40, 0.35	-0.93, -0.78, -0.69	Epi-A	Depleted

Appendix I. The genes for subtype-specific depleted and amplified shRNAs. (continued)

Index	Gene	NES	*False Discovery Rate q*-value	Hairpin ID	Hairpin score	Effect size	Subtype	Depleted/ Amplified
49	*SARNP*	1.68	0.0035	TRCN0000151631,TRCN0000152985	0.54, 0.50	-0.86, -0.79	Epi-A	Depleted
50	*SEC13*	1.68	0.0033	TRCN0000064985,TRCN0000064983	0.46, 0.38	-0.92, -0.72	Epi-A	Depleted
51	*DCUN1D1*	1.67	0.0041	TRCN0000137624,TRCN0000134715,TRCN0000134676	0.41, 0.37, 0.32	-0.60, -0.58, -0.52	Epi-A	Depleted
52	*FOLR3*	1.67	0.0042	TRCN0000060528,TRCN0000060529,TRCN0000060530	0.62, 0.59, 0.38	-0.97, -1.01, -0.61	Epi-A	Depleted
53	*GPR176*	1.67	0.0042	TRCN0000011490,TRCN0000011491	0.53, 0.53	-0.94, -0.92	Epi-A	Depleted
54	*LRRFIP2*	1.67	0.0042	TRCN0000061978,TRCN0000061980	0.52, 0.51	-0.89, -0.93	Epi-A	Depleted
55	*CDK8*	1.66	0.0044	TRCN0000000493,TRCN0000000490,TRCN0000000489	0.43, 0.35, 0.32	-0.73, -0.58, -0.51	Epi-A	Depleted
56	*MYO1C*	1.66	0.0005	TRCN0000122927,TRCN0000122926	0.58, 0.45	-0.97, -0.76	Epi-A	Depleted
57	*SEMG2*	1.65	0.0049	TRCN0000154196,TRCN0000156481	0.71, 0.46	-1.08, -0.74	Epi-A	Depleted
58	*WDR67*	1.65	0.0049	TRCN0000143325,TRCN0000142816	0.53, 0.41	-0.82, -0.69	Epi-A	Depleted
59	*MYH10*	1.64	0.001	TRCN0000123075	0.49	-0.86	Epi-A	Depleted
60	*SIM2*	1.63	0.0017	TRCN0000015150,TRCN0000015148	0.57, 0.51	-1.01, -0.90	Epi-A	Depleted
61	*C1orf14*	1.62	0.0024	TRCN0000136159,TRCN0000159649	0.82, 0.56	-1.29, -0.88	Epi-A	Depleted
62	*PRAMEF7*	1.62	0.0021	TRCN0000130745,TRCN0000128088	0.57, 0.41	-0.98, -0.64	Epi-A	Depleted
63	*CASP10*	1.61	0.0028	TRCN0000003586,TRCN0000003588	0.50, 0.47	-0.87, -0.88	Epi-A	Depleted
64	*OR51T1*	1.61	0.0029	TRCN0000061471,TRCN0000061469	0.99, 0.54	-1.94, -1.08	Epi-A	Depleted
65	*SFRS8*	1.61	0.0027	TRCN0000017226,TRCN0000017224	0.52, 0.48	-0.97, -0.90	Epi-A	Depleted
66	*SAMSN1*	1.6	0.0034	TRCN0000136656,TRCN0000138187	0.47, 0.41	-0.82, -0.65	Epi-A	Depleted
67	*MAP2K2*	1.59	0.0037	TRCN0000007007	0.72	-1.34	Epi-A	Depleted
68	*PALLD*	1.59	0.0035	TRCN0000073463	0.55	-0.86	Epi-A	Depleted

Appendix I. The genes for subtype-specific depleted and amplified shRNAs. (continued)

Index	Gene	NES	*False Discovery Rate q*-value	Hairpin ID	Hairpin score	Effect size	Subtype	Depleted/ Amplified
69	*CLDND1*	1.58	0.0044	TRCN0000146451	0.59	-0.89	Epi-A	Depleted
70	*KLHL17*	1.58	0.0044	TRCN0000155542	0.61	-0.91	Epi-A	Depleted
71	*EYS*	1.57	0.0046	TRCN0000040249	0.59	-1.15	Epi-A	Depleted
72	*PAX6*	1.57	0.0046	TRCN0000016126,TRCN0000016127	0.55, 0.37	-0.98, -0.73	Epi-A	Depleted
73	*C20orf19*	1.53	0.0011	TRCN0000133823	0.57	-0.85	Epi-A	Depleted
74	*SLC15A1*	1.52	0.0013	TRCN0000043300	0.74	-1.32	Epi-A	Depleted
75	*LZTS2*	1.51	0.0021	TRCN0000021124,TRCN0000021126	0.51, 0.50	-0.90, -0.85	Epi-A	Depleted
76	*MAD1L1*	1.49	0.0041	TRCN0000006563	0.49	-0.86	Epi-A	Depleted
77	*WFDC12*	1.49	0.0039	TRCN0000073672	0.5	-0.82	Epi-A	Depleted
78	*PLEKHA3*	1.9	0	TRCN0000147627,TRCN0000149526,TRCN0000149956	0.50, 0.49, 0.43	-0.82, -0.72, -0.78	Mes	Depleted
79	*EMILIN1*	1.88	0	TRCN0000142626,TRCN0000144904,TRCN0000141739	0.45, 0.42, 0.38	-0.78, -0.71, -0.67	Mes	Depleted
80	*PRAMEF3*	1.88	0	TRCN0000129627,TRCN0000128569,TRCN0000128976 ,TRCN0000130446	0.50, 0.38, 0.38, 0.34	-0.78, -0.61, -0.72, -0.62	Mes	Depleted
81	*FATE1*	1.86	0	TRCN0000130192,TRCN0000128985,TRCN0000146597 ,TRCN0000128805,TRCN0000149011	0.53, 0.48, 0.38, 0.37, 0.32	-0.99, -0.74, -0.74, -0.61, -0.53	Mes	Depleted
82	*NTRK2*	1.83	0.0002	TRCN0000002245,TRCN0000002246,TRCN0000002242	0.41, 0.41, 0.36	-0.70, -0.78, -0.66	Mes	Depleted
83	*C22orf34*	1.8	0.0006	TRCN0000147028,TRCN0000148869,TRCN0000149153	0.50, 0.37, 0.34	-0.83, -0.68, -0.67	Mes	Depleted
84	*GNPTG*	1.8	0.0006	TRCN0000036051,TRCN0000036052,TRCN0000036050 ,TRCN0000036053,TRCN0000036049	0.38, 0.33, 0.31, 0.28, 0.28	-0.75, -0.63, -0.61, -0.53, -0.53	Mes	Depleted

Appendix I. The genes for subtype-specific depleted and amplified shRNAs. (continued)

Index	Gene	NES	*False Discovery Rate q*-value	Hairpin ID	Hairpin score	Effect size	Subtype	Depleted/ Amplified
85	*GAL3ST2*	1.79	0.0007	TRCN0000035072,TRCN0000035071	0.42, 0.34	-0.68, -0.66	Mes	Depleted
86	*HEBP2*	1.79	0.0002	TRCN0000151159,TRCN0000158096	0.75, 0.57	-1.12, -0.94	Mes	Depleted
87	*KCNG1*	1.79	0.0007	TRCN0000045112,TRCN0000045108	0.53, 0.51	-1.04, -0.86	Mes	Depleted
88	*SPEG*	1.79	0.0007	TRCN0000037429,TRCN0000037432,TRCN0000037431 ,TRCN0000037430	0.47, 0.46, 0.39, 0.30	-0.93, -0.87, -0.62, -0.60	Mes	Depleted
89	*ZC3HC1*	1.79	0.0008	TRCN0000037541,TRCN0000037540,TRCN0000037543 ,TRCN0000037539	0.47, 0.41, 0.38, 0.38	-0.88, -0.80, -0.76, -0.72	Mes	Depleted
90	*APOF*	1.77	0.0004	TRCN0000146962,TRCN0000148916	0.50, 0.38	-0.88, -0.67	Mes	Depleted
91	*SPINT1*	1.77	0.001	TRCN0000073577,TRCN0000073574,TRCN0000073573	0.45, 0.40, 0.39	-0.76, -0.73, -0.73	Mes	Depleted
92	*TIAF1*	1.76	0.0005	TRCN0000107202,TRCN0000107201,TRCN0000107204	0.65, 0.48, 0.34	-1.27, -0.92, -0.66	Mes	Depleted
93	*UNK_interferon responsive gene 15*	1.76	0.0014	TRCN0000143471,TRCN0000140968,TRCN0000141875	0.56, 0.50, 0.49	-0.83, -0.82, -0.92	Mes	Depleted
94	*CYP1A2*	1.75	0.0005	TRCN0000064634,TRCN0000064635,TRCN0000064637	0.56, 0.48, 0.36	-0.98, -0.93, -0.62	Mes	Depleted
95	*LRP5*	1.75	0.0017	TRCN0000033403,TRCN0000033399	0.75, 0.48	-1.20, -0.89	Mes	Depleted
96	*NAT8L*	1.75	0.0005	TRCN0000147770,TRCN0000149334,TRCN0000146484	0.60, 0.59, 0.34	-1.08, -1.02, -0.55	Mes	Depleted
97	*APC2*	1.74	0.0006	TRCN0000154929	0.59	-1	Mes	Depleted
98	*ADRM1*	1.73	0.0024	TRCN0000115945,TRCN0000115944,TRCN0000115942	0.49, 0.34, 0.30	-0.81, -0.64, -0.60	Mes	Depleted
99	*HTATSF1*	1.73	0.0006	TRCN0000006587,TRCN0000006588,TRCN0000006590	0.42, 0.38, 0.37	-0.71, -0.63, -0.64	Mes	Depleted

Appendix I. The genes for subtype-specific depleted and amplified shRNAs. (continued)

Index	Gene	NES	*False Discovery Rate q*-value	Hairpin ID	Hairpin score	Effect size	Subtype	Depleted/ Amplified
100	*IMMP2L*	1.73	0.0025	TRCN0000046674,TRCN0000046673,TRCN0000046677	0.58, 0.56, 0.41	-1.08, -1.12, -0.77	Mes	Depleted
101	*LRRC15*	1.73	0.0025	TRCN0000144278,TRCN0000139477,TRCN0000143971 ,TRCN0000139627,TRCN0000140863	0.50, 0.42, 0.33, 0.27, 0.24	-0.83, -0.68, -0.61, -0.45, -0.46	Mes	Depleted
102	*TACC1*	1.73	0.0024	TRCN0000155122	0.4	-0.63	Mes	Depleted
103	*YEATS2*	1.73	0.0025	TRCN0000142732,TRCN0000144134,TRCN0000144252 ,TRCN0000139940	0.46, 0.44, 0.33, 0.28	-0.74, -0.83, -0.57, -0.45	Mes	Depleted
104	*CDK10*	1.72	0.0032	TRCN0000010653,TRCN0000000687,TRCN0000001822	0.44, 0.39, 0.30	-0.75, -0.73, -0.59	Mes	Depleted
105	*CSPP1*	1.72	0.0025	TRCN0000143063,TRCN0000121664,TRCN0000122820	0.43, 0.31, 0.30	-0.73, -0.61, -0.50	Mes	Depleted
106	*SLC37A2*	1.71	0.001	TRCN0000043324,TRCN0000043323,TRCN0000043325 ,TRCN0000043326	0.44, 0.35, 0.32, 0.31	-0.83, -0.63, -0.58, -0.58	Mes	Depleted
107	*DNMT3B*	1.7	0.0013	TRCN0000035686,TRCN0000035685,TRCN0000035688	0.81, 0.41, 0.33	-1.39, -0.82, -0.62	Mes	Depleted
108	*FRMD6*	1.7	0.0013	TRCN0000142296,TRCN0000145454	0.53, 0.41	-0.94, -0.64	Mes	Depleted
109	*GRM7*	1.7	0.0013	TRCN0000009033	0.48	-0.86	Mes	Depleted
110	*MAST2*	1.7	0.0012	TRCN0000001733,TRCN0000010650,TRCN0000001736	0.32, 0.31, 0.30	-0.53, -0.57, -0.61	Mes	Depleted
111	*MRPS23*	1.7	0.0013	TRCN0000155167,TRCN0000154022	0.57, 0.54	-0.86, -0.82	Mes	Depleted
112	*NSUN5C*	1.7	0.0012	TRCN0000139787,TRCN0000139509,TRCN0000144522	0.46, 0.34, 0.33	-0.75, -0.67, -0.66	Mes	Depleted
113	*ABCC2*	1.69	0.0037	TRCN0000059307,TRCN0000059304	0.59, 0.43	-1.06, -0.71	Mes	Depleted
114	*CTTN*	1.69	0.0015	TRCN0000040274,TRCN0000040276	0.56, 0.48	-1.10, -0.87	Mes	Depleted
115	*DEFB118*	1.69	0.0018	TRCN0000149422,TRCN0000149580	0.58, 0.42	-1.05, -0.76	Mes	Depleted

Appendix I. The genes for subtype-specific depleted and amplified shRNAs. (continued)

Index	Gene	NES	*False Discovery Rate q*-value	Hairpin ID	Hairpin score	Effect size	Subtype	Depleted/ Amplified
116	*LGI2*	1.69	0.0042	TRCN0000138972,TRCN0000145222	0.59, 0.34	-0.90, -0.62	Mes	Depleted
117	*NHEDC2*	1.69	0.0018	TRCN0000128451,TRCN0000130075,TRCN0000127770	0.35, 0.34, 0.34	-0.69, -0.67, -0.67	Mes	Depleted
118	*PTPN3*	1.69	0.0018	TRCN0000002788,TRCN0000010741	0.42, 0.40	-0.69, -0.68	Mes	Depleted
119	*UFSP2*	1.69	0.0038	TRCN0000130335,TRCN0000149929,TRCN0000149702 ,TRCN0000150139	0.64, 0.50, 0.49, 0.28	-1.18, -0.76, -0.72, -0.54	Mes	Depleted
120	*UNK_ATPase, Class I, type 8B family pseudogene*	1.69	0.0042	TRCN0000148337,TRCN0000147683,TRCN0000147097 ,TRCN0000148159,TRCN0000149690	0.65, 0.53, 0.41, 0.23, 0.22	-0.97, -0.98, -0.74, -0.39, -0.38	Mes	Depleted
121	*UNK_LOC442601*	1.69	0.0037	TRCN0000137047,TRCN0000135854,TRCN0000137504	0.50, 0.34, 0.30	-0.83, -0.61, -0.59	Mes	Depleted
122	*USE1*	1.69	0.0036	TRCN0000157187,TRCN0000156767,TRCN0000158060 ,TRCN0000157522	0.48, 0.38, 0.29, 0.26	-0.80, -0.61, -0.55, -0.46	Mes	Depleted
123	*XPR1*	1.69	0.0018	TRCN0000014298,TRCN0000014301,TRCN0000014299	0.46, 0.33, 0.32	-0.79, -0.62, -0.52	Mes	Depleted
124	*CACYBP*	1.68	0.0023	TRCN0000146815,TRCN0000130068,TRCN0000148456	0.47, 0.46, 0.29	-0.81, -0.82, -0.59	Mes	Depleted
125	*CBLL1*	1.68	0.0043	TRCN0000033939,TRCN0000033942	0.33, 0.32	-0.65, -0.64	Mes	Depleted
126	*GPR63*	1.68	0.0042	TRCN0000011637,TRCN0000011639	0.64, 0.39	-1.15, -0.65	Mes	Depleted
127	*PLB1*	1.68	0	TRCN0000157010,TRCN0000155628	0.52, 0.51	-0.90, -0.85	Mes	Depleted
128	*TBC1D20*	1.68	0.0043	TRCN0000148772,TRCN0000130793,TRCN0000148575 ,TRCN0000129790	0.46, 0.45, 0.37, 0.28	-0.86, -0.86, -0.60, -0.56	Mes	Depleted
129	*SYNPR*	1.67	0.0047	TRCN0000059641,TRCN0000059642,TRCN0000059639	0.56, 0.40, 0.29	-1.08, -0.68, -0.57	Mes	Depleted

Appendix I. The genes for subtype-specific depleted and amplified shRNAs. (continued)

Index	Gene	NES	*False Discovery Rate q*-value	Hairpin ID	Hairpin score	Effect size	Subtype	Depleted/ Amplified
130	*UNK_hypothetical gene supported by AK056895*	1.67	0.0048	TRCN0000130215,TRCN0000130602,TRCN0000127897,TRCN0000127903	0.40, 0.34, 0.31, 0.30	-0.73, -0.67, -0.50, -0.49	Mes	Depleted
131	*COMMD8*	1.66	0	TRCN0000137729,TRCN0000134226	0.66, 0.46	-1.28, -0.77	Mes	Depleted
132	*RFX3*	1.66	0.0034	TRCN0000014875,TRCN0000014873,TRCN0000014874	0.52, 0.32, 0.32	-0.88, -0.52, -0.53	Mes	Depleted
133	*TMEM206*	1.66	0	TRCN0000138000,TRCN0000136154,TRCN0000135806	0.64, 0.57, 0.43	-1.00, -1.03, -0.76	Mes	Depleted
134	*C12orf64*	1.65	0	TRCN0000149380,TRCN0000147442,TRCN0000148411	0.57, 0.48, 0.42	-0.95, -0.87, -0.68	Mes	Depleted
135	*RMND1*	1.65	0.0042	TRCN0000135089,TRCN0000135730	0.53, 0.42	-0.88, -0.69	Mes	Depleted
136	*ALKBH5*	1.64	0	TRCN0000064785,TRCN0000064787	0.53, 0.46	-0.81, -0.82	Mes	Depleted
137	*KRT72*	1.64	0.0045	TRCN0000116779	0.47	-0.94	Mes	Depleted
138	*NANS*	1.64	0.0042	TRCN0000045438,TRCN0000045439	0.48, 0.45	-0.91, -0.79	Mes	Depleted
139	*NEK11*	1.64	0.0042	TRCN0000001961,TRCN0000001965,TRCN0000001962	0.47, 0.42, 0.27	-0.85, -0.73, -0.51	Mes	Depleted
140	*PHC1*	1.64	0.0045	TRCN0000153561,TRCN0000153821,TRCN0000156138	0.50, 0.40, 0.27	-0.82, -0.77, -0.46	Mes	Depleted
141	*PYCR1*	1.64	0.0049	TRCN0000038982,TRCN0000038983	0.41, 0.41	-0.77, -0.74	Mes	Depleted
142	*RAB3IL1*	1.64	0.0045	TRCN0000144359,TRCN0000140552	0.41, 0.30	-0.67, -0.55	Mes	Depleted

Appendix I. The genes for subtype-specific depleted and amplified shRNAs. (continued)

Index	Gene	NES	*False Discovery Rate q*-value	Hairpin ID	Hairpin score	Effect size	Subtype	Depleted/ Amplified
143	*UNK_similar to ATP-binding cassette sub-family E member 1 (RNase L inhibitor) (Ribonuclease 4 inhibitor) (RNS4I)*	1.64	0	TRCN0000021590	0.54	-0.94	Mes	Depleted
144	*VSX2*	1.64	0.0048	TRCN0000018065,TRCN0000018067	0.65, 0.43	-1.16, -0.76	Mes	Depleted
145	*GLRB*	1.63	0.0006	TRCN0000061708,TRCN0000061710	0.61, 0.42	-1.18, -0.70	Mes	Depleted
146	*CLEC3B*	1.62	0.0008	TRCN0000062475,TRCN0000062474	0.40, 0.40	-0.77, -0.73	Mes	Depleted
147	*MRC1*	1.62	0.0006	TRCN0000029669	0.69	-1.27	Mes	Depleted
148	*PYGB*	1.62	0.0008	TRCN0000153819	0.47	-0.71	Mes	Depleted
149	*CMYA5*	1.61	0.0009	TRCN0000128399,TRCN0000130845	0.48, 0.48	-0.82, -0.82	Mes	Depleted
150	*NDUFA4L2*	1.61	0.0009	TRCN0000046591,TRCN0000046590	0.71, 0.39	-1.41, -0.78	Mes	Depleted
151	*SLC7A5*	1.6	0.0012	TRCN0000043010,TRCN0000043011	0.47, 0.42	-0.72, -0.80	Mes	Depleted
152	*XDH*	1.6	0.0015	TRCN0000028089,TRCN0000028064	0.51, 0.37	-0.89, -0.70	Mes	Depleted

Appendix I. The genes for subtype-specific depleted and amplified shRNAs. (continued)

Index	Gene	NES	*False Discovery Rate q*-value	Hairpin ID	Hairpin score	Effect size	Subtype	Depleted/ Amplified
153	*UNK_uncharacterized serine/threonine-protein kinase SgK494*	1.59	0.0018	TRCN0000002413,TRCN0000002412	0.58, 0.46	-1.04, -0.91	Mes	Depleted
154	*GLP2R*	1.58	0.0031	TRCN0000008795	0.4	-0.72	Mes	Depleted
155	*TRPC5*	1.58	0.0034	TRCN0000044078,TRCN0000044082,TRCN0000044079	0.44, 0.37, 0.33	-0.83, -0.70, -0.53	Mes	Depleted
156	*UNK_hypothetical gene supported by AK128188*	1.57	0.0039	TRCN0000146604	0.42	-0.75	Mes	Depleted
157	*ZNF619*	1.57	0.0035	TRCN0000017793,TRCN0000017796	0.43, 0.36	-0.70, -0.64	Mes	Depleted
158	*MAB21L1*	1.56	0.0043	TRCN0000144537,TRCN0000142724,TRCN0000145271	0.65, 0.38, 0.32	-1.09, -0.59, -0.52	Mes	Depleted
159	*SMYD5*	1.51	0.0011	TRCN0000155095,TRCN0000155068	0.68, 0.49	-1.16, -0.83	Mes	Depleted
160	*ZNF264*	1.5	0.0016	TRCN0000019141,TRCN0000019143	0.53, 0.46	-0.91, -0.88	Mes	Depleted
161	*FAM129B*	1.49	0.0019	TRCN0000122833	0.51	-0.82	Mes	Depleted
162	*LMX1B*	1.48	0.0037	TRCN0000017514,TRCN0000017517	0.46, 0.42	-0.88, -0.75	Mes	Depleted
163	*EGFR*	1.96	0.0006	TRCN0000121067,TRCN0000121327,TRCN0000121070,TRCN0000121206,TRCN0000121069,TRCN0000121202,TRCN0000039636	0.68, 0.57, 0.34, 0.30, 0.28, 0.27, 0.25	-1.01, -0.92, -0.67, -0.54, -0.56, -0.53, -0.50	Stem-A	Depleted

Appendix I. The genes for subtype-specific depleted and amplified shRNAs. (continued)

Index	Gene	NES	*False Discovery Rate q*-value	Hairpin ID	Hairpin score	Effect size	Subtype	Depleted/ Amplified
164	*MESDC2*	1.91	0	TRCN0000131214,TRCN0000146350	0.79, 0.56	-1.50, -0.94	Stem-A	Depleted
165	*VPS13B*	1.89	0	TRCN0000083955,TRCN0000083953,TRCN0000083956 ,TRCN0000083954	0.46, 0.42, 0.40, 0.36	-0.92, -0.83, -0.80, -0.71	Stem-A	Depleted
166	*C10orf129*	1.88	0	TRCN0000154168,TRCN0000152516,TRCN0000156093	0.47, 0.38, 0.36	-0.76, -0.70, -0.59	Stem-A	Depleted
167	*SFRS2*	1.86	0.0016	TRCN0000000094,TRCN0000000090,TRCN0000000089 ,TRCN0000000085,TRCN0000000099,TRCN000000008 2,TRCN0000000081	0.46, 0.35, 0.35, 0.34, 0.33, 0.29, 0.25	-0.78, -0.58, -0.64, -0.58, -0.58, -0.46, -0.49	Stem-A	Depleted
168	*FAM153A*	1.85	0.0003	TRCN0000148967,TRCN0000147331,TRCN0000148441 ,TRCN0000127581	0.48, 0.35, 0.33, 0.31	-0.86, -0.62, -0.61, -0.56	Stem-A	Depleted
169	*ASZ1*	1.81	0.0008	TRCN0000131236,TRCN0000128986,TRCN0000130915	0.39, 0.37, 0.32	-0.71, -0.73, -0.64	Stem-A	Depleted
170	*TAPBP*	1.81	0.0002	TRCN0000118833,TRCN0000118835	0.57, 0.50	-0.99, -0.96	Stem-A	Depleted
171	*NAB2*	1.8	0.0008	TRCN0000019548,TRCN0000019547,TRCN0000019544	0.59, 0.39, 0.32	-1.02, -0.68, -0.54	Stem-A	Depleted
172	*CHPT1*	1.79	0.0012	TRCN0000035937,TRCN0000035938	0.43, 0.34	-0.84, -0.66	Stem-A	Depleted
173	*DAZL*	1.79	0.0014	TRCN0000083433,TRCN0000083436	0.59, 0.50	-1.14, -0.94	Stem-A	Depleted
174	*MUC15*	1.79	0.0014	TRCN0000128034,TRCN0000128885	0.45, 0.43	-0.79, -0.77	Stem-A	Depleted
175	*C1orf187*	1.78	0.0008	TRCN0000136368,TRCN0000134037	0.41, 0.41	-0.75, -0.65	Stem-A	Depleted
176	*LGR6*	1.78	0.0016	TRCN0000063622,TRCN0000063618	0.53, 0.37	-0.85, -0.71	Stem-A	Depleted
177	*ZFR*	1.78	0.0007	TRCN0000016964,TRCN0000016965	0.45, 0.40	-0.77, -0.69	Stem-A	Depleted
178	*ZNF827*	1.78	0.0017	TRCN0000144574,TRCN0000144745	0.48, 0.43	-0.77, -0.86	Stem-A	Depleted
179	*COX5A*	1.77	0.0019	TRCN0000045961,TRCN0000045958,TRCN0000045962 ,TRCN0000045960	0.46, 0.40, 0.36, 0.26	-0.83, -0.76, -0.69, -0.50	Stem-A	Depleted

Appendix I. The genes for subtype-specific depleted and amplified shRNAs. (continued)

Index	Gene	NES	*False Discovery Rate q*-value	Hairpin ID	Hairpin score	Effect size	Subtype	Depleted/ Amplified
180	*HIST1H2AI*	1.77	0.0019	TRCN0000106668,TRCN0000106666,TRCN0000106665	0.69, 0.62, 0.47	-1.14, -0.99, -0.89	Stem-A	Depleted
181	*ZIC2*	1.77	0.0019	TRCN0000062368,TRCN0000062369	0.37, 0.32	-0.73, -0.64	Stem-A	Depleted
182	*CCL3L1*	1.76	0.0023	TRCN0000058044,TRCN0000058045,TRCN0000058046 ,TRCN0000058047	0.51, 0.48, 0.45, 0.26	-0.98, -0.85, -0.80, -0.52	Stem-A	Depleted
183	*UNK_hypothetical LOC389791*	1.76	0.0008	TRCN0000141064,TRCN0000142116,TRCN0000141392	0.43, 0.40, 0.37	-0.82, -0.62, -0.69	Stem-A	Depleted
184	*KCTD21*	1.75	0.0009	TRCN0000139215,TRCN0000145150,TRCN0000139704	0.44, 0.39, 0.37	-0.78, -0.73, -0.68	Stem-A	Depleted
185	*SLC8A3*	1.75	0.0009	TRCN0000044868	0.69	-1.03	Stem-A	Depleted
186	*UNK_hypothetical protein LOC283874*	1.75	0.0008	TRCN0000152683	0.53	-0.76	Stem-A	Depleted
187	*WDR5*	1.75	0.0008	TRCN0000118048,TRCN0000118047	0.40, 0.36	-0.64, -0.61	Stem-A	Depleted
188	*KLHL2*	1.74	0.0033	TRCN0000064966,TRCN0000064964	0.77, 0.42	-1.49, -0.82	Stem-A	Depleted
189	*OR2L3*	1.74	0.0033	TRCN0000061295,TRCN0000061294,TRCN0000061297	0.38, 0.35, 0.34	-0.73, -0.68, -0.62	Stem-A	Depleted
190	*ADAMTSL3*	1.73	0.0037	TRCN0000118272,TRCN0000118275,TRCN0000118273	0.41, 0.30, 0.29	-0.76, -0.59, -0.58	Stem-A	Depleted
191	*CA8*	1.72	0.0018	TRCN0000151892,TRCN0000153276,TRCN0000151716	0.77, 0.44, 0.41	-1.17, -0.86, -0.77	Stem-A	Depleted
192	*CYP1A1*	1.72	0.0039	TRCN0000064621,TRCN0000064620,TRCN0000064622	0.47, 0.45, 0.29	-0.89, -0.89, -0.54	Stem-A	Depleted

Appendix I. The genes for subtype-specific depleted and amplified shRNAs. (continued)

Index	Gene	NES	*False Discovery Rate q*-value	Hairpin ID	Hairpin score	Effect size	Subtype	Depleted/ Amplified
193	*DGKH*	1.72	0.0016	TRCN0000001359,TRCN0000001360	0.39, 0.37	-0.76, -0.60	Stem-A	Depleted
194	*GLB1*	1.72	0.0039	TRCN0000083273,TRCN0000083275	0.65, 0.31	-1.15, -0.57	Stem-A	Depleted
195	*HIST1H3G*	1.72	0.0039	TRCN0000106934,TRCN0000106930,TRCN0000106932	0.80, 0.42, 0.30	-1.45, -0.80, -0.60	Stem-A	Depleted
196	*SPATA18*	1.72	0.0017	TRCN0000142371,TRCN0000121623,TRCN0000141968	0.45, 0.34, 0.31	-0.71, -0.63, -0.59	Stem-A	Depleted
197	*C6orf192*	1.71	0.0049	TRCN0000059460,TRCN0000059462,TRCN0000059459	0.36, 0.33, 0.25	-0.71, -0.64, -0.50	Stem-A	Depleted
198	*CALML4*	1.71	0.0044	TRCN0000053533,TRCN0000053537,TRCN0000053535 ,TRCN0000053536	0.45, 0.36, 0.31, 0.27	-0.84, -0.71, -0.62, -0.54	Stem-A	Depleted
199	*FETUB*	1.71	0.0044	TRCN0000073617,TRCN0000073615	0.54, 0.40	-0.92, -0.78	Stem-A	Depleted
200	*LENG1*	1.71	0.0019	TRCN0000060394,TRCN0000060393,TRCN0000060396	0.82, 0.32, 0.31	-1.55, -0.63, -0.59	Stem-A	Depleted
201	*LRRC59*	1.71	0.0018	TRCN0000078740,TRCN0000078739	0.59, 0.47	-1.06, -0.92	Stem-A	Depleted
202	*RWDD3*	1.71	0.0018	TRCN0000004094,TRCN0000004096,TRCN0000004093	0.44, 0.34, 0.31	-0.88, -0.57, -0.60	Stem-A	Depleted
203	*C1orf105*	1.7	0.0022	TRCN0000140677,TRCN0000142864	0.76, 0.43	-1.25, -0.81	Stem-A	Depleted
204	*C22orf25*	1.7	0.0024	TRCN0000129777,TRCN0000130981	0.47, 0.43	-0.80, -0.79	Stem-A	Depleted
205	*FAM38B*	1.7	0.0024	TRCN0000123251	0.79	-1.3	Stem-A	Depleted
206	*GORASP2*	1.7	0.0024	TRCN0000130898,TRCN0000127975	0.67, 0.53	-1.29, -0.80	Stem-A	Depleted
207	*HIPK2*	1.7	0.0022	TRCN0000003202,TRCN0000003204	0.41, 0.40	-0.79, -0.68	Stem-A	Depleted
208	*HIST1H4A*	1.7	0.0022	TRCN0000106699,TRCN0000106698,TRCN0000106696	0.58, 0.57, 0.43	-0.89, -1.14, -0.80	Stem-A	Depleted
209	*NAT12*	1.7	0.0024	TRCN0000154958,TRCN0000155086	0.71, 0.47	-1.10, -0.76	Stem-A	Depleted

Appendix I. The genes for subtype-specific depleted and amplified shRNAs. (continued)

Index	Gene	NES	*False Discovery Rate q*-value	Hairpin ID	Hairpin score	Effect size	Subtype	Depleted/ Amplified
210	*VPS41*	1.7	0.0024	TRCN0000034324,TRCN0000034326	0.36, 0.34	-0.62, -0.68	Stem-A	Depleted
211	*AGPAT4*	1.69	0.0026	TRCN0000035163,TRCN0000035161	0.35, 0.34	-0.66, -0.66	Stem-A	Depleted
212	*BIK*	1.69	0.0024	TRCN0000033528,TRCN0000033526	0.46, 0.32	-0.85, -0.57	Stem-A	Depleted
213	*CDKL3*	1.69	0.0024	TRCN0000002376,TRCN0000002377,TRCN0000002378	0.60, 0.40, 0.36	-1.08, -0.66, -0.66	Stem-A	Depleted
214	*EPN2*	1.69	0.0024	TRCN0000077917,TRCN0000077916,TRCN0000077914	0.50, 0.36, 0.31	-0.92, -0.71, -0.57	Stem-A	Depleted
215	*PIR*	1.69	0.0024	TRCN0000019258,TRCN0000019257	0.70, 0.49	-1.29, -0.84	Stem-A	Depleted
216	*SPATA1*	1.69	0.0024	TRCN0000136814,TRCN0000135064,TRCN0000137509 ,TRCN0000134784	0.40, 0.35, 0.32, 0.29	-0.62, -0.66, -0.56, -0.55	Stem-A	Depleted
217	*ST6GALNAC5*	1.69	0.0026	TRCN0000035090,TRCN0000035091	0.69, 0.40	-1.37, -0.77	Stem-A	Depleted
218	*PCDHB5*	1.68	0.0026	TRCN0000056218,TRCN0000056222	0.68, 0.55	-1.23, -1.06	Stem-A	Depleted
219	*MAD2L1*	1.67	0.0041	TRCN0000006564,TRCN0000006565	0.49, 0.39	-0.83, -0.74	Stem-A	Depleted
220	*RALGPS1*	1.67	0.0038	TRCN0000154931,TRCN0000152217	0.43, 0.40	-0.73, -0.79	Stem-A	Depleted
221	*REEP1*	1.67	0.0035	TRCN0000061733,TRCN0000061736	0.41, 0.39	-0.78, -0.71	Stem-A	Depleted
222	*WDR24*	1.67	0.0039	TRCN0000130142,TRCN0000130106,TRCN0000130105	0.44, 0.33, 0.32	-0.75, -0.66, -0.52	Stem-A	Depleted
223	*ZNF800*	1.67	0.0035	TRCN0000021157,TRCN0000021155,TRCN0000021156	0.46, 0.34, 0.31	-0.79, -0.57, -0.51	Stem-A	Depleted
224	*HEXIM1*	1.66	0.0046	TRCN0000074176,TRCN0000074174	0.55, 0.30	-0.85, -0.54	Stem-A	Depleted
225	*RFC3*	1.66	0.0005	TRCN0000072650,TRCN0000072649	0.57, 0.52	-0.93, -0.86	Stem-A	Depleted
226	*VWA1*	1.66	0.0044	TRCN0000117178,TRCN0000117177	0.44, 0.44	-0.81, -0.77	Stem-A	Depleted
227	*FBXO16*	1.65	0.0049	TRCN0000149016,TRCN0000147114	0.67, 0.44	-0.99, -0.76	Stem-A	Depleted

Appendix I. The genes for subtype-specific depleted and amplified shRNAs. (continued)

Index	Gene	NES	*False Discovery Rate q*-value	Hairpin ID	Hairpin score	Effect size	Subtype	Depleted/ Amplified
228	*QRICH1*	1.65	0.0005	TRCN0000153106,TRCN0000151753	0.64, 0.45	-1.06, -0.83	Stem-A	Depleted
229	*UNK_hypothetical protein LOC284581*	1.65	0.0047	TRCN0000121848,TRCN0000142210,TRCN0000122163,TRCN0000143749	0.33, 0.29, 0.27, 0.27	-0.65, -0.57, -0.52, -0.53	Stem-A	Depleted
230	*CREBZF*	1.63	0.0019	TRCN0000017687	0.44	-0.82	Stem-A	Depleted
231	*PPP1R13L*	1.63	0.0015	TRCN0000022212,TRCN0000022210	0.56, 0.50	-0.97, -0.86	Stem-A	Depleted
232	*MAP3K7IP2*	1.62	0.002	TRCN0000004453,TRCN0000004456	0.42, 0.39	-0.71, -0.66	Stem-A	Depleted
233	*TCERG1L*	1.62	0.0021	TRCN0000015482,TRCN0000015480	0.42, 0.40	-0.78, -0.70	Stem-A	Depleted
234	*LIPA*	1.61	0.0026	TRCN0000029247,TRCN0000029248,TRCN0000029245	0.55, 0.39, 0.36	-1.06, -0.65, -0.70	Stem-A	Depleted
235	*ZNF548*	1.61	0.0027	TRCN0000015379,TRCN0000015380	0.45, 0.37	-0.80, -0.74	Stem-A	Depleted
236	*BLOC1S1*	1.6	0.0034	TRCN0000107374,TRCN0000107372	0.51, 0.36	-1.02, -0.69	Stem-A	Depleted
237	*UBXN1*	1.6	0.003	TRCN0000004112,TRCN0000004111	0.43, 0.42	-0.76, -0.77	Stem-A	Depleted
238	*C6orf165*	1.59	0.0035	TRCN0000134261,TRCN0000135274	0.50, 0.47	-0.89, -0.84	Stem-A	Depleted
239	*SCGB1A1*	1.59	0.0034	TRCN0000083113,TRCN0000083117	0.58, 0.36	-1.12, -0.71	Stem-A	Depleted
240	*ZNF577*	1.59	0.0038	TRCN0000016695,TRCN0000016696	0.36, 0.35	-0.64, -0.60	Stem-A	Depleted
241	*KBTBD4*	1.58	0.0039	TRCN0000141375,TRCN0000139228	0.53, 0.52	-0.77, -0.89	Stem-A	Depleted
242	*SAMD9*	1.58	0.0038	TRCN0000122029,TRCN0000122106,TRCN0000121519	0.53, 0.43, 0.33	-1.01, -0.64, -0.59	Stem-A	Depleted
243	*DTX2*	1.57	0.0049	TRCN0000004560,TRCN0000004561	0.44, 0.37	-0.73, -0.69	Stem-A	Depleted
244	*HLA-DMA*	1.57	0.0045	TRCN0000057332	0.46	-0.93	Stem-A	Depleted
245	*OR56B1*	1.57	0.0049	TRCN0000060669,TRCN0000060672	0.40, 0.36	-0.69, -0.69	Stem-A	Depleted
246	*INSC*	1.51	0.0016	TRCN0000138732	0.48	-0.82	Stem-A	Depleted

Appendix I. The genes for subtype-specific depleted and amplified shRNAs. (continued)

Index	Gene	NES	*False Discovery Rate q*-value	Hairpin ID	Hairpin score	Effect size	Subtype	Depleted/ Amplified
247	*NPY*	1.5	0.0034	TRCN0000009207	0.5	-0.96	Stem-A	Depleted
248	*AFG3L1*	1.49	0.0039	TRCN0000006680,TRCN0000006677	0.50, 0.42	-0.86, -0.71	Stem-A	Depleted
249	*PRKAG2*	1.49	0.0042	TRCN0000003145	0.42	-0.79	Stem-A	Depleted
250	*RAB25*	1.49	0.0049	TRCN0000021851	0.43	-0.73	Stem-A	Depleted
1	*HRAS*	1.76	0.0013	TRCN0000033265,TRCN0000040090	0.57, 0.47	0.90, 0.94	Epi-A	Amplified
2	*USE1*	1.76	0.0005	TRCN0000158060,TRCN0000157522,TRCN0000157032	0.51, 0.48, 0.45	0.98, 0.81, 0.83	Epi-A	Amplified
3	*RAC2*	1.73	0.001	TRCN0000047275,TRCN0000047277,TRCN0000047273	0.56, 0.49, 0.47	1.07, 0.87, 0.91	Epi-A	Amplified
4	*SLC38A10*	1.73	0.0009	TRCN0000151835,TRCN0000154868,TRCN0000155811 ,TRCN0000155211	0.40, 0.39, 0.35, 0.27	0.74, 0.68, 0.64, 0.53	Epi-A	Amplified
5	*ZNF804A*	1.72	0.0003	TRCN0000128318,TRCN0000128661	0.44, 0.43	0.83, 0.84	Epi-A	Amplified
6	*PROZ*	1.71	0.0016	TRCN0000056028,TRCN0000056029	0.56, 0.32	0.91, 0.11	Epi-A	Amplified
7	*SMC5*	1.71	0.0018	TRCN0000146759,TRCN0000147918,TRCN0000147948	0.62, 0.48, 0.29	1.16, 0.91, 0.57	Epi-A	Amplified
8	*CA4*	1.7	0.001	TRCN0000158178,TRCN0000157938	1.21, 0.58	2.01, 1.04	Epi-A	Amplified
9	*RGPD5*	1.7	0.0021	TRCN0000155995,TRCN0000153068,TRCN0000150710 ,TRCN0000155941	0.36, 0.29, 0.27, 0.24	0.70, 0.54, 0.53, 0.48	Epi-A	Amplified
10	*ECM2*	1.69	0.0025	TRCN0000157144,TRCN0000150882	0.30, 0.30	0.59, 0.60	Epi-A	Amplified
11	*C5orf34*	1.68	0.001	TRCN0000148489,TRCN0000146578,TRCN0000130044	0.41, 0.38, 0.32	0.78, 0.66, 0.64	Epi-A	Amplified
12	*ZFP106*	1.68	0.0028	TRCN0000107376,TRCN0000107377	0.70, 0.35	1.37, 0.69	Epi-A	Amplified
13	*C1orf35*	1.67	0.0029	TRCN0000159276,TRCN0000159258,TRCN0000121643	0.41, 0.26, 0.25	0.80, 0.51, 0.49	Epi-A	Amplified
14	*DEFB118*	1.67	0.0013	TRCN0000149422	0.63	1.16	Epi-A	Amplified

Appendix I. The genes for subtype-specific depleted and amplified shRNAs. (continued)

Index	Gene	NES	*False Discovery Rate q*-value	Hairpin ID	Hairpin score	Effect size	Subtype	Depleted/ Amplified
15	*IQCA1*	1.67	0.0028	TRCN0000135122,TRCN0000135715,TRCN0000138576	0.62, 0.43, 0.31	1.23, 0.85, 0.62	Epi-A	Amplified
16	*TMSB15A*	1.67	0.0013	TRCN0000139504,TRCN0000143842,TRCN0000143553	0.48, 0.41, 0.32	0.89, 0.81, 0.61	Epi-A	Amplified
17	*B3GNT1*	1.66	0.003	TRCN0000035909,TRCN0000035911	0.43, 0.37	0.79, 0.71	Epi-A	Amplified
18	*STMN3*	1.66	0.0013	TRCN0000063856,TRCN0000063853,TRCN0000063857	0.47, 0.47, 0.33	0.93, 0.90, 0.64	Epi-A	Amplified
19	*WDR75*	1.66	0.0017	TRCN0000152085,TRCN0000156084	0.40, 0.39	0.76, 0.73	Epi-A	Amplified
20	*SGOL2*	1.65	0.0039	TRCN0000074153,TRCN0000074155,TRCN0000074154	0.32, 0.25, 0.23	0.64, 0.48, 0.47	Epi-A	Amplified
21	*UNK_PIN2 -interacting protein 1*	1.65	0.0021	TRCN0000128607	0.79	1.57	Epi-A	Amplified
22	*ZNF180*	1.65	0.0021	TRCN0000013002,TRCN0000013000	0.52, 0.43	0.95, 0.79	Epi-A	Amplified
23	*PAPD4*	1.64	0.0044	TRCN0000139535,TRCN0000139631,TRCN0000144693	1.33, 0.26, 0.24	2.25, 0.52, 0.49	Epi-A	Amplified
24	*PLOD3*	1.64	0.0043	TRCN0000064734,TRCN0000064735,TRCN0000064737	0.36, 0.31, 0.28	0.72, 0.59, 0.54	Epi-A	Amplified
25	*LHX4*	1.63	0.0037	TRCN0000017492,TRCN0000017488	0.39, 0.32	0.70, 0.63	Epi-A	Amplified
26	*CABP7*	1.62	0.0038	TRCN0000054282,TRCN0000054278,TRCN0000054279	0.44, 0.32, 0.26	0.84, 0.59, 0.53	Epi-A	Amplified
27	*PCDHB5*	1.62	0.0038	TRCN0000056218	0.55	1.09	Epi-A	Amplified

Appendix I. The genes for subtype-specific depleted and amplified shRNAs. (continued)

Index	Gene	NES	*False Discovery Rate q*-value	Hairpin ID	Hairpin score	Effect size	Subtype	Depleted/ Amplified
28	*ZNF575*	1.62	0.0038	TRCN0000107260,TRCN0000107262,TRCN0000107264	0.38, 0.36, 0.36	0.75, 0.71, 0.69	Epi-A	Amplified
29	*H2AFJ*	1.61	0.0048	TRCN0000106749,TRCN0000106746	0.80, 0.32	1.42, 0.62	Epi-A	Amplified
30	*EGR1*	1.6	0.0007	TRCN0000013837	0.51	0.8	Epi-A	Amplified
31	*CXCR6*	1.58	0.0017	TRCN0000011323,TRCN0000011319	0.57, 0.36	1.03, 0.66	Epi-A	Amplified
32	*WDR59*	1.57	0.0021	TRCN0000157708,TRCN0000156940,TRCN0000157812	0.42, 0.42, 0.34	0.76, 0.84, 0.66	Epi-A	Amplified
33	*ZNF33A*	1.57	0.0028	TRCN0000014950	0.44	0.83	Epi-A	Amplified
34	*PPP1R13L*	1.56	0.0028	TRCN0000022210,TRCN0000022212	0.50, 0.44	0.94, 0.86	Epi-A	Amplified
35	*SMG5*	1.56	0.0038	TRCN0000130550,TRCN0000130700,TRCN0000128697	0.46, 0.45, 0.33	0.83, 0.71, 0.59	Epi-A	Amplified
36	*CTSD*	1.48	0.0022	TRCN0000003661,TRCN0000003660	0.46, 0.45	0.80, 0.83	Epi-A	Amplified
37	*RAX*	1.48	0.0019	TRCN0000018085	0.48	0.89	Epi-A	Amplified
38	*ZYG11A*	1.48	0.0013	TRCN0000135348,TRCN0000137844	0.61, 0.48	1.22, 0.82	Epi-A	Amplified
39	*C12orf66*	1.47	0.0025	TRCN0000137567	0.47	0.83	Epi-A	Amplified
40	*HCRTR1*	1.47	0.0024	TRCN0000004747	0.5	0.94	Epi-A	Amplified
41	*MARK2*	1.47	0.0024	TRCN0000001585,TRCN0000001582	0.47, 0.44	0.77, 0.83	Epi-A	Amplified
42	*ATF5*	1.46	0.0033	TRCN0000017638,TRCN0000017641	0.47, 0.42	0.86, 0.78	Epi-A	Amplified
43	*ZNF773*	1.46	0.0031	TRCN0000107859	0.54	1.08	Epi-A	Amplified
44	*C11orf60*	1.94	0	TRCN0000074374,TRCN0000074375,TRCN0000074376 ,TRCN0000074377	0.61, 0.57, 0.46, 0.44	1.21, 1.12, 0.89, 0.86	Mes	Amplified
45	*TSPAN7*	1.89	0	TRCN0000118808,TRCN0000118807,TRCN0000118809 ,TRCN0000118810,TRCN0000118811	0.53, 0.40, 0.39, 0.37, 0.33	1.01, 0.79, 0.73, 0.73, 0.61	Mes	Amplified
46	*AKAP8L*	1.84	0.0001	TRCN0000038003,TRCN0000037999	0.58, 0.48	1.12, 0.90	Mes	Amplified

Appendix I. The genes for subtype-specific depleted and amplified shRNAs. (continued)

Index	Gene	NES	*False Discovery Rate q*-value	Hairpin ID	Hairpin score	Effect size	Subtype	Depleted/ Amplified
47	*KISS1*	1.83	0.0001	TRCN0000059066,TRCN0000059064,TRCN0000059065	0.57, 0.45, 0.45	0.90, 0.86, 0.82	Mes	Amplified
48	*PIPOX*	1.82	0.0002	TRCN0000046134,TRCN0000046133,TRCN0000046136 ,TRCN0000046135	0.43, 0.39, 0.34, 0.30	0.85, 0.78, 0.68, 0.57	Mes	Amplified
49	*SLIT3*	1.82	0.0005	TRCN0000053413,TRCN0000053416,TRCN0000053414	0.60, 0.47, 0.38	1.19, 0.95, 0.76	Mes	Amplified
50	*AP3B1*	1.77	0.0013	TRCN0000065059,TRCN0000065058,TRCN0000065062	0.67, 0.42, 0.34	1.24, 0.81, 0.68	Mes	Amplified
51	*DGKB*	1.77	0.001	TRCN0000000764,TRCN0000000767	0.64, 0.49	1.18, 0.91	Mes	Amplified
52	*PRR16*	1.77	0.0011	TRCN0000123216,TRCN0000123217,TRCN0000123215 ,TRCN0000123214	0.42, 0.40, 0.34, 0.29	0.75, 0.79, 0.66, 0.57	Mes	Amplified
53	*TRIP10*	1.77	0.0012	TRCN0000063183,TRCN0000063185,TRCN0000063186	0.55, 0.42, 0.35	1.09, 0.84, 0.69	Mes	Amplified
54	*UNK_similar to Kinase suppressor of ras-1 (Kinase suppressor of ras)*	1.77	0.001	TRCN0000082444	0.69	1.3	Mes	Amplified
55	*ADAMTSL3*	1.76	0.0013	TRCN0000118272,TRCN0000118275,TRCN0000118274	0.60, 0.54, 0.35	1.16, 1.06, 0.69	Mes	Amplified
56	*ITIH5*	1.76	0.0005	TRCN0000118263,TRCN0000118266,TRCN0000118265 ,TRCN0000118264	0.53, 0.50, 0.40, 0.33	1.03, 0.98, 0.78, 0.53	Mes	Amplified
57	*CEPT1*	1.75	0.0018	TRCN0000035969,TRCN0000035971	0.65, 0.37	1.30, 0.74	Mes	Amplified
58	*HKR1*	1.75	0.0015	TRCN0000017636,TRCN0000017637,TRCN0000017635 ,TRCN0000017633	0.54, 0.49, 0.33, 0.27	0.95, 0.96, 0.52, 0.53	Mes	Amplified

Appendix I. The genes for subtype-specific depleted and amplified shRNAs. (continued)

Index	Gene	NES	*False Discovery Rate q*-value	Hairpin ID	Hairpin score	Effect size	Subtype	Depleted/ Amplified
59	*CD2BP2*	1.74	0.0019	TRCN0000057483,TRCN0000057486,TRCN0000057484	0.56, 0.45, 0.29	1.10, 0.90, 0.58	Mes	Amplified
60	*PNPT1*	1.74	0.0019	TRCN0000035908,TRCN0000035906,TRCN0000035905 ,TRCN0000035907	0.42, 0.39, 0.26, 0.25	0.83, 0.78, 0.52, 0.48	Mes	Amplified
61	*RPL5*	1.74	0.0018	TRCN0000074994,TRCN0000074995,TRCN0000074996 ,TRCN0000074993	0.46, 0.33, 0.29, 0.26	0.84, 0.62, 0.57, 0.50	Mes	Amplified
62	*SEMA3D*	1.74	0.0019	TRCN0000063213,TRCN0000063215,TRCN0000063217 ,TRCN0000063214	0.50, 0.36, 0.27, 0.26	0.99, 0.72, 0.53, 0.51	Mes	Amplified
63	*MS4A14*	1.73	0.002	TRCN0000060356,TRCN0000060357,TRCN0000060355 ,TRCN0000060353	0.49, 0.42, 0.40, 0.30	0.97, 0.83, 0.79, 0.59	Mes	Amplified
64	*STX17*	1.73	0.0009	TRCN0000060122,TRCN0000060118,TRCN0000060121	0.44, 0.41, 0.33	0.87, 0.82, 0.66	Mes	Amplified
65	*ATP6V0E1*	1.72	0.0009	TRCN0000038520,TRCN0000038522	0.78, 0.50	1.54, 0.93	Mes	Amplified
66	*C6orf130*	1.72	0.0024	TRCN0000129418,TRCN0000128685	0.54, 0.30	1.05, 0.61	Mes	Amplified
67	*IL1F7*	1.72	0.0026	TRCN0000058176,TRCN0000058177,TRCN0000058174 ,TRCN0000058173	0.62, 0.46, 0.44, 0.23	1.23, 0.91, 0.84, 0.46	Mes	Amplified
68	*LY6K*	1.72	0.0023	TRCN0000117955,TRCN0000117956	0.62, 0.39	1.22, 0.73	Mes	Amplified
69	*MYCT1*	1.72	0.0022	TRCN0000135843,TRCN0000136533	0.38, 0.30	0.73, 0.59	Mes	Amplified
70	*WNT8B*	1.72	0.0009	TRCN0000062095,TRCN0000062096	0.46, 0.37	0.89, 0.74	Mes	Amplified
71	*SRPRB*	1.71	0.0027	TRCN0000063103,TRCN0000063106,TRCN0000063107	0.52, 0.50, 0.27	1.00, 0.99, 0.54	Mes	Amplified
72	*YTHDC2*	1.71	0.0009	TRCN0000153934,TRCN0000154178,TRCN0000157638	0.51, 0.46, 0.39	1.00, 0.88, 0.65	Mes	Amplified
73	*BTNL2*	1.7	0.0015	TRCN0000156514,TRCN0000155485	0.58, 0.48	1.09, 0.85	Mes	Amplified
74	*CD151*	1.69	0.0017	TRCN0000057643,TRCN0000057646	0.56, 0.39	1.08, 0.77	Mes	Amplified

Appendix I. The genes for subtype-specific depleted and amplified shRNAs. (continued)

Index	Gene	NES	*False Discovery Rate q*-value	Hairpin ID	Hairpin score	Effect size	Subtype	Depleted/ Amplified
75	*FAM160B1*	1.69	0.0019	TRCN0000129856,TRCN0000130062	0.65, 0.54	1.10, 1.02	Mes	Amplified
76	*FBXL3*	1.69	0.0017	TRCN0000004283,TRCN0000004281	0.60, 0.42	0.98, 0.69	Mes	Amplified
77	*UTP3*	1.69	0.004	TRCN0000134646,TRCN0000134895,TRCN0000136463 ,TRCN0000135598,TRCN0000133824	0.33, 0.27, 0.24, 0.24, 0.21	0.64, 0.53, 0.47, 0.48, 0.40	Mes	Amplified
78	*C20orf158*	1.68	0.0045	TRCN0000074348,TRCN0000074351,TRCN0000074350	0.45, 0.34, 0.23	0.89, 0.67, 0.46	Mes	Amplified
79	*CASC3*	1.68	0.0024	TRCN0000059920,TRCN0000059921	0.68, 0.44	1.35, 0.88	Mes	Amplified
80	*GSTM3*	1.68	0.0019	TRCN0000149566	0.41	0.68	Mes	Amplified
81	*NKX3-1*	1.68	0.0025	TRCN0000040122,TRCN0000040119	0.35, 0.34	0.69, 0.67	Mes	Amplified
82	*NPSR1*	1.68	0.0045	TRCN0000063361,TRCN0000063358	0.27, 0.27	0.55, 0.53	Mes	Amplified
83	*OR1S2*	1.68	0.0043	TRCN0000063099,TRCN0000063101,TRCN0000063102	0.41, 0.39, 0.37	0.82, 0.77, 0.74	Mes	Amplified
84	*TMEM123*	1.68	0.0021	TRCN0000061730,TRCN0000061729	0.52, 0.40	0.91, 0.75	Mes	Amplified
85	*DTX2*	1.67	0	TRCN0000004560	0.69	1.14	Mes	Amplified
86	*LANCL1*	1.67	0.0027	TRCN0000011687,TRCN0000011691,TRCN0000011688	0.46, 0.36, 0.31	0.90, 0.69, 0.58	Mes	Amplified
87	*ERN1*	1.66	0.0002	TRCN0000000532,TRCN0000000528	0.61, 0.50	1.00, 0.98	Mes	Amplified
88	*KBTBD6*	1.66	0.0031	TRCN0000138270,TRCN0000135111	0.52, 0.43	0.97, 0.84	Mes	Amplified
89	*AIMP2*	1.65	0.0002	TRCN0000072468	0.51	0.97	Mes	Amplified
90	*CENPL*	1.65	0.0038	TRCN0000136105,TRCN0000134136	0.42, 0.29	0.80, 0.57	Mes	Amplified
91	*SLITRK5*	1.65	0.0042	TRCN0000078706,TRCN0000078707	0.34, 0.30	0.65, 0.57	Mes	Amplified
92	*TAS2R60*	1.65	0.0041	TRCN0000014138,TRCN0000014141,TRCN0000014140 ,TRCN0000014142	0.46, 0.36, 0.27, 0.26	0.73, 0.67, 0.52, 0.50	Mes	Amplified

Appendix I. The genes for subtype-specific depleted and amplified shRNAs. (continued)

Index	Gene	NES	*False Discovery Rate q*-value	Hairpin ID	Hairpin score	Effect size	Subtype	Depleted/ Amplified
93	*PGAM2*	1.64	0.0048	TRCN0000049044,TRCN0000049045,TRCN0000049043	0.53, 0.40, 0.32	1.05, 0.73, 0.63	Mes	Amplified
94	*SHANK1*	1.64	0.0003	TRCN0000138405,TRCN0000136791	0.57, 0.43	1.09, 0.81	Mes	Amplified
95	*TCL1A*	1.64	0.0047	TRCN0000107143,TRCN0000107144,TRCN0000107141	0.39, 0.36, 0.29	0.78, 0.72, 0.56	Mes	Amplified
96	*SLITRK6*	1.62	0.0008	TRCN0000153177	0.69	1.13	Mes	Amplified
97	*THNSL1*	1.59	0.0017	TRCN0000045420,TRCN0000045419	0.65, 0.43	1.29, 0.87	Mes	Amplified
98	*SDAD1*	1.58	0.0032	TRCN0000129836	0.51	0.77	Mes	Amplified
99	*TOMM40*	1.57	0.0037	TRCN0000072436,TRCN0000072434	0.51, 0.46	1.01, 0.91	Mes	Amplified
100	*UNK_SLC7 A5 pseudogene*	1.57	0.0039	TRCN0000060268,TRCN0000060271	0.53, 0.38	1.00, 0.76	Mes	Amplified
101	*UNK_testis serine protease 1*	1.57	0.0039	TRCN0000074056,TRCN0000074057	0.53, 0.39	0.85, 0.73	Mes	Amplified
102	*UNK_SLC7 A5*	1.57	0.0039	TRCN0000060268,TRCN0000060271	0.53, 0.38	1.00, 0.76	Mes	Amplified
103	*S1PR5*	1.56	0.0042	TRCN0000004749,TRCN0000004748	0.61, 0.44	0.99, 0.86	Mes	Amplified
104	*SEMA3G*	1.56	0.0045	TRCN0000060855	0.38	0.71	Mes	Amplified
105	*TAS2R7*	1.56	0.0044	TRCN0000014152,TRCN0000014148	0.53, 0.34	0.97, 0.53	Mes	Amplified
106	*TMEM128*	1.52	0.0006	TRCN0000128524	0.58	1.08	Mes	Amplified
107	*LDHAL6B*	1.51	0.0007	TRCN0000028399	0.51	0.82	Mes	Amplified
108	*FBXO25*	1.5	0.0017	TRCN0000004317,TRCN0000004320	0.50, 0.45	0.89, 0.71	Mes	Amplified
109	*RFXANK*	1.5	0.0017	TRCN0000013263,TRCN0000013267	0.50, 0.45	0.87, 0.72	Mes	Amplified
110	*RHO*	1.5	0.0012	TRCN0000003752	0.68	1.29	Mes	Amplified

Appendix I. The genes for subtype-specific depleted and amplified shRNAs. (continued)

Index	Gene	NES	*False Discovery Rate q*-value	Hairpin ID	Hairpin score	Effect size	Subtype	Depleted/ Amplified
111	*WFDC2*	1.5	0.0012	TRCN0000073678,TRCN0000073682	0.60, 0.47	0.94, 0.73	Mes	Amplified
112	*CHRM4*	1.49	0.0019	TRCN0000011268	0.54	1	Mes	Amplified
113	*MT3*	1.49	0.0023	TRCN0000072598,TRCN0000072599	0.48, 0.44	0.88, 0.80	Mes	Amplified
114	*CAMKK1*	1.48	0.0035	TRCN0000001980,TRCN0000001983	0.50, 0.42	0.97, 0.83	Mes	Amplified
115	*UNK_plasma glutamate carboxypeptidase*	1.48	0.0036	TRCN0000073950	0.49	0.92	Mes	Amplified
116	*GLIPR1*	1.84	0	TRCN0000123177,TRCN0000123175,TRCN0000123178	0.65, 0.54, 0.51	1.26, 0.99, 0.99	Stem-A	Amplified
117	*SLC4A9*	1.8	0.0002	TRCN0000038251,TRCN0000038253,TRCN0000038252,TRCN0000038250,TRCN0000038249	0.46, 0.44, 0.41, 0.32, 0.27	0.92, 0.86, 0.83, 0.63, 0.52	Stem-A	Amplified
118	*IRAK1BP1*	1.78	0.0003	TRCN0000052533,TRCN0000052534,TRCN0000052535,TRCN0000052537	0.49, 0.38, 0.33, 0.31	0.96, 0.76, 0.65, 0.61	Stem-A	Amplified
119	*SPTLC1*	1.77	0.0004	TRCN0000035013,TRCN0000035012	0.62, 0.43	1.07, 0.83	Stem-A	Amplified
120	*CHEK1*	1.75	0.0032	TRCN0000000501,TRCN0000000499,TRCN0000039854,TRCN0000039856,TRCN0000009827	0.34, 0.34, 0.34, 0.30, 0.27	0.64, 0.66, 0.67, 0.57, 0.53	Stem-A	Amplified
121	*LY75*	1.75	0.0009	TRCN0000057364,TRCN0000057365,TRCN0000057363	0.54, 0.41, 0.35	1.05, 0.77, 0.66	Stem-A	Amplified
122	*CFHR4*	1.73	0.0014	TRCN0000150861,TRCN0000152424,TRCN0000151444	0.33, 0.31, 0.28	0.63, 0.62, 0.56	Stem-A	Amplified
123	*SLC22A15*	1.73	0.0011	TRCN0000038257,TRCN0000038256,TRCN0000038258,TRCN0000038255	0.29, 0.27, 0.25, 0.24	0.57, 0.54, 0.50, 0.49	Stem-A	Amplified
124	*FBXL16*	1.72	0.0017	TRCN0000118573,TRCN0000118574,TRCN0000118575	0.48, 0.42, 0.33	0.94, 0.80, 0.51	Stem-A	Amplified

Appendix I. The genes for subtype-specific depleted and amplified shRNAs. (continued)

Index	Gene	NES	*False Discovery Rate q*-value	Hairpin ID	Hairpin score	Effect size	Subtype	Depleted/ Amplified
125	*KDELC1*	1.72	0.0015	TRCN0000152313,TRCN0000152479	0.61, 0.49	1.21, 0.99	Stem-A	Amplified
126	*TMCO1*	1.72	0.0005	TRCN0000062123,TRCN0000062126,TRCN0000062125 ,TRCN0000062124	0.39, 0.37, 0.37, 0.30	0.78, 0.73, 0.74, 0.59	Stem-A	Amplified
127	*UNK_ATPase, Class I, type 8B family pseudogene*	1.71	0.0019	TRCN0000148337,TRCN0000149690,TRCN0000148159	0.45, 0.44, 0.35	0.82, 0.80, 0.57	Stem-A	Amplified
128	*B3GNT8*	1.69	0.0028	TRCN0000035776,TRCN0000035777,TRCN0000035774 ,TRCN0000035775	0.36, 0.29, 0.24, 0.21	0.72, 0.57, 0.47, 0.42	Stem-A	Amplified
129	*MAGEE1*	1.69	0.0028	TRCN0000115851,TRCN0000115847,TRCN0000115848	0.40, 0.35, 0.30	0.79, 0.66, 0.59	Stem-A	Amplified
130	*PTPRG*	1.69	0.0028	TRCN0000002862,TRCN0000002863,TRCN0000002861	0.55, 0.28, 0.23	0.95, 0.54, 0.46	Stem-A	Amplified
131	*C22orf34*	1.67	0.0028	TRCN0000147028,TRCN0000148869,TRCN0000149311 ,TRCN0000149153	0.49, 0.27, 0.24, 0.23	0.89, 0.54, 0.47, 0.46	Stem-A	Amplified
132	*CBX5*	1.67	0.0013	TRCN0000062240	0.93	1.71	Stem-A	Amplified
133	*SLC22A18AS*	1.67	0.0028	TRCN0000043185,TRCN0000043187	0.45, 0.38	0.88, 0.75	Stem-A	Amplified
134	*UNK_similar to FK506 binding protein 52*	1.67	0.003	TRCN0000049180,TRCN0000049182,TRCN0000049181	0.42, 0.34, 0.31	0.82, 0.67, 0.60	Stem-A	Amplified
135	*GUCA1B*	1.66	0.0036	TRCN0000056299,TRCN0000056302,TRCN0000056300	0.33, 0.28, 0.22	0.64, 0.52, 0.44	Stem-A	Amplified

Appendix I. The genes for subtype-specific depleted and amplified shRNAs. (continued)

Index	Gene	NES	*False Discovery Rate q*-value	Hairpin ID	Hairpin score	Effect size	Subtype	Depleted/ Amplified
136	*UNK_ubiquinol-cytochrome c reductase complex (7.2 kD)*	1.66	0.0035	TRCN0000046360,TRCN0000046359,TRCN0000046358	0.70, 0.31, 0.26	1.36, 0.61, 0.48	Stem-A	Amplified
137	*CDSN*	1.65	0.0041	TRCN0000083131,TRCN0000083128,TRCN0000083129	0.55, 0.40, 0.40	1.02, 0.77, 0.79	Stem-A	Amplified
138	*LRRC15*	1.65	0.0041	TRCN0000139627,TRCN0000144278,TRCN0000143971 ,TRCN0000139477	0.47, 0.23, 0.22, 0.21	0.76, 0.45, 0.43, 0.43	Stem-A	Amplified
139	*UNK_HERV-FRD provirus ancestral Env polyprotein*	1.65	0.0026	TRCN0000062254,TRCN0000062256	0.57, 0.43	1.14, 0.86	Stem-A	Amplified
140	*ANO1*	1.64	0	TRCN0000040264	0.48	0.86	Stem-A	Amplified
141	*ATF7IP*	1.64	0.0031	TRCN0000020824,TRCN0000020827,TRCN0000020828	0.38, 0.35, 0.32	0.76, 0.66, 0.53	Stem-A	Amplified
142	*CLN6*	1.63	0.0038	TRCN0000083612,TRCN0000083610	0.63, 0.33	1.26, 0.62	Stem-A	Amplified
143	*SCG5*	1.62	0.0046	TRCN0000060172	0.39	0.72	Stem-A	Amplified
144	*LNX1*	1.61	0.0005	TRCN0000073124,TRCN0000073126	0.49, 0.39	0.80, 0.74	Stem-A	Amplified
145	*PLEKHO2*	1.6	0.0005	TRCN0000138801	0.78	1.23	Stem-A	Amplified
146	*GAK*	1.59	0.0015	TRCN0000002156,TRCN0000002157	0.55, 0.37	1.06, 0.74	Stem-A	Amplified
147	*IFNA1*	1.58	0.0017	TRCN0000005874,TRCN0000005875	0.47, 0.40	0.74, 0.78	Stem-A	Amplified
148	*PTGDS*	1.57	0.0024	TRCN0000045506,TRCN0000045503	0.46, 0.33	0.80, 0.66	Stem-A	Amplified

Appendix I. The genes for subtype-specific depleted and amplified shRNAs. (continued)

Index	Gene	NES	*False Discovery Rate q*-value	Hairpin ID	Hairpin score	Effect size	Subtype	Depleted/ Amplified
149	*ITGA5*	1.56	0.0037	TRCN0000029652,TRCN0000029651	0.51, 0.36	0.95, 0.67	Stem-A	Amplified
150	*TEAD1*	1.56	0.0037	TRCN0000015799,TRCN0000015802,TRCN0000015801	0.39, 0.33, 0.30	0.76, 0.58, 0.48	Stem-A	Amplified
151	*NFAT5*	1.55	0.0049	TRCN0000020021,TRCN0000020020,TRCN0000020023	0.33, 0.30, 0.29	0.56, 0.61, 0.58	Stem-A	Amplified
152	*FTL*	1.49	0.0008	TRCN0000029434	0.61	1.04	Stem-A	Amplified
153	*NDUFS8*	1.49	0.001	TRCN0000036669	0.46	0.89	Stem-A	Amplified
154	*ATOH8*	1.48	0.0018	TRCN0000016994,TRCN0000016995	0.43, 0.43	0.66, 0.71	Stem-A	Amplified
155	*NFIL3*	1.48	0.0023	TRCN0000014742	0.61	0.98	Stem-A	Amplified
156	*TLE1*	1.48	0.0021	TRCN0000019595,TRCN0000019597	0.46, 0.42	0.73, 0.77	Stem-A	Amplified
157	*MAP3K2*	1.47	0.0025	TRCN0000002044	0.71	1.18	Stem-A	Amplified
158	*UNK_similar to ENSANGP00000020885*	1.47	0.0027	TRCN0000015987	0.45	0.82	Stem-A	Amplified
159	*ZNF281*	1.46	0.0044	TRCN0000019685	0.6	0.94	Stem-A	Amplified

Appendix II. Common pathway response in OVCA433, HeyA8 and PA-1 to *TUBGCP4* and *NAT10* knockdown.

Index	Gene set	Gene knocked down	Positive/Negative fold change	Source
1	HOFFMANN_IMMATURE_TO_MATURE_B_LYMPHOCYTE_UP	TUBGCP4	+	GSEA.c2
2	V$STAT5A_04	TUBGCP4	+	GSEA.c3
3	TURASHVILI_BREAST_DUCTAL_CARCINOMA_VS_LOBULAR_NORMAL_DN	TUBGCP4	+	GSEA.c2
4	PROTEIN_MODIFICATION_PROCESS	TUBGCP4	+	GSEA.c5
5	GAUTSCHI_SRC_SIGNALING	TUBGCP4	+	GSEA.c2
6	TP63_DN	TUBGCP4	+	Path.Sig.SAM
7	PHOSPHORIC_MONOESTER_HYDROLASE_ACTIVITY	TUBGCP4	+	GSEA.c5
8	CHR6P	TUBGCP4	+	GSEA.c1
9	STEMABR_DN	TUBGCP4	+	Subtype.BR
10	YAO_TEMPORAL_RESPONSE_TO_PROGESTERONE_CLUSTER_3	TUBGCP4	+	GSEA.c2
11	BIOPOLYMER_MODIFICATION	TUBGCP4	+	GSEA.c5
12	VESICLE_MEDIATED_TRANSPORT	TUBGCP4	+	GSEA.c5
13	LUND_SILENCED_BY_METHYLATION	TUBGCP4	+	GSEA.c2
14	WANG_RESPONSE_TO_FORSKOLIN_DN	TUBGCP4	+	GSEA.c2
15	BIOCARTA_IL17_PATHWAY	TUBGCP4	+	GSEA.c5
16	WANG_HCP_PROSTATE_CANCER	TUBGCP4	+	GSEA.c2
17	SINGLE_STRANDED_RNA_BINDING	TUBGCP4	+	GSEA.c5
18	WANG_BARRETTS_ESOPHAGUS_AND_ESOPHAGUS_CANCER_UP	TUBGCP4	+	GSEA.c2
19	AMIT_EGF_RESPONSE_20_MCF10A	TUBGCP4	+	GSEA.c2
20	ST_STAT3_PATHWAY	TUBGCP4	+	GSEA.c2
21	TATTATA,MIR-374	TUBGCP4	+	GSEA.c3
22	PROTEASE_INHIBITOR_ACTIVITY	TUBGCP4	+	GSEA.c5
23	TRANSCRIPTION_REPRESSOR_ACTIVITY	TUBGCP4	+	GSEA.c5

Appendix II. Common pathway response in OVCA433, HeyA8 and PA-1 to *TUBGCP4* and *NAT10* knockdown. (continued)

Index	Gene set	Gene knocked down	Positive/Negative fold change	Source
24	CHR3Q22	TUBGCP4	+	GSEA.c1
25	ACTGCCT,MIR-34B	TUBGCP4	+	GSEA.c3
26	LIAN_LIPA_TARGETS_3M	TUBGCP4	+	GSEA.c2
27	LIAN_LIPA_TARGETS_6M	TUBGCP4	+	GSEA.c2
28	BOYLAN_MULTIPLE_MYELOMA_D_DN	TUBGCP4	+	GSEA.c2
29	PROTEIN_PROCESSING	TUBGCP4	+	GSEA.c5
30	WILLIAMS_ESR1_TARGETS_DN	TUBGCP4	+	GSEA.c2
31	HORIUCHI_WTAP_TARGETS_UP	TUBGCP4	+	GSEA.c2
32	BUYTAERT_PHOTODYNAMIC_THERAPY_STRESS_UP	TUBGCP4	+	GSEA.c5
33	BIOCARTA_FIBRINOLYSIS_PATHWAY	TUBGCP4	+	GSEA.c5
34	SCIBETTA_KDM5B_TARGETS_UP	TUBGCP4	+	GSEA.c2
35	SWEET_KRAS_ONCOGENIC_SIGNATURE	TUBGCP4	+	GSEA.c2
36	ACTIVATION_OF_NF_KAPPAB_TRANSCRIPTION_FACTOR	TUBGCP4	+	GSEA.c5
37	MAHAJAN_RESPONSE_TO_IL1A_UP	TUBGCP4	+	GSEA.c2
38	SMALL_GTPASE_REGULATOR_ACTIVITY	TUBGCP4	+	GSEA.c5
39	POSITIVE_REGULATION_OF_CELLULAR_PROTEIN_METABOLIC_PROCESS	TUBGCP4	+	GSEA.c5
40	V$CREB_02	TUBGCP4	+	GSEA.c3
41	NUCLEAR_SPECK	TUBGCP4	+	GSEA.c5
42	V$ATF4_Q2	TUBGCP4	+	GSEA.c3
43	V$HNF6_Q6	TUBGCP4	+	GSEA.c3
44	WNT_TARGETS	TUBGCP4	+	GSEA.c5
45	INTRACELLULAR_SIGNALING_CASCADE	TUBGCP4	+	GSEA.c5
46	MITSIADES_RESPONSE_TO_APLIDIN_UP	TUBGCP4	+	GSEA.c2

Appendix II. Common pathway response in OVCA433, HeyA8 and PA-1 to *TUBGCP4* and *NAT10* knockdown. (continued)

Index	Gene set	Gene knocked down	Positive/Negative fold change	Source
47	PATTERN_BINDING	TUBGCP4	+	GSEA.c5
48	V$HOXA4_Q2	TUBGCP4	+	GSEA.c3
49	SH2_DOMAIN_BINDING	TUBGCP4	+	GSEA.c5
50	GUTIERREZ_WALDENSTROEMS_MACROGLOBULINEMIA_1_DN	TUBGCP4	+	GSEA.c2
51	KHETCHOUMIAN_TRIM24_TARGETS_UP	TUBGCP4	+	GSEA.c2
52	TTGCACT,MIR-130A,MIR-301,MIR-130B	TUBGCP4	+	GSEA.c3
53	KYNG_DNA_DAMAGE_UP	TUBGCP4	+	GSEA.c2
54	RUNNE_GENDER_EFFECT_DN	TUBGCP4	+	GSEA.c2
55	NEGATIVE_REGULATION_OF_APOPTOSIS	TUBGCP4	+	GSEA.c5
56	CAIRO_HEPATOBLASTOMA_CLASSES_DN	TUBGCP4	+	GSEA.c2
57	POSITIVE_REGULATION_OF_PROTEIN_METABOLIC_PROCESS	TUBGCP4	+	GSEA.c5
58	GESERICK_TERT_TARGETS_DN	TUBGCP4	+	GSEA.c2
59	AROMATIC_COMPOUND_METABOLIC_PROCESS	TUBGCP4	-	GSEA.c5
60	CHR11Q25	TUBGCP4	-	GSEA.c1
61	ACEVEDO_LIVER_CANCER_WITH_H3K9ME3_DN	TUBGCP4	-	GSEA.c2
62	LIU_SOX4_TARGETS_DN	TUBGCP4	-	GSEA.c2
63	V$E2F_01	TUBGCP4	-	GSEA.c3
64	WINNEPENNINCKX_MELANOMA_METASTASIS_UP	TUBGCP4	-	GSEA.c2
65	PYEON_CANCER_HEAD_AND_NECK_VS_CERVICAL_UP	TUBGCP4	-	GSEA.c2
66	REACTOME_CELL_CYCLE_MITOTIC	TUBGCP4	-	GSEA.c5
67	V$USF_Q6_01	TUBGCP4	-	GSEA.c3
68	SGCGSSAAA_V$E2F1DP2_01	TUBGCP4	-	GSEA.c3
69	BIOCARTA_RB_PATHWAY	TUBGCP4	-	GSEA.c5

Appendix II. Common pathway response in OVCA433, HeyA8 and PA-1 to *TUBGCP4* and *NAT10* knockdown. (continued)

Index	Gene set	Gene knocked down	Positive/Negative fold change	Source
70	KEGG_STEROID_BIOSYNTHESIS	TUBGCP4	-	GSEA.c5
71	V$E2F_02	TUBGCP4	-	GSEA.c3
72	BYSTRYKH_HEMATOPOIESIS_STEM_CELL_AND_BRAIN_QTL_TRANS	TUBGCP4	-	GSEA.c2
73	V$E2F_Q3	TUBGCP4	-	GSEA.c3
74	PUJANA_BRCA2_PCC_NETWORK	TUBGCP4	-	GSEA.c2
75	UBIQUITIN_LIGASE_COMPLEX	TUBGCP4	-	GSEA.c5
76	GRASEMANN_RETINOBLASTOMA_WITH_6P_AMPLIFICATION	TUBGCP4	-	GSEA.c2
77	STARK_BRAIN_22Q11_DELETION	TUBGCP4	-	GSEA.c2
78	SEMBA_FHIT_TARGETS_DN	TUBGCP4	-	GSEA.c2
79	V$E2F1DP1_01	TUBGCP4	-	GSEA.c3
80	V$E2F1DP2_01	TUBGCP4	-	GSEA.c3
81	V$E2F4DP2_01	TUBGCP4	-	GSEA.c3
82	MORF_DEAF1	TUBGCP4	-	GSEA.c4
83	V$E2F1_Q3	TUBGCP4	-	GSEA.c3
84	ZHAN_V1_LATE_DIFFERENTIATION_GENES_DN	TUBGCP4	-	GSEA.c2
85	KEGG_ALPHA_LINOLENIC_ACID_METABOLISM	TUBGCP4	-	GSEA.c5
86	FINETTI_BREAST_CANCER_BASAL_VS_LUMINAL	TUBGCP4	-	GSEA.c2
87	FINETTI_BREAST_CANCER_KINOME_RED	TUBGCP4	-	GSEA.c2
88	CAFFAREL_RESPONSE_TO_THC_DN	TUBGCP4	-	GSEA.c2
89	MORF_GNB1	TUBGCP4	-	GSEA.c4
90	GNF2_HAT1	TUBGCP4	-	GSEA.c4
91	KTGGYRSGAA_UNKNOWN	TUBGCP4	-	GSEA.c3
92	S_PHASE	TUBGCP4	-	GSEA.c5

Appendix II. Common pathway response in OVCA433, HeyA8 and PA-1 to *TUBGCP4* and *NAT10* knockdown. (continued)

Index	Gene set	Gene knocked down	Positive/Negative fold change	Source
93	V$E2F1DP1RB_01	TUBGCP4	-	GSEA.c3
94	BLUM_RESPONSE_TO_SALIRASIB_DN	TUBGCP4	-	GSEA.c2
95	CROONQUIST_NRAS_SIGNALING_DN	TUBGCP4	-	GSEA.c2
96	KINSEY_TARGETS_OF_EWSR1_FLII_FUSION_UP	TUBGCP4	-	GSEA.c2
97	WEBER_METHYLATED_LCP_IN_FIBROBLAST_DN	TUBGCP4	-	GSEA.c2
98	MORF_G22P1	TUBGCP4	-	GSEA.c4
99	PUJANA_BRCA1_PCC_NETWORK	TUBGCP4	-	GSEA.c2
100	V$E2F_03	TUBGCP4	-	GSEA.c3
101	CHANG_CYCLING_GENES	TUBGCP4	-	GSEA.c2
102	MODULE_147	TUBGCP4	-	GSEA.c4
103	WHITEFORD_PEDIATRIC_CANCER_MARKERS	TUBGCP4	-	GSEA.c2
104	SCIAN_CELL_CYCLE_TARGETS_OF_TP53_AND_TP73_DN	TUBGCP4	-	GSEA.c2
105	CASORELLI_ACUTE_PROMYELOCYTIC_LEUKEMIA_DN	TUBGCP4	-	GSEA.c2
106	REACTOME_INACTIVATION_OF_APC_VIA_DIRECT_INHIBITION_OF_THE_APC OMPLEX	TUBGCP4	-	GSEA.c5
107	MITOTIC_CELL_CYCLE	TUBGCP4	-	GSEA.c5
108	CREIGHTON_ENDOCRINE_THERAPY_RESISTANCE_4	TUBGCP4	-	GSEA.c2
109	WEST_ADRENOCORTICAL_TUMOR_UP	TUBGCP4	-	GSEA.c2
110	GNF2_CKS2	TUBGCP4	-	GSEA.c4
111	MORF_PTPN11	TUBGCP4	-	GSEA.c4
112	V$E2F4DP1_01	TUBGCP4	-	GSEA.c3
113	GCM_CBFB	TUBGCP4	-	GSEA.c4
114	V$E2F1_Q4_01	TUBGCP4	-	GSEA.c3

Appendix II. Common pathway response in OVCA433, HeyA8 and PA-1 to *TUBGCP4* and *NAT10* knockdown. (continued)

Index	Gene set	Gene knocked down	Positive/Negative fold change	Source
115	TANG_SENESCENCE_TP53_TARGETS_DN	TUBGCP4	-	GSEA.c2
116	CHR9P11	TUBGCP4	-	GSEA.c1
117	MORF_EI24	TUBGCP4	-	GSEA.c4
118	M_PHASE_OF_MITOTIC_CELL_CYCLE	TUBGCP4	-	GSEA.c5
119	NUYTTEN_EZH2_TARGETS_DN	TUBGCP4	-	GSEA.c2
120	MODULE_244	TUBGCP4	-	GSEA.c4
121	MODULE_198	TUBGCP4	-	GSEA.c4
122	REACTOME_PACKAGING_OF_TELOMERE_ENDS	TUBGCP4	-	GSEA.c5
123	WEBER_METHYLATED_LCP_IN_SPERM_DN	TUBGCP4	-	GSEA.c2
124	MORF_CSNK2B	TUBGCP4	-	GSEA.c4
125	CHEMNITZ_RESPONSE_TO_PROSTAGLANDIN_E2_UP	TUBGCP4	-	GSEA.c2
126	MORF_BUB1B	TUBGCP4	-	GSEA.c4
127	KEGG_OOCYTE_MEIOSIS	TUBGCP4	-	GSEA.c5
128	T_CELL_DIFFERENTIATION	TUBGCP4	-	GSEA.c5
129	LIANG_SILENCED_BY_METHYLATION_DN	TUBGCP4	-	GSEA.c2
130	MODULE_203	TUBGCP4	-	GSEA.c4
131	MORF_AATF	TUBGCP4	-	GSEA.c4
132	SISTER_CHROMATID_SEGREGATION	TUBGCP4	-	GSEA.c5
133	MITOSIS	TUBGCP4	-	GSEA.c5
134	GNF2_CCNB2	TUBGCP4	-	GSEA.c4
135	G1_PHASE	TUBGCP4	-	GSEA.c5

Appendix II. Common pathway response in OVCA433, HeyA8 and PA-1 to *TUBGCP4* and *NAT10* knockdown. (continued)

Index	Gene set	Gene knocked down	Positive/Negative fold change	Source
136	MORF_RAD23A	TUBGCP4	-	GSEA.c4
137	VECCHI_GASTRIC_CANCER_EARLY_UP	TUBGCP4	-	GSEA.c2
138	MORF_ERH	TUBGCP4	-	GSEA.c4
139	VANTVEER_BREAST_CANCER_METASTASIS_DN	TUBGCP4	-	GSEA.c2
140	MICROTUBULE	TUBGCP4	-	GSEA.c5
141	S_PHASE_OF_MITOTIC_CELL_CYCLE	TUBGCP4	-	GSEA.c5
142	HAHTOLA_MYCOSIS_FUNGOIDES_CD4_DN	TUBGCP4	-	GSEA.c2
143	MODULE_372	TUBGCP4	-	GSEA.c4
144	LIANG_HEMATOPOIESIS_STEM_CELL_NUMBER_LARGE_VS_TINY_UP	TUBGCP4	-	GSEA.c2
145	MORF_SS18	TUBGCP4	-	GSEA.c4
146	GNF2_SMC4L1	TUBGCP4	-	GSEA.c4
147	REACTOME_G2_M_CHECKPOINTS	TUBGCP4	-	GSEA.c5
148	GNF2_DEK	TUBGCP4	-	GSEA.c4
149	MORF_DDB1	TUBGCP4	-	GSEA.c4
150	MORF_ACP1	TUBGCP4	-	GSEA.c4
151	GNF2_CDC2	TUBGCP4	-	GSEA.c4
152	MORF_BUB3	TUBGCP4	-	GSEA.c4
153	MORF_XRCC5	TUBGCP4	-	GSEA.c4
154	NUCLEAR_UBIQUITIN_LIGASE_COMPLEX	TUBGCP4	-	GSEA.c5
155	HOFFMANN_LARGE_TO_SMALL_PRE_BII_LYMPHOCYTE_UP	TUBGCP4	-	GSEA.c2
156	STARK_HYPPOCAMPUS_22Q11_DELETION_UP	TUBGCP4	-	GSEA.c2
157	PUJANA_BREAST_CANCER_LIT_INT_NETWORK	TUBGCP4	-	GSEA.c2
158	MOLENAAR_TARGETS_OF_CCND1_AND_CDK4_DN	TUBGCP4	-	GSEA.c2

Appendix II. Common pathway response in OVCA433, HeyA8 and PA-1 to *TUBGCP4* and *NAT10* knockdown. (continued)

Index	Gene set	Gene knocked down	Positive/Negative fold change	Source
159	GNF2_RRM1	TUBGCP4	-	GSEA.c4
160	ZHAN_MULTIPLE_MYELOMA_PR_UP	TUBGCP4	-	GSEA.c2
161	GNF2_CENPF	TUBGCP4	-	GSEA.c4
162	V$E2F_Q3_01	TUBGCP4	-	GSEA.c3
163	CHR1P11	TUBGCP4	-	GSEA.c1
164	GNF2_MLH1	TUBGCP4	-	GSEA.c4
165	SHEDDEN_LUNG_CANCER_POOR_SURVIVAL_A6	TUBGCP4	-	GSEA.c2
166	CHEN_HOXA5_TARGETS_9HR_DN	TUBGCP4	-	GSEA.c2
167	KANG_DOXORUBICIN_RESISTANCE_UP	TUBGCP4	-	GSEA.c2
168	RUIZ_TNC_TARGETS_DN	TUBGCP4	-	GSEA.c2
169	SA_REG_CASCADE_OF_CYCLIN_EXPR	TUBGCP4	-	GSEA.c2
170	V$MYC_Q2	TUBGCP4	-	GSEA.c3
171	MORF_SOD1	TUBGCP4	-	GSEA.c4
172	GNF2_MCM5	TUBGCP4	-	GSEA.c4
173	CONDENSED_NUCLEAR_CHROMOSOME	TUBGCP4	-	GSEA.c5
174	NUCLEAR_CHROMATIN	TUBGCP4	-	GSEA.c5
175	GNF2_PCNA	TUBGCP4	-	GSEA.c4
176	GRAHAM_NORMAL_QUIESCENT_VS_NORMAL_DIVIDING_DN	TUBGCP4	-	GSEA.c2
177	DANG_BOUND_BY_MYC	TUBGCP4	-	GSEA.c2
178	KEGG_CELL_CYCLE	TUBGCP4	-	GSEA.c5
179	GNF2_HMMR	TUBGCP4	-	GSEA.c4
180	GNF2_RFC3	TUBGCP4	-	GSEA.c4
181	PUJANA_BREAST_CANCER_WITH_BRCA1_MUTATED_UP	TUBGCP4	-	GSEA.c2

Appendix II. Common pathway response in OVCA433, HeyA8 and PA-1 to *TUBGCP4* and *NAT10* knockdown. (continued)

Index	Gene set	Gene knocked down	Positive/Negative fold change	Source
182	G1_PHASE_OF_MITOTIC_CELL_CYCLE	TUBGCP4	-	GSEA.c5
183	SOTIRIOU_BREAST_CANCER_GRADE_1_VS_3_UP	TUBGCP4	-	GSEA.c2
184	GNF2_CCNA2	TUBGCP4	-	GSEA.c4
185	NUCLEAR_CHROMOSOME	TUBGCP4	-	GSEA.c5
186	GRAHAM_CML_QUIESCENT_VS_NORMAL_QUIESCENT_UP	TUBGCP4	-	GSEA.c2
187	GNF2_FEN1	TUBGCP4	-	GSEA.c4
188	MORF_SMC1L1	TUBGCP4	-	GSEA.c4
189	MORF_EIF3S2	TUBGCP4	-	GSEA.c4
190	MORF_MTA1	TUBGCP4	-	GSEA.c4
191	FERRANDO_T_ALL_WITH_MLL_ENL_FUSION_DN	TUBGCP4	-	GSEA.c2
192	LY_AGING_PREMATURE_DN	TUBGCP4	-	GSEA.c2
193	GNF2_APEX1	TUBGCP4	-	GSEA.c4
194	SCHUHMACHER_MYC_TARGETS_UP	TUBGCP4	-	GSEA.c2
195	MANALO_HYPOXIA_DN	TUBGCP4	-	GSEA.c2
196	MYLLYKANGAS_AMPLIFICATION_HOT_SPOT_3	TUBGCP4	-	GSEA.c2
197	REACTOME_REPAIR_SYNTHESIS_OF_PATCH_27_30_BASES_LONG_BY_DNA_POLYMERASE	TUBGCP4	-	GSEA.c5
198	BIOCARTA_SRCRPTP_PATHWAY	TUBGCP4	-	GSEA.c5
199	AKT_UP	TUBGCP4	-	Path.Sig.SAM
200	MITOTIC_SISTER_CHROMATID_SEGREGATION	TUBGCP4	-	GSEA.c5
201	MODULE_17	TUBGCP4	-	GSEA.c4
202	MOOTHA_GLUCONEOGENESIS	TUBGCP4	-	GSEA.c2
203	REACTOME_ACTIVATION_OF_THE_PRE_REPLICATIVE_COMPLEX	TUBGCP4	-	GSEA.c5
204	MORF_GMPS	TUBGCP4	-	GSEA.c4

Appendix II. Common pathway response in OVCA433, HeyA8 and PA-1 to *TUBGCP4* and *NAT10* knockdown. (continued)

Index	Gene set	Gene knocked down	Positive/Negative fold change	Source
205	V$AHR_Q5	TUBGCP4	-	GSEA.c3
206	RICKMAN_TUMOR_DIFFERENTIATED_MODERATELY_VS_POORLY_DN	TUBGCP4	-	GSEA.c2
207	RICKMAN_TUMOR_DIFFERENTIATED_MODERATELY_VS_POORLY_UP	TUBGCP4	-	GSEA.c2
208	MORF_HDAC1	TUBGCP4	-	GSEA.c4
209	MITSIADES_RESPONSE_TO_APLIDIN_DN	TUBGCP4	-	GSEA.c2
210	GNF2_BUB1	TUBGCP4	-	GSEA.c4
211	MYLLYKANGAS_AMPLIFICATION_HOT_SPOT_15	TUBGCP4	-	GSEA.c2
212	ROSTY_CERVICAL_CANCER_PROLIFERATION_CLUSTER	TUBGCP4	-	GSEA.c2
213	MODULE_439	TUBGCP4	-	GSEA.c4
214	KEGG_PYRUVATE_METABOLISM	TUBGCP4	-	GSEA.c5
215	LINDGREN_BLADDER_CANCER_CLUSTER_3_UP	TUBGCP4	-	GSEA.c2
216	MATTIOLI_MGUS_VS_PCL	TUBGCP4	-	GSEA.c2
217	YU_MYC_TARGETS_UP	TUBGCP4	-	GSEA.c2
218	REACTOME_TELOMERE_MAINTENANCE	TUBGCP4	-	GSEA.c5
219	CHROMATIN_BINDING	TUBGCP4	-	GSEA.c5
220	ENDODEOXYRIBONUCLEASE_ACTIVITY	TUBGCP4	-	GSEA.c5
221	MODULE_54	TUBGCP4	-	GSEA.c4
222	LEE_EARLY_T_LYMPHOCYTE_UP	TUBGCP4	-	GSEA.c2
223	ISOPRENOID_METABOLIC_PROCESS	TUBGCP4	-	GSEA.c5
224	GCM_ANP32B	TUBGCP4	-	GSEA.c4
225	GCM_PPP1CC	TUBGCP4	-	GSEA.c4
226	MORF_FBL	TUBGCP4	-	GSEA.c4
227	REACTOME_CHOLESTEROL_BIOSYNTHESIS	TUBGCP4	-	GSEA.c5
228	MISSIAGLIA_REGULATED_BY_METHYLATION_DN	TUBGCP4	-	GSEA.c2

Appendix II. Common pathway response in OVCA433, HeyA8 and PA-1 to *TUBGCP4* and *NAT10* knockdown. (continued)

Index	Gene set	Gene knocked down	Positive/Negative fold change	Source
229	BIOCARTA_SKP2E2F_PATHWAY	TUBGCP4	-	GSEA.c5
230	NUNODA_RESPONSE_TO_DASATINIB_IMATINIB_UP	TUBGCP4	-	GSEA.c2
231	SHIPP_DLBCL_VS_FOLLICULAR_LYMPHOMA_UP	TUBGCP4	-	GSEA.c2
232	BENPORATH_MYC_TARGETS_WITH_EBOX	TUBGCP4	-	GSEA.c2
233	SHEPARD_BMYB_MORPHOLINO_DN	TUBGCP4	-	GSEA.c2
234	MODULE_538	TUBGCP4	-	GSEA.c4
235	KERLEY_RESPONSE_TO_CISPLATIN_DN	TUBGCP4	-	GSEA.c2
236	BIOCARTA_P27_PATHWAY	TUBGCP4	-	GSEA.c5
237	PRAMOONJAGO_SOX4_TARGETS_DN	TUBGCP4	-	GSEA.c2
238	DAIRKEE_CANCER_PRONE_RESPONSE_BPA_E2	TUBGCP4	-	GSEA.c2
239	KYNG_DNA_DAMAGE_BY_4NQO_OR_GAMMA_RADIATION	NAT10	+	GSEA.c2
240	RUGO_STRESS_RESPONSE_SUBSET_F	NAT10	+	GSEA.c2
241	REACTOME_CHAPERONIN_MEDIATED_PROTEIN_FOLDING	NAT10	+	GSEA.c5
242	BIOCARTA_EPHA4_PATHWAY	NAT10	+	GSEA.c5
243	WU_SILENCED_BY_METHYLATION_IN_BLADDER_CANCER	NAT10	+	GSEA.c2
244	EXTRACELLULAR_STRUCTURE_ORGANIZATION_AND_BIOGENESIS	NAT10	+	GSEA.c5
245	MODULE_491	NAT10	+	GSEA.c4
246	GOLGI_VESICLE_TRANSPORT	NAT10	+	GSEA.c5
247	TURASHVILI_BREAST_DUCTAL_CARCINOMA_VS_LOBULAR_NORMAL_DN	NAT10	+	GSEA.c2
248	V$FOXO4_02	NAT10	+	GSEA.c3
249	NOJIMA_SFRP2_TARGETS_UP	NAT10	+	GSEA.c2
250	LANDIS_ERBB2_BREAST_TUMORS_65_UP	NAT10	+	GSEA.c2
251	CHIANG_LIVER_CANCER_SUBCLASS_UNANNOTATED_UP	NAT10	+	GSEA.c2

Appendix II. Common pathway response in OVCA433, HeyA8 and PA-1 to *TUBGCP4* and *NAT10* knockdown. (continued)

Index	Gene set	Gene knocked down	Positive/Negative fold change	Source
252	REACTOME_ACTIVATED_AMPK_STIMULATES_FATTY_ACID_OXIDATION_IN_MUSCLE	NAT10	+	GSEA.c5
253	TATTATA,MIR-374	NAT10	+	GSEA.c3
254	SYNAPSE_ORGANIZATION_AND_BIOGENESIS	NAT10	+	GSEA.c5
255	SILIGAN_TARGETS_OF_EWS_FLI1_FUSION_UP	NAT10	+	GSEA.c2
256	V$CEBPA_01	NAT10	+	GSEA.c3
257	PHOSPHOLIPID_BINDING	NAT10	+	GSEA.c5
258	TRANSPORT_VESICLE	NAT10	+	GSEA.c5
259	SHEPARD_CRUSH_AND_BURN_MUTANT_UP	NAT10	+	GSEA.c2
260	REACTOME_SIGNALING_BY_WNT	NAT10	+	GSEA.c5
261	SASAKI_TARGETS_OF_TP73_AND_TP63	NAT10	+	GSEA.c2
262	CHR6Q12	NAT10	+	GSEA.c1
263	HEIDENBLAD_AMPLIFIED_IN_PANCREATIC_CANCER	NAT10	+	GSEA.c2
264	DAZARD_UV_RESPONSE_CLUSTER_G1	NAT10	+	GSEA.c2
265	BLUM_RESPONSE_TO_SALIRASIB_UP	NAT10	+	GSEA.c2
266	SA_CASPASE_CASCADE	NAT10	+	GSEA.c2
267	CELLULAR_MACROMOLECULE_METABOLIC_PROCESS	NAT10	+	GSEA.c5
268	GCTCTTG,MIR-335	NAT10	+	GSEA.c3
269	DOANE_RESPONSE_TO_ANDROGEN_UP	NAT10	+	GSEA.c2
270	KAAB_HEART_ATRIUM_VS_VENTRICLE_DN	NAT10	+	GSEA.c2
271	HORIUCHI_WTAP_TARGETS_UP	NAT10	+	GSEA.c2
272	V$POU3F2_01	NAT10	+	GSEA.c3
273	FRASOR_RESPONSE_TO_SERM_OR_FULVESTRANT_UP	NAT10	+	GSEA.c2
274	INTRACELLULAR_TRANSPORT	NAT10	+	GSEA.c5

Appendix II. Common pathway response in OVCA433, HeyA8 and PA-1 to *TUBGCP4* and *NAT10* knockdown. (continued)

Index	Gene set	Gene knocked down	Positive/Negative fold change	Source
275	PROTEASE_INHIBITOR_ACTIVITY	NAT10	+	GSEA.c5
276	DANG_REGULATED_BY_MYC_DN	NAT10	+	GSEA.c2
277	BRUNEAU_HEART_GREAT_VESSELS_AND_VALVULOGENESIS	NAT10	+	GSEA.c2
278	GTGCAAT,MIR-25,MIR-32,MIR-92,MIR-363,MIR-367	NAT10	+	GSEA.c3
279	EXOCYTOSIS	NAT10	+	GSEA.c5
280	JIANG_HYPOXIA_NORMAL	NAT10	+	GSEA.c2
281	CELLULAR_PROTEIN_METABOLIC_PROCESS	NAT10	+	GSEA.c5
282	BIOCARTA_D4GDI_PATHWAY	NAT10	+	GSEA.c5
283	ACID_AMINO_ACID_LIGASE_ACTIVITY	NAT10	+	GSEA.c5
284	CHR7P11	NAT10	+	GSEA.c1
285	V$HNF3B_01	NAT10	+	GSEA.c3
286	OXIDOREDUCTASE_ACTIVITY_GO_0016706	NAT10	+	GSEA.c5
287	CHIANG_LIVER_CANCER_SUBCLASS_POLYSOMY7_DN	NAT10	+	GSEA.c2
288	NEGATIVE_REGULATION_OF_CELLULAR_COMPONENT_ORGANIZATION_AND_BIOGENESIS	NAT10	+	GSEA.c5
289	V$FOXD3_01	NAT10	+	GSEA.c3
290	CHR5Q32	NAT10	+	GSEA.c1
291	ZHOU_INFLAMMATORY_RESPONSE_FIMA_UP	NAT10	+	GSEA.c2
292	GCAAGAC,MIR-431	NAT10	+	GSEA.c3
293	BOHN_PRIMARY_IMMUNODEFICIENCY_SYNDROM_DN	NAT10	+	GSEA.c2
294	KOKKINAKIS_METHIONINE_DEPRIVATION_96HR_UP	NAT10	+	GSEA.c2
295	EMBRYONIC_DEVELOPMENT	NAT10	+	GSEA.c5
296	NOUZOVA_METHYLATED_IN_APL	NAT10	+	GSEA.c2
297	REGULATION_OF_T_CELL_PROLIFERATION	NAT10	+	GSEA.c5

Appendix II. Common pathway response in OVCA433, HeyA8 and PA-1 to *TUBGCP4* and *NAT10* knockdown. (continued)

Index	Gene set	Gene knocked down	Positive/Negative fold change	Source
298	GENTILE_UV_RESPONSE_CLUSTER_D8	NAT10	+	GSEA.c2
299	FUJII_YBX1_TARGETS_UP	NAT10	+	GSEA.c2
300	BEGUM_TARGETS_OF_PAX3_FOXO1_FUSION_AND_PAX3	NAT10	+	GSEA.c2
301	UDAYAKUMAR_MED1_TARGETS_DN	NAT10	+	GSEA.c2
302	ABDULRAHMAN_KIDNEY_CANCER_VHL_DN	NAT10	+	GSEA.c2
303	MODULE_447	NAT10	+	GSEA.c4
304	KEGG_SNARE_INTERACTIONS_IN_VESICULAR_TRANSPORT	NAT10	+	GSEA.c5
305	EMBRYO_IMPLANTATION	NAT10	+	GSEA.c5
306	V$ELK1_01	NAT10	+	GSEA.c3
307	V$POU6F1_01	NAT10	+	GSEA.c3
308	POSITIVE_REGULATION_OF_MAPKKK_CASCADE	NAT10	+	GSEA.c5
309	SCIBETTA_KDM5B_TARGETS_UP	NAT10	+	GSEA.c2
310	CHIARADONNA_NEOPLASTIC_TRANSFORMATION_CDC25_UP	NAT10	+	GSEA.c2
311	TAKEDA_TARGETS_OF_NUP98_HOXA9_FUSION_16D_DN	NAT10	+	GSEA.c2
312	REACTOME_REGULATED_PROTEOLYSIS_OF_P75NTR	NAT10	+	GSEA.c5
313	MODULE_543	NAT10	+	GSEA.c4
314	BIOCARTA_VITCB_PATHWAY	NAT10	+	GSEA.c5
315	CAIRO_HEPATOBLASTOMA_DN	NAT10	+	GSEA.c2
316	SHARMA_ASTROCYTOMA_WITH_NF1_SYNDROM	NAT10	+	GSEA.c2
317	GTCTACC,MIR-379	NAT10	+	GSEA.c3
318	POSITIVE_REGULATION_OF_PROTEIN_METABOLIC_PROCESS	NAT10	+	GSEA.c5
319	MODULE_259	NAT10	+	GSEA.c4
320	CHR3P23	NAT10	+	GSEA.c1
321	BLALOCK_ALZHEIMERS_DISEASE_INCIPIENT_UP	NAT10	+	GSEA.c2

Appendix II. Common pathway response in OVCA433, HeyA8 and PA-1 to *TUBGCP4* and *NAT10* knockdown. (continued)

Index	Gene set	Gene knocked down	Positive/Negative fold change	Source
322	BOYAULT_LIVER_CANCER_SUBCLASS_G2	NAT10	+	GSEA.c2
323	CHR3P22	NAT10	+	GSEA.c1
324	REACTOME_ASSOCIATION_OF_TRIC_CCT_WITH_TARGET_PROTEINS_DURING_BIOSYNTHESIS	NAT10	+	GSEA.c5
325	REACTOME_SIGNALING_BY_NOTCH	NAT10	+	GSEA.c5
326	HYDROLASE_ACTIVITY_ACTING_ON_ESTER_BONDS	NAT10	+	GSEA.c5
327	TTCCGTT,MIR-191	NAT10	+	GSEA.c3
328	CAIRO_HEPATOBLASTOMA_CLASSES_DN	NAT10	+	GSEA.c2
329	SECRETION	NAT10	+	GSEA.c5
330	V$GATA1_02	NAT10	+	GSEA.c3
331	BROWNE_HCMV_INFECTION_20HR_DN	NAT10	+	GSEA.c2
332	TGGTGCT,MIR-29A,MIR-29B,MIR-29C	NAT10	+	GSEA.c3
333	RODRIGUES_DCC_TARGETS_DN	NAT10	+	GSEA.c2
334	CHR4P12	NAT10	+	GSEA.c1
335	GCAAGGA,MIR-502	NAT10	+	GSEA.c3
336	POSITIVE_REGULATION_OF_CELLULAR_PROTEIN_METABOLIC_PROCESS	NAT10	+	GSEA.c5
337	CHRXQ26	NAT10	-	GSEA.c1
338	THUM_MIR21_TARGETS_HEART_DISEASE_DN	NAT10	-	GSEA.c2
339	APPIERTO_RESPONSE_TO_FENRETINIDE_DN	NAT10	-	GSEA.c2
340	XU_HGF_SIGNALING_NOT_VIA_AKT1_48HR_DN	NAT10	-	GSEA.c2
341	MODULE_471	NAT10	-	GSEA.c4
342	MORF_RAN	NAT10	-	GSEA.c4
343	GARGALOVIC_RESPONSE_TO_OXIDIZED_PHOSPHOLIPIDS_RED_UP	NAT10	-	GSEA.c2

Appendix II. Common pathway response in OVCA433, HeyA8 and PA-1 to *TUBGCP4* and *NAT10* knockdown. (continued)

Index	Gene set	Gene knocked down	Positive/Negative fold change	Source
344	MORF_UBE2I	NAT10	-	GSEA.c4
345	MICROTUBULE_POLYMERIZATION_OR_DEPOLYMERIZATION	NAT10	-	GSEA.c5
346	MODULE_18	NAT10	-	GSEA.c4
347	BIOCARTA_NEUROTRANSMITTERS_PATHWAY	NAT10	-	GSEA.c5
348	BETA_TUBULIN_BINDING	NAT10	-	GSEA.c5
349	BASE_EXCISION_REPAIR	NAT10	-	GSEA.c5
350	MORF_RAF1	NAT10	-	GSEA.c4
351	DNA_DAMAGE_RESPONSESIGNAL_TRANSDUCTION_RESULTING_IN_INDUCTION_OF_APOPTOSIS	NAT10	-	GSEA.c5
352	KENNY_CTNNB1_TARGETS_UP	NAT10	-	GSEA.c2
353	BIOCARTA_SHH_PATHWAY	NAT10	-	GSEA.c5
354	CHR11Q24	NAT10	-	GSEA.c1
355	GAMETE_GENERATION	NAT10	-	GSEA.c5
356	MODULE_428	NAT10	-	GSEA.c4
357	REACTOME_TRANSMEMBRANE_TRANSPORT_OF_SMALL_MOLECULES	NAT10	-	GSEA.c5
358	REACTOME_BASE_EXCISION_REPAIR	NAT10	-	GSEA.c5
359	WELCSH_BRCA1_TARGETS_1_DN	NAT10	-	GSEA.c2
360	MORF_G22P1	NAT10	-	GSEA.c4
361	V$NFY_01	NAT10	-	GSEA.c3
362	KEGG_ACUTE_MYELOID_LEUKEMIA	NAT10	-	GSEA.c5
363	SA_G1_AND_S_PHASES	NAT10	-	GSEA.c2
364	CHR7P13	NAT10	-	GSEA.c1
365	FERRANDO_HOX11_NEIGHBORS	NAT10	-	GSEA.c2

Appendix II. Common pathway response in OVCA433, HeyA8 and PA-1 to *TUBGCP4* and *NAT10* knockdown. (continued)

Index	Gene set	Gene knocked down	Positive/Negative fold change	Source
366	CONCANNON_APOPTOSIS_BY_EPOXOMICIN_DN	NAT10	-	GSEA.c2
367	REACTOME_APOPTOSIS_INDUCED_DNA_FRAGMENTATION	NAT10	-	GSEA.c5
368	GAL_LEUKEMIC_STEM_CELL_DN	NAT10	-	GSEA.c2
369	V$E2F1_Q3_01	NAT10	-	GSEA.c3
370	DAIRKEE_TERT_TARGETS_UP	NAT10	-	GSEA.c2
371	MORF_ERH	NAT10	-	GSEA.c4
372	V$MYC_Q2	NAT10	-	GSEA.c3
373	REGULATION_OF_NEUROTRANSMITTER_LEVELS	NAT10	-	GSEA.c5
374	ATPASE_ACTIVITY_COUPLED	NAT10	-	GSEA.c5
375	HASLINGER_B_CLL_WITH_CHROMOSOME_12_TRISOMY	NAT10	-	GSEA.c2
376	PASQUALUCCI_LYMPHOMA_BY_GC_STAGE_DN	NAT10	-	GSEA.c2
377	MODULE_303	NAT10	-	GSEA.c4
378	MODULE_16	NAT10	-	GSEA.c4
379	PODAR_RESPONSE_TO_ADAPHOSTIN_DN	NAT10	-	GSEA.c2
380	TTTNNANAGCYR_UNKNOWN	NAT10	-	GSEA.c3
381	MODULE_149	NAT10	-	GSEA.c4
382	CHR9P11	NAT10	-	GSEA.c1
383	REACTOME_ASSOCIATION_OF_LICENSING_FACTORS_WITH_THE_PREREPLICATIVE_COMPLEX	NAT10	-	GSEA.c5
384	ACTIVATION_OF_JNK_ACTIVITY	NAT10	-	GSEA.c5
385	MODULE_253	NAT10	-	GSEA.c4
386	PAL_PRMT5_TARGETS_UP	NAT10	-	GSEA.c2

Appendix II. Common pathway response in OVCA433, HeyA8 and PA-1 to *TUBGCP4* and *NAT10* knockdown. (continued)

Index	Gene set	Gene knocked down	Positive/Negative fold change	Source
387	NUCLEOBASENUCLEOSIDENUCLEOTIDE_AND_NUCLEIC_ACID_TRANSMEMBRANE_TRANSPORTER_ACTIVITY	NAT10	-	GSEA.c5
388	BIOCARTA_SET_PATHWAY	NAT10	-	GSEA.c5
389	SHEPARD_CRUSH_AND_BURN_MUTANT_DN	NAT10	-	GSEA.c2
390	SESTO_RESPONSE_TO_UV_C7	NAT10	-	GSEA.c2
391	MARKEY_RB1_CHRONIC_LOF_UP	NAT10	-	GSEA.c2
392	REACTOME_REMOVAL_OF_DNA_PATCH_CONTAINING_ABASIC_RESIDUE	NAT10	-	GSEA.c5
393	REACTOME_AMINO_ACID_TRANSPORT_ACROSS_THE_PLASMA_MEMBRANE	NAT10	-	GSEA.c5
394	CELL_DIVISION	NAT10	-	GSEA.c5
395	MODULE_115	NAT10	-	GSEA.c4
396	NAKAYAMA_SOFT_TISSUE_TUMORS_PCA2_UP	NAT10	-	GSEA.c2
397	REACTOME_EARLY_PHASE_OF_HIV_LIFE_CYCLE	NAT10	-	GSEA.c5
398	BENPORATH_ES_CORE_NINE_CORRELATED	NAT10	-	GSEA.c2
399	MORF_ORC1L	NAT10	-	GSEA.c4
400	GLINSKY_CANCER_DEATH_UP	NAT10	-	GSEA.c2
401	CUI_GLUCOSE_DEPRIVATION	NAT10	-	GSEA.c2
402	SEXUAL_REPRODUCTION	NAT10	-	GSEA.c5
403	CHIARETTI_T_ALL_RELAPSE_PROGNOSIS	NAT10	-	GSEA.c2
404	V$CMYB_01	NAT10	-	GSEA.c3
405	LAMELLIPODIUM	NAT10	-	GSEA.c5
406	AROMATIC_COMPOUND_METABOLIC_PROCESS	NAT10	-	GSEA.c5
407	BIOCARTA_CARM1_PATHWAY	NAT10	-	GSEA.c5
408	GCM_HDAC1	NAT10	-	GSEA.c4

Appendix II. Common pathway response in OVCA433, HeyA8 and PA-1 to *TUBGCP4* and *NAT10* knockdown. (continued)

Index	Gene set	Gene knocked down	Positive/Negative fold change	Source
409	BOGNI_TREATMENT_RELATED_MYELOID_LEUKEMIA_UP	NAT10	-	GSEA.c2
410	TP63_UP	NAT10	-	Path.Sig.SAM
411	MORF_MYST2	NAT10	-	GSEA.c4
412	SHEPARD_BMYB_TARGETS	NAT10	-	GSEA.c2
413	KTGGYRSGAA_UNKNOWN	NAT10	-	GSEA.c3
414	LEE_LIVER_CANCER_MYC_UP	NAT10	-	GSEA.c2
415	SA_REG_CASCADE_OF_CYCLIN_EXPR	NAT10	-	GSEA.c2
416	CYTOKINESIS	NAT10	-	GSEA.c5
417	MODULE_56	NAT10	-	GSEA.c4
418	PRODUCTION_OF_MOLECULAR_MEDIATOR_OF_IMMUNE_RESPONSE	NAT10	-	GSEA.c5
419	MYLLYKANGAS_AMPLIFICATION_HOT_SPOT_15	NAT10	-	GSEA.c2
420	MODULE_21	NAT10	-	GSEA.c4
421	SHEPARD_BMYB_MORPHOLINO_DN	NAT10	-	GSEA.c2
422	REACTOME_REMOVAL_OF_THE_FLAP_INTERMEDIATE_FROM_THE_C_STRAND	NAT10	-	GSEA.c5
423	PUIFFE_INVASION_INHIBITED_BY_ASCITES_UP	NAT10	-	GSEA.c2
424	MODULE_53	NAT10	-	GSEA.c4
425	OHASHI_AURKB_TARGETS	NAT10	-	GSEA.c2

GSEA: Curated gene sets from GSEA database.
Path.Sig.SAM: Gene sets generated using significance analysis of microarrays (SAM) from Gatza et al (2010).
Subtype.BR: Gene sets generated for each subtype by binary regression (BinReg) analysis from Tan et al (2013).
Subtype.SAM: Gene sets generated for each subtype by SAM and receiver operating characteristics (ROC) analysis from Tan et al (2013).

Appendix III. List of PA-1 specific down-regulated pathways that overlapped with Stem-A cell lines enriched gene sets.

Index	Gene set	Gene knocked down	Source	Recurrence
1	CENTRAL_NERVOUS_SYSTEM_DEVELOPMENT	*NAT10*	GSEA.c5	No
2	TGCGCANK_UNKNOWN	*NAT10*	GSEA.c3	No
3	GCM_NF2	*NAT10*	GSEA.c4	No
4	GNF2_MLF1	*NAT10*	GSEA.c4	No
5	MOOTHA_VOXPHOS	*NAT10*	GSEA.c2	No
6	MITOCHONDRIAL_MEMBRANE_PART	*NAT10*	GSEA.c5	Yes
7	MODULE_519	*NAT10*	GSEA.c4	No
8	MORF_BECN1	*NAT10*	GSEA.c4	No
9	YATGNWAAT_V$OCT_C	*NAT10*	GSEA.c3	No
10	GNF2_CCNA1	*NAT10*	GSEA.c4	Yes
11	HEME_BIOSYNTHETIC_PROCESS	*NAT10*	GSEA.c5	Yes
12	GLUTATHIONE_TRANSFERASE_ACTIVITY	*NAT10*	GSEA.c5	Yes
13	UBIQUITIN_PROTEIN_LIGASE_ACTIVITY	*NAT10*	GSEA.c5	Yes
14	KEGG_VALINE_LEUCINE_AND_ISOLEUCINE_BIOSYNTHESIS	*NAT10*	GSEA.c5	No
15	MICROBODY_MEMBRANE	*NAT10*	GSEA.c5	Yes
16	PEROXISOMAL_MEMBRANE	*NAT10*	GSEA.c5	Yes
17	KEGG_PYRUVATE_METABOLISM	*NAT10*	GSEA.c5	No
18	SMITH_LIVER_CANCER	*NAT10*	GSEA.c2	No
19	TRANSITION_METAL_ION_TRANSMEMBRANE_TRANSPORTER_ACTIVITY	*NAT10*	GSEA.c5	No
20	HOEGERKORP_CD44_TARGETS_TEMPORAL_DN	*NAT10*	GSEA.c2	Yes
21	GARGALOVIC_RESPONSE_TO_OXIDIZED_PHOSPHOLIPIDS_BLUE_DN	*NAT10*	GSEA.c2	Yes
22	HASLINGER_B_CLL_WITH_17P13_DELETION	*NAT10*	GSEA.c2	No
23	BROWNE_HCMV_INFECTION_10HR_UP	*NAT10*	GSEA.c2	Yes

Appendix III. List of PA-1 specific down-regulated pathways that overlapped with Stem-A cell lines enriched gene sets. (continued)

Index	Gene set	Gene knocked down	Source	Recurrence
24	MODULE_152	*NAT10*	GSEA.c4	No
25	PENG_RAPAMYCIN_RESPONSE_DN	*NAT10*	GSEA.c2	Yes
26	PIGMENT_METABOLIC_PROCESS	*NAT10*	GSEA.c5	No
27	PIGMENT_BIOSYNTHETIC_PROCESS	*NAT10*	GSEA.c5	Yes
28	HETEROCYCLE_METABOLIC_PROCESS	*NAT10*	GSEA.c5	Yes
29	SPERM_MOTILITY	*NAT10*	GSEA.c5	Yes
30	V$PAX3_01	*NAT10*	GSEA.c3	Yes
31	VALK_AML_CLUSTER_16	*NAT10*	GSEA.c2	No
32	GTTGNYNNRGNAAC_UNKNOWN	*NAT10*	GSEA.c3	Yes
33	GGTGAAG,MIR-412	*NAT10*	GSEA.c3	Yes
34	KEGG_OXIDATIVE_PHOSPHORYLATION	*NAT10*	GSEA.c5	No
35	ISOMERASE_ACTIVITY	*NAT10*	GSEA.c5	Yes
36	DACOSTA_UV_RESPONSE_VIA_ERCC3_XPCS_UP	*NAT10*	GSEA.c2	Yes
37	AGGAGTG,MIR-483	*NAT10*	GSEA.c3	No
38	MODULE_221	*NAT10*	GSEA.c4	Yes
39	MODULE_22	*NAT10*	GSEA.c4	No
40	MODULE_184	*NAT10*	GSEA.c4	Yes
41	PURINE_NUCLEOTIDE_METABOLIC_PROCESS	*NAT10*	GSEA.c5	No
42	SMALL_PROTEIN_CONJUGATING_ENZYME_ACTIVITY	*NAT10*	GSEA.c5	No
43	MITOCHONDRIAL_MEMBRANE	*NAT10*	GSEA.c5	No
44	ZHAN_MULTIPLE_MYELOMA_CD1_AND_CD2_UP	*NAT10*	GSEA.c2	No
45	FAELT_B_CLL_WITH_VH3_21_DN	*NAT10*	GSEA.c2	No
46	MODULE_42	*NAT10*	GSEA.c4	No

Appendix III. List of PA-1 specific down-regulated pathways that overlapped with Stem-A cell lines enriched gene sets. (continued)

Index	Gene set	Gene knocked down	Source	Recurrence
47	MODULE_62	*NAT10*	GSEA.c4	No
48	MODULE_77	*NAT10*	GSEA.c4	No
49	GAUSSMANN_MLL_AF4_FUSION_TARGETS_B_UP	*NAT10*	GSEA.c2	Yes
50	BARRIER_COLON_CANCER_RECURRENCE_UP	*NAT10*	GSEA.c2	No
51	BIOCARTA_ACTINY_PATHWAY	*NAT10*	GSEA.c5	No
52	MITOCHONDRIAL_ENVELOPE	*NAT10*	GSEA.c5	No
53	CHOI_ATL_STAGE_PREDICTOR	*NAT10*	GSEA.c2	No
54	V$CREB_Q3	*NAT10*	GSEA.c3	Yes
55	MYLLYKANGAS_AMPLIFICATION_HOT_SPOT_25	*NAT10*	GSEA.c2	No
56	V$VDR_Q3	*NAT10*	GSEA.c3	No
57	MITOCHONDRIAL_RESPIRATORY_CHAIN_COMPLEX_I	*NAT10*	GSEA.c5	No
58	NADH_DEHYDROGENASE_COMPLEX	*NAT10*	GSEA.c5	No
59	RESPIRATORY_CHAIN_COMPLEX_I	*NAT10*	GSEA.c5	No
60	HISTONE_DEACETYLASE_COMPLEX	*NAT10*	GSEA.c5	No
61	ACAACCT,MIR-453	*NAT10*	GSEA.c3	No
62	DING_LUNG_CANCER_MUTATED_FREQUENTLY	*NAT10*	GSEA.c2	No
63	LIN_MELANOMA_COPY_NUMBER_UP	*NAT10*	GSEA.c2	No
64	GGGGCCC,MIR-296	*NAT10*	GSEA.c3	No
65	GCM_CSNK1D	*NAT10*	GSEA.c4	No
66	HOEGERKORP_CD44_TARGETS_TEMPORAL_DN	*TUBGCP4*	GSEA.c2	Yes
67	GTTGNYNNRGNAAC_UNKNOWN	*TUBGCP4*	GSEA.c3	Yes
68	ISOMERASE_ACTIVITY	*TUBGCP4*	GSEA.c5	Yes
69	BROWNE_HCMV_INFECTION_10HR_UP	*TUBGCP4*	GSEA.c2	Yes

Appendix III. List of PA-1 specific down-regulated pathways that overlapped with Stem-A cell lines enriched gene sets. (continued)

Index	Gene set	Gene knocked down	Source	Recurrence
70	PENG_RAPAMYCIN_RESPONSE_DN	*TUBGCP4*	GSEA.c2	Yes
71	HETEROCYCLE_METABOLIC_PROCESS	*TUBGCP4*	GSEA.c5	Yes
72	SPERM_MOTILITY	*TUBGCP4*	GSEA.c5	Yes
73	V$PAX3_01	*TUBGCP4*	GSEA.c3	Yes
74	MICROBODY_MEMBRANE	*TUBGCP4*	GSEA.c5	Yes
75	PEROXISOMAL_MEMBRANE	*TUBGCP4*	GSEA.c5	Yes
76	GGTGAAG,MIR-412	*TUBGCP4*	GSEA.c3	Yes
77	HEME_BIOSYNTHETIC_PROCESS	*TUBGCP4*	GSEA.c5	Yes
78	PIGMENT_BIOSYNTHETIC_PROCESS	*TUBGCP4*	GSEA.c5	Yes
79	UBIQUITIN_PROTEIN_LIGASE_ACTIVITY	*TUBGCP4*	GSEA.c5	Yes
80	CREIGHTON_ENDOCRINE_THERAPY_RESISTANCE_2	*TUBGCP4*	GSEA.c2	No
81	GLUTATHIONE_TRANSFERASE_ACTIVITY	*TUBGCP4*	GSEA.c5	Yes
82	GAUSSMANN_MLL_AF4_FUSION_TARGETS_B_UP	*TUBGCP4*	GSEA.c2	Yes
83	MITOCHONDRIAL_MEMBRANE_PART	*TUBGCP4*	GSEA.c5	Yes
84	V$CREB_Q3	*TUBGCP4*	GSEA.c3	Yes
85	MODULE_356	*TUBGCP4*	GSEA.c4	No
86	GNF2_CCNA1	*TUBGCP4*	GSEA.c4	Yes
87	GARGALOVIC_RESPONSE_TO_OXIDIZED_PHOSPHOLIPIDS_BLUE_DN	*TUBGCP4*	GSEA.c2	Yes
88	MODULE_49	*TUBGCP4*	GSEA.c4	No
89	MODULE_184	*TUBGCP4*	GSEA.c4	Yes
90	MODULE_221	*TUBGCP4*	GSEA.c4	Yes
91	DACOSTA_UV_RESPONSE_VIA_ERCC3_XPCS_UP	*TUBGCP4*	GSEA.c2	Yes

GSEA: Curated gene sets from GSEA database.

Appendix IV. Cisplatin resistance candidate genes and cisplatin sensitizing genes identified from RNAi screen ($q < 0.005$).

Index	Gene	NES	False Discovery Rate *q*-value	Hairpin ID	Hairpin score	Category
1	SLC5A1	0.91	0	TRCN0000043588,TRCN0000043589,TRCN0000043590,TRCN0000043591,TRCN0000043592	0.39,0.72,0.62,0.57,0.43	Resistance
2	RB1	0.96	0	TRCN0000040164,TRCN0000040167,TRCN0000040163,TRCN0000040165	1.01,0.91,0.66,0.52	Resistance
3	PABPC4	0.83	0	TRCN0000074659,TRCN0000074660,TRCN0000074661,TRCN0000074662,TRCN0000074658	0.39,0.55,0.32,0.27,0.40	Resistance
4	SLC6A13	0.94	0	TRCN0000042915,TRCN0000042917,TRCN0000042916	0.49,0.49,0.47	Resistance
5	ANAPC11	0.99	0	TRCN0000038800,TRCN0000038799	0.84,0.69	Resistance
6	SLC22A6	0.84	0	TRCN0000043253,TRCN0000043254,TRCN0000043255,TRCN0000043256,TRCN0000043257	0.28,0.80,0.37,0.81,0.59	Resistance
7	CAV3	0.87	0	TRCN0000082933,TRCN0000082934,TRCN0000082935,TRCN0000082936,TRCN0000082937	0.61,0.43,0.56,0.37,0.32	Resistance
8	AKR1B10	0.83	0	TRCN0000046343,TRCN0000046344,TRCN0000046345,TRCN0000046346,TRCN0000046347	0.27,0.37,0.45,0.40,0.50	Resistance
9	ATP6V0A1	0.81	0.0001	TRCN0000038429,TRCN0000038430,TRCN0000038431,TRCN0000038432,TRCN0000038433	0.24,0.58,0.54,0.32,0.66	Resistance
10	NF2	0.81	0.0001	TRCN0000039973,TRCN0000039974,TRCN0000039975,TRCN0000039976,TRCN0000039977	0.30,0.59,0.30,0.25,0.61	Resistance
11	SLC22A1	0.81	0.0001	TRCN0000043208,TRCN0000043209,TRCN0000043210,TRCN0000043211,TRCN0000043212	0.25,0.59,0.27,0.36,0.68	Resistance
12	KCND1	0.8	0.0001	TRCN0000044973,TRCN0000044974,TRCN0000044975,TRCN0000044976,TRCN0000044977	0.23,0.26,0.26,0.31,0.52	Resistance
13	TNFRSF8	0.81	0.0001	TRCN0000058833,TRCN0000058834,TRCN0000058835,TRCN0000058836,TRCN0000058837	0.29,0.27,0.41,0.34,0.24	Resistance
14	KCNN1	0.79	0.0003	TRCN0000043818,TRCN0000043819,TRCN0000043820,TRCN0000043821,TRCN0000043822	0.23,0.29,0.50,0.36,0.31	Resistance
15	TBL3	0.88	0.0003	TRCN0000078058,TRCN0000078059,TRCN0000078061,TRCN0000078062	0.43,0.54,0.48,0.34	Resistance
16	CLDN14	0.91	0.0003	TRCN0000082913,TRCN0000082914,TRCN0000082917	0.51,0.52,0.40	Resistance

Appendix IV. Cisplatin resistance candidate genes and cisplatin sensitizing genes identified from RNAi screen (q < 0.005). (continued)

Index	Gene	NES	False Discovery Rate q-value	Hairpin ID	Hairpin score	Category
17	RPS6KA1	0.73	0.0004	TRCN0000001385,TRCN0000001388,TRCN0000039753,TRCN0000039754,TRCN0000039755,TRCN0000039757	0.67,0.34,0.68,0.44,0.62,-0.05	Resistance
18	MLH1	0.73	0.0004	TRCN0000010381,TRCN0000040053,TRCN0000040054,TRCN0000040055,TRCN0000040056,TRCN0000040057	0.36,0.16,0.28,0.31,0.21,0.42	Resistance
19	RIT2	0.79	0.0004	TRCN0000047943,TRCN0000047944,TRCN0000047945,TRCN0000047946,TRCN0000047947	0.36,0.29,0.22,0.29,0.30	Resistance
20	EXOC3	0.91	0.0004	TRCN0000074303,TRCN0000074306,TRCN0000074307	0.40,0.46,0.55	Resistance
21	HIST1H4F	0.97	0.0004	TRCN0000106726,TRCN0000106729	0.69,0.59	Resistance
22	KRTHA1	0.78	0.0005	TRCN0000116792,TRCN0000116793,TRCN0000116794,TRCN0000116795,TRCN0000116796	0.40,0.38,0.54,0.21,0.42	Resistance
23	VTI1A	0.78	0.0005	TRCN0000043358,TRCN0000043359,TRCN0000043360,TRCN0000043361,TRCN0000043362	0.34,0.40,0.21,0.28,0.48	Resistance
24	CATSPER3	0.78	0.0005	TRCN0000043813,TRCN0000043814,TRCN0000043815,TRCN0000043816,TRCN0000043817	0.49,0.86,0.49,0.01,0.62	Resistance
25	AP1M1	0.85	0.0006	TRCN0000065089,TRCN0000065090,TRCN0000065091,TRCN0000065092	0.80,0.30,0.32,0.32	Resistance
26	RPL7L1	0.86	0.0006	TRCN0000117687,TRCN0000117689,TRCN0000117690,TRCN0000117691	0.32,0.36,0.34,0.31	Resistance
27	XRCC4	0.76	0.0008	TRCN0000009874,TRCN0000040113,TRCN0000040114,TRCN0000040115,TRCN0000040116	0.43,0.19,0.56,0.60,0.65	Resistance
28	SLC23A2	0.76	0.0008	TRCN0000038204,TRCN0000038205,TRCN0000038206,TRCN0000038207,TRCN0000038208	0.61,0.19,0.57,0.26,0.35	Resistance
29	TNPO3	0.76	0.0008	TRCN0000038329,TRCN0000038330,TRCN0000038331,TRCN0000038332,TRCN0000038333	0.19,0.22,0.97,0.20,0.60	Resistance
30	SLC6A17	0.84	0.0008	TRCN0000038514,TRCN0000038515,TRCN0000038517,TRCN0000038518	1.47,0.29,0.29,0.32	Resistance
31	CTAG2	0.89	0.0008	TRCN0000115762,TRCN0000115764,TRCN0000115765	0.36,0.49,0.53	Resistance
32	CYB5R3	0.84	0.0009	TRCN0000038974,TRCN0000038975,TRCN0000038976,TRCN0000038978	0.75,0.28,0.45,0.72	Resistance
33	SLC27A5	0.89	0.0009	TRCN0000043380,TRCN0000043381,TRCN0000043382	0.54,0.74,0.36	Resistance

Appendix IV. Cisplatin resistance candidate genes and cisplatin sensitizing genes identified from RNAi screen (q < 0.005). (continued)

Index	Gene	NES	False Discovery Rate q-value	Hairpin ID	Hairpin score	Category
34	ZNF510	0.75	0.0009	TRCN0000107660,TRCN0000107661,TRCN0000107662,TRCN0000107663,TRCN0000107664	0.50,0.18,0.21,0.39,0.45	Resistance
35	FKSG30	0.96	0.001	TRCN0000117202,TRCN0000117204	0.53,0.54	Resistance
36	LOC393062	0.96	0.0011	TRCN0000038484,TRCN0000038487	0.52,0.63	Resistance
37	MRPL3	0.75	0.0011	TRCN0000117582,TRCN0000117583,TRCN0000117584,TRCN0000117585,TRCN0000117586	0.17,0.54,0.67,0.33,0.37	Resistance
38	SLC5A12	0.82	0.0012	TRCN0000043653,TRCN0000043654,TRCN0000043656,TRCN0000043657	0.33,0.26,0.37,0.64	Resistance
39	DUOX2	0.82	0.0012	TRCN0000045963,TRCN0000045964,TRCN0000045966,TRCN0000045967	0.35,0.33,0.54,0.26	Resistance
40	SPTBN4	0.82	0.0012	TRCN0000113936,TRCN0000113937,TRCN0000113938,TRCN0000113940	0.38,0.28,0.28,0.26	Resistance
41	KIFC3	0.74	0.0012	TRCN0000116462,TRCN0000116463,TRCN0000116464,TRCN0000116465,TRCN0000116466	0.19,0.33,0.36,0.17,0.22	Resistance
42	ABCC3	0.88	0.0013	TRCN0000059404,TRCN0000059406,TRCN0000059407	0.70,0.74,0.34	Resistance
43	MR1	0.81	0.0014	TRCN0000057288,TRCN0000057289,TRCN0000057290,TRCN0000057291	0.58,0.25,0.36,0.27	Resistance
44	VKORC1	0.95	0.0015	TRCN0000038970,TRCN0000038973	0.50,0.66	Resistance
45	RAB3GAP2	0.87	0.0016	TRCN0000047218,TRCN0000047219,TRCN0000047222	0.33,0.48,0.51	Resistance
46	PPL	0.81	0.0016	TRCN0000116937,TRCN0000116938,TRCN0000116939,TRCN0000116941	0.24,0.51,0.53,0.25	Resistance
47	SLCO4C1	0.8	0.0018	TRCN0000038310,TRCN0000038311,TRCN0000038312,TRCN0000038313	0.88,0.24,0.29,0.38	Resistance
48	SLC35E2	0.74	0.0018	TRCN0000044373,TRCN0000044374,TRCN0000044375,TRCN0000044376,TRCN0000044377	0.88,0.28,0.77,0.16,0.35	Resistance
49	PEX5	0.95	0.0018	TRCN0000082820,TRCN0000082822	0.82,0.49	Resistance
50	SLCO2A1	0.95	0.0019	TRCN0000043063,TRCN0000043064	0.49,0.58	Resistance
51	ATP6V0D2	0.8	0.002	TRCN0000043518,TRCN0000043519,TRCN0000043520,TRCN0000043521	0.23,0.54,0.26,0.55	Resistance
52	TRPC3	0.73	0.002	TRCN0000044028,TRCN0000044029,TRCN0000044030,TRCN0000044031,TRCN0000044032	0.55,0.42,0.44,-0.15,0.58	Resistance

Appendix IV. Cisplatin resistance candidate genes and cisplatin sensitizing genes identified from RNAi screen (q < 0.005). (continued)

Index	Gene	NES	False Discovery Rate q-value	Hairpin ID	Hairpin score	Category
53	BIN1	0.73	0.002	TRCN0000118037,TRCN0000118038,TRCN0000118039,TRCN0000118040,TRCN0000118041	0.48,0.16,0.65,0.25,0.43	Resistance
54	AKAP8	0.79	0.0021	TRCN0000037944,TRCN0000037945,TRCN0000037946,TRCN0000037947	0.37,0.46,0.22,0.43	Resistance
55	ATP6V0A2	0.79	0.0021	TRCN0000043493,TRCN0000043494,TRCN0000043495,TRCN0000043496	0.99,0.23,0.27,0.38	Resistance
56	CLCN1	0.79	0.0021	TRCN0000043883,TRCN0000043884,TRCN0000043885,TRCN0000043887	0.31,0.23,0.25,0.34	Resistance
57	ST3GAL6	0.73	0.0022	TRCN0000035499,TRCN0000035500,TRCN0000035501,TRCN0000035502,TRCN0000035503	0.18,0.47,0.48,0.16,0.20	Resistance
58	KCNJ3	0.78	0.0022	TRCN0000044328,TRCN0000044329,TRCN0000044330,TRCN0000044332	0.22,0.25,0.32,0.25	Resistance
59	SLC35B1	0.73	0.0024	TRCN0000044403,TRCN0000044404,TRCN0000044405,TRCN0000044406,TRCN0000044407	0.39,0.15,0.43,0.45,0.40	Resistance
60	CKAP1	0.78	0.0025	TRCN0000117032,TRCN0000117033,TRCN0000117034,TRCN0000117035	0.68,0.32,0.21,0.47	Resistance
61	ZNF694	0.78	0.0025	TRCN0000107350,TRCN0000107351,TRCN0000107353,TRCN0000107354	0.34,0.21,0.44,0.33	Resistance
62	RBM15	0.72	0.0025	TRCN0000074703,TRCN0000074704,TRCN0000074705,TRCN0000074706,TRCN0000074707	0.75,0.21,0.23,0.15,0.73	Resistance
63	ATP1B3	0.78	0.0026	TRCN0000043368,TRCN0000043369,TRCN0000043370,TRCN0000043371	0.30,0.47,0.27,0.21	Resistance
64	SLC25A17	0.78	0.0026	TRCN0000043908,TRCN0000043909,TRCN0000043910,TRCN0000043912	0.43,0.31,0.55,0.21	Resistance
65	ZNF546	0.78	0.0026	TRCN0000108170,TRCN0000108171,TRCN0000108172,TRCN0000108174	0.21,0.21,0.30,0.55	Resistance
66	CKS1B	0.72	0.0027	TRCN0000037919,TRCN0000037920,TRCN0000037921,TRCN0000037922,TRCN0000037923	0.15,0.60,0.45,0.26,0.28	Resistance
67	SCN4A	0.72	0.0027	TRCN0000044418,TRCN0000044419,TRCN0000044420,TRCN0000044421,TRCN0000044422	0.33,0.15,0.28,0.24,0.46	Resistance
68	TRPV3	0.72	0.0028	TRCN0000044318,TRCN0000044319,TRCN0000044320,TRCN0000044321,TRCN0000044322	0.17,0.60,0.37,0.15,0.15	Resistance
69	WDR57	0.72	0.0029	TRCN0000074608,TRCN0000074609,TRCN0000074610,TRCN0000074611,TRCN0000074612	0.37,-0.26,0.36,0.56,0.76	Resistance
70	TPCN2	0.71	0.0029	TRCN0000043918,TRCN0000043919,TRCN0000043920,TRCN0000043921,TRCN0000043922	-0.40,0.47,0.52,0.40,0.50	Resistance

Appendix IV. Cisplatin resistance candidate genes and cisplatin sensitizing genes identified from RNAi screen (q < 0.005). (continued)

Index	Gene	NES	False Discovery Rate q-value	Hairpin ID	Hairpin score	Category
71	DUOX1	0.71	0.0029	TRCN0000045973,TRCN0000045974,TRCN0000045975,TRCN0000045976,TRCN0000045977	0.40,0.46,-0.16,0.48,0.43	Resistance
72	CACNA2D1	0.85	0.003	TRCN0000043768,TRCN0000043769,TRCN0000043770	0.34,0.55,0.30	Resistance
73	KCNH3	0.77	0.003	TRCN0000044593,TRCN0000044594,TRCN0000044595,TRCN0000044596	0.33,0.20,0.34,0.21	Resistance
74	HIST1H4B	0.85	0.003	TRCN0000106686,TRCN0000106687,TRCN0000106689	0.30,0.66,0.34	Resistance
75	NMRAL1	0.77	0.0033	TRCN0000036909,TRCN0000036911,TRCN0000036912,TRCN0000036913	0.20,0.61,0.46,0.28	Resistance
76	INCENP	0.77	0.0033	TRCN0000074143,TRCN0000074144,TRCN0000074145,TRCN0000074146	0.26,0.20,0.35,0.26	Resistance
77	TMEM16A	0.85	0.0034	TRCN0000040265,TRCN0000040266,TRCN0000040267	0.29,0.34,0.79	Resistance
78	AKAP13	0.77	0.0034	TRCN0000037970,TRCN0000037971,TRCN0000037972,TRCN0000037973	0.40,0.20,0.35,0.62	Resistance
79	CBR1	0.71	0.0035	TRCN0000046373,TRCN0000046374,TRCN0000046375,TRCN0000046376,TRCN0000046377	0.37,0.14,0.15,0.60,0.46	Resistance
80	TNPO2	0.76	0.0036	TRCN0000043468,TRCN0000043469,TRCN0000043470,TRCN0000043471	0.20,0.68,0.27,0.19	Resistance
81	DPP10	0.71	0.0036	TRCN0000046663,TRCN0000046664,TRCN0000046665,TRCN0000046666,TRCN0000046667	0.23,0.14,0.29,0.15,0.15	Resistance
82	GPC3	0.76	0.0036	TRCN0000078558,TRCN0000078559,TRCN0000078561,TRCN0000078562	0.22,0.77,0.77,0.19	Resistance
83	MYO15A	0.76	0.0036	TRCN0000083324,TRCN0000083325,TRCN0000083326,TRCN0000083327	0.35,0.31,0.19,0.31	Resistance
84	ZNF418	0.71	0.0036	TRCN0000107465,TRCN0000107466,TRCN0000107467,TRCN0000107468,TRCN0000107469	0.37,0.19,0.27,0.14,0.53	Resistance
85	SLC26A4	0.71	0.0039	TRCN0000044283,TRCN0000044284,TRCN0000044285,TRCN0000044286,TRCN0000044287	0.81,0.69,0.33,0.51,-0.09	Resistance
86	ACE	0.71	0.0039	TRCN0000046613,TRCN0000046614,TRCN0000046615,TRCN0000046616,TRCN0000046617	-0.44,0.57,0.36,0.56,0.55	Resistance
87	ART4	0.7	0.004	TRCN0000083628,TRCN0000083629,TRCN0000083630,TRCN0000083631,TRCN0000083632	0.16,1.03,0.13,0.18,0.61	Resistance
88	PODXL	0.7	0.004	TRCN0000117017,TRCN0000117018,TRCN0000117019,TRCN0000117020,TRCN0000117021	0.09,0.58,0.35,0.36,0.64	Resistance

Appendix IV. Cisplatin resistance candidate genes and cisplatin sensitizing genes identified from RNAi screen (q < 0.005). (continued)

Index	Gene	NES	False Discovery Rate q-value	Hairpin ID	Hairpin score	Category
89	SARS2	0.7	0.0041	TRCN0000045498,TRCN0000045499,TRCN0000045500,TRCN0000045501,TRCN0000045502	0.16,0.31,0.32,0.15,0.13	Resistance
90	ARL6	0.7	0.0041	TRCN0000047993,TRCN0000047994,TRCN0000047995,TRCN0000047996,TRCN0000047997	0.65,0.22,0.21,0.17,0.13	Resistance
91	AOF1	0.84	0.0042	TRCN0000046073,TRCN0000046076,TRCN0000046077	0.48,0.52,0.28	Resistance
92	NDST3	0.7	0.0043	TRCN0000035989,TRCN0000035990,TRCN0000035991,TRCN0000035992,TRCN0000035993	0.73,0.30,0.22,0.13,0.41	Resistance
93	KCNN4	0.7	0.0044	TRCN0000043933,TRCN0000043934,TRCN0000043935,TRCN0000043936,TRCN0000043937	0.12,0.78,0.71,0.29,0.36	Resistance
94	SLC25A18	0.7	0.0044	TRCN0000043953,TRCN0000043954,TRCN0000043955,TRCN0000043956,TRCN0000043957	0.53,0.12,0.18,0.23,0.22	Resistance
95	SSX9	0.7	0.0045	TRCN0000115722,TRCN0000115723,TRCN0000115724,TRCN0000115725,TRCN0000115726	0.41,0.40,0.44,0.37,0.01	Resistance
96	PKIG	0.93	0.0047	TRCN0000037965,TRCN0000037966	0.43,0.45	Resistance
97	OGFOD2	0.69	0.0047	TRCN0000064893,TRCN0000064894,TRCN0000064895,TRCN0000064896,TRCN0000064897	0.26,0.24,0.57,0.56,0.12	Resistance
98	ASCC3L1	0.86	0	TRCN0000051828,TRCN0000051829,TRCN0000051830,TRCN0000051832,TRCN0000051831	0.98,1.08,0.75,0.63,0.53	Sensitizing
99	SIRPB2	0.82	0	TRCN0000052753,TRCN0000052754,TRCN0000052755,TRCN0000052756,TRCN0000052757	0.65,0.56,0.58,0.67,0.49	Sensitizing
100	POLE2	0.97	0	TRCN0000052983,TRCN0000052984,TRCN0000052985,TRCN0000052986,TRCN0000052987	0.77,0.88,0.83,0.76,0.95	Sensitizing
101	CLEC4C	0.9	0	TRCN0000055458,TRCN0000055460,TRCN0000055461,TRCN0000055462	0.63,0.60,0.59,0.71	Sensitizing
102	DNTTIP2	0.94	0	TRCN0000061513,TRCN0000061514,TRCN0000061515	1.07,0.71,0.68	Sensitizing
103	CTGF	0.92	0	TRCN0000061949,TRCN0000061950,TRCN0000061951,TRCN0000061952	0.66,0.70,0.65,0.63	Sensitizing
104	LEPREL1	0.95	0	TRCN0000064793,TRCN0000064795,TRCN0000064797	0.77,0.70,1.03	Sensitizing
105	LOC440606	0.8	0.0001	TRCN0000049312,TRCN0000049308,TRCN0000049309,TRCN0000049310,TRCN0000049311	1.32,0.47,0.53,0.46,0.52	Sensitizing

Appendix IV. Cisplatin resistance candidate genes and cisplatin sensitizing genes identified from RNAi screen (q < 0.005). (continued)

Index	Gene	NES	False Discovery Rate q-value	Hairpin ID	Hairpin score	Category
106	AP1GBP1	0.93	0.0001	TRCN0000054121,TRCN0000054118,TRCN0000054120	0.77,0.69,0.64	Sensitizing
107	SOS1	0.81	0.0001	TRCN0000048143,TRCN0000048144,TRCN0000048145,TRCN0000048146,TRCN0000048147	0.56,0.79,0.69,0.50,0.48	Sensitizing
108	SND1	0.81	0.0001	TRCN0000049653,TRCN0000049654,TRCN0000049655,TRCN0000049656,TRCN0000049657	0.54,0.59,0.47,0.68,0.69	Sensitizing
109	SCG2	0.92	0.0001	TRCN0000055603,TRCN0000055605,TRCN0000055606	0.67,0.66,0.64	Sensitizing
110	CABP2	0.81	0.0001	TRCN0000056138,TRCN0000056139,TRCN0000056140,TRCN0000056141,TRCN0000056142	0.56,0.57,1.09,0.47,0.70	Sensitizing
111	PKD2L2	0.8	0.0001	TRCN0000056288,TRCN0000056289,TRCN0000056290,TRCN0000056291,TRCN0000056292	0.47,0.60,0.51,0.73,0.46	Sensitizing
112	CLEC2B	0.79	0.0001	TRCN0000056488,TRCN0000056489,TRCN0000056490,TRCN0000056491,TRCN0000056492	0.66,0.77,0.43,0.64,1.30	Sensitizing
113	CXorf9	0.91	0.0003	TRCN0000062584,TRCN0000062585,TRCN0000062586	0.72,0.64,0.62	Sensitizing
114	PCDHB2	0.79	0.0003	TRCN0000055493,TRCN0000055494,TRCN0000055495,TRCN0000055496,TRCN0000055497	0.50,0.51,0.61,0.63,0.45	Sensitizing
115	GMDS	0.77	0.0004	TRCN0000052468,TRCN0000052469,TRCN0000052470,TRCN0000052471,TRCN0000052472	0.93,0.70,0.28,0.61,0.72	Sensitizing
116	CDH9	0.86	0.0004	TRCN0000054253,TRCN0000054254,TRCN0000054255,TRCN0000054257	0.76,0.58,0.54,0.64	Sensitizing
117	PCDH11Y	0.79	0.0004	TRCN0000056283,TRCN0000056284,TRCN0000056285,TRCN0000056286,TRCN0000056287	0.53,0.44,0.62,0.65,0.72	Sensitizing
118	MRPS26	0.97	0.0004	TRCN0000146373,TRCN0000179426	0.82,0.77	Sensitizing
119	CPXCR1	0.97	0.0005	TRCN0000134254,TRCN0000135021	0.87,0.76	Sensitizing
120	TNKS2	0.85	0.0006	TRCN0000053238,TRCN0000053239,TRCN0000053240,TRCN0000053241	0.56,0.52,1.03,0.53	Sensitizing
121	ANXA7	0.86	0.0006	TRCN0000056303,TRCN0000056305,TRCN0000056306,TRCN0000056307	0.74,0.54,0.62,0.73	Sensitizing
122	GUCA1A	0.9	0.0008	TRCN0000056259,TRCN0000056260,TRCN0000056262	1.00,0.57,0.77	Sensitizing
123	FGD1	0.74	0.0009	TRCN0000048168,TRCN0000048169,TRCN0000048170,TRCN0000048171,TRCN0000048172	0.63,0.59,0.63,0.76,0.35	Sensitizing

Appendix IV. Cisplatin resistance candidate genes and cisplatin sensitizing genes identified from RNAi screen (q < 0.005). (continued)

Index	Gene	NES	False Discovery Rate q-value	Hairpin ID	Hairpin score	Category
124	ABCC12	0.75	0.0009	TRCN0000059268,TRCN0000059269,TRCN0000059270,TRCN0000059271,TRCN0000059272	1.25,0.26,-0.30,1.03,0.92	Sensitizing
125	RAB20	0.83	0.001	TRCN0000048093,TRCN0000048094,TRCN0000048096,TRCN0000048097	0.60,0.58,0.67,0.50	Sensitizing
126	NCOA6	0.89	0.001	TRCN0000063263,TRCN0000063264,TRCN0000063265	2.98,0.14,1.12	Sensitizing
127	TATDN2	0.89	0.0011	TRCN0000049828,TRCN0000049830,TRCN0000049831	0.96,0.56,0.81	Sensitizing
128	PCDHA8	0.83	0.0011	TRCN0000056018,TRCN0000056019,TRCN0000056020,TRCN0000056022	0.70,0.50,0.65,0.55	Sensitizing
129	PRRG1	0.83	0.0011	TRCN0000056433,TRCN0000056434,TRCN0000056436,TRCN0000056437	0.50,0.53,0.71,0.56	Sensitizing
130	PCDHB5	0.82	0.0012	TRCN0000056218,TRCN0000056220,TRCN0000056221,TRCN0000056222	0.51,0.72,0.48,0.60	Sensitizing
131	EPS15L1	0.74	0.0014	TRCN0000053823,TRCN0000053824,TRCN0000053825,TRCN0000053826,TRCN0000053827	0.82,0.43,0.56,1.43,0.46	Sensitizing
132	RPS11	0.74	0.0014	TRCN0000074978,TRCN0000074979,TRCN0000074980,TRCN0000074981,TRCN0000074982	0.80,0.43,0.43,0.50,0.43	Sensitizing
133	PATE	0.81	0.0015	TRCN0000055671,TRCN0000055672,TRCN0000055669,TRCN0000055670	0.54,0.83,0.47,0.72	Sensitizing
134	DNM3	0.81	0.0015	TRCN0000051404,TRCN0000051405,TRCN0000051406,TRCN0000051407	0.47,0.60,0.59,0.53	Sensitizing
135	ZZEF1	0.81	0.0015	TRCN0000055663,TRCN0000055664,TRCN0000055665,TRCN0000055667	0.47,0.54,0.62,0.51	Sensitizing
136	ACTN3	0.8	0.0016	TRCN0000055908,TRCN0000055909,TRCN0000055910,TRCN0000055911	0.70,0.63,0.96,0.46	Sensitizing
137	RPL23	0.87	0.0016	TRCN0000117542,TRCN0000117543,TRCN0000117544	0.55,0.80,1.28	Sensitizing
138	EFEMP1	0.73	0.0017	TRCN0000055963,TRCN0000055964,TRCN0000055965,TRCN0000055966,TRCN0000055967	0.94,0.47,0.42,1.16,0.64	Sensitizing
139	CSF2RB	0.86	0.0018	TRCN0000059219,TRCN0000059221,TRCN0000059222	0.81,0.54,0.54	Sensitizing
140	CEP164	0.95	0.0018	TRCN0000147245,TRCN0000148591	0.70,0.70	Sensitizing
141	RHBDF2	0.79	0.0019	TRCN0000048683,TRCN0000048684,TRCN0000048685,TRCN0000048687	0.44,0.72,0.79,0.65	Sensitizing
142	PCDH8	0.79	0.0019	TRCN0000055863,TRCN0000055864,TRCN0000055865,TRCN0000055866	-0.39,1.20,0.71,0.70	Sensitizing
143	PLSCR1	0.79	0.0019	TRCN0000056269,TRCN0000056270,TRCN0000056271,TRCN0000056272	1.45,0.74,0.44,0.52	Sensitizing

Appendix IV. Cisplatin resistance candidate genes and cisplatin sensitizing genes identified from RNAi screen (q < 0.005). (continued)

Index	Gene	NES	False Discovery Rate q-value	Hairpin ID	Hairpin score	Category
144	CDH7	0.79	0.002	TRCN0000054158,TRCN0000054159,TRCN0000054160,TRCN0000054161	0.52,0.44,0.52,0.47	Sensitizing
145	PCDHA12	0.78	0.002	TRCN0000055749,TRCN0000055750,TRCN0000055751,TRCN0000055752	0.64,0.48,0.43,0.45	Sensitizing
146	SNAI3	0.95	0.0022	TRCN0000033299,TRCN0000033303	0.70,0.70	Sensitizing
147	FAHD1	0.72	0.0022	TRCN0000050068,TRCN0000050069,TRCN0000050070,TRCN0000050071,TRCN0000050072	0.42,0.56,0.61,1.16,0.40	Sensitizing
148	SPOCK3	0.72	0.0022	TRCN0000053618,TRCN0000053619,TRCN0000053620,TRCN0000053621,TRCN0000053622	0.72,0.40,0.72,0.61,0.53	Sensitizing
149	PCDHB8	0.72	0.0022	TRCN0000054208,TRCN0000054209,TRCN0000054210,TRCN0000054211,TRCN0000054212	0.65,0.49,0.58,0.40,0.62	Sensitizing
150	PCDHGC3	0.72	0.0022	TRCN0000055638,TRCN0000055639,TRCN0000055640,TRCN0000055641,TRCN0000055642	1.22,-0.24,0.53,0.85,0.55	Sensitizing
151	TPTEps1	0.72	0.0023	TRCN0000052829,TRCN0000052832,TRCN0000052828,TRCN0000052830,TRCN0000052831	1.10,0.39,0.52,0.41,0.43	Sensitizing
152	ACOT9	0.72	0.0023	TRCN0000048903,TRCN0000048904,TRCN0000048905,TRCN0000048906,TRCN0000048907	1.07,0.45,0.39,0.84,0.54	Sensitizing
153	GOLGA4	0.86	0.0023	TRCN0000061990,TRCN0000061991,TRCN0000061992	0.65,0.53,0.93	Sensitizing
154	KNDC1	0.51	0.0024	TRCN0000048293,TRCN0000048294,TRCN0000048295,TRCN0000048296,TRCN0000048297,TRCN0000048298,TRCN0000048299,TRCN0000048300,TRCN000... <Preview truncated at 128 characters>	0.57,0.74,-0.09,-0.16,0.18,0.49,0.66,1.17,0.28,0.64	Sensitizing
155	EFHA2	0.77	0.0025	TRCN0000056083,TRCN0000056084,TRCN0000056085,TRCN0000056086	0.56,-0.19,0.63,2.57	Sensitizing
156	GJA8	0.71	0.0027	TRCN0000059838,TRCN0000059839,TRCN0000059840,TRCN0000059841,TRCN0000059842	0.53,0.73,1.02,-0.48,0.65	Sensitizing
157	LOC402282	0.71	0.0028	TRCN0000048258,TRCN0000048259,TRCN0000048260,TRCN0000048261,TRCN0000048262	0.77,0.01,0.60,0.73,0.54	Sensitizing
158	GCLC	0.76	0.0029	TRCN0000048483,TRCN0000048484,TRCN0000048485,TRCN0000048486	-0.17,0.72,0.65,1.11	Sensitizing
159	CDH10	0.7	0.0029	TRCN0000054288,TRCN0000054289,TRCN0000054290,TRCN0000054291,TRCN0000054292	0.53,0.37,0.67,0.38,0.51	Sensitizing

Appendix IV. Cisplatin resistance candidate genes and cisplatin sensitizing genes identified from RNAi screen (q < 0.005). (continued)

Index	Gene	NES	False Discovery Rate q-value	Hairpin ID	Hairpin score	Category
160	WNT9A	0.7	0.0029	TRCN0000062073,TRCN0000062074,TRCN0000062075,TRCN0000062076,TRCN0000062077	0.68,0.55,0.64,0.16,0.68	Sensitizing
161	LTBP4	0.85	0.003	TRCN0000055828,TRCN0000055830,TRCN0000055831	0.52,0.59,0.65	Sensitizing
162	PSMD13	0.85	0.003	TRCN0000058109,TRCN0000058110,TRCN0000058111	0.95,0.52,0.55	Sensitizing
163	PCDHGA6	0.7	0.0031	TRCN0000053548,TRCN0000053549,TRCN0000053550,TRCN0000053551,TRCN0000053552	-0.10,0.59,0.97,0.50,1.22	Sensitizing
164	CD40LG	0.76	0.0031	TRCN0000059113,TRCN0000059115,TRCN0000059116,TRCN0000059117	0.54,0.59,0.43,0.44	Sensitizing
165	CANT1	0.85	0.0032	TRCN0000051898,TRCN0000051900,TRCN0000051901	0.52,0.54,0.66	Sensitizing
166	POLH	0.7	0.0032	TRCN0000053008,TRCN0000053009,TRCN0000053010,TRCN0000053011,TRCN0000053012	1.05,0.70,0.19,-0.40,1.24	Sensitizing
167	POLR2H	0.7	0.0033	TRCN0000053068,TRCN0000053069,TRCN0000053070,TRCN0000053071,TRCN0000053072	0.50,0.76,0.94,0.02,0.99	Sensitizing
168	IFNA4	0.94	0.0034	TRCN0000005814,TRCN0000005817	0.67,0.70	Sensitizing
169	PCDHA1	0.69	0.004	TRCN0000053268,TRCN0000053269,TRCN0000053270,TRCN0000053271,TRCN0000053272	0.71,-0.03,-0.17,0.92,1.08	Sensitizing
170	OR51B6	0.75	0.0043	TRCN0000060783,TRCN0000060784,TRCN0000060785,TRCN0000060786	0.65,0.57,0.51,0.43	Sensitizing
171	PCDHGA9	0.84	0.0045	TRCN0000053404,TRCN0000053405,TRCN0000053407	1.58,0.51,0.61	Sensitizing
172	GABRA5	0.68	0.0046	TRCN0000061268,TRCN0000061269,TRCN0000061270,TRCN0000061271,TRCN0000061272	0.17,1.08,-0.03,0.95,0.70	Sensitizing
173	GNB3	0.74	0.0047	TRCN0000036784,TRCN0000036786,TRCN0000036787,TRCN0000036788	1.17,0.38,0.61,0.62	Sensitizing
174	MMAB	0.74	0.0047	TRCN0000083903,TRCN0000083905,TRCN0000083906,TRCN0000083907	0.88,0.57,0.43,0.73	Sensitizing